



THE UNIVERSITY
of ADELAIDE

Hydrothermal Carbonisation of Novel Biomasses



Benjamin Geoffrey Keiller



Thesis Submitted for the degree of Doctor of Philosophy

School of Agriculture, Food and Wine

Faculty of Science

School of Chemical Engineering and Advanced Materials

Faculty of Engineering, Computer & Mathematical Sciences

University of Adelaide, Australia

January 2020

Table of Contents

List of Figures.....	i
List of Tables.....	iii
Abstract.....	iv
Declaration.....	vi
Acknowledgments.....	vii
Preface.....	viii
Chapter 1 – Introduction.....	1
1.0 Background.....	2
1.1 Scope, Structure and Summary of Thesis.....	3
Chapter 2 – Literature Review.....	9
2.0 Introduction to Biofuels.....	10
2.1 Hydrothermal Biofuels.....	11
2.1.1 Hydrothermal Carbonisation.....	12
2.2 Composition of biomass.....	14
2.2.1 Cellulose.....	15
2.2.2 Hemicellulose.....	16
2.2.3 Lignin.....	16
2.2.4 Proteins.....	17
2.2.5 Ash.....	17
2.3 Mechanism of HTC.....	18
2.3.1 Degradation Reactions.....	21
2.3.2 Polymerisation Reactions.....	24
2.4 Reaction Kinetics of HTC.....	27
Aim and Objectives of Thesis.....	34
Chapter 3 (Paper I) - Hydrothermal Carbonisation of Australian Saltbush.....	36
3.0 Abstract.....	37
3.1 Introduction.....	37
3.2 Methods and Materials.....	40
3.2.1 Preparation of saltbush sample.....	40
3.2.2 Hydrothermal Carbonisation.....	41
3.2.3 Fuel Analysis.....	42
3.2.4 Experimental Statistical Analysis.....	44
3.3. Results and Discussion.....	44

3.4 Conclusion.....	58
3.5 Acknowledgments.....	58
Chapter 4 (Paper II) – Biochemical Composition & Kinetic Modelling of HTC of Saltbush.....	60
4.0 Abstract.....	63
4.1 Introduction.....	63
4.2 Methods and Materials.....	68
4.2.1 Hydrothermal Carbonisation.....	68
4.2.2 Compositional analysis.....	69
4.2.3 Kinetics method.....	71
4.3 Results and Discussion.....	73
4.3.1 Overall changes to feedstock during HTC.....	73
4.3.2 Biochemical Changes in HTC.....	77
4.4 Conclusions.....	88
4.5 Acknowledgments.....	89
Chapter 5 (Paper III) – Biochemical Composition & Kinetic Modelling of HTC of Hemp.....	90
5.0 Abstract.....	93
5.1 Introduction.....	93
5.2 Methods and Materials.....	96
5.2.1 Hydrothermal Carbonisation.....	96
5.2.2 Compositional Analysis.....	98
5.2.3 Kinetic modelling.....	99
5.3. Results and Discussion.....	101
5.3.1 Global changes in biomass composition.....	101
5.3.2 Mechanism of hydrochar production.....	106
5.4 Conclusion.....	119
5.5 Acknowledgments.....	120
Chapter 6 (Paper IV) – Biochemical Composition & Kinetic Modelling of HTC of Macroalgae	121
6.0 Abstract.....	124
6.1 Introduction.....	124
6.2 Methods and Materials.....	129
6.2.1 Hydrothermal Carbonisation.....	129
6.2.2 Compositional Analysis.....	131
6.2.3 Kinetic modeling.....	131
6.3 Results and Discussion.....	133

6.4 Conclusion.....	152
6.5 Acknowledgments.....	152
Chapter 7 – Thesis Conclusions and Future Directions.....	153
7.1 Thesis Conclusions and Key Findings.....	154
7.1.1 Fuel Properties of HTC of novel biomasses.....	155
7.1.2 Compositional Analysis of Hydrochars.....	156
7.1.3 Kinetics of the Principle Biochemical Components of biomass.....	157
7.2 Future Directions.....	158
7.2.1 Develop a database on the compositions of different biomasses and hydrochars.....	158
7.2.2 Develop better methods of differentiating primary and secondary char.....	159
7.2.3 Investigate the mechanisms by which hydrochar reabsorbs inorganic elements.....	159
Appendix.....	160
Bibliography.....	164

List of Figures

Figure 1: Overview of the structure of lignocellulose in a terrestrial plant cell wall.....	15
Figure 2: Three-pathway mechanism proposed by Jatzwauk and Schempe 2015.....	19
Figure 3: Twin-pathway model of HTC proposed by Karayıldırım <i>et al.</i> 2008 and Dinjus <i>et al.</i> 2011.....	19
Figure 4: Hydrolysis of an ester bond.....	21
Figure 5: Decarboxylation of a carboxylic acid.....	21
Figure 6: Dehydration of a secondary alcohol.....	22
Figure 7: Aromatisation of glucose to form 5-HMF.....	23
Figure 8: Condensation reaction of an alcohol and a carboxylic acid.....	23
Figure 9: Summary of the conversion of cellulose into secondary hydrochar.....	25
Figure 10: Solid product mass yield, product energy yield and higher heating values following HTC of saltbush.....	43
Figure 11: Proximate Analysis, Ultimate Analysis and Ash Retention of untreated saltbush and HTC hydrochars.....	46
Figure 12: Pyrolysis Behaviour of untreated saltbush and hydrochars.....	47
Figure 13: Retentions of Carbon, Hydrogen, Nitrogen and Oxygen within hydrochars.....	49
Figure 14: Van Krevelen Chart comparing the H:C and O:C ratios of untreated saltbush and hydrochars compared with Victorian Brown Coals.....	50
Figure 15: Elemental concentrations of Na, Cl, Ca, K, S and P in untreated saltbush and hydrochars.....	52
Figure 16: FTIR spectra of untreated saltbush and select hydrochars following HTC.....	69
Figure 17: Total biochemical composition of untreated saltbush and hydrochars.....	72
Figure 18: Model of lignocellulose degradation during HTC.....	76
Figure 19: Degradation and first order Arrhenius kinetic modeling of hemicellulose within saltbush following HTC.....	77
Figure 20: Degradation and 0.5 th order Arrhenius kinetic modeling of cellulose within saltbush following HTC.....	78
Figure 21: Degradation and first order Arrhenius kinetic modeling of lignin within saltbush following HTC.....	81

Figure 22: Yields of liquid, gas, and biochemical macromolecule across whole HTC reaction system of hemp stems, seed hulls and hydrochars.....98

Figure 23: Ultimate analysis and higher heating values of untreated feedstock and HTC hydrochars of hemp stems and seed hulls.....101

Figure 24: Proposed mechanism for the conversion of biomass into hydrochar during HTC...103

Figure 25: Degradation and Arrhenius kinetic modeling of hemicellulose within hemp following HTC.....105

Figure 26: Monosaccharide profiles of untreated hemp stem and seed hull, and select hydrochars following HTC.....107

Figure 27: Degradation and Arrhenius kinetic modeling of cellulose within hemp following HTC.....108

Figure 28: Degradation and Arrhenius kinetic modeling of lignin within hemp following HTC.111

Figure 29: Global changes in macroalgae biomass composition during HTC.....130

Figure 30: Ultimate Analysis and higher heating values of untreated macroalgae and HTC hydrochars.....134

Figure 31: Proposed Mechanism of biomass degradation in HTC.....135

Figure 32: Monosaccharide profiles of untreated *Oedogonium* and *Ulva*, and select hydrochars following HTC.....138

Figure 33: Degradation and Arrhenius kinetic modeling of hemicellulose within macroalgae following HTC.....139

Figure 34: Degradation and Arrhenius kinetic modeling of cellulose within macroalgae following HTC.....140

Figure 35: Degradation and Arrhenius kinetic modeling of protein within macroalgae following HTC.....145

List of Tables

Table 1: Summary of literature investigating the degradation kinetics of a given feedstock during a variety of hydrothermal treatments.....	32
Table 2: FTIR Resonances of untreated saltbush and hydrochars.....	71
Table 3: Kinetic parameters for the degradation of saltbush lignocellulose during HTC.....	76
Table 4: Published values for hemicellulose and cellulose in pure refined feedstock and biomass HTC experiments.....	82
Table 5: Kinetic parameters for the degradation of key biochemical components during HTC of hemp.....	107
Table 6: Kinetic parameters for the degradation of key biochemical components during HTC of macroalgae.....	136
Table 7: Summary of concentrations of each biochemical macromolecule (% w/w) in each feedstock (untreated, and select hydrochars) studied in this thesis.....	152
Table 8: Summary of Kinetic Parameters of the biochemical macromolecules and feedstocks and models examined within this thesis.....	154

Abstract

Renewable sources of thermal and chemical energy are needed in order to satisfy the world's ever growing energy needs while limiting the rise of global temperatures below 2 °C above pre-industrial levels. Plant biomass is a vast resource which if harnessed properly could help revolutionise the global energy economy. Hydrothermal Carbonisation (HTC) is a technology wherein biomass exposed to subcritical water at 180 °C – 260 °C is thermochemically converted into an energy-dense “hydrochar” with strong thermal and elemental similarities to fossil coal. However, key aspects of the HTC reaction remain unknown, especially with regard to the degradation of the key biochemical macromolecules hemicellulose, cellulose, lignin and protein. In this thesis, three novel biomasses, Australian saltbush, hemp and macroalgae, were subjected to HTC and the hydrochars analysed for fuel properties and biochemical composition. The breakdown of the key macromolecules was then described using kinetic modelling to build a mechanistic model of the overall conversion of biomass to hydrochar.

Each of the three biomasses underwent profound chemical changes during the HTC reaction, resulting in much lower oxygen content, and much higher carbon content. This caused the energy content of the hydrochars to rise to levels that rivaled or even exceeded those observed in fossil lignites. In addition, the ash content of the biomass was reduced, although certain reaction conditions at higher intensities saw the reabsorbence of inorganic elements back into the char.

A twin-pathway mechanistic model was adapted and developed from the literature to describe the overall HTC process and the formation of two different kinds of hydrochar: Mechanism 1, involving solid phase conversions that yield “primary char” derived directly from undissolved and partially converted starting material; and Mechanism 2, a two-step pathway that involves the degradation of the feedstock into dissolved intermediates, and the subsequent repolymerisation of those intermediates into “secondary char”. Using this model as a framework of the backdrop of the HTC reaction, the kinetics of the degradation step in each macromolecule were then analysed in detail.

There were numerous broad similarities in the behaviour of the key macromolecules between the different biomasses, in spite of their different origins. The degradation of polysaccharides was determined mainly by the degree of crystallinity; non-crystalline hemicellulose degraded very quickly in every biomass in a pseudo-first order reaction, often being completely eliminated from the feedstock within minutes. On the other hand, highly crystalline cellulose was more recalcitrant, and the reaction orders and rates of degradation of cellulose varied considerably across the three biomasses, although it was consistently slower than its non-crystalline counterparts. Variations in the degree of crystallinity in both cellulose and hemicellulose appeared to result in dramatic differences in the degradation kinetics. Lignin was found to be partially susceptible to HTC degradation, with the majority being dissolved with similar kinetics to hemicellulose, and the remainder being inert. The mechanism of the degradation of protein in macroalgae was opaque and difficult to model, with proteins possibly undergoing Maillard reactions with carbohydrates.

It is hoped that the methods presented here, especially regarding the biochemical analyses of the hydrochars, can form a major facet of future research and industrial development of HTC.

Declaration

I certify that this work contains no material which has been accepted for the award of any other degree or diploma in my name, in any university or other tertiary institution and, to the best of my knowledge and belief, contains no material previously published or written by another person, except where due reference has been made in the text. In addition, I certify that no part of this work will, in the future, be used in a submission in my name, for any other degree or diploma in any university or other tertiary institution without the prior approval of the University of Adelaide and where applicable, any partner institution responsible for the joint-award of this degree.

I acknowledge that copyright of published works contained within this thesis resides with the copyright holder(s) of those works.

I also give permission for the digital version of my thesis to be made available on the web, via the University's digital research repository, the Library Search and also through web search engines, unless permission has been granted by the University to restrict access for a period of time.

I acknowledge the support I have received for my research through the provision of an Australian Government Research Training Program Scholarship.

Benjamin Geoffrey Keiller

2020

Acknowledgments

This crazy, wild ride that some might call a PhD could not possibly have been completed without the expertise, insight, love and support of so many very remarkable people to whom I am deeply indebted to, and to whom I would like to extend my most sincere thanks and acknowledgments.

First of all, I would like to thank my supervisors, Rachel Burton and Phil van Eyk for their invaluable guidance and support over these tumultuous, yet fulfilling four years. In especial, I would like to thank Rachel for her patience, wit, and humour, vast knowledge of plants and their cell walls, and for always believing in me even when I stumbled. I would like to thank Phil for graciously adopting me into the chemical engineering world, for introducing me to the magic of hydrothermal tech, and for being an all around top bloke and good mate. I would be deeply remiss not to also thank Richard Muhlack for being my independent advisor, for providing his essential aid with statistics, and for his good nature. I would like to sincerely thank the Australian Federal Government for their financial support to me personally in providing me with a Research Training Scholarship (originally an Australian Postgraduate Award), and to the Australian Research Council Centre of Excellence in Plant Cell Walls for their financial support for this project.

Speaking of, I would like to extend my deep gratitude to the Wallies of the ARC CoE PCW for their guidance and companionship. I would like to thank Jelle Lahnstein for teaching me how to use HPLC, Andrea Matros for helping me to develop the lignin assay, and Kylie Neumann and Sandy Khor for teaching me how to do everything else, as well as being great friends. At the School of Chemical Engineering, I would like to extend a special thanks to Dan Lane, who taught me all the ropes of HTC, and without whom I would never have been able to find my feet so well. I would like to thank the Honours students Matthew Potter and Phoebe Chilman for their sterling work on the hemp and macroalgae projects, as well as my fellow HT postgrad students for their dear friendship.

Finally, I would like to thank all the family and friends who have helped me and lifted me up along the way. I say a truly heartfelt thank you to my Mum and Dad for their love and encouragement, to Mark and all the swords lads and ladies at ASA, to my dearest friends Simon and Charné, as well as to my beloved peach Monika. This is dedicated to you all.

Preface

This thesis is submitted as a portfolio of four journal papers, with two published online in *Energy & Fuels*, and two awaiting submission for publication.

I) Hydrothermal Carbonisation of Australian Saltbush

Benjamin G Keiller, Philip J van Eyk, Daniel J Lane, Richard Muhlack, and Rachel A. Burton
Energy & Fuels (2018) doi:10.1021/acs.energyfuels.8b03416.

II) Biochemical Compositional Analysis and Kinetic Modelling of Hydrothermal Carbonisation of Australian Saltbush

Benjamin G Keiller, Richard Muhlack, Rachel A. Burton, and Philip J van Eyk
Energy & Fuels (2019) doi:10.1021/acs.energyfuels.9b02931.

III) Biochemical Compositional Analysis and Kinetic Modelling of Hydrothermal Carbonisation of Hemp

Benjamin G Keiller, Matthew Potter, Rachel A. Burton, and Philip J van Eyk

IV) Biochemical Compositional Analysis and Kinetic Modelling of Hydrothermal Carbonisation of Macroalgae

Benjamin G Keiller, Phoebe Chilman, Rocky de Nys, Rachel A. Burton, and Philip J van Eyk

Chapter 1

Introduction

1.0 Background

Human-induced climate change is accelerating at a time when conventional energy sources are becoming scarcer and more politically contentious. Without a rapid transition to renewable, low-carbon sources of energy, while simultaneously developing means of sequestering carbon from the atmosphere and boosting agricultural productivity in a volatile environment, modern industrial civilization faces an almost existential threat by the end of the century¹⁻³. The imperative to develop new energy sources is undeniable, yet sourcing such an immense amount of energy (up to 17.8 billion tonnes of oil equivalent per annum by 2040⁴) that is cheap, clean, and readily available across the globe is a formidable challenge. Plant biomass, the organic material produced from the photosynthetic growth of plants, offers one potential opportunity for meeting this challenge. By fixing the energy of the sun into chemical energy, and then using this energy to construct their bodies in the form of sugars and other organic molecules, plants generate an astonishing quantity of biomass across the world each year, with an estimated 100 billion tonnes of land biomass and 50 billion tonnes of aquatic biomass produced every year⁵. Such abundance makes plant biomass a strong contender as a bedrock to replace fossil fuels based on availability alone, if nothing else.

However, there are numerous drawbacks to using raw biomass as an energy source, not least of which is the high water content, which necessitates lengthy, energy-intensive predrying. Dry biomass is typically only suitable as a solid fuel, and cannot replace the various petroleum fuels such as petrol, diesel, naphtha, gasoline and so on. Biomass is also less thermally dense than fossil fuels, meaning that greater masses must be combusted to deliver the same energy output, and it also tends to have high levels of inorganics, which leads to the formation of ash^{6,7}. Thus, biomass must be processed in order to convert it to a more suitable fuel. Thermochemical treatments, such as torrefaction and pyrolysis, expose a feedstock to high temperatures under anoxic conditions, whereupon the feedstock is converted into an energy-rich char at lower temperatures, a liquid product at medium temperatures, or gaseous products at high temperatures⁸. These products, in terms of composition and energy content, are very similar to fossil coal, oil and natural gas, and can be used as sustainable, low-carbon replacements for these fossil fuels in most applications. While relatively simple and cheap, air-based technologies such as pyrolysis are limited in that for very wet feedstocks, such as fresh

biomass, the high water content leads to excessive drying requirements, and they also tend to concentrate the levels inorganic elements, exacerbating ash-related issues. These issues can however be alleviated by treating the feedstocks in water, instead of air, in a process called hydrothermal conversion. Due to the conversion taking place water, there is no need to predry the feedstock, and it also allows for the ash to be dissolved out of the solid phase into the surrounding water. In addition, the aqueous medium allows for the formation of an aqueous product that is rich in nitrogen, phosphorous and valuable organic chemicals, creating additional value chains as liquid fertilisers and a source for precursor compounds for the chemical industry. Under mild temperatures, between 180 °C and 260 °C, Hydrothermal Carbonisation (HTC) takes place, and yields a solid char as its primary product. This char, or “hydrochar”, can be used as an energy-dense, low-ash solid fuel, as a soil amendment for sustainable agriculture, or buried as a means of sequestering carbon. The tremendous versatility of hydrothermal conversion makes it a highly promising technology, and it has the potential to revolutionise energy production, agriculture and sustainable civilization if it can be applied to high-growth, low-impact biomasses at industrial scales.

Presented in this thesis is a study of the hydrothermal carbonisation of novel biomasses and the reactions that take place therein.

1.1 Scope, Structure and Summary of Thesis

The major scope of this thesis is two-fold. In the first instance, the suitability of novel biomass sources that are fast growing, environmentally friendly, and potentially economically productive as HTC feedstocks for fuel purposes is investigated. Important factors in this context include hydrochar yield, energy content, and ash properties. In the second instance, the underlying mechanisms that drive the hydrothermal conversion of biomass to hydrochar are studied. Key aspects of the HTC reaction remain unknown, not least of which is the manner in which the major biochemical constituents are degraded within whole biomass. Without knowing this, it is not possible to obtain the mechanistic and kinetic understanding necessary to build industrial scale reactors. The sheer complexity of whole biomass HTC, with all the interconnected reactions and products and side products contained within, makes studying whole biomass reaction kinetics very difficult. A common means of getting around

this is to use idealised, purified model compounds that simulate each component individually. However, these model compound experiments cannot capture the effect of the various cross-linkages and interactions present throughout the biomass structure, nor the overall chemical environment. The major breakthrough presented in this thesis is the development of biochemical assays that are capable of measuring the breakdown of the key macromolecules hemicellulose, cellulose, lignin and protein, both within untreated biomass and hydrochar. Using these, is it possible to measure in detail the breakdown of the biochemical macromolecules in their natural state as a function of time, something which has not been achieved before. From this, simple kinetic models were developed to describe the degradations of these components, and using the insights gathered from fitting these models, a mechanistic model of the degradation step of the HTC reaction was built. This process was applied to three biomasses: Australian saltbush, hemp and macroalgae.

These biomasses were chosen because they all possess the ability to grow on marginal land, while still maintaining a high growth rate on said marginal land. The ability to grow biomass for non-food processes purposes on marginal land is considered essential, because this mitigates any competition with food crops for land and water. Macroalgae in particular can be grown in vats on arid land, thereby completely avoiding the use of fertile soil, or even fresh water in the case of marine algae. Additionally each of these biomasses also has numerous other uses beyond biofuels, such as grazing fodder for saltbush, textiles, bioplastics, foodstuffs and others for hemp, and nutraceuticals, food additives, medical dressings and others for macroalgae. As such, HTC can act as an embedded component within a broader-scale adoption of each of these novel biomasses, creating a richer and more diversified bioeconomy. Further justifications for each biomass are detail below.

The overall structure and summarisation of the thesis is as follows. After a review of the state-of-the-art of hydrothermal carbonisation as it stands at the time of publication (Chapter 2), this project begins with the analysis of Australian Saltbush as a potential feedstock for HTC. Saltbush is a group of arid and semi-arid dwelling plants that are native to a broad area of the Australian Outback, and are notable for their high salt-tolerance. In a time when drought and soil salinity are serious concerns for Australian farmers in the drylands, saltbush is growing in

prominence and popularity due to its ability to remediate salt-stricken soils, and also sustain sheep in areas where other forage is unavailable due to a lack of water. On account of its hardiness, native status, high growth rate under appropriate conditions, and numerous human applications, saltbush was chosen as a potential HTC feedstock specifically for arid areas. The study of saltbush HTC is divided into two parts, an analysis of the combustion properties of the hydrochar (Chapter 3, Paper I), and an investigation of the breakdown of the key lignocellulosic constituents (Chapter 4, Paper II).

In the combustion study, saltbush was subjected to HTC under 3 temperatures (200 °C, 230 °C and 260 °C) and four reaction times (0 min, 15 min, 30 min, and 60 min), whereupon it was found to have hydrochar yields of between 66% after an hour at 200 °C, and 35% after an hour at 260 °C, comparable to similar woody biomasses. The hydrochars demonstrated significantly different elemental compositions compared to the untreated feedstock, with increased carbon content accompanied by much reduced oxygen content, especially at higher reaction severities. These elemental changes produced hydrochars with very similar chemical properties to fossil lignite, and had correspondingly similar higher heating values (HHV), with the hydrochars borne of the highest reaction severities boasting HHVs of up to 35 MJ kg⁻¹, well within or even slightly exceeding the range observed in brown coal (24 – 30 MJ kg⁻¹)⁹. Because of the tendency of saltbush to sequester salt within itself, this biomass had a higher ash content than other woody biomasses, so this was another key focus of this first study. Total ash content fell precipitously over the course of the HTC reaction, with almost 80% of the total ash removed after one hour at 260 °C. On an individual element basis, sodium, potassium, and sulphur were consistently and rapidly removed across all reaction temperatures and times. Calcium was more or less inert at 200 °C and 230 °C, but was also removed at 260 °C, while the behaviour of phosphorus is rather complex, falling rapidly at 200 °C and 230 °C in line with sodium and potassium, yet is reabsorbed at 260 °C. With so many similarities and lower ash content compared to fossil coal, saltbush hydrochars show a great deal of promise as a potential solid fuel.

The second saltbush study shifted focus to understanding the underlying mechanics and kinetics of the degradation of the biomass. Using the same chars produced for the combustion

study, the biochemical compositions of the untreated saltbush and hydrochars were analysed to measure the amount of hemicellulose, cellulose, lignin and protein, and how these change over the course of the HTC reaction. Using this information, mechanistic and kinetic models were built to describe this breakdown. It was found that hemicellulose reacted extremely quickly, being completely removed from the hydrochar within minutes at any temperature in a first-order reaction ($E_a = 33 \text{ kJ mol}^{-1}$), while cellulose was more resistant, and degraded in a 0.5th-order reaction ($E_a = 127 \text{ kJ mol}^{-1}$). Lignin was found to be partially susceptible to hydrothermal degradation, with 78% degrading rapidly in a first order reaction, and the remaining 22% being completely inert under the conditions tested. The portion that did react had almost identical kinetic parameters as hemicellulose ($E_a = 32 \text{ kJ mol}^{-1}$), suggesting that the two seemingly very different macromolecules share similar mechanisms. This was very surprising, and contrary to large portions of the literature, as it is commonly (but not universally) held that lignin is highly resistant to hydrothermal carbonisation, or even entirely inert. This study, and the biochemical assays and kinetic methods introduced in it, formed the foundation for Chapters 5 and 6, both of which were extensions of the saltbush work into different feedstocks.

In Chapter 5 (Paper III), the hydrothermal carbonisation of hemp was investigated. Hemp for industrial purposes is rapidly growing as more and more governments across the world decriminalise its usage, and as a result hemp products in food, textiles, plastics, fertilisers and myriad other applications aside are burgeoning. It can therefore be anticipated that a large amount of waste biomass will be generated, which could potentially be value-recovered through the use of HTC. Thus, hemp stem residue and seed hulls were subjected the HTC at three temperatures (200 °C, 230 °C and 260 °C) and four reaction times (0 min, 15 min, 30 min, and 60 min), and compared to saltbush. It was found that on the whole, both hemp residues behaved very similarly to saltbush, with a near identical range hydrochar yields of between 70% and 31% after an hour at 200 °C and 260 °C respectively. Both residues revealed similar patterns of carbon enrichment, oxygen loss, increase in HHV (with both residues rising to lignite values), and removal of ash as shown in the saltbush study, demonstrating the versatility of HTC. On a biochemical level, however, there were a few notable differences between saltbush and the hemp residues. The portion of inert lignin differed between the two tissues, with hulls having an HTC-stable portion of 31%, while determining the inert portion of stem lignin was

more opaque than the other biomasses. So, two separate kinetic models were built, one assuming a lower value of 21% inert, and the other an upper boundary of 34%. The 34% inert model degraded in a first order reaction, same as the hull lignin, although the stem lignin had a much higher activation energy than the saltbush lignin, while the hull lignin had a much lower one ($E_a^{\text{Stem}} = 98 \text{ kJ mol}^{-1}$, $E_a^{\text{Hull}} = 22 \text{ kJ mol}^{-1}$). If the stem inert portion was assumed to be 21%, however, the best fitting model was a second order reaction with a slightly lower activation energy to the 34% model ($E_a = 81 \text{ kJ mol}^{-1}$) but with much lower reaction rate constants. Hemicellulose in both hemp tissues degraded with 1.3rd order reactions, with higher activation energies than in saltbush ($E_a^{\text{Stem}} = 58 \text{ kJ mol}^{-1}$, $E_a^{\text{Hull}} = 67 \text{ kJ mol}^{-1}$), while stem cellulose underwent a first order reaction ($E_a = 113 \text{ kJ mol}^{-1}$) and hull cellulose underwent a 1.5th order reaction ($E_a = 112 \text{ kJ mol}^{-1}$). These differences between similar lignocellulosic feedstocks, even between different kinds of tissue of the same species, highlight that the general assumptions about the behaviour of a given macromolecule as held by the HTC literature cannot be relied upon universally in whole biomass.

With hemp and saltbush being terrestrial lignocellulosic biomasses, the scope of the study was expanded in Chapter 6 (Paper IV) to include macroalgae. As aquatic plants, macroalgae exhibit numerous key differences to terrestrial plants, most notable of which is the lack of lignin. Marine macroalgae (seaweeds) have been used by humans for millennia, and have in recent times been the subject of considerable interest for its bioactivity, high growth rates and ability to be cultivated in vats on marginal land. The notable differences between aquatic plants and terrestrial lignocellulosic plants also make it an interesting comparison case for the investigation of HTC mechanics. Two species of macroalgae, the freshwater *Oedogonium intermedium* and the saltwater *Ulva ohnoi*, were subjected to HTC at three reaction temperatures (200 °C, 220 °C, and 240 °C) and five retention times (0 min, 5 min, 15 min, 30 min, and 60 min). The reaction temperatures for macroalgae were lower than for terrestrial plants due to the fact that it was observed in previous research that algae was highly susceptible to HTC, and resulted in very low mass yields at 260 °C¹⁰. It was found that hydrochar yields for *Oedogonium* were consistently higher than for *Ulva* for any temperature or time. As with the terrestrial biomasses, the hydrochars showed an increase in energy content comparable with that of coal, with the concomitant changes in carbon and oxygen content. *Ulva*, being a

saltwater seaweed, presented the highest ash content of any biomass examined in the study (25% w/w), but even that was reduced by 95% after 60 minutes at 200 °C. Interestingly, under high reaction severities, *Ulva* hydrochars began to reabsorb inorganics, potentially in a similar manner to that observed for phosphorus in saltbush. As with the other feedstocks, hemicellulose degraded extremely rapidly, with a first order reaction in both species ($E_a^{Ulva} = 136 \text{ kJ mol}^{-1}$, $E_a^{Oedogonium} = 115 \text{ kJ mol}^{-1}$), while cellulose degraded more slowly. Surprisingly, macroalgal cellulose degrades with different mechanisms between the two species; *Oedogonium* cellulose degraded via a simple first order reaction ($E_a = 130 \text{ kJ mol}^{-1}$), while *Ulva* cellulose appeared to degrade in two parallel first order reactions, one fast and the other slow ($E_a^{Fast} = 148 \text{ kJ mol}^{-1}$, $E_a^{Slow} = 112 \text{ kJ mol}^{-1}$). Protein was suspected to undergo Maillard reactions, and as such was difficult to model, but may undergo a similar parallel mechanism in both species, with *Ulva* ($E_a^{Fast} = 88 \text{ kJ mol}^{-1}$, $E_a^{Slow} = 74 \text{ kJ mol}^{-1}$) degrading faster on the whole than *Oedogonium* ($E_a^{Fast} = 148 \text{ kJ mol}^{-1}$, $E_a^{Slow} = 112 \text{ kJ mol}^{-1}$). The notably different behaviour of the *Ulva* cellulose compared to that of every other biomass studied here, and the complex behaviour of the macroalgae protein illustrate vividly the profound variances in the responses different feedstocks have to hydrothermal conversion, even if the overall properties of the resultant hydrochars are similar.

Overall, the work presented in this thesis describes the biochemical changes that occur in the hydrothermal carbonisation of a variety of biomasses in more detail than has been possible to date. In doing so, the behaviours of key biochemical compounds have been demonstrated to be more complex than previously realised, in manners which are impossible to elucidate in idealised feedstock experiments. These findings strongly underline the need for whole biomass HTC compositional studies, and it is hoped that the methodologies, data, and techniques presented here can be used as a foundation for further in-depth studies into the kinetics and mechanisms of biomass HTC. With the knowledge gained from a molecular-level understanding of the HTC reaction, it may be possible to one day realise the wide-scale adoption of advanced thermochemical biofuels.

Chapter 2

Literature Review

2.0 Introduction to Biofuels

It is projected that by 2040, global energy needs will increase by around a third, with the renewable energy industry the fastest growing sector at 7.1% per annum, and accounting for 40% of all new energy sources⁴. Renewable, low-carbon fuels derived from biomass, or “biofuels”, offer a means of replacing fossil fuels in situations where a transportable, combustible energy source is required, for example in internal combustion engines.

Because the carbon contained within biofuels ultimately comes from atmospheric CO₂ fixed via photosynthesis, biofuels have the potential to be a near limitless, carbon-neutral fuel source, and this has prompted much interest in their wider adoption; as of 2016 there are 64 countries and numerous states and territories within countries that now have biofuel mandates and targets¹¹. These typically come in the form of low blending requirements of petrol with bioethanol (often $\leq 10\%$ ethanol/petrol), which is almost always produced via the fermentation of crops such as corn and sugarcane. As a result, ethanol production in the US surged from 6.5 million gallons in 2007 to over 16 million gallons in 2018, accounting for 56% of global fuel ethanol production¹². However, recently the uptake of biofuels in developed markets has slowed dramatically over the past 8 years, with the US exhibiting a projected growth from 2019-2024 of just 1%, and the EU just 0.5%¹³. This is in large portion due to the negative reputation of so-called “first generation biofuels” that are produced from edible crops. There have been numerous controversies over the fears of first generation biofuels competing directly with edible crops and the natural environment for space and water, potentially causing spikes in global food prices¹⁴⁻²⁰, and causing significant issues with deforestation and releases of carbon emissions as more land is converted to grow food crops²¹⁻²³. In addition, the utility of ethanol as a fuel is restricted to light internal combustion engines, and even there has limitations; ethanol blends have a lower energy content than petrol or diesel and tend to have an adverse effect on engine performance²⁴. It is completely unsuitable for applications that require high levels of thermal output, and does nothing to replace the various petroproducts that are derived from crude oil, such as plastics, chemicals, adhesives, paints and so on.

There is therefore a great need for a technology that is capable of leveraging the immense potential of biomass as an unlimited, sustainable energy source that can fit seamlessly into current energy and chemical infrastructure.

2.1 Hydrothermal Biofuels

A highly promising biofuel technology is hydrothermal conversion, wherein biomass is subjected to high-temperature, high-pressure water within the ranges of 180 °C – 374 °C, and 4 – 22 MPa, in an oxygen-free environment^{25–27}. Such conditions, being higher than the atmospheric boiling point of 100 °C yet lower than the critical point of water (374 °C, 22 MPa) endow this “subcritical water” with numerous properties that make it extremely useful for the biofuels engineer. As the temperature of subcritical water rises, so does the ionic product of water (K_w) that describes the dissociation of water into the ions H_3O^+ and OH^- , as shown in Equation 1²⁸.



Thus, under subcritical conditions there is a greater profusion of hydronium and hydroxide ions than at room temperature, and this allows water to become a highly effective medium for acid and base catalysed reactions. The viscosity of water also decreases under subcritical conditions, and continues to decrease as temperatures are raised, eventually approaching the viscosity of water vapour near the critical point²⁸. This has the effect of raising the diffusion coefficient, which in turn boosts the rate of reaction²⁹. But among the most interesting of properties subcritical water gains is the ability to become a reactant in and of itself, becoming involved in self-catalysed hydrolysis reactions^{27,30}. These properties, combined with the high reaction temperatures, allow water to auto-catalyse a great variety of different reactions in biomass, including hydrolysis, decarboxylation, polymerisation, aromatisation, and many others^{25–27,31}. Biomass thus exposed to subcritical water thereby rapidly decomposes in conditions that approximate those present deep beneath the Earth’s surface during the conversion process that generated fossil fuels from primordial wood and algae hundreds of millions of years ago, meaning that the solid, liquid and gaseous products of this decomposition possess very similar physical, thermal, and chemical properties to fossil coal, oil and natural

gas^{25–27,32}. The extraordinary promise of such “hydrothermal biofuels” is that they potentially offer a renewable, low- or even zero-net carbon replacement for conventional fossil fuels that can simply “drop in” to existing infrastructure and usage.

2.1.1 Hydrothermal Carbonisation

Hydrothermal Carbonisation (HTC) is the hydrothermal process which occurs at temperatures between 180 °C and 260 °C, the main product of which is a solid, black, porous char, called “hydrochar”. HTC was developed in 1913 as a potential method of energetically upgrading lignite and peat³³, but has received great attention in recent decades due to the potential of hydrochar as a possible renewable replacement for coal. Numerous studies have demonstrated that one of the principle effects of HTC is to thermally and chemically upgrade biomass^{25,31,32,34}, which is in and of itself a poor quality solid fuel, owing to high moisture and ash content, and low higher heating value (HHV) compared to other solid fuels like charcoal and coke. Further, fresh untreated biomass has a limited storage life, as it tends to be subject to microbial decomposition and degradation over time, often leading to health and safety concerns. Biomass is therefore frequently dried before storage, but this is highly energy intensive, and due to the hygroscopic nature of biomass, it tends to reabsorb water from the surrounding air^{35,36}. HTC alleviates this problem by converting the biomass to a hydrophobic, biologically inert char that can be easily dried, ground and pelleted for ease of storage, transportation, and combustion³⁷. The hydrophobic nature of the hydrochar has further benefits, in that it makes it far easier to separate from the aqueous reaction medium, and also reduces the energy and time requirements to dry the nascent hydrochar post-reaction³⁸. The principle benefit of HTC, however, is the ability to boost the typically low HHV of biomass to levels where it is competitive with fossil coal. Upon combustion, untreated biomass releases on the order of 15 – 20 MJ kg⁻¹ of energy⁶, which is lower than the range of values seen for higher-grade lignite (22 – 27 MJ kg⁻¹)⁹. Many studies over the decades have demonstrated that for a wide range of feedstocks including wood, bamboo, municipal solid waste, olive stones, sewerage sludge, biosolids, poultry litter, seaweed, and many others, the HHV of the feedstock is raised after hydrothermal treatment, frequently to levels that are comparable with lignite^{37,39–44}. Such a rise in the HHV dramatically raises the thermal utility of the hydrochars, making

them a far more useful solid fuel than the untreated feedstocks they were produced from, possibly even allowing hydrochar to replace coal in thermal applications.

In addition to the obvious thermal applications, hydrochars may also be able to fulfill other applications. The highly carbonaceous nature of hydrochar renders it chemically and biologically inert, thereby making it potentially useful for long-term carbon sequestration⁴⁵⁻⁴⁷. There is some evidence that applying hydrochar to soil for such sequestration purposes also has additional effects in raising soil fertility and water retention, as in *terra pietra*⁴⁸⁻⁵⁰. The high porosity of hydrochars makes them valuable as activated carbons⁵¹⁻⁵³, which can be used in such diverse applications as CO₂ capture⁵⁴, dye absorption⁵⁵, supercapacitors^{56,57} and others⁵². The HTC reaction also produces numerous water-soluble compounds such as 5-HMF, acetic acid, levulinic acid, glycolic acid, formic acid etc., all of which are very valuable as precursor compounds in the chemical industry^{58,59}.

The versatility of HTC is belied by its simplicity and efficiency. Water has a very high heat capacity, which is the energy required to raise the temperature of a given amount of water by a given degree. At $75.5 \text{ J (mol}\cdot\text{K)}^{-1}$ at $25 \text{ }^\circ\text{C}$ ⁶⁰, this is higher than many other common liquids, such as ethanol and acetic acid⁶¹. It also has a comparatively high enthalpy of vapourisation ($40.65 \text{ kJ mol}^{-1}$)⁶⁰, the energy required to convert the liquid water into gas at the boiling point. Because HTC occurs under pressure equal to or above the vapour pressure of water, even at highly elevated temperatures, the water never boils, and thus the enthalpy of vapourisation is avoided. As a result of this, it requires less energy to heat a mole of pressurised, liquid water to $260 \text{ }^\circ\text{C}$ from $25 \text{ }^\circ\text{C}$ (17 kJ mol^{-1}) than it does to boil the same volume of water at $100 \text{ }^\circ\text{C}$ (40 kJ mol^{-1}). Additionally, there is evidence that the carbonisation reaction is exothermic, and begins spontaneously at temperatures above $180 \text{ }^\circ\text{C}$ ²⁵. Thus, once the reaction has begun, it is not necessary to continuously add energy to the system, making the carbonisation process more energy efficient than one might expect. If the energy to heat the water can be sourced renewably, such as in a solar-thermal plant, then HTC potentially represents a carbon-neutral or even carbon-negative method of producing biofuels, as the only carbon emissions released across the process are during the combustion of the fuel, which originally came from the CO₂ absorbed by the biomass in the first place.

HTC and related technologies such as hydrothermal liquifaction have the potential to completely revolutionise the global economy, and yet there is still much that remains unknown. In particular, the incredibly complex mechanism by which biomass is converted to hydrochar, and the kinetics thereof, are very difficult to elucidate. This is in large part due to the highly heterogenous nature of biomass, which is a rich mixture of various compounds and structures, each of which have been shown to behave in HTC in differing manners. A closer investigation of the primary components of biomass is required before any holistic kinetic and mechanistic understanding of the HTC process can be attained.

2.2 Composition of biomass

Biomass is a broad term encompassing almost any kind of organic material, yet the most commonly utilised type of biomass is plant-based. Plant cells develop an encompassing cell wall composed of a variety of complex biopolymers, including long polysaccharides (cellulose and hemicellulose), proteins and in the case of terrestrial plants, disordered aromatic polymers (lignin). The cell-wall composites of terrestrial plants are thus called “lignocellulose”. These biopolymers are covalently networked together into an insoluble, rigid and robust hetero-matrix (Figure 1), which plants use as a structural support against osmotic pressure within the cell and also against the force of gravity, allowing plants to grow vertically to great heights⁶².

2.2.1 Cellulose

Of the major components of the cell wall, cellulose is by far the most abundant, making up 35% – 50% of a plant's dry mass⁶³. Indeed, by some estimates, cellulose is the most abundant biopolymer in the world, with over 10^{11} tonnes produced annually⁶⁴, and is found in plants, algae and some animals⁶³. Cellulose is composed of long strands of between 8000 and 15,000 D-glucose molecules linked via β -(1→4) glycosidic bonds, which then stack upon one another via Van der Waals forces and intermolecular hydrogen bonds between the adjacent chains into a highly regular matrix^{64,65}. Repeated stacking leads to the creation of long insoluble microfibrils that form the backbone of the plant cell wall, and provide the basis of the structural strength of lignocellulose.

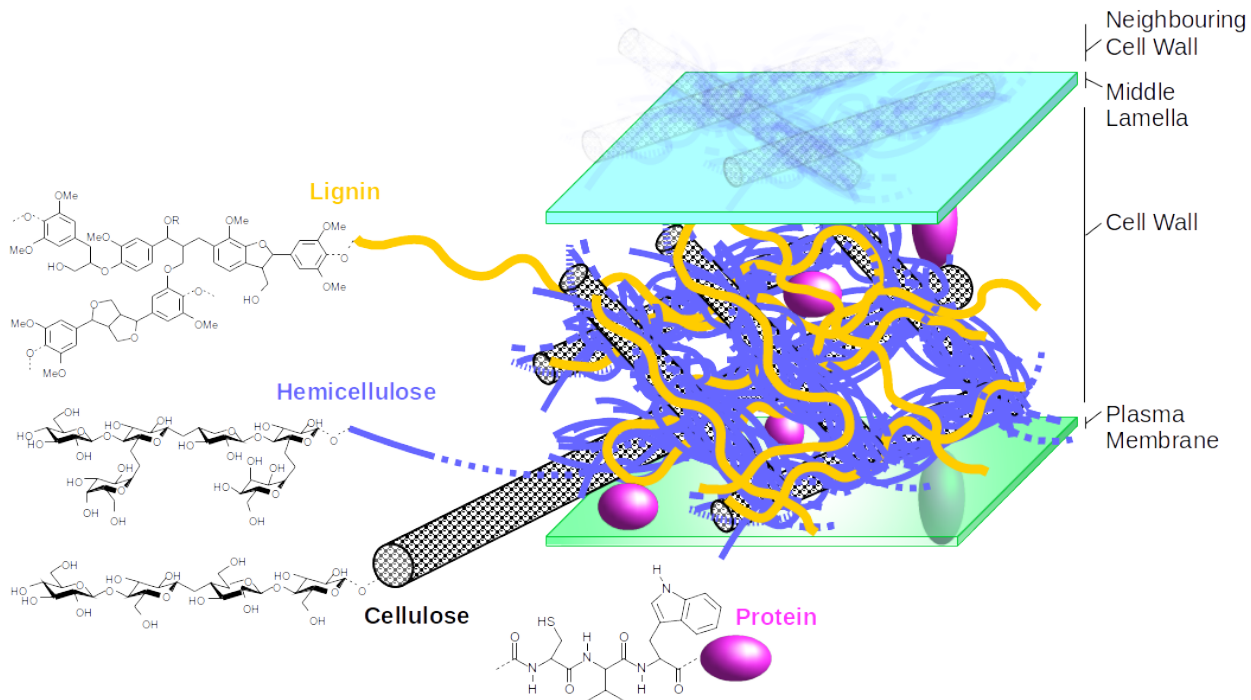


Figure 1: Overview of the structure of lignocellulose in a terrestrial plant cell wall. Algae typically lack lignin.

2.2.2 Hemicellulose

In addition to the very highly regular, crystalline cellulose, there is a great abundance of non-crystalline, heterogenous polysaccharides that entwine and enmesh the cellulose fibrils, historically described with the catch-all term hemicellulose. Hemicellulose typically makes up between 20 – 25% of a plant's dry weight⁶³, and the polysaccharide chains are generally shorter and more structurally complex than cellulose. Hemicellulose monosaccharides are bound to one another with β -(1 \rightarrow 4) or β -(1 \rightarrow 3) glycosidic bonds, forming branched and unbranched strands composed of a variety of different sugar monomers including hexoses, pentoses and sugar acids⁶⁶. The types and sugar composition of hemicelluloses vary considerably between species^{66,67}, with xylans being the most widespread, featuring heavily in hardwoods (glucuronoxylan), cereals (arabinoxylans) and grasses (glucuronoarabinoxylans)⁶⁸, whilst glucomannans are present in high quantities in softwoods^{66,68}. Aquatic plants such as macroalgae have a variety of unique monosaccharides that are not present in terrestrial plants, such as agarose, gluconic acid, uronic acid and mannuronic acid⁶⁹. Through this heterogeneity,

hemicelluloses can perform many functions within the plant cell, including structural reinforcement of the cell wall, energy storage, and also acting as signaling molecules⁷⁰.

2.2.3 Lignin

Lignin, in contrast to the aforementioned polysaccharides is not sugar-based; instead, it is a complex, disordered three-dimensional polymer built from phenolic alcohols called monolignols^{71,72}. It is present in particularly high quantities in the secondary cell wall, where it fills the space between hemicellulose and cellulose, and performs an adhesive role within the lignocellulosic hetero-matrix. It typically makes up 5 – 30% of a plant's dry mass⁶³, provides added strength and support, and is also highly insoluble, waterproofing the plant, and helping to ward off microbial attack^{62,73}. There are three main phenolpropane monolignols, each differentiated by the degree of methoxylation: *p*-coumeryl, coniferyl and sinapyl alcohol⁷². Upon being synthesised, the monolignols are transported to the plant cell wall, and then radicalised with a peroxidase. These radicals then conjoin via a highly complex, chaotic and much debated series of radical coupling and nucleophilic H₂O reactions to form a highly irregular, amorphous aromatic polymer. There is great diversity in the linkages between lignin monomers, including β -O-4 and β -O-5 ether bonds and carbon-carbon β - β and β -5 bonds⁷². This high degree of covalent cross-linking confers on lignin its strength, and while this is of great utility to the plant, it presents numerous issues for human applications of lignified tissues, such as paper-making or biofuel production.

2.2.4 Protein

Proteins are differentiated from the aforementioned biochemical components in being made of L- α -amino acids, which comprise of an amine, a carboxylic acid, and a variable side group. The amino acids are bound together via a peptide bond, while the combinations of different side residues and the intra- and intermolecular interactions thereof comport the protein into innumerable different shapes and sizes, allowing them to perform a vast array of different functions within the cell. Proteins make up only a very small portion of lignocellulosic biomass, generally between 1% – 11% for straws, woods, grasses and grains, but can make up a much larger proportion of algae, ranging from 6% – 71%⁷⁴⁻⁷⁶. Because of the

nitrogen of the amine group, as well as the nitrogen contained within such residues as arginine, histidine and lysine, biomasses with a high protein content correspondingly have a high nitrogen content, and this has consequences in a combustion context, as it results in the production of NO_x pollutants^{77,78}.

2.2.5 Ash

In addition to the organic biochemical components explored above, there is also a portion of inorganic elements contained within the biomass. The inorganic content varies across different forms of biomass, with typical mean values ranging around 3.6%, 4.8% and 8.6% for wood, grasses and straws respectively⁷⁹. Agricultural waste, such as rice hulls, sugarcane bagasse, grape marc and so on, can have greatly elevated inorganic contents, sometimes up to 20%^{6,79}, while certain kinds of marine algae can have ash contents of up to 36.6%⁸⁰. The inorganic content of biomass has particular relevance for fuel applications, as it is incombustible, and therefore remains after burning as ash. Ash in a combustion furnace or boiler melts and is deposited on the sides of the furnace (slagging), or is entrained away from the heat of the furnace and eventually condenses on the cooler convection surfaces (fouling)⁸¹. Slagging and fouling are significant operational issues that can lead to costly furnace downtime and repairs, and therefore means of reducing the ash content of a given feedstock is of great interest.

The different morphological structures of each of these components means that in the hydrothermal medium, each of these will respond in a different manner. Certain chemical bonds, such as the glycosidic linkages that bind the sugar monomers of the polysaccharides, are highly susceptible to hydrothermal degradation, while others, such as the carbon-carbon cross linkages of lignin, are not^{25,26,82}. The macromolecular habit of the component can be of tremendous influence on reactivity, with the highly crystalline cellulose capable of resisting hydrothermal degradation at temperatures up to 307 °C²⁶, while the non-crystalline xylose begins to dissolve at 180 °C⁸², despite both polysaccharides having the β-(1→4) bond as their primary linkage. The mechanisms of these reactions are as multifaceted as the components themselves, and any attempt at elucidating the fine detail of the HTC reaction would rely heavily on understanding the underlying mechanics.

2.3 Mechanism of HTC

Hydrothermal carbonisation yields three different kinds of products: solid, liquid and gaseous. During the HTC treatment of biomass, the reactions that yield each of these three products are almost fractally complex. With so many different macromolecules reacting together, determining the underlying mechanisms of HTC becomes very difficult. Nonetheless, there have been several proposed mechanisms that attempt to describe the conversion of the initial feedstock to the various products. Jazwauck and Schempe⁸³ offered a simple three-step mechanism that involved an initial degradation of the solid substrate into dissolved intermediates, which in turn either became the solid hydrochar, or gaseous and dissolved byproducts (Figure 2).

More detailed mechanistic models stem from the observation that the hydrochar is itself comprised of two different varieties of char: primary char, which consists of the unreacted remainder of the feedstock (which may be subject to solid-solid reactions), and secondary char, which manifests as carbonaceous nanospheres⁸⁴. In sections of the literature, primary and secondary char may be referred to as “char” and “coke” respectively^{85,86}. The primary char is the remainder of the initial feedstock that did not dissolve into the hydrothermal medium. It has been observed that under even very harsh conditions, such as hydrothermal gasification conditions of 600 °C for 1 hour, a small portion of the original feedstock remains, albeit showing signs of thermal conversion, such as softening and melting⁸⁵. Other kinds of conversion of the undissolved feedstock are the phase changes that lignin undergoes at elevated temperatures under acidic conditions. At 150 °C in a mildly acidic medium, lignin was observed in maize to dissociate and coalesce and then migrate through the plant cell wall for some distance due to diffusion and thermal expansion, before eventually extruding out onto the surface of the biomass in small droplets⁸⁷. The coalescence and migration of lignin under elevated temperatures (80 – 193 °C) is associated with a shift to a glassy transition stage wherein the cross-linkages within lignin are broken, and the lignin superstructure is converted into an amorphous solid. Thus emancipated, the amorphous lignin can then undergo a rubbery flow which allows it to pass through and escape from the cell wall⁸⁸.

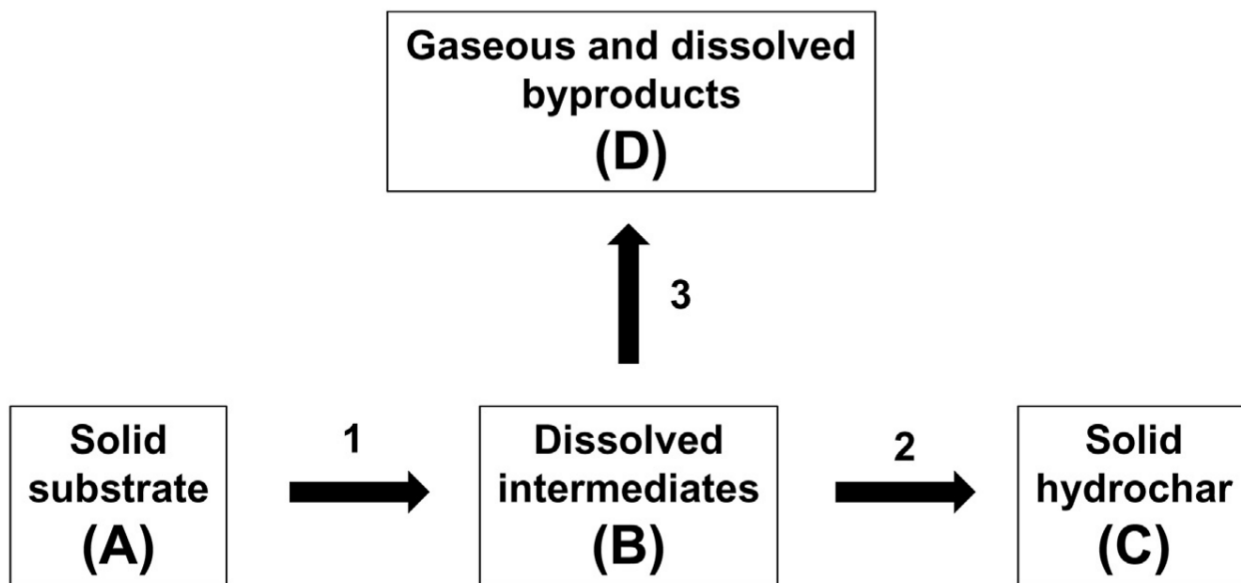


Figure 2: Three-pathway mechanism proposed by Jatzwauk and Schempe 2015⁸³

The primary char is frequently observed, across temperatures ranging from 180 °C to 600 °C^{82,85}, as being covered across its surface with small, regularly shaped carbon spheres. These nanospheres consist of a hydrophobic, aromatic core surrounded by a hydrophilic shell featuring a high concentration of oxygenated functional groups, including hydroxyl groups, phenolics, carbonyls and carboxylic acids⁸⁹. The core is constructed of a superstructure of interconnected polyfuranic rings, originating from the polymerisation of 5-hydroxymethyl furfural (5-HMF), in turn derived from the successive dehydration of free sugars liberated from the digested biomass^{27,34,82,89}. Thus, a dual-pathway mechanistic model has been proposed, with primary char being formed from a single-step solid-solid conversion, and secondary char formed from a two-step reaction involving the degradation of biomass into soluble intermediaries that then repolymerise (Figure 3)^{85,86}. Despite these two pathways being seemingly very distinct, they are in fact closely inter-connected, and readily influence each other.

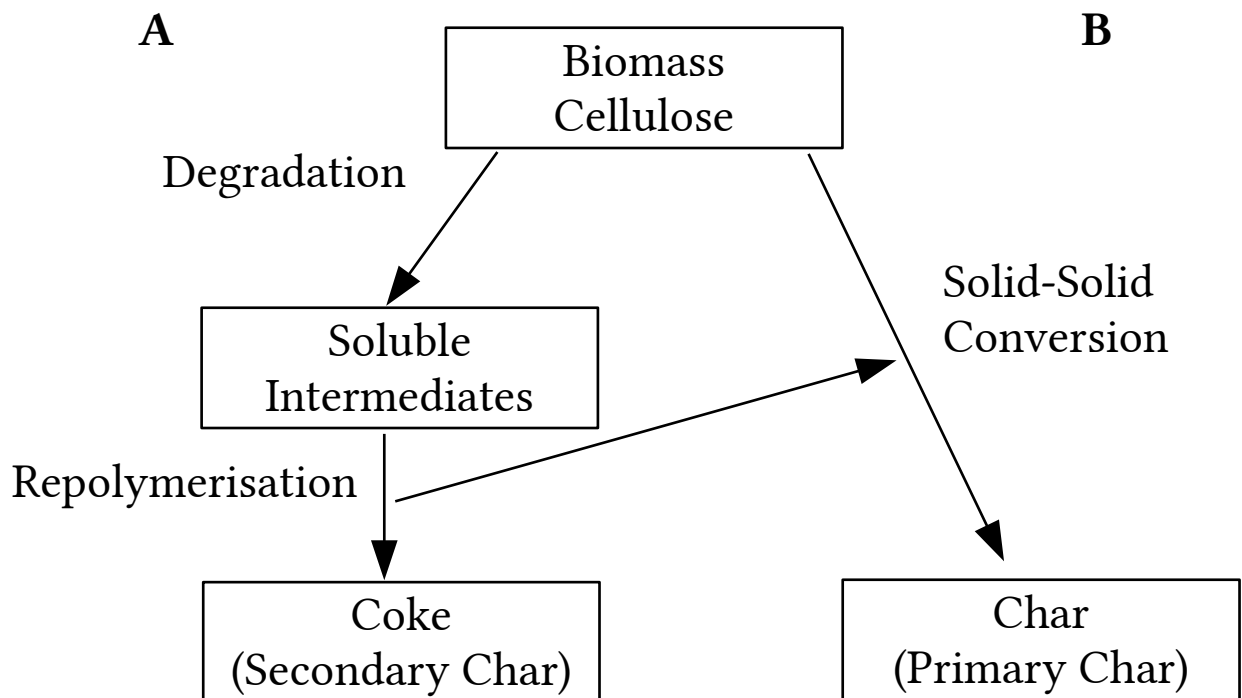


Figure 3: Twin-pathway model of HTC proposed by Karayıldırım et al. 2008 and Dinjus et al. 2011^{85,86}

2.3.1 Degradation Reactions

The main degradation reactions that lead to the formation of soluble intermediates include hydrolysis, decarboxylation, and dehydration. Hydrolysis is the addition of water which results in the cleavage of bonds, especially ester and ether bonds (Figure 4)⁹⁰. Hydrolysis is one of the most important reactions in HTC, being responsible for the rapid digestion of glycosidic linkages between sugar monomers within carbohydrates (beginning at 180 °C for hemicellulose, 200 °C for cellulose), and the ether bonds within lignin (beginning at 200 °C)²⁵. In whole biomass (sugarcane bagasse), as part of a shrinking cylindrical model, it has been found that hydrolysis occurs along the inner surface of pores in the biomass particle, with hydrolytic conversion being completed after 5 minutes at 270 °C⁹¹. Because the products of the hydrolysis of ester bonds are alcohols and carboxylic acids, hydrolysis is an important precursor step to subsequent dehydration (requires alcohol) and decarboxylation (requires carboxylic acid) reactions. This cascading effect gives birth to complex reaction chains even with simple feedstocks; the HTC of D-glucose alone is modelled to involve 8-9 steps and produces at least 21 products and side products (>1% yield)⁹².

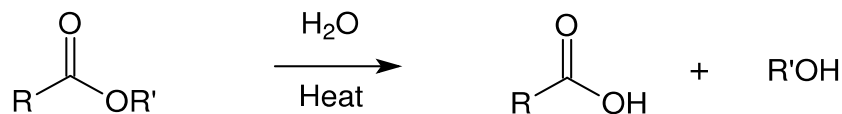


Figure 4: Hydrolysis of an ester bond

Decarboxylation is the removal of CO₂ from a molecule, typically from an oxocarboxylic acid (Figure 5)⁹⁰. Such a reaction produces a ketone, as well as gaseous carbon dioxide, the major gas product of HTC²⁵. Decarboxylation occurs readily under mild heating (>50 °C), and can be accelerated greatly if performed under acid conditions (beginning at ~30 °C)⁹⁰, and as such proceeds very rapidly under hydrothermal conditions.

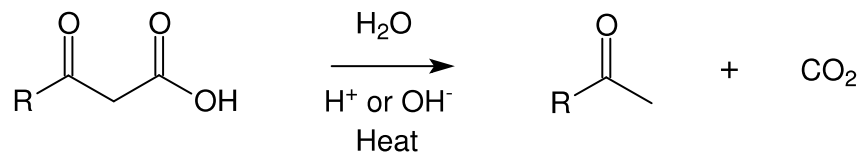


Figure 5: Decarboxylation of a carboxylic acid

Dehydration, to be differentiated from the physical removal of free liquid water from a substance (dewatering), is the elimination reaction wherein hydroxyl groups (OH) are lost in the form of H₂O (Figure 6)⁹⁰. Dehydration occurs predominately via the E1 mechanism in secondary and tertiary alcohols, and is a key hydrothermal reaction for cellulose and lignin²⁵. As with hydrolysis, it was found that in a shrinking cylindrical particle model, sugarcane bagasse undergoes dehydration reactions on the interior surface of pores of the particle, occurring between the temperature ranges 200 °C to 300 °C, with conversion being complete after 20 minutes at 270 °C, and 5 minutes at 300 °C⁹¹. Dehydration and decarboxylation are responsible for removing a significant amount of oxygen from the feedstock by converting it into water or carbon dioxide respectively. This purging of oxygen has the effect of dramatically raising the higher heating value of the hydrochar, often pushing the energy content into the range of thermal coal^{32,93}. Dehydration reactions are also essential to the conversion of free monosaccharides into 5-member ring aromatics such as furfural and 5-HMF.

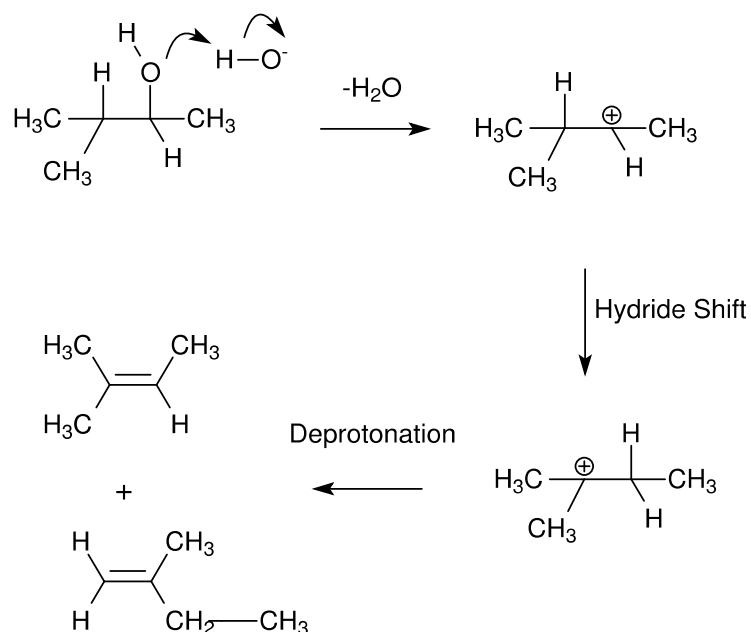


Figure 6: Dehydration of a secondary alcohol

Beginning at around 210 °C, glucose and fructose, either in purified form, or evolved as a result of the hydrolysis of hemicellulose or cellulose, undergoes a series of dehydration reactions, and eventually aromatises into the compounds 5-HMF and furfural (Figure 7)^{82,92,94}. These compounds command high market prices as precursor and platform chemicals, and as such are highly desired by-products or even primary products of the HTC reaction^{40,95,96}. Once synthesised, these 5-member aromatic rings undergo further reactions that lead to their repolymerisation.

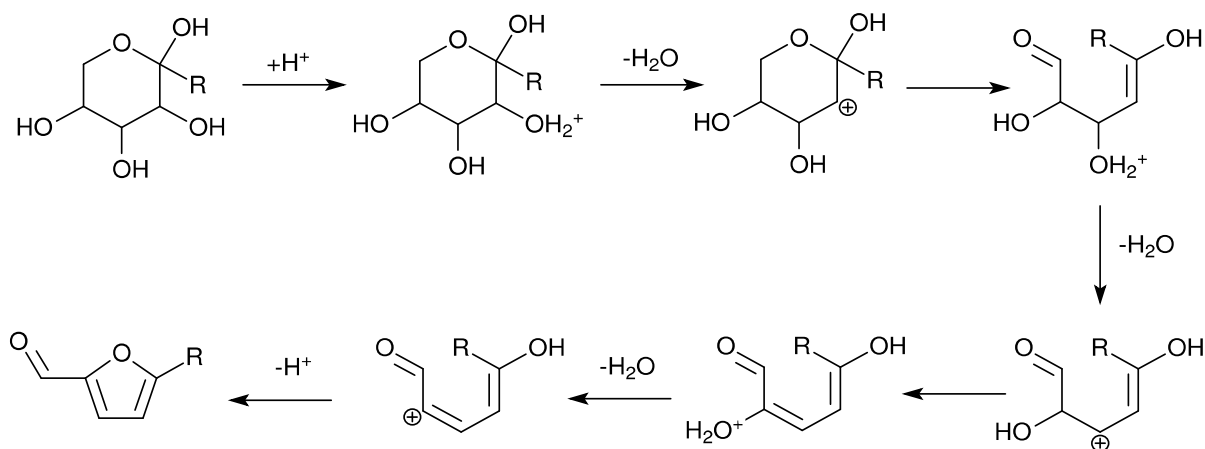


Figure 7: Aromatisation of glucose to form 5-HMF

2.3.2 Polymerisation Reactions

Polymerisation is the linking of multiple monomer molecules together to form a larger synthetic molecule. In HTC, one of the most important polymerisation reactions is the condensation reaction. Condensation reactions link monomers together via the removal of a small molecule, typically water or an alcohol (Figure 8)⁹⁰. Condensation reactions are versatile, and can occur between a broad range of different functional groups, such as between an alcohol and a carboxylic acid (such as those formed by the hydrolysis of esters), between enols and carbonyls (aldol condensation), a pair of esters (Claisen condensation), or even intramolecularly in diesters (Dieckman condensation).

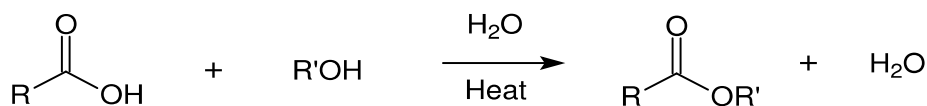


Figure 8: Condensation reaction of an alcohol and a carboxylic acid

In the aforementioned furfuranic products, successive condensation reactions under prolonged exposure to hydrothermal conditions leads to the formation of aromatic clusters, which then act as nucleation sites for further polymerisation (the Lamer model). Aromatic moieties, including phenolics derived from lignin, continue to build up into a polyaromatic and

polyfuranic structure, which eventually coalesces into the tarry, black, carbonaceous nanospheres of the secondary char (Figure 9)^{54,82,89,97}.

These reactions occur together in a great “soup” of intermediaries and side products. The sheer complexity of these reactions means that many mechanistic studies have chosen to focus on the reactions that occur within a single model compound, such as purified crystalline cellulose, xylose, or Klason lignin. A key tool for understanding the underlying mechanics of a given complex reaction is to determine the reaction kinetics.

2.4 Reaction Kinetics of HTC

The kinetics of a chemical reaction describe the energy requirements and the speed of the reaction at a given temperature. It is dependent on the nature of the chemicals reacting, on the strength of the bonds, and the number of chemicals which must come together in order to execute the reaction. Understanding the kinetics of the HTC reaction is essential in order to develop reactors at greater scales, efficacies and efficiencies as the technology is commercialised, and as such there have been numerous attempts at calculating the kinetic parameters of HTC⁹⁸. The majority of these studies have used a basic dimensionless (0D) kinetic model, typically utilising a first order Arrhenius model as described fully in Equation 2:

$$r = \frac{-dm}{dt} = k(t) \times m = A_0 \exp\left(\frac{-E_a}{RT}\right) \times m \quad (2)$$

Wherein r is the temperature-dependent reaction rate (time^{-1}), t is time (often measured in seconds), $k(t)$ is the reaction rate coefficient at time t (time^{-1}), and m is the mass of the solid phase, R is the universal gas constant of $8.314 \text{ J mol}^{-1} \text{ K}^{-1}$, and $T =$ Temperature at time t (K). The key Arrhenius factors are A_0 as the Arrhenius pre-exponential factor, and E_a as the Activation energy (J mol^{-1})

Hydrothermal Carbonisation of Novel Biomasses

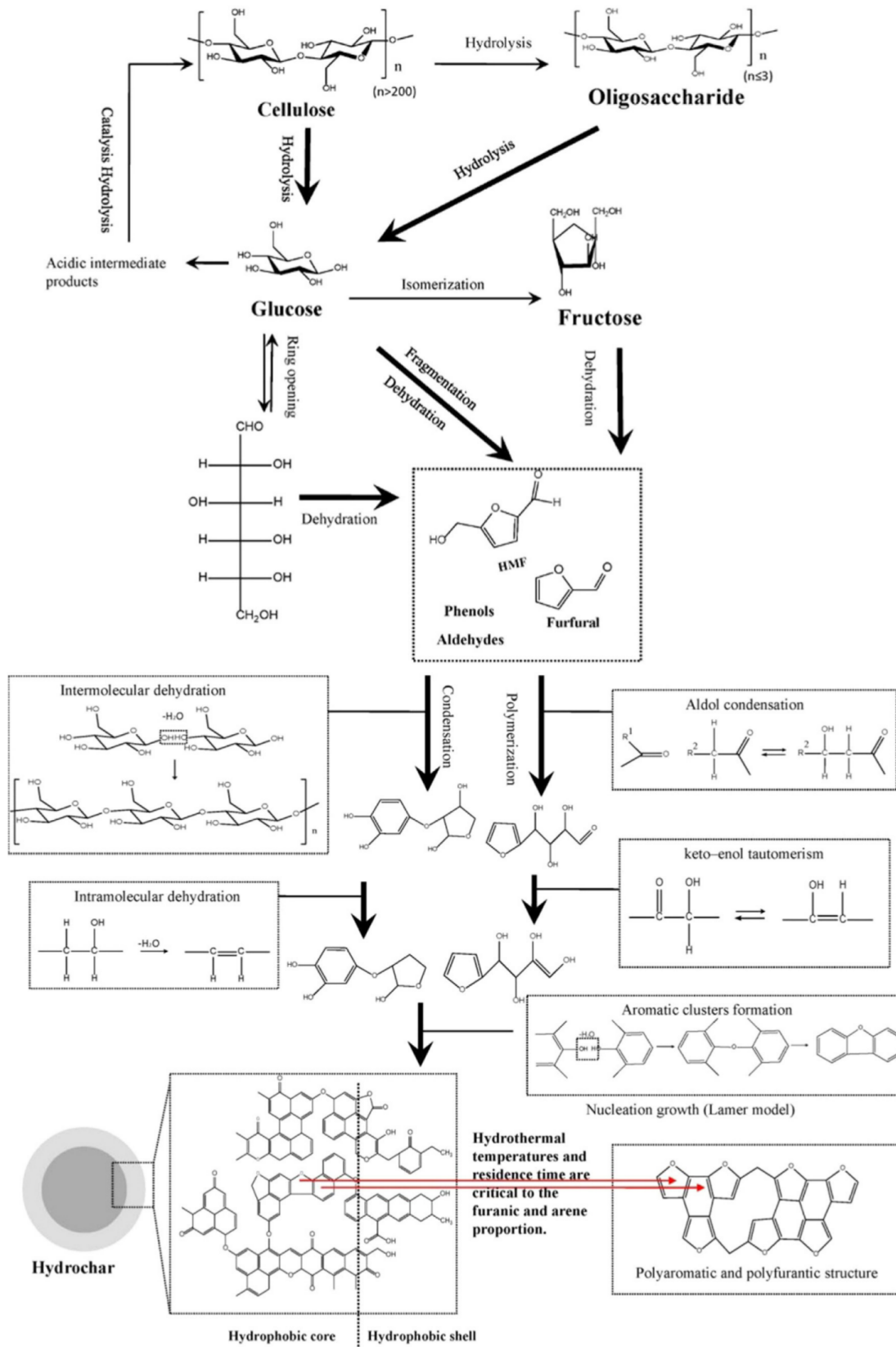


Figure 9: Summary of the conversion of cellulose into secondary hydrochar⁸²

Practically speaking, Equation 2 is frequently simplified to assume a constant temperature across the duration of the reaction, resulting in Equation 3:

$$X(t) = \exp(-k \times t) = \exp\left(-A_0 \exp\left(\frac{-E_a}{RT}\right) \times t\right) \quad (3)$$

Wherein $X(t)$ is the conversion of the solid fraction at time t at a given temperature. This allows the activation energy and Arrhenius constants to be calculated by fitting the model to the experimental data, using for example a least sum of squares methodology. In doing so, it is possible to quickly and easily build a model that provides a good fit to the mass yields of the HTC reaction. As a result, first order Arrhenius models are far and away the most common model found in the literature, with many studies applying a basic first order Arrhenius model to a wide variety of feedstocks, including various kinds of biomasses as well as purified compounds such as glucose and tannin (Table 1). When applied to whole biomass experiments, while it is possible to gain an estimate of the overall energy requirements of the reaction and the overall rate of reaction, these simple models are not capable of providing information about the underlying mechanisms of the reaction, especially about the disparate reactions of the biochemical constituents. The simple three-step model provided by Jatzwauck and Schumpe (Figure 2) allowed for the construction of a slightly more complex lumped model, meaning that the three reaction pathways could be solved simultaneously using a Runge-Kutta method⁸³. However, the reactions of the biomass remained simplified into an overall first order reaction, with the only insight into the underlying biochemical changes coming from the solid mass yield and the mean carbon content. Jung and Kruse 2017 constructed a lumped coalification model described in Equation 4 that attempted to predict the carbon and oxygen content as well as the hydrochar yield using published data⁹⁹.

$$At^B \exp\left[\frac{-C}{T}\right] = \frac{O_{feed} - O_t}{O_{feed} - 6} \quad (4)$$

Where A , B and C are adjustable variables, t is reaction time, T the reaction temperature, O_{feed} is the oxygen content of the feedstock, and O_t is the oxygen content after reaction time t .

This coalification model was tested against a linear regression model (Equation 5), a severity model (Equation 6), and a dose-response model (Equation 7), the latter two using the severity factor R_0 given in Equation 8.

$$f = a \cdot T + b \cdot t + c \quad (5)$$

$$f = a \ln(R_0) + b \quad (6)$$

$$f = a + \frac{b - a}{1 + 10^{(c - \ln(R_0))d}} \quad (7)$$

$$R_0 = t \exp\left[\frac{T - T_{Ref}}{\omega}\right] \quad (8)$$

Where a , b , c , d and ω are adjustable variables, and T_{Ref} is a reference temperature. It was found that this coalification model was capable of predicting the carbon content, oxygen content and hydrochar yield with reasonable accuracy, as measured by mean absolute error, although the dose-response model demonstrated the lowest mean absolute error of the four models tested by far. The authors of this study concluded that it was possible to use the models presented to predict the hydrochar yield of a given biomass, without the need to do any experiments. However, this statement rests on the assumption that lignin was unreactive, which is known to be untrue^{88,100}. Furthermore, the model was inaccurate when applied to large temperature ranges, and discounted the effect of the varying levels of hemicellulose, cellulose and lignin. Such a lumped model is useful in gaining a quick estimate of a desired property, but cannot by its nature inform or be informed by the underlying chemical changes in the feedstock.

Iryani *et al.* (2016) attempted to gain some mechanistic information from the HTC of sugarcane bagasse by constructing a shrinking core model that specifically modelled the dehydration and hydrolysis reactions as a pair of first order reactions⁹¹. It was found that degradation reactions occurred on the interior of the cracked, disintegrating surface of the solid particles, and that the rates of both reactions are controlled by the rate of diffusion of water through the solid hydrochar product being deposited on the surface of the particle. While this

model did provide important insight into the fundamentals of the degradation reactions of HTC in whole biomass and where they occur, the model could say little about how the individual components themselves degraded.

A common means for studying the reactions of the biochemical constituents of biomass is to isolate each component and observe them separately. Such model compound experiments are simple and easy, and there is a substantial amount of literature describing first order reactions for glucose¹⁰¹⁻¹⁰⁵, cellulose²⁶, and alkaline lignin^{106,107}. The degree to which these model compound experiments reflect the reactions that occur in whole biomass is questionable, however. It can be expected that the chemical environments that occur in model compound reactions differ from those in whole biomass experiments, for example with the addition of inorganic elements altering the ionic profile of the hydrothermal medium, or excess carbonic acid evolved from a high concentration of carbohydrates altering the pH, or phenolics released from lignin affecting the hydrophobicity of the medium, to say nothing of the effect of the multitude of crosslinks between the various components in their natural state. It would be far more informative to track and analyse the degradation of the biomass constituents as they degrade in whole biomass over the course of the HTC reaction. Reza *et al.* (2013) constructed a model that estimated the degradation of hemicellulose and cellulose within the wood of loblolly pine as a pair of first order reactions, using the initial biochemical composition of the untreated biomass, and the solid mass yield of the HTC reaction, as given in Equation 9¹⁰⁸.

$$Y(t) = \frac{M(t)}{M_0} = Y_{H_0} e^{-k_1 t} + Y_{C_0} e^{-k_2 t} + \beta Y_{C_0} (1 - e^{-k_2 t}) + Y_{L_0} \quad (9)$$

Where $Y(t)$ is the hydrochar yield, $M(t)$ is the mass of unreacted biomass, M_0 is the initial mass of biomass, Y_{H_0} , Y_{C_0} , and Y_{L_0} are the initial mass fractions of hemicellulose, cellulose and lignin, respectively, k_1 and k_2 are the first order reaction rate constants of hemicellulose and cellulose respectively, and β is the mass yield of the solid products of the conversion of cellulose to char. Hemicellulose was assumed to degrade into aqueous and gaseous products, while cellulose was assumed to evolve gaseous, aqueous, and solid products. Lignin was assumed to be inert, while the biochemical remainder, termed “aqueous extractives”, were assumed to instantly degrade into aqueous and gaseous products. Using these estimations, it was possible to attain activation

energies of 29 kJ mol⁻¹ for hemicellulose, and 77 kJ mol⁻¹ for cellulose, which were dramatically lower than those attained for the purified model compounds (135 kJ mol⁻¹ and 215 kJ mol⁻¹ respectively) (Table 1).

Such discrepancy highlights the limitations of model compound experiments, and underlines the necessity of studying biomass HTC using whole biomass material. Yet, the Reza model itself has limitations, as the levels of hemicellulose, cellulose and lignin within the hydrochars were not directly measured, but were instead estimated using the composition of the untreated wood, which in turn was quantified using a Van Soest fibre analysis¹⁰⁹. The Van Soest method was developed for quantifying crude fibre in an animal feed context, and does not provide accurate or precise measurements for polysaccharides or phenolics, but instead estimates them based on acid and detergent solubility¹¹⁰. In particular, it is not capable of distinguishing lignin from undigested material, a potentially significant issue with biomasses with high levels of crystalline polysaccharides, and also cannot be used to measure the compositions of hydrochar. Hence, while a valuable first step in understanding the reactions of hemicellulose and cellulose in their native state, and a marked step up from the most basic first order models common in the literature, the Reza model is not likely to be reflective of the true nature of the HTC reaction.

A persistent hole in the state-of-the-art of hydrothermal carbonisation is the inability to accurately and precisely measure the levels of hemicellulose, cellulose, lignin, protein and other macromolecules within hydrochar as well as the untreated biomass. Without understanding how these macromolecules behave in their native state within an HTC environment, further knowledge of the HTC reaction is by necessity obscured. Model compound experiments cannot capture the complexities of whole biomass reactions, and therefore there is a driving need to develop techniques that are capable of tracking the biochemical changes within the reacting biomass with great precision and detail. Only then will it be possible to develop more sophisticated kinetic and mechanistic models that more effectively reflect the reality of the hydrothermal reaction. The rewards in doing so should not be understated; in a world with ever increasing energy requirements and ever diminishing environmental resilience and stability, the need for new, sustainable energy sources is of the utmost concern. Better

understandings of the HTC reaction will allow for the exploitation of new biomass sources that do not infringe on the needs of agriculture, provide a truly sustainable source of energy, are carbon-neutral or negative with carbon sequestering, and which provide multifaceted benefits and products in a new and growing bioeconomy.

Table 1: Summary of literature investigating the degradation kinetics of a given feedstock during a variety of hydrothermal treatments.

Feedstock	Temperature (°C)	Model Type	Activation Energy (kJ mol⁻¹)
Glucose	250 - 350	Simple Arrhenius first order	114 ¹⁰¹ , 96 ¹⁰² , 121 ^{103,104} , 88 ¹⁰⁵
Xylan	152 - 175	Simple Arrhenius first order	112 (sugar maple wood chips) ¹¹¹ 114 (sugar maple wood meal) ¹¹²
Cellulose	200 - 350	Simple Arrhenius first order	215 (purified) ²⁶ , 77 (loblolly pine) ¹⁰⁸ ,
Hemicellulose	150 - 260	Simple Arrhenius first order	29 (loblolly pine) ¹⁰⁸ , 135 (spruce extract) ¹¹³
Lignin	300 - 450	Simple Arrhenius first order	34 ¹⁰⁶ , 43 ¹⁰⁷ (alkali lignin), 37 (soft wood) ¹¹⁴
Soft Rush	180 - 240	Three-step first order reaction model	141 ⁸³
Synthetic Faeces	140 - 200	Simple Arrhenius first order	78 ¹¹⁵
Tannins	130 - 200	Simple Arrhenius first order	91 ¹¹⁶
Grape Marc	180 - 250	Simple Arrhenius first order	95 ¹¹⁷
Sugarcane Bagasse	200 - 300	Parallel first-order with shrinking core mechanism	88 (hydrolysis), 129 (dehydration) ⁹¹

Aim and Objectives of Thesis

The overall aim of the study presented here is to understand the various reactions that occur within novel feedstocks during hydrothermal carbonisation for fuel applications. In order to satisfy this aim, this study proceeded with four aims.

Firstly, the feasibility of novel feedstocks such as saltbush, macroalgae and hemp as HTC feedstocks was investigated. The investigation was performed from the context of solid fuel applications, and factors such as hydrochar yield, higher heating value, carbon, oxygen and nitrogen content, and ash content, were key points of interest.

Secondly, biochemical compositional assays that accurately and precisely track the changes that occur during the HTC of biomass were developed. Specifically, hemicellulose, cellulose, lignin and protein were individually quantified for each temperature and time point, such that there was no interference that could occur from synchronous measurement, as in the case of the Van Soest method.

Thirdly, using the data obtained from the Second Objective, a mechanistic model of the biochemical changes that occur during HTC of biomass was developed. This model incorporated the degradation of each biochemical component into intermediates, and the fates of those intermediates.

Fourthly, using data from the Second and Third Objectives, a kinetic model of the degradation of hemicellulose, cellulose, lignin (Chapters 2 and 3) and protein (Chapter 4) could be formulated. This model was in essence a validation of the mechanistic model presented in the Third Objective, and used to inform the refinement of the mechanistic understanding.

This study is presented to the reader as a demonstration of the utility of the biochemical assays detailed herein, and the potential they possess to dramatically increase the current knowledge of HTC. The models and methodologies contained herein are offered as a first step exploring what can be done with the power of these techniques, and it is hoped that they may form a foundation for hydrothermal research in the future.

Chapter 3

Paper I

Hydrothermal Carbonisation of Australian Saltbush

Benjamin G. Keiller[†], Philip J. van Eyk[‡], Daniel J. Lane[‡], Richard Muhlack[†], and Rachel A. Burton[†]*

[†] School of Agriculture, Food and Wine, University of Adelaide, Waite Campus, Glen Osmond, SA 5064

[‡] School of Chemical Engineering and Advanced Materials, University of Adelaide, Adelaide, SA 5005

* Corresponding Author: philip.vaneyk@adelaide.edu.au

This manuscript was written with contributions from all authors. All authors have given approval to the final version of the manuscript

Statement of Authorship

Title of Paper	Hydrothermal Carbonisation of Australian Saltbush
Publication Status	<input checked="" type="checkbox"/> Published <input type="checkbox"/> Accepted for Publication <input type="checkbox"/> Submitted for Publication <input type="checkbox"/> Unpublished and Unsubmitted work written in manuscript style
Publication Details	Keiller, B. G., van Eyk, P. J., Lane, D. J., Muhlack, R. & Burton, R. A. Hydrothermal Carbonization of Australian Saltbush. <i>Energy Fuels</i> (2018) doi:10.1021/acs.energyfuels.8b03416.

Principal Author

Name of Principal Author (Candidate)	Benjamin Keiller		
Contribution to the Paper	Conception, Analysis, Drafting		
Overall percentage (%)	70%		
Certification:	This paper reports on original research I conducted during the period of my Higher Degree by Research candidature and is not subject to any obligations or contractual agreements with a third party that would constrain its inclusion in this thesis. I am the primary author of this paper.		
Signature		Date	10-12-19

Co-Author Contributions

By signing the Statement of Authorship, each author certifies that:

- i. the candidate's stated contribution to the publication is accurate (as detailed above);
- ii. permission is granted for the candidate to include the publication in the thesis; and
- iii. the sum of all co-author contributions is equal to 100% less the candidate's stated contribution.

Name of Co-Author	Philip J van Eyk		
Contribution to the Paper	Conception, Analysis, Drafting		
Signature		Date	13-01-20

Name of Co-Author	Daniel J Lane		
Contribution to the Paper	Conception, Analysis, Drafting		
Signature		Date	16.12.2019

Chapter 3 (Paper I) - Hydrothermal Carbonisation of Australian Saltbush

Name of Co-Author	Richard Muhlack		
Contribution to the Paper	Conception, Analysis, Drafting		
Signature		Date	10.12.2019

Name of Co-Author	Rachel A. Burton		
Contribution to the Paper	Conception, Analysis, Drafting		
Signature		Date	7/12/19

3.0 Abstract

Hydrothermal carbonisation (HTC) is a thermochemical process wherein biomass is subjected to high-pressure, high-temperature subcritical water to improve the combustion characteristics of biomass as a solid fuel. Australian saltbush was subjected to HTC at three temperatures (200 °C, 230 °C, 260 °C) and four holding times (0 min, 15 min, 30 min, 60 min), using a custom-built batch reactor. The resultant hydrochars demonstrated improved higher-heating values, with temperature more influential than time. At the most severe condition of 60 minutes, 260 °C, the hydrochar possessed numerous key similarities to fossil coal, such as a higher heating value of 27.5 MJ kg⁻¹, similar ratios of carbon/oxygen and hydrogen/oxygen, and equivalent levels of volatile matter, fixed carbon and ash. The HTC process also proved effective in reducing the high levels of inorganic elements naturally present within saltbush, with 60 minutes at 260 °C again shown to be the most effective condition, removing almost 95% of sodium, chloride, and potassium.

3.1 Introduction

Concern over the effects of climate change combined with the drawbacks of using conventional fossil fuels is driving tremendous growth in renewable energy development. It is projected that by 2040, global energy consumption will increase by 35%, with the renewable energy sector growing the fastest, eventually coming to occupy 40 of the energy mix¹¹⁸. Biofuels, that is, combustible fuels derived from living matter (biomass), are poised to play a significant role in the coming sustainable economy. While most biofuels research is focused around liquid fuels for use in internal combustion and jet turbine engines, there is still likely to be a need for solid fuels to replace coal and coke, particularly in high-temperature applications other than electricity production, such as steel foundries.

Hydrothermal carbonisation (HTC) is a technique for producing renewable solid biofuels wherein biomass is subjected to subcritical water at temperatures between 180 °C and 260 °C. In this manner, it is possible to simulate and accelerate the conditions deep beneath the Earth's crust during coalification, with the resultant solid product (known as “hydrochar”) exhibiting many similarities to conventional fossil coal²⁵. The advantages of HTC over similar

pyrolytic technologies such as torrefaction are numerous, and in large part due to the aqueous reaction medium. These include a high degree of energy efficiency due to avoiding the enthalpy of vapourisation, removal of inorganic elements within the feedstock, ease of separation of liquids and solids, and because there is little need for costly predrying of the biomass, a greater versatility of feedstocks is permitted^{26,119}. Over the course of the HTC reaction, the principle biopolymer components of biomass (hemicellulose, cellulose and lignin, collectively termed lignocellulose) are subject to a variety of reactions catalysed by the high temperature subcritical water, including hydrolysis, dehydration, decarboxylation, repolymerisation, and aromatisation which lead to the degradation of the lignocellulose and its conversion to hydrochar^{25,120}. Previous literature has indicated that this conversion process has numerous benefits in upgrading the biomass, including increasing the heating values, producing more favourable carbon:oxygen ratios, and purging volatile matter from the biomass^{32,93,121}. The exact properties of the resultant hydrochar fuels, however, are highly feedstock dependent; numerous studies on a wide variety of feedstocks ranging from loblolly pine, willow, oak and other woods to algae to biosolids and even municipal waste have revealed profound variances in mass and ash yield^{43,109,122}. Because of this variance, it is difficult to predict the nature of the hydrochars produced from a given biomass, as well as the optimum conditions such as ideal residence times and temperatures required to produce said hydrochars.

The choice of biomass feedstock is constrained by important considerations such as availability, cost, the possibility of environmental degradation caused by its collection, pollution from its use, or the potential for competition for land and water used usually for conventional agriculture. A novel approach to generating sustainable biomass for heat and power application is to use material from marginal land that is unsuitable for agricultural use. In Australia, where some 70% of the land area is considered arid¹²³, there is a great deal of marginal land that is unsuitable for most kinds of intensive agriculture, and yet supports many native plant species that thrive in these harsh conditions, such as saltbush. Saltbush is a term used somewhat broadly to describe a selection of halophytic species from the Chenopodiaceae family (mainly *Atriplex* and similar geni) that are highly adapted to growing on such marginal lands, particularly in soils with high salinity. In fact, some species are so well adapted to saline conditions that they actually receive a growth bonus with increased NaCl concentrations, up to

a certain limit¹²⁴. Because of this supreme hardiness, saltbushes range widely across many different environments in Australia, and form an important foundation for many dryland ecosystems where other plant species struggle. This hardiness has also lent itself to many human applications; saltbush is an important forage for the sheep grazing industry. Many species of saltbush are palatable for sheep, and therefore it is possible to rear livestock on otherwise inhospitable land. Saltbush contains a high level of protein important for sheep growth¹²⁵, and additionally has a desirable effect on the taste of lamb meat. As a result, there is a growing market for saltbush lamb and beef, which commands a premium in restaurants. Therefore, there is already an existing value chain for saltbush, and in 2014 a startup company, Wilson Pastoral, was established in South Australia to commercially grow saltbush to produce livestock fodder pellets. In addition to this, saltbush is also being investigated as an agent for remediation of soil salinity caused by rising watertables. With its affinity for salt and deep taproots, saltbush can be established on hypersaline soils to reduce the water table, and can also sequester a small portion of the salt within its leaves¹²⁶. The fact that saltbush is a reasonably fast-growing biomass with little ecological impact, high tolerance for harsh Australian conditions, and large economic importance, makes it worth investigating as a novel feedstock. However, there is at present zero published information as to the behaviour and suitability of saltbush-derived solid biofuel, and it is possible that the high salt content will present challenges in the form of a high ash content.

During combustion, salt and other inorganic compounds are deposited as ash, which is responsible for slagging and fouling in industrial processes such as coal-fired boilers^{127,128}. Slagging occurs when molten or softened ash particles adhere to the cooler sides of the furnace or convection surface, while fouling occurs when vapourised inorganic particles are entrained and eventually condense on convection surfaces away from the heat of the furnace⁸¹. Both slagging and fouling cause significant operational issues, and can lead to greatly reduced thermal efficiency, as well as damage and corrosion to key furnace infrastructure¹²⁷. It is therefore essential to have a good understanding of the inorganic elements present in a given solid fuel, and in the case of HTC, of the behaviour of those inorganics over the course of the hydrothermal reaction. Of particular note are the elements Na, Cl, K, P, S, all of which are heavily implicated in ash-related issues¹²⁹. All are utilised by living organisms in varying

quantities, and thus are all present in biomass. Previous studies have investigated the removal of inorganics via HTC of a wide variety of feedstocks including sawdust, algae, food waste, sewage, biosolids, municipal waste including polycomposite packaging, and agricultural waste^{43,130–133}. In each of these studies, levels of inorganics decreased with higher HTC reaction temperatures, although the effect was dependent upon the specific element, and feedstock type. Feedstocks derived from lignocellulosic biomass, such as wood or algae, displayed a marked reduction in inorganic compounds, in some cases up to 97% of important cations⁴³. However, most of the inorganics associated with these biomasses are present in relatively low quantities, as the organisms they are derived from seek to tightly regulate the amount of inorganics within their system; it is unknown how the higher salt content of saltbush will affect the HTC process relative to similar, non-salty woody biomasses.

The aim of this paper is therefore to assess the potential of Australian saltbush as a suitable biomass feedstock for hydrothermal carbonisation for solid fuel applications. To achieve this aim, the key objectives are: to investigate the impact of reaction time and temperature on the characteristics of the resultant fuel, including higher heating values, pyrolysis behaviour ultimate analysis and proximate composition; and to quantify the retention of inorganic elements within the hydrochars.

3.2 Methods and Materials

3.2.1 Preparation of saltbush sample

A sample of harvested saltbush was supplied by Wilson Pastoral (location, South Australia), as a sun-dried, unmilled mixture of mainly *Enchylaena tomentosa* and *Atriplex amnicola*. The biomass was collected from a semi-domesticated, multi-purpose field in a native saltland environment sown with *E. tomentosa* and *A. amnicola* seeds, but which also had other native saltland species such as *Atriplex nummularia* growing wildly, with no preventative measures in place to ensure a monocrop. Intended to be an environmentally sustainable crop for saltbush pellet production, the heterogeneity of the field also allowed for a nutritionally varied grazing for sheep, a much higher level of biodiversity compared to surrounding sheep paddocks, and also a closer simulation of wild native saltland. Because of the versatility of such

saltland usage, the mixed saltbush sample was used as provided, just as in any potential future industrial application, with no attempt to separate the various constituents.

The biomass was finely ground in a knife mill, and then sieved to obtain the 150 – 500 μm size fraction. The ground biomass was oven-dried at 105 °C, 24 hours prior to the hydrothermal reaction.

3.2.2 Hydrothermal Carbonisation

The hydrothermal carbonisation reactions were carried out in a custom-built batch reactor (Supplementary Figure 1). The reactor was a stainless steel grade 316 tube with an outside diameter of $\frac{3}{4}$ " , a wall thickness of $\frac{1}{8}$ " , and an internal volume of 30 mL. The reactor tube was sealed with a $\frac{3}{4}$ " cap on the bottom, and a $\frac{3}{4}$ " to $\frac{1}{8}$ " Swagelok reducing union on top. The upper section of the reactor consisted of $\frac{1}{8}$ " tubing to minimise the cold headspace above the reaction vessel. This $\frac{1}{8}$ " tubing connected the main reaction vessel to a 1.5 mm diameter K-type thermocouple positioned in the centre of the main reactor tube, as well as a Wika brand pressure transducer (4 – 20 mA) and an emergency release valve. Both the thermocouple and the pressure transducer were connected to a digital logger. The uppermost section of the reactor contained a pair of Hoke hand-operated ball-valves mounted on either side of a T-section to facilitate the sequential pressurising and releasing of N_2 gas prior to the HTC reaction. To minimise the likelihood of entrained fluid/solids clogging the tubing, the upper section was equipped with a sintered steel filter between the safety release valve and the T-section.

Saltbush was mixed with deionised water to produce a slurry with a 15% w/w solids loading, a typical loading in the literature for lignocellulosic feedstocks^{10,134,135}. The slurry was added to the reactor (80% of maximum capacity), which was sealed. The seal of the reactor was pressure tested up to 100bar in nitrogen, and the oxygen within the reactor was purged. This was achieved by sequentially pressurising the reactor to 20bar of nitrogen and then releasing this pressure three times. The saturation pressure of water at the desired reaction temperature was calculated, and the reaction vessel was pre-pressurised with nitrogen to ensure that the saturation pressure was met or exceeded during the reaction. The reactor was fully immersed

in an electronically heated fluidised bed (Techne, model: SBL-2D) equipped with alumina sand as a bedding material, and heated to the desired reaction temperature. HTC reactions were carried out at three reaction temperatures (200 °C, 230 °C, 260 °C) with four isothermal holding times (0 minutes, 15 minutes, 30 minutes, 60 minutes). The reaction condition 200 °C, 30 mins was performed in quadruplicate. Isothermal holding time was counted from when the reactant mixture reached 98% of the setpoint temperature. An isothermal holding time of 0 minutes represents conditions where the internal temperature of the reaction vessel was raised to reaction temperature, and then immediately quenched. After the desired residence time, the reactor was removed from the reactor and quenched in water. The 0 minute element of experimental design was chosen because it enables the distinction between the reactions that occur during the initial heat-up phase, which can take up to 10 minutes with the present reactor design, and those that occur during the isothermal holding period.

Gaseous products were released to exhaust, and the solid and liquid fractions of the reaction products were separated via vacuum filtration, using filter paper with a 2.5 µm pore size. The bulk of the reaction products were collected by simply pouring the contents of the reaction vessel over the filter paper, and manually scraping the sides of the reactor with a spatula. The remainder of the reaction products, the small portion that remained stuck to the reactor sides, was rinsed off using deionised water over a second filter paper. Because rinsing in deionised water affects the concentrations of inorganic components within the product, this second filter paper was only used to determine mass yields, and then discarded. The filter papers containing the solid product were dried at 105 °C for 24 hours, while the liquid fraction was discarded.

3.2.3 Fuel Analysis

For all fuel analyses, the untreated saltbush (in triplicate) as well as the HTC hydrochars were tested. The Higher Heating Values (HHV) were determined using a Leco AC-350 bomb calorimeter. Proximate analysis was performed using thermogravimetric analysis (TGA). Hydrochar (~5 mg) was loaded into cylindrical alumina crucibles (70 µl), and loaded into a Mettler Toledo Thermogravimetric Analyser (TGA)/Differential Scanning Calorimeter (DSC) 2. Samples were progressively heated at a rate of 10 °C min⁻¹ up to 105 °C under N₂ (80 mL min⁻¹ @

Hydrothermal Carbonisation of Novel Biomasses

STP), which was held for 30 minutes to purge any residual moisture. The samples were then heated to 550 °C at a rate of 10 °C min⁻¹ and held at this temperature for a period of 1 hour to determine the volatile matter content. The samples, still at 550 °C, were then exposed to air and combusted to determine the ash content, and the fixed carbon content by difference. Samples were prepared for ultimate, inorganic and pyrolysis behaviour analysis by finely grinding in an agate mortar and pestle. Samples for pyrolysis behaviour analysis were further prepared by sieving to obtain the <105 µm size fraction. The ultimate analysis (CHN) was determined using a Perkin Elmer 2400 series II CHNS analyser.

Inorganic elemental concentrations of Na, K, P S were obtained using a total metals by acid hydrolysis method: The finely ground sample was digested in a microwave oven with nitric acid and the solution was then analysed for a wide range of elements by inductively coupled plasma optical emission spectrometry (ICP-OES) on an Agilent 5100 SVDV instrument¹³⁶. Cl levels were determined using an automated colorimetric determination after water extraction. The 0.1 g sample was extracted with 10 mL water then filtered and determined by ion chromatography (IC) utilising a Dionex ICS-2500 system¹³⁷.

Pyrolysis behaviour of the hydrochars was determined using a Netzsch Simultaneous Thermal Analyser STA 449. Following an atmospheric purge of oxygen using N₂ (120 mL min⁻¹ @ STP), samples of unprocessed feedstock and hydrochar (2 mg) were progressively heated up to 105 °C at 5 °C min⁻¹ and held at this temperature for 40 minutes to purge moisture. The samples were then progressively heated again at 5 °C min⁻¹ up to a maximum temperature of 800 °C. All pyrolysis experiments were performed under N₂ (120 mL min⁻¹ @ STP).

3.2.4 Experimental Statistical Analysis

The reaction condition of 200 °C, 30 mins was performed in quadruplicate, and was used to estimate the experimental error via a propagation of error analysis¹³⁸. Student's t-tests were used to compare means of each process condition to determine statistically significant groupings (See supplementary data, Supplementary Table 1). A factorial analysis was used to determine the effect of temperature and time on the higher heating value, as well as mass yield¹³⁹.

3.3. Results and Discussion

A mixed sample of Australian saltbush was subjected to HTC with varying reaction severity with regards to reaction temperature and holding time, in order to identify the optimum conditions for producing high quality hydrochars for combustion purposes. For each given HTC temperature, the saturation pressure was calculated, and the reactor was pre-pressurised with nitrogen gas to that pressure. In this manner, at all times for each experiment, the interior pressure was equal to or in excess of the saturation pressure, thus ensuring that the water remained a liquid. This is critical for HTC, as the high temperature water acts as the medium, solvent and reactant of the carbonisation reaction. Over the course of the experiment, the gas pressure would increase, as gaseous products were produced by the HTC reaction, and as the gas phase was compressed by the expansion of the water under HTC conditions. While there is some evidence to suggest that increased reaction pressure has an impact on the various reactions that occur during HTC (such as depressed rates of decarboxylation and dehydration reactions), numerous studies have determined that in practical terms, reaction pressure has little overall effect on HTC²⁵. As a result, reaction pressure was not chosen as a variable in experimental design. Temperature and pressure profiles may be found in the supplementary data (Supplementary Figure 2)

The mass yield of the solid product of HTC dropped over time from between 66% to 60% after 60 minutes, with increased temperatures leading to the lowest yield of 35% (Figure 10A). Over the course of the carbonisation reaction, the feedstock undergoes a series of dehydration and decarboxylation reactions, causing the main components of the biomass (principally the polysaccharides cellulose and hemicellulose, as well as the aromatic polymer lignin) to break down into smaller molecules²⁶. Previous literature indicates that in addition to the solid hydrochar, these products may be gaseous or water-soluble²⁵, and therefore are released from the body of the carbonising biomass, causing the mass yield to fall over time. The behaviour of the saltbush sample is consistent with this trend.

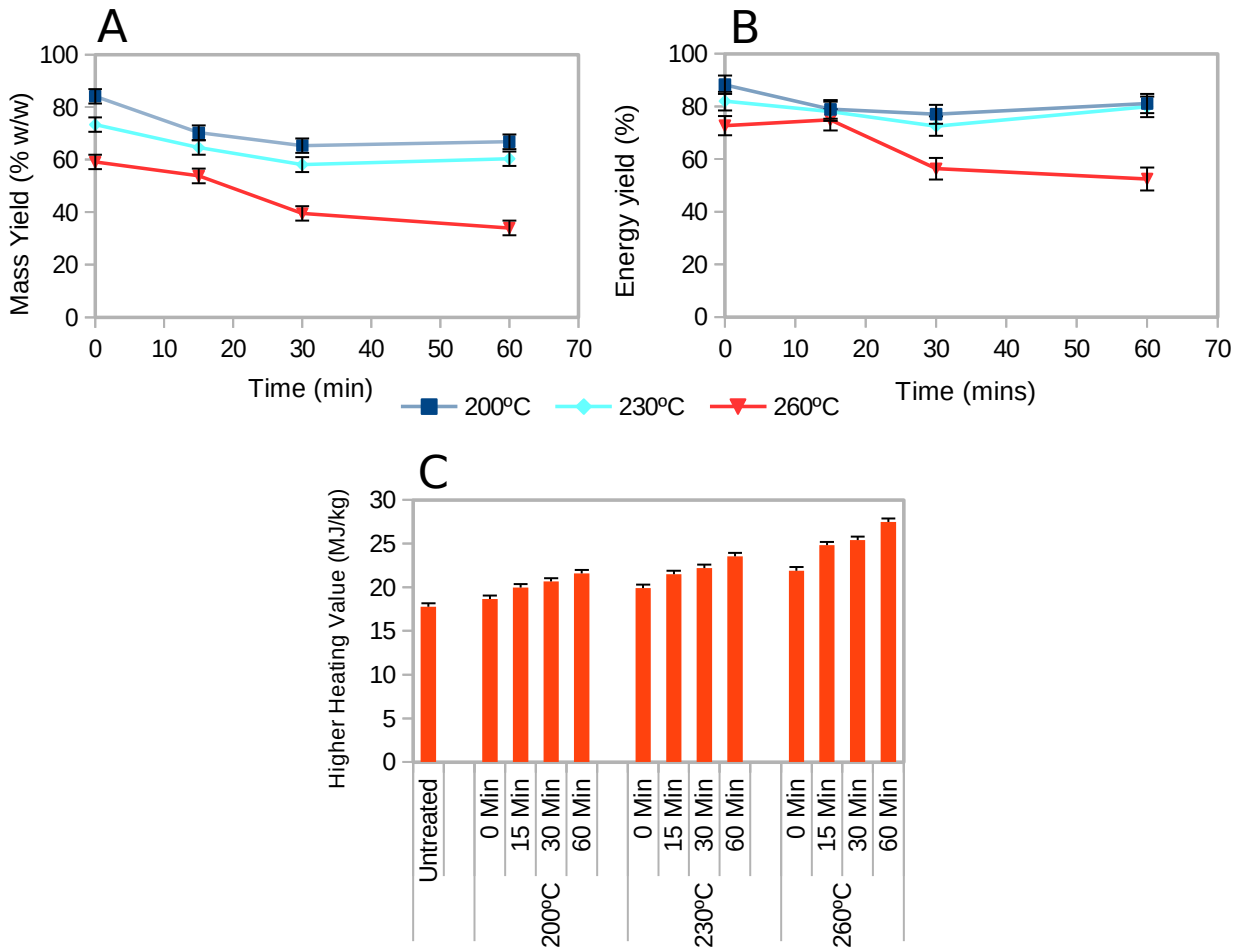


Figure 10: (A) Solid product mass yield, (B) product energy yield and (C) higher heating values following HTC at different temperatures (200 °C - 260 °C) and different isothermal holding times (0 min – 60 min). Error bars represent one standard deviation.

A factorial analysis was used to determine the relative impact of temperature and time on the mass yield, and whether there was any additional interaction between the two factors. Of the two primary variables, temperature and time, temperature appeared to be the more dominant factor, although both were found to be statistically significant, with p-values of 1.31×10^{-3} for time and 1.30×10^{-4} for temperature. The factorial analysis also indicated an additional interaction between temperature and time beyond the mere additive effect of the two factors, with an interaction p-value of 0.04.

This led to complex interactions between the two variables during the HTC process. At 200 °C and 230 °C, the mass yields followed very similar curves that initially dropped smoothly to 76% and 69% at 30 minutes respectively, after which they plateaued off. In comparison, at 260 °C the reduction in mass yield over time was more pronounced and continuous, proceeding to drop to a minimum of 35% at 60 minutes (Figure 10A). Compared with similar woody biomasses, these mass yields are consistent with published data. HTC of the softwoods Jeffrey Pine and White Fir for 30 minutes at 215 °C, 235 °C and 255 °C produced yields of 69%, 64% and 50% respectively¹¹⁹. A combined investigation of several feedstocks, including oak, *miscanthus* and willow wood at 200 °C and 250 °C for 60 minutes produced mass yields ranging from 58% to 70% at the cooler temperature, and between 40% to 60% at the higher temperature⁴³. In this context, it can be seen that saltbush behaves in a similar manner to more “conventional” feedstocks, which highlights the robustness and versatility of the hydrothermal process.

The energy yield (defined as the higher heating value (HHV) of the char divided by the HHV of the untreated feedstock, multiplied by the mass yield of the char) of HTC (Figure 10B) remained stable for the entirety of the 200 °C and 230 °C reactions, but nearly halved over the course of the 260 °C reaction, vividly illustrating the influence of temperature as opposed to time on the reaction. The energy yield for 200 °C and 230 °C was constant at around 80%, while that for 260 °C decreased steadily after 15 minutes to a minimum of 52%. This indicated that for the initial stages of the 260 °C reaction, and the entirety of the 200 °C and 230 °C reactions, the mass that was lost over the course of carbonisation did not contribute greatly to the total energy content, or higher heating value (HHV).

All reactions led to a statistically significant increase in HHV, with higher temperatures again producing greater increases (Figure 10C and Supplementary Table 1). A factorial analysis was used to determine the relative impact of temperature and time on the higher heating value, and whether there was any additional interaction between the two factors. The factorial analysis returned p-values of 2.9×10^{-4} for time, and 3.6×10^{-5} for temperature, indicating that temperature has a much more significant effect on the change in HHV than time, although both factors were highly significant. This can be directly observed where after 60 minutes at the

reaction temperature, the heating values of the hydrochars relative to the untreated feedstock increased by 17%, 24%, and 35% at 200 °C, 230 °C and 260 °C respectively. Conversely, between 0 minutes and 60 minutes at the reaction temperature, the heating values rose by only 14%, 15%, and 20% at 200 °C, 230 °C and 260 °C respectively. There was also an additional interactive effect between the two values, with an interaction p-value of 0.04. Notably, after 15 minutes at 260 °C, the higher heating value is beginning to enter the range typically seen for Australian lignites (24-30 MJ kg⁻¹)⁹. At 60 minutes, the energy densification ratio, defined as the ratio between the HHV of the hydrochar to the untreated feedstock rose to a maximum of 1.54. This increase in HHV is consistent with previous literature^{32,93} and the ability to energetically upgrade a wide variety of feedstocks is one of the greatest strengths of HTC.

To better understand the finer similarities between the saltbush hydrochars and fossil coal, the hydrochars were submitted for proximate and ultimate analysis, as well as being tested for pyrolysis behaviour. Proximate analysis (Figure 11A) is a thermogravimetric analytical technique used to grade different varieties of coals according to the relative mass fractions of moisture, volatile matter, fixed carbon and ash¹⁴⁰. The relative abundance of such fractions has a profound impact on the combustion behaviour of a given coal or char, and can also be used to identify and compare different coals or chars, and is thus an important metric to obtain.

Every reaction condition led to a relative increase in the mass fraction of fixed carbon, attended by a matched relative decrease in the mass fraction of volatile matter. Untreated saltbush exhibits features commonly seen in woody biomass: a very high level of volatile matter (71%) compared to the amount of fixed carbon (24%). This is similar to values seen for other woody materials, such as cedar wood (77% volatiles, 21% fixed carbon), Douglas fir bark (73% volatiles, 25% fixed carbon) and pine bark (74% volatiles, 24% fixed carbon)⁷⁹. The changes in the volatile matter and fixed carbon mass fractions were particularly affected by temperature; across both the entire 200 °C and 230 °C reaction series, there were many conditions that share statistically significant groupings, indicating that relatively little change occurred at low and mid temperatures. However, at 260 °C, every consecutive time point produced a statistically significant increase over the previous one. Indeed, each time interval at 260 °C increased the volatile matter to fixed carbon ratio more than the total difference across the whole of either

the 200 °C or the 230 °C tests. In particular, at the most severe conditions of 260 °C at 30 and 60 minutes, the ratio between volatiles and fixed carbon approaches 1:1, which is characteristic of many lignites^{9,79}, and is another measure in which these hydrochars closely approximate fossil coals. This trend of increasing the volatile matter:fixed carbon ratio is a common feature of HTC, and has been observed across a wide variety of feedstocks⁹³, and even applies to predominately non-lignocellulosic biomass like poultry litter⁴².

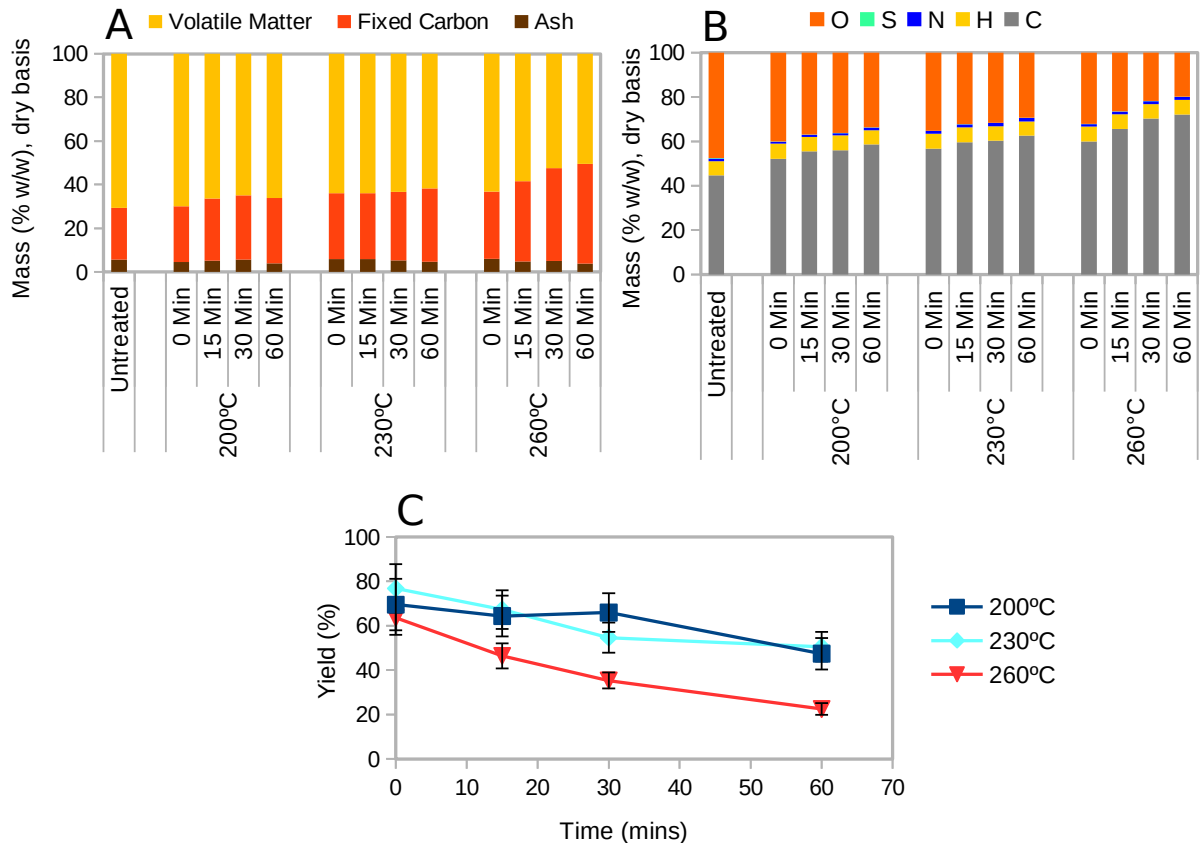


Figure 11: (A) Proximate Analysis, (B) Ultimate Analysis and (C) Ash Retention of untreated saltbush and HTC hydrochars at different temperatures (200 °C – 260 °C) and different isothermal holding times (0 min – 60 min). Relative standard deviation for the proximate analysis measurement of volatile matter, fixed carbon and ash were approximately 1% , 1% and 0.5% respectively, while error bars for the ash retention represent one standard deviation. Carbon, Hydrogen and Nitrogen determined via CHNS analysis, Sulphur levels determined via ICP-OES, Oxygen levels determined by difference.

As expected, saltbush contained a high percentage of ash compared to other lignocellulosic biomasses, at around 5% ash (Figure 11A) compared to an average of 2.7% for similar woods and barks⁷⁹. This high ash content was a result of the high level of salts, typically sodium chloride, that saltbush sequesters in its leaves as a salinity tolerance measure. As a total percentage, the level of ash in the hydrochars changed little with increasing reaction severity, instead staying relatively constant at between 4% and 5%. Such values compare very favourably to both brown and black coals (3% - 12% ash)⁹, as well as to hydrochars produced from other lignocellulosic feedstocks, which can vary between 0.1 and 29.8%^{43,93,130}.

The untreated feedstock and the hydrochars were subjected to further thermogravimetric analysis to determine the manner in which the volatile matter contained within the fuel is released during devolatilisation. To that end, the mass fraction (Y), and the first time derivative of the mass fraction divided by the mass fraction ($[dY/dt]/Y$) were determined (Figure 12).

As the severity of the HTC reaction was increased, the temperature at which rapid and significant mass loss (devolatilisation) begins was pushed higher and higher (Figure 12A). After an initial period of lag, devolatilisation began to accelerate dramatically after 200 °C for untreated saltbush, compared to around 270 °C for hydrochars treated for 60 minutes at 200 °C and 230 °C, while hydrochars treated under the most

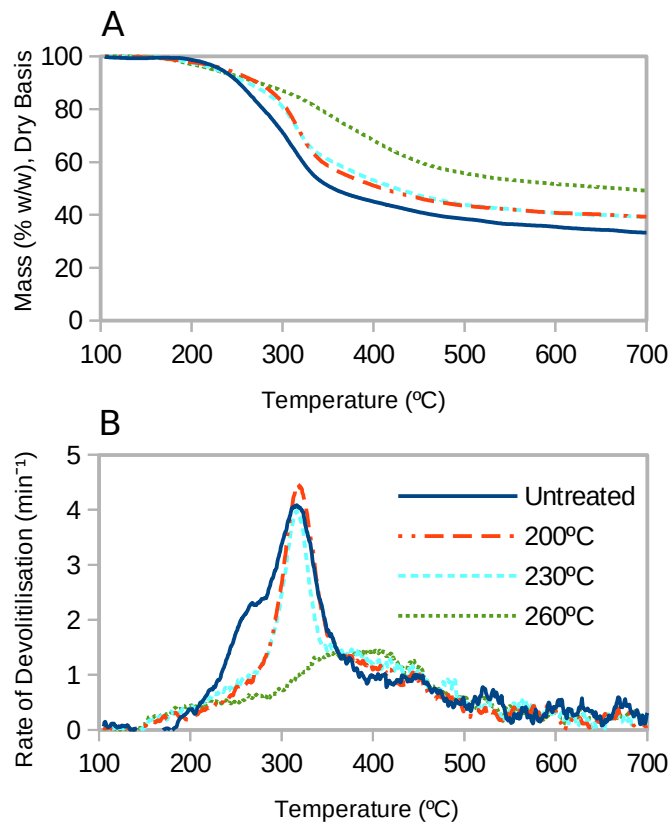


Figure 12: Pyrolysis Behaviour of untreated saltbush and hydrochars at different temperatures after 60 minutes of HT treatment. (A) Mass loss over temperature under nitrogen atmosphere. (B) First derivative of mass loss of function in A.

severe conditions underwent rapid, albeit diminished devolatilisation after 300 °C. This is due to the progressive loss of volatile matter in the hydrochars as reaction temperature was increased (Figure 11A), with the lighter volatile matter likely to be lost first. The delay in the onset of rapid devolatilisation has implications for the combustion behaviour of the hydrochars in industrial applications. Solid fuels with a high proportion of light-mass volatile matter and a rapid rate of devolatilisation, such as biomass, tend to ignite almost instantly upon exposure to high temperatures within a furnace¹⁴¹. The result of this is that, depending on the furnace design, the majority of combustion may occur very near to the fuel feed, potentially leading to hot-spotting and inadequate heat-transfer. The delayed onset and reduced rate of volatile release within the hydrochars implies a longer, more controlled burn than the untreated saltbush and other forms of biomass, particularly at 260 °C for 60 minutes. Under such HTC conditions, the main peak of the derivative was greatly reduced compared to the feedstock and other hydrochars, and is much broader. This suggests a much slower release of volatile matter over a greater period of time. Previous studies have attempted to utilise thermogravimetric analysis to elucidate the composition of various lignocellulosic biomasses¹⁴². To this end, the main peak has been associated with cellulose, and the distinctive “shoulder” on the unprocessed feedstock peak has been associated with the presence of hemicellulose. It is interesting to note, therefore, that this shoulder is not present in any of the hydrochars, save for 200 °C at 0 minutes, indicating that hemicellulose degrades extremely rapidly in the hydrothermal process. This is consistent with previous literature^{26,27}.

Ultimate analysis of the hydrochars compared to the unprocessed feedstock indicated that as absolute weight by weight percentages, carbon was enriched during HTC, while oxygen was removed (Figure 11B). Changes in carbon and oxygen content were very very common with increasing reaction severity, with almost every reaction condition producing statistically discreet groupings, and often in a clear step-wise progression (Supplementary Table 1). The mass percentage of carbon rose from 47.5% in unprocessed saltbush to a maximum of 69.5% after one hour at 260 °C. Meanwhile, oxygen as a mass percentage was more than halved, falling from 39% to just 18% under the same conditions. Such levels of carbon and oxygen compare very favourably with typical values observed for Victorian brown coals, indicating that the carbonisation process is altering the chemical composition of the hydrochars in a

similar fashion to coalification. These trends are well described in the literature^{32,93,120}. Sulphur made up a very small portion of both the untreated feedstock and hydrochars, and changed very little regardless of reaction severity, hovering around 1%. This is markedly lower than for typical values for brown coal, which can possess sulphur contents of up to 2.8%, almost three times greater⁹. This is very promising for the potential use of saltbush hydrochar as a coal replacement, as sulphur produces toxic sulphur dioxide upon combustion, which is a strictly regulated air pollutant under Australian law¹⁴³.

The elemental retentions (Figure 13) indicate that, while the total mass percentage of carbon increased across all reaction conditions, the carbon yield was actually more or less flat for most reaction conditions, with 260 °C leading to a greater loss of carbon after 30 minutes. The observed enrichment was due to the loss of hydrogen over all reaction conditions, and a

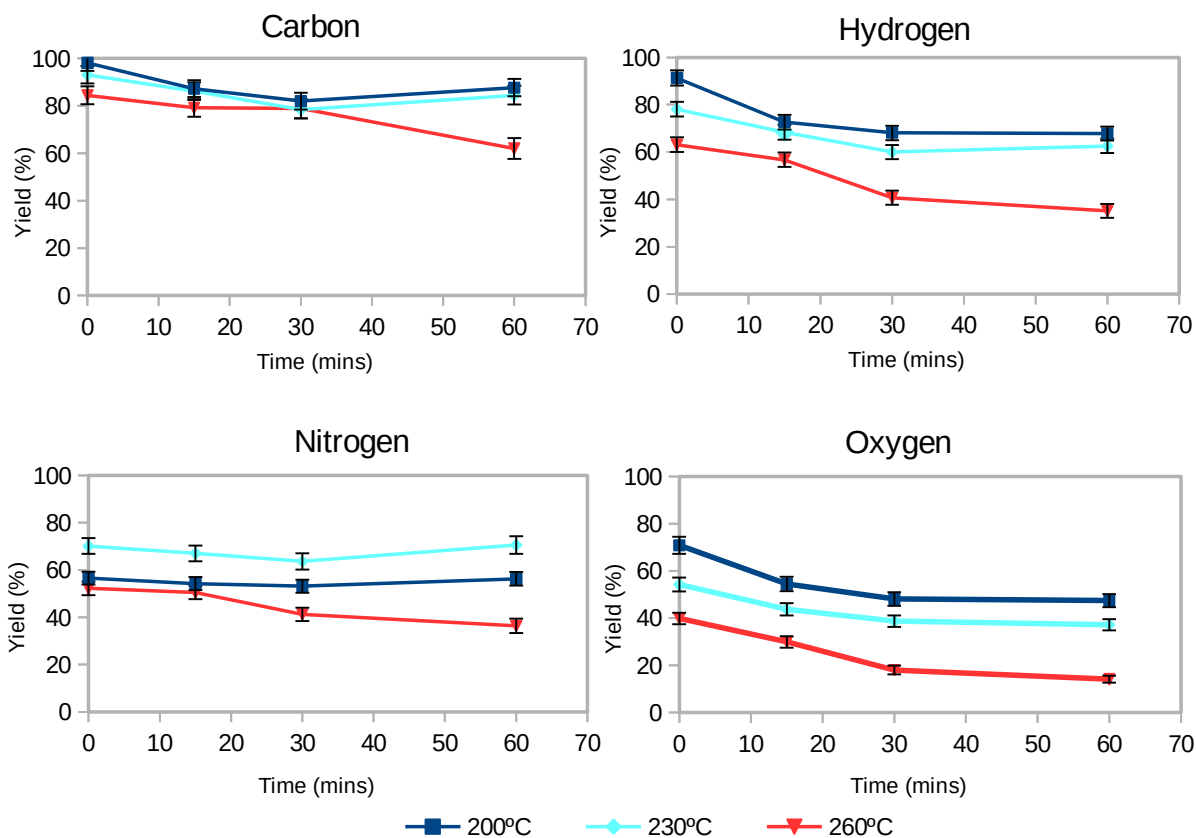


Figure 13: Retentions of Carbon, Hydrogen, Nitrogen and Oxygen within hydrochars at different temperatures (200 °C - 260 °C) and different isothermal holding times (0 min – 60 min). Error bars represent one standard deviation.

pronounced removal of oxygen, with oxygen retention falling by 84.1%. The removal of oxygen is an especially important function of HTC, as a reduced oxygen content within a solid fuel leads to an increase in higher heating value⁶. (Figure 10C)

The ultimate analysis can also be used to characterise and compare different varieties and grades of solid fuels by way of a Van Krevelen chart (Figure 14), which plots the ratios of hydrogen : carbon over oxygen : carbon, thereby visualising the profound chemical changes that occur during HTC.

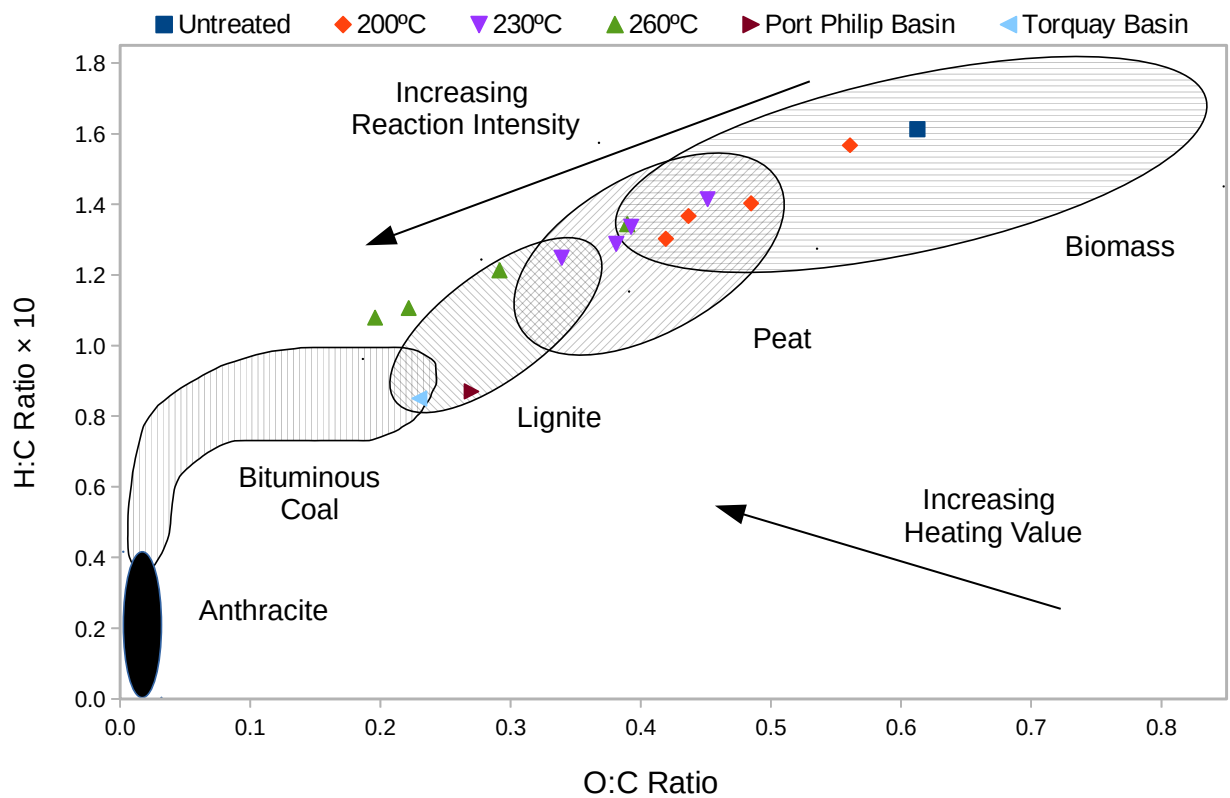


Figure 14: Van Krevelen Chart comparing the H:C and O:C ratios of untreated saltbush and hydrochars compared with Victorian Brown Coals⁹. Figure adapted from Trif-Tordai and Ionel, 2011²³⁰. Reaction holding time for each temperature is not shown, but rises linearly with increasing reaction intensity.

The H:C and O:C ratios for unprocessed saltbush fit completely within the typical range for biomass, while each sequential HTC condition acted to decrease the ratios. HTC at 200 °C

did not really enhance fuel beyond the biomass range, although at longer holding times the ratios began to move into the ranges shown in peat. The whole 230 °C reaction series fits entirely within the peat range, with the 60min treatment moving toward lignite values. The reaction condition of 260 °C for 0min produced a more enriched fuel than any of the 200 °C samples. Hydrochars produced in the most severe reaction conditions of 30 and 60 minutes at 260 °C possessed H:C and O:C ratios that began to surpass lignite, and enter the range seen for bituminous coal. These highest quality hydrochars compare very favourably to Victorian brown coals, although it is noteworthy that while they have comparable or even superior O:C ratios, they each tend to have higher H:C values. Similar trends have also been observed for HTC for other feedstocks^{25,32,93}. That these hydrochars, especially those produced under the most severe reaction conditions, so closely resemble fossil coal across so many parameters is encouraging, and as a proof of concept, it is clear that there is great potential for saltbush-derived hydrochars as a possible coal replacement.

The question of whether high levels of salt and other inorganics would lead to excessive levels of ash was addressed next. Previous studies of both woody and non-woody feedstocks have demonstrated that HTC is capable of reducing inorganic elements in the hydrochar^{43,130,144}, but it was unknown whether this would hold true for a high-salt, high-ash woody feedstock like saltbush. From the proximate analysis (Figure 11A), it was determined that there were only slight changes in the mass fraction of ash of the hydrochars after HTC. While HTC at any temperature produced a statistically significant change in the ash content compared to the untreated feedstock, that change as a weight by weight percentage of the hydrochars did not change dramatically over time or temperature, with the notable exception of 260 °C for 60 minutes, which elicited a significant reduction in ash (Supplementary Table 1). However, when the ash yield of the hydrochars over the course of the HTC reaction was determined (Figure 11C), it can be seen that all reaction conditions caused a drop in the total levels of ash. Reactions at 260 °C were particularly efficient at removing ash, with almost 80% removed after one hour.

On an individual elemental basis (Figure 15A), concentrations of the most important elements implicated in slagging and fouling (Na, Cl, Ca, K, S, P) were for the most part reduced,

some quite precipitously. Na and Cl in particular were greatly reduced, with sodium falling from around 1.4% in the untreated feedstock to 0.2% after one hour at 260 °C, while chloride fell by an entire order of magnitude, from 2% to 0.2% under the same conditions. At 200 °C and 230 °C, Ca is almost inert during hydrothermal treatment (Figure 15B), leading to an overall enrichment of Ca in hydrochars over time at these lower temperatures (Figure 15A). At 260 °C, however, Ca levels begin to fall, reducing to 62% after 60 minutes.

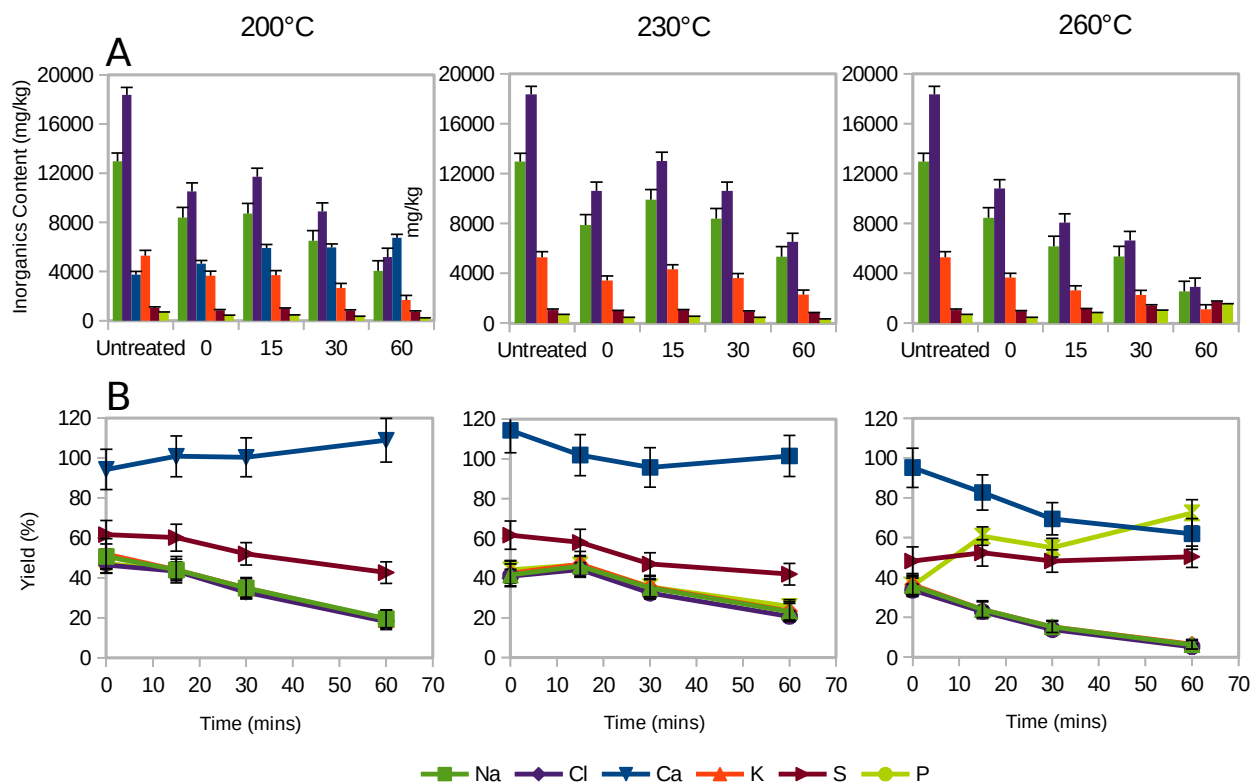


Figure 15: Elemental concentrations of Na, Cl, Ca, K, S and P in untreated saltbush and hydrochars at different temperatures (200 °C - 260 °C) and different isothermal holding times (0 min – 60 min). (A) w/w Concentration of inorganic elements in over time (minutes) at each reaction temperature. (B) Yields of inorganic elements over time at each reaction temperature. Error bars represent one standard deviation.

The rate at which Na, Cl and K were lost was almost identical within each temperature condition (Figure 15B), which suggests that the primary mechanism by which these elements are reduced was through the dissolution of water-soluble NaCl and KCl to the hydrothermal medium. Sulphur retention tended to lag behind the other elements, and was statistically

constant (Supplementary Table 1), which may be attributable to the fact that sulphur is predominantly found in proteins, which may be more likely to incorporate into the body of the hydrochar, instead of dissolving and degrading into the aqueous and gaseous phases¹⁴⁵. For all these elements, the rate of loss was fastest during the heat-up phase; for sulphur, the most recalcitrant of the diminishing inorganics, 40% of the starting sulphur content was removed during the roughly 8 minutes of heat-up time before the isothermal reaction time of 0 minutes was achieved. For the remaining hour of reaction time at any temperature, sulphur yield was statistically unchanged. Similar trends can be seen for Na, Cl and K; even at 260 °C, where inorganics were purged the most rapidly, the overwhelming majority of that removal occurred before the reaction temperature was even reached, with comparatively slower reductions occurring thereafter. During the 10 minute heat-up period, over 65% of Na, Cl and K were removed from the biomass. Over the next hour at 260 °C, further reductions totalled a mere 25% of the initial value. The reduction of these major slagging and fouling agents is of great importance for potential use as a combustible fuel.

Of particular note is the behaviour of phosphorus at 260 °C; in clear contrast to the other elements, as well as its own behaviour at 200 °C and 230 °C, phosphorus appears to be reabsorbed back into the hydrochar at higher temperatures over time. As with the lower temperature trials, phosphorus initially dropped to about 36% of the feedstock concentration after 0 minutes. Over the course of the next hour, however, the retention of phosphorus rose, until almost three quarters of the starting concentration had been restored. Phosphorus in solid fuels is a significant issue, as high concentrations can be highly deleterious to certain applications, such as steel making¹⁴⁶.

Studies on the HTC of microalgae and distillery grains have indicated that the principle form of phosphorous present in carbonising biomass is as water-soluble phosphates, which readily dissolve into the aqueous phase during the reaction^{145,147}. The enrichment of P may be a result of water-soluble P being reabsorbed back into the hydrochar after being initially purged. HTC hydrochars are known to become porous as a result of the hemicellulose within the feedstock fully degrading, leaving the lignocellulose superstructure partially intact, but riddled with micropores, with higher temperatures leading to greater porosity^{148,149}. It has been

suggested that this porosity allows the hydrochars to reabsorb inorganics, including P, back from the aqueous phase^{130,150}. Such a mechanism could account for the behaviour observed here; at lower temperatures, and at 0 minutes at 260 °C, the hydrochars may have been insufficiently porous to facilitate the reabsorption of P, and so P was lost to the aqueous phase. Over the course of the 260 °C reaction, however, the porosity of the hydrochars may have increased, thus allowing the absorbance of P.

Overall, HTC proved to be highly effective at removing most of the important ash-producing inorganic elements from saltbush, proving that the high salt content is no barrier to the potential of saltbush as a hydrothermal biomass feedstock candidate.

3.4 Conclusion

Australian saltbush was subjected to hydrothermal carbonisation at three temperatures and four holding times. Of these, it was determined that 30 and 60 minutes at 260 °C produced the highest quality fuel. Treatment under these conditions produced the hydrochars possessed of very similar higher heating values, volatile/fixed carbon ratios, oxygen content, and H/C and O/C ratios to high quality lignites and bituminous coals. The ash content of the feedstock was greatly reduced, with slagging and fouling salts purged from the hydrochars, with the interesting exception of phosphorous at the highest temperature. In this context, it can be concluded that saltbush has great promise as a potential feedstock for HTC.

3.5 Acknowledgments

This project was funded and supported by the Australian Research Council Centre of Excellence in Plant Cell Walls CE110001007. The authors would like to acknowledge Wilson Pastoral for supplying the dried saltbush material; John Gouzos of the Commonwealth Scientific and Industrial Research Institute (CSIRO), Land and Water Division, South Australia for performing the ICP-OES inorganic analysis; and Tony Hall of the University of Adelaide, Physical Sciences, for performing the CHNS analysis.

Chapter 4

Paper II

Biochemical Compositional and Kinetic Modelling of Hydrothermal Carbonisation of Australian Saltbush

Benjamin G. Keiller[†], Richard Muhlack[†], Rachel A. Burton[†], and Philip J. van Eyk^{ ‡}*

[†] School of Agriculture, Food and Wine, University of Adelaide, Waite Campus, Glen Osmond, SA 5064

[‡] School of Chemical Engineering and Advanced Materials, University of Adelaide, Adelaide, SA 5005

* Corresponding Author: philip.vaneyk@adelaide.edu.au

This manuscript was written with contributions from all authors. All authors have given approval to the final version of the manuscript

Statement of Authorship

Title of Paper	Biochemical Compositional Analysis and Kinetic Modeling of Hydrothermal Carbonisation of Australian Saltbush
Publication Status	<input checked="" type="checkbox"/> Published <input type="checkbox"/> Accepted for Publication <input type="checkbox"/> Submitted for Publication <input type="checkbox"/> Unpublished and Unsubmitted work written in manuscript style
Publication Details	Keiller, B. G., Muhlack, R., Burton, R. A. & van Eyk, P. J. Biochemical Compositional Analysis and Kinetic Modeling of Hydrothermal Carbonisation of Australian Saltbush. <i>Energy Fuels</i> (2019) doi:10.1021/acs.energyfuels.9b02931.

Principal Author

Name of Principal Author (Candidate)	Benjamin Keiller		
Contribution to the Paper	Conception, Analysis, Drafting		
Overall percentage (%)	70%		
Certification:	This paper reports on original research I conducted during the period of my Higher Degree by Research candidature and is not subject to any obligations or contractual agreements with a third party that would constrain its inclusion in this thesis. I am the primary author of this paper.		
Signature		Date	10.12.19

Co-Author Contributions

By signing the Statement of Authorship, each author certifies that:

- i. the candidate's stated contribution to the publication is accurate (as detailed above);
- ii. permission is granted for the candidate to include the publication in the thesis; and
- iii. the sum of all co-author contributions is equal to 100% less the candidate's stated contribution.

Name of Co-Author	Richard Muhlack		
Contribution to the Paper	Conception, Analysis, Drafting		
Signature		Date	10.12.2019

Name of Co-Author	Rachel A. Burton		
Contribution to the Paper	Conception, Analysis, Drafting		
Signature		Date	11/12/19

Hydrothermal Carbonisation of Novel Biomasses

Name of Co-Author	Philip J van Eyk		
Contribution to the Paper	Conception, Analysis, Drafting		
Signature		Date	13-01-20

4.0 Abstract

Hydrothermal Carbonisation (HTC) is the thermochemical conversion of biomass in sub-critical water to form an energy-enriched “hydrochar” as a renewable replacement for coal. Lignocellulosic biomass contains a variety of complex, interconnected biopolymers with very different physical and chemical structures, including hemicellulose, cellulose, lignin and protein. These differing structures lead to different rates of decomposition during the HTC reaction. Where previous studies have attempted to elucidate these various rates through the use of individual, purified model compounds, the complexity of whole biomass makes understanding these reactions in their natural state difficult. This present study offers a first step towards gaining a more thorough knowledge of the HTC reaction by accurately quantifying the degradation of hemicellulose, cellulose and lignin within whole biomass, and producing a simple kinetic and mechanistic model to describe this degradation. Australian saltbush was subjected to HTC at three temperatures (200 °C, 230 °C, 260 °C), and four residence times (0, 15, 30, 60 minutes). The resultant hydrochars were assayed for hemicellulose, cellulose, and lignin content, via HPLC, Updegraff assay, and acetyl bromide assay respectively. The degradation of each component was measured, and the reaction order n and key Arrhenius parameters reaction rate constant k , activation energy E_a , and the pre-exponential factor A_0 were calculated. It was found that hemicellulose degraded fastest ($n = 1$, $E_a = 61 \text{ kJ mol}^{-1}$), cellulose the slowest ($n = 0.5$, $E_a = 127 \text{ kJ mol}^{-1}$), and only a portion of lignin reacted ($n = 1$, $E_a = 66 \text{ kJ mol}^{-1}$), the remaining 22% being stable under HTC conditions.

4.1 Introduction

As global awareness of the risk climate change poses to modern civilization grows, greater efforts are being made to develop and adopt alternative energy sources to the polluting fossil fuels that currently underpin the global economy. Hydrothermal Carbonisation (HTC) of biomass offers one such alternative. By subjecting biomass to high temperature, high pressure subcritical water between 180 °C – 260 °C and 20 – 70 bar, a black, granular, porous char or “hydrochar” can be produced^{25,26}. Such hydrochars exhibit similar energy and compositional properties to fossil coal, meaning that hydrochar could potentially serve as a renewable

substitute for solid fuels in heating and electricity production, soil remediation and enrichment, and carbon sequestration^{32,120,121}.

While HTC is versatile enough to successfully convert a wide variety of different feedstock types, ranging from straw to wood to algae to biosolids and even mixed municipal waste, the most common HTC feedstock, and the most commonly used type of biomass¹⁵¹, is lignocellulosic biomass. Lignocellulose is a highly complex composite of biopolymers produced by plants in their cell walls in vast quantities across the world. It has been estimated that global production of cellulose is within the realm of 10^{11} to 1.5×10^{12} tonnes per annum^{64,152}, making lignocellulose the largest source of renewable carbon on the planet. HTC of lignocellulosic biomass therefore presents an extraordinary opportunity for renewable energy production, especially if sourced from feedstocks that do not compete directly with edible crop for space and water. One such feedstock may be native Australian saltbush, a diverse group of saline-tolerant plants within the *Atriplex* and *Enchylaena* geni, which range widely across a great variety of different habitats and ecological conditions within Australia. These plants thrive in low-water, high-salinity areas, have numerous synergistic human applications in agriculture and soil remediation, and has proven to be suitable for HTC treatment¹⁵³. However, there are still many unknowns about the process of HTC, especially with regard to the behaviour of lignocellulose during the carbonisation reaction.

Lignocellulose is comprised principally of three main biopolymers: cellulose, hemicellulose and lignin^{154,155}, of which the principle component (35 – 55% dry weight) is cellulose⁶³. Cellulose is a glucan, comprised of long chains of glucose moieties attached to one another via β -(1 \rightarrow 4) glycosidic bonds. These chains aggregate into a crystalline matrix to form long, insoluble fibrils that form the backbone of the plant cell wall¹⁵². These crystalline fibrils are entwined and enmeshed within a web of other, non-cellulosic polysaccharides that historically have been described with the catch-all term hemicellulose. Hemicelluloses are very structurally diverse compared to cellulose, and are made up from a wider variety of monosaccharide sugars beyond just glucose, such as xylose, arabinose, galactose, and mannose. The heterogeneity across hemicelluloses is considerable, and manifests in structure (branched vs unbranched chains), composition (glucans vs xyloglucans etc.), substitution (methylated vs unmethylated)

and other parameters^{156,157}. The third major component, lignin, is not sugar-based, but is instead a complex, highly disordered aromatic polymer. Lignin is comprised of three aromatic phenolic monomers, or monolignols: *p*-coumeryl alcohol, coniferyl alcohol, and sinapyl alcohol. These phenols migrate to the cell wall and undergo enzyme-catalysed radicalisation, followed by radical coupling and nucleophilic H₂O addition to form *p*-hydroxyphenyl (H), guaiacyl (G), and syrigyl (S) lignin subunits, which polymerise to form the lignin superstructure^{72,158}.

Across different types of biomass, there is considerable variation in the ratios of hemicellulose, cellulose and lignin^{93,159}, which likely impacts the properties of the resultant hydrochar after the biomass is processed via HTC. As a result, there has been much research into attempting to elucidate the changes that each of the primary lignocellulosic biopolymers undergoes during HTC. The carbohydrate monomers of both hemicellulose and cellulose are bound to one another via β -(1→4) or β -(1→3) glycosidic bonds, which are easily hydrolysable in acidic liquid media. Under hydrothermal conditions, excited water molecules become capable of auto-catalysing acidic reactions such as hydrolysis and decarboxylation, leading to the ready depolymerisation of carbohydrates²⁶. Hemicellulose has been described as the most susceptible to HTC^{26,27}. Studies utilising refined xylan as a model for hemicellulose have indicated that hydrochar mass yields are typically lower for xylan than for cellulose, lignin, or indeed whole biomass such as pine wood meal, at any given temperature^{160,161}. Cellulose by contrast appears to be more resistant. Pure crystalline cellulose has been demonstrated to be insoluble in water below 307 °C, above which the crystalline fibrils begin to soften and dissolve, until 340 °C where they completely dissolve within 15 minutes¹⁶². Such temperatures are well above the ranges required for the carbonisation reaction, so one might expect cellulose to be inert during HTC. However, numerous studies have demonstrated HTC of purified cellulose can produce hydrochar; Kim *et al.* obtained mass yields of 50.4% after performing HTC at 250 °C for 30 mins, while Kang *et al.* reported very similar mass yields after 20 hours at 265 °C, indicating that cellulose does indeed have some reactivity under HTC conditions. In contrast to the polysaccharides, lignin lacks the glycosidic bonds typical of carbohydrates, instead featuring a plethora of different types of crosslinks, such as β -O-4 and β -O-5 ether bonds and carbon-carbon β - β and β -5 bonds. As a result of these strong covalent linkages, lignin has been widely described as highly resistant or even inert under HTC conditions^{86,88,114}.

Despite a steadily growing body of literature on the effect of HTC on lignocellulose, most such studies have been focused on isolated, purified components, which exist in a very different chemical environment to reacting biomass. As a result, the behaviour of lignocellulose as it reacts within a naturalistic biomass environment is little understood. One study conducted on HTC of bagasse utilised compositional analysis to track the changes in lignocellulose content over time and temperature¹⁶³. Hemicellulose was found to be highly susceptible to degradation, completely disappearing after 10 minutes at 200 °C and just 3 minutes at 270 °C, while cellulose content declined to around 50% after 30 minutes at 200 °C, and was almost completely degraded after 20 minutes at 270 °C. The compositional techniques utilised in this study were not able to discern the levels of lignin as separate from the hydrochar product, nor were they able to determine the overall hemicellulose content, measuring just xylose and glucose levels. More refined and comprehensive analytical techniques are required to accurately track the changes in the feedstock during HTC. Should such techniques be applied to hydrochars produced via HTC, it would be possible to track the degradation of each lignocellulosic component over the course of the HTC reaction.

Related to the lack of information on the behaviour of lignocellulose during HTC is the poor understanding of the hydrothermal reaction mechanism and kinetics. Understanding the kinetics of the HTC reaction is essential for designing large scale larger scale reactors during any potential industrialisation of this technology, and intrinsically tied to the kinetics of a given reaction is the chemical mechanism. Furthermore, understanding the mechanisms and kinetics involved allows a prediction to be made as to how a given feedstock may respond to hydrothermal processing if the composition of that feedstock was known. Previous work on HTC kinetics has been focused on building simplified Arrhenius kinetic models, with some additional work looking to produce statistical (frequently factorial) models, as well as an attempt to computationally model the reaction in three-dimensional space⁹⁸. The advantage of the kinetic model approach over the other modeling systems is dramatically greater simplicity, at the cost of some depth of understanding. Many of the models presented in the literature boast quite close fits to their respective experimental data, suggesting that while such models are on their own unsuitable for full-scale applications, they offer a useful starting point towards further study. A common approach in HTC kinetics is to describe the solid product mass yields

using first order reaction models. This has been performed with tannins ($E_a = 91 \text{ kJ mol}^{-1}$), synthetic feces ($A_0 = 1.5 \times 10^7 \text{ min}^{-1}$, $E_a = 78 \text{ kJ mol}^{-1}$), and glucose ($A_0 = 7.7 \times 10^8 \text{ s}^{-1}$, $E_a = 114 \text{ kJ mol}^{-1}$)^{101,115,116}. Such models do little to reveal the underlying behaviour of the lignocellulosic components during HTC, however. Jatzwauck and Schumpe 2015 offered a mechanistic and kinetic model where the lignocellulosic components underwent a two-step degradation pathway, first degrading to soluble intermediates, which then either degrade further into gaseous and soluble byproducts, or recondense into solid hydrochar⁸³. Reza *et al.* 2013 proposed a different model, postulating that hemicellulose degrades to gas and soluble fractions, cellulose degrades to gas, liquid, and solid products, and lignin is inert¹⁰⁸. Through this model, both hemicellulose and cellulose were proposed to degrade via first order reactions (hemicellulose: $A_0 = 58.6 \times 10^5 \text{ s}^{-1}$, $E_a = 29 \text{ kJ mol}^{-1}$; cellulose: $A_0 = 8.2 \times 10^5 \text{ s}^{-1}$, $E_a = 77 \text{ kJ mol}^{-1}$). Notably, the activation energies for both hemicellulose and cellulose within biomass were determined to be dramatically lower than that for refined hemicellulose (135 kJ mol^{-1}) and cellulose ($E_a = 215 \text{ kJ mol}^{-1}$)^{26,113}, indicating that for kinetic and compositional studies to be accurate, they must be conducted using biomass. However, the Reza model merely estimated the changes in the hydrochars by using the compositional ratios in the untreated feedstock, and then adjusting them using a proposed mechanistic model and the HTC mass yield. An alternative approach, where the lignocellulosic compositions of both the feedstock and the resultant hydrochars are directly and accurately determined, and then used to derive a kinetic model, would offer greater certainty and understanding than current models which rely on compositional estimates.

The aim of this paper is therefore to develop methods of compositional analysis to accurately determine the lignocellulosic composition of biomass and hydrochars, and then utilise such methods to determine the degradation of each lignocellulosic component over the course of the HTC reaction in Australian saltbush, and then use this data to arrive at a kinetic model of the HTC reaction.

4.2 Methods and Materials

4.2.1 Hydrothermal Carbonisation

Saltbush feedstock (a mix of predominantly *Enchylaena tomentosa* and *Atriplex amnicola*) was supplied by Wilson Pastoral, South Australia. This mixed feedstock was ground and dried before HTC treatment. The HTC reaction was performed using a stainless steel custom-built reactor with an electronically heated fluidised bed (Techne, model: SBL-2D) as a heat source, according to previously published methods¹⁵³. In brief, a stainless steel reactor tube with an internal volume of 30mL, and equipped with a thermocouple, pressure transducer, safety valve and a pair of hand-operated ball valves, was filled to 80% maximum capacity with a biomass-water slurry with a 15% solids loading. The reactor was sealed, and gaseous oxygen within the reactor was purged with nitrogen, resulting in a completely nitrogenous reaction atmosphere. The reactor was then pressurised with nitrogen gas such that the calculated saturation pressure at a given reaction temperature was met or exceeded, and then the reactor was immersed in the fluidised bed. Upon completion of the run, the reactor was removed from the fluidised bed, and quenched in water. Reactions were performed at 200 °C, 230 °C and 260 °C, with residence times at reaction temperature of 0, 15, 30, and 60 minutes. These conditions have been commonly used in previous studies of the thermal properties of hydrochar, and are thus relevant for obtaining a greater understanding of the kinetics of HTC under likely industrial conditions^{89,93,130,164}. Residence time refers to the period of time the interior of the reactor spent at 98% or more of the desired reaction temperature. Thus, a residence time of 15 minutes indicates that the reactor was heated up to 98% of the desired reaction temperature over the course of several minutes, and held isothermally at that temperature for a further 15 minutes before quenching in water. A residence time of 0 minutes indicates that the reactor was heated to 98% of reaction temperature, and then immediately quenched. Owing to differences in the heating rate, due to factors such as ambient temperature, the total experimental time varied slightly between experiments. The HTC reaction condition of 200 °C, 30 minutes was repeated in quadruplicate, and used to estimate the error of the compositional analyses via a propagation of error analysis¹³⁸.

4.2.2 Compositional Analysis

Hemicellulose, cellulose, and lignin experiments were performed in duplicate, and the total error estimated via propagation of error analysis using the HTC error estimate.

Alcohol-Insoluble Residue (AIR) preparation

Samples were washed sequentially in organic solvents (described below) to remove the alcohol soluble components of the sample, thereby isolating the plant cell walls and the remnants thereof. 1 mL of solvent was added to 20-50 mg of dried, ground sample, vortexed thoroughly, and incubated at room temperature for one hour. The samples were centrifuged (10,000 g, 5 minutes), and the supernatant removed. The solvents and sequence used was 70% ethanol (twice), 100% ethanol (twice), acetone, and finally methanol. After the removal of the methanol, the tubes were dried overnight in a fumehood. The remaining pellet was weighed as AIR.

Hemicellulose

Hemicellulose content was determined via HPLC of acid-hydrolysed monosaccharides derivatised with 1-phenyl-3-methyl-5-pyrazoline (PMP)¹⁶⁵. Dried, ground biomass and hydrochars were hydrolysed in 1 M sulphuric acid (1 mL) for 3 hours at 100 °C, and centrifuged (23,000 g, 5 minutes). A 1 in 20 dilution of the supernatant (10 µL) was transferred to fresh tubes, along with 0.5 mM 2-deoxy glucose (10 µL), which acted as an internal standard. A solution of 0.5 M PMP in methanol (20 µL), as well as 1 M ammonium hydroxide (18.5 µL) were added to the tubes, which were vortexed, pulse spun, and incubated at 70 °C for 1 hour. The tubes were cooled, and 10 M formic acid (10 µL) was added. Excess PMP was removed by vigorously washing twice with dibutyl ether (1 mL), which was removed completely via vacuum centrifugation. PMP-derivatised monosaccharides were quantified via reverse-phase chromatography^{166,167}. Liquid Chromatography was performed using an Agilent 1100 Instrument (Agilent, Forest Hill, VIC, Australia), equipped with a quaternary pump, diode array detector (DAD), using gradient elution at a flowrate of 0.8 mL/min at 30 °C with a Kintex 2.5 µm C18 100×3mm 100A column. Three eluents were used: (A) 10% acetonitrile, 40 mM ammonium acetate (pH ~6.8), (B) 70% acetonitrile, and (C) 40 mM acetic acid. Initial conditions were 92% (A), 8% (B), 0% (C), which moved to 83% (A), 17% (B), 0% (C) over 9.5 minutes. The gradient

Hydrothermal Carbonisation of Novel Biomasses

shifted to 0% (A), 90% (B), 10% (C) over 30 seconds, and held for one minute. The gradient shifted again to 92% (A), 8% (B), 0% (C) over 50 seconds, and held for three minutes. UV absorbance was measured at 250 nm, and the concentration of PMP-derivatives was determined by comparing peak area and retention times to standard curves of xylose, arabinose, mannose, glucose and galactose.

Cellulose

The crystalline cellulose content was determined using a modified Updegraff method¹⁶⁸. In brief, 30mg samples were subjected to an AIR preparation, and boiled in a mixture (1 mL) of 2:8:1 water : glacial acetic acid : 70% nitric acid for 90 minutes, with the tubes gently mixed every 30 minutes. The tubes were cooled to room temperature, and centrifuged (16,000 g, 5 minutes). The supernatant was removed, and the pellets were washed sequentially in water, 80% ethanol (twice), and finally acetone, and the pellets were dried overnight at 60 °C. The crystalline cellulose content was determined by taking the mass difference between the pellet and the unprocessed sample.

Lignin

Lignin content was determined by acetyl bromide solubilisation¹⁶⁹. In brief, 5 mg of AIR was digested in 0.3 mL 25% acetyl bromide in glacial acetic acid at 70 °C for one hour, gently mixing the tubes every 10 minutes. The tubes were immediately cooled on ice, and while on ice, they were diluted with 1.5 mL glacial acetic acid. The tubes were centrifuged (1,400 g, 5 minutes), and 0.3 mL of the uppermost supernatant was transferred to new tubes. Volumes of 0.4 mL 2M NaOH and 0.3 mL freshly made 0.5 M hydroxylamine hydrochloride were added, and the mixture was mixed thoroughly. A 0.1 mL aliquot of the mixture was transferred to a quartz cuvette containing 0.9 mL glacial acetic acid, the dilution was mixed thoroughly, and the absorbance was immediately read at 280 nm on a Varian Cary 50 Bio UV-Vis photospectrometer. The lignin content was determined against a standard curve using TCI alkaline lignin (TCI L0082, CAS RN 8068-05-1) as the standard.

Protein

The nitrogen content of the hydrochars was determined using a Perkin Elmer 2400 series II CHNS analyser. The crude protein content was determined by multiplying the percentage nitrogen content by 6.25¹⁷⁰.

Fourier Transform Infrared spectroscopy (FTIR)

The overall diversity and relative quantity of various functional groups within the biomass and hydrochars were monitored on a Nicolet 6700 FTIR photospectrometer.

4.2.3 Kinetics Method

The degradation of the principle lignocellulosic components was modelled using Arrhenius kinetics, so as to gain an insight into the underlying mechanisms involved. The temperature profile of the HTC reaction was used with the Arrhenius equation to determine the rate constant k at each time and temperature (in 15 second intervals) during the reaction.

For a given, n^{th} order reaction:

$$\frac{-dc_t}{dt} = k_n c_t^n \quad (10)$$

Where:

c_t is the concentration of a particular biomass component in weight by weight percentage,

k is the temperature dependent reaction rate constant in joules per minute,

t is time in minutes,

n is the reaction order.

With an initial concentration of c_i and a concentration of c_t at time t , Equation 10 can be integrated and rearranged to give Equation 11 for a first order reaction:

$$c_t = c_i \exp(-kt) \quad (11)$$

And Equation 12 for a general n^{th} order reaction

$$c_t = \left(\frac{1}{kt \times (n-1)} + \frac{1}{c_i^{n-1}} \right)^{\frac{1}{n-1}} \quad (12)$$

The reactor setup utilised in this study required a starting heat-up period before reaching the final holding temperature, meaning that the temperature dependent reaction constant varied over time. To account for this, the reaction rate k was sequentially recalculated at each temperature point over 15 second intervals using the Arrhenius equation, as given in Equation 13:

$$k = A_0 \exp\left(\frac{-E_a}{RT}\right) \quad (13)$$

Where:

E_a is the activation energy in Joules,

R is the universal gas constant of $8.314 \text{ J mol}^{-1} \text{ K}^{-1}$,

A_0 is the pre-exponential factor,

T is the temperature in Kelvin

Because of this variance in k over the changes in temperature, the k value given here is the average k value across the holding time period, between 0 and 60 minutes, and does not include the initial heat up period. After quenching the reactor in water, the interior temperature of the reactor dropped at a maximum rate of $20 \text{ }^\circ\text{C sec}^{-1}$, meaning that the temperature fell below the lower limit for HTC reactions ($180 \text{ }^\circ\text{C}$) within seconds. As a result, the cooling rates were considered to have a negligible effect on the kinetics in this case.

Using the k thus found for each reaction temperature ($200 \text{ }^\circ\text{C}$, $230 \text{ }^\circ\text{C}$, $260 \text{ }^\circ\text{C}$), the activation energy E_a and pre-exponential factor A_0 were each calculated by minimising the square root of the sum of squares between the model and the experimental data using DEPS evolutionary algorithm in LibreOffice Solver. Models were produced with reaction orders from $n = 0.1$ to $n = 2$ in increments of 0.1 .

The principle metrics used to judge the goodness of the fit of the model were the minimised difference between the data and the model, as well as the coefficient of determination (r^2). Only data for those models having the best fit are reported.

4.3 Results and Discussion

A mixed sample of Australian saltbush was subjected to HTC at three reaction temperatures (200 °C, 230 °C, 260 °C) and four residence times (0 minutes, 15 minutes, 30 minutes, and 60 minutes).

4.3.1 Overall changes to feedstock during HTC

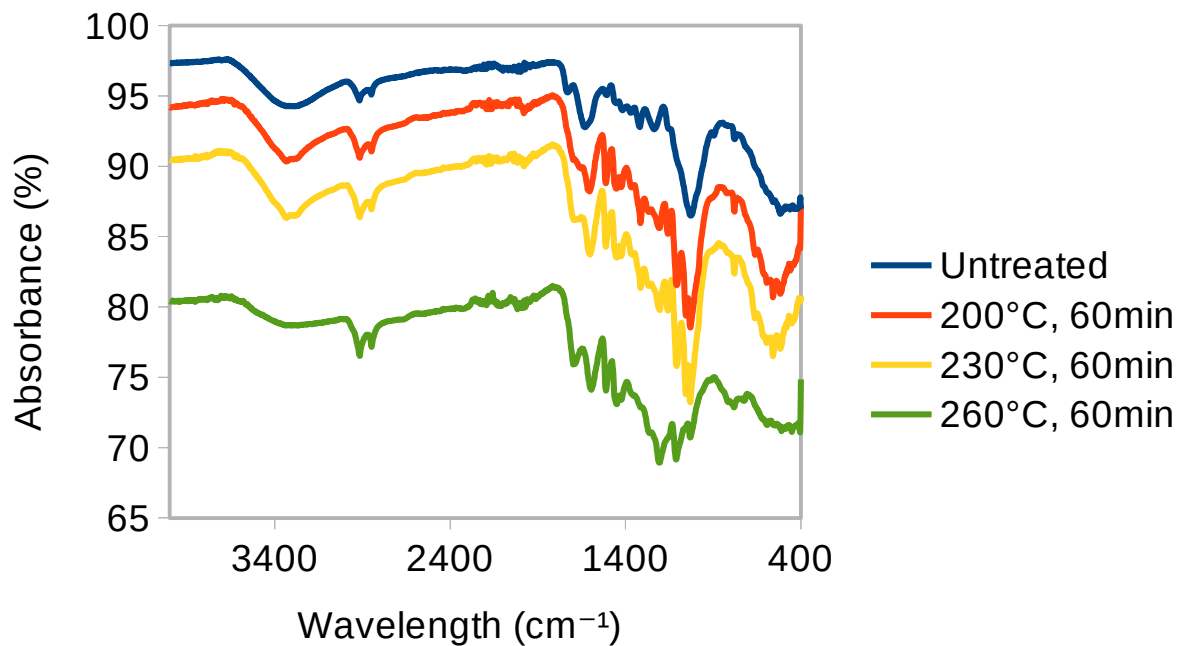


Figure 16: FTIR spectra of untreated saltbush and select hydrochars following HTC

Table 2: FTIR Resonances of untreated saltbush and hydrochars. *s*: Strong, *m*: Medium, *w*: Weak. *H*: Hemicellulose, *C*: Cellulose, *L*: Lignin, *Hy*: Hydrochar, *P*: Protein

Band	Peak Wavenumber (cm ⁻¹)	Functional group (Biopolymer) ¹⁷¹
1	3320 (<i>s</i> → <i>m</i>)	O-H stretching (H, C, L)
2	2920 (<i>m</i>)	Alkane C-H _n stretching (H, C)
3	2850 (<i>m</i>)	Aromatic C-H stretching (L)
4	1730 – 1698 (<i>w</i> → <i>m</i>)	(Aldehyde, ketone, carbonyl) C=O stretching (H, C)
5	1630 – 1596 (<i>m</i>)	Benzene aromatic stretching C=C (L)
6	1510 (<i>m</i>)	N-O or N-H (P)
7	1455 – 1425 (<i>w</i> → <i>m</i>)	Alcohol and Carboxylic acid O-H bending
8	1370 (<i>w</i>)	Aromatic O-H (L)
9	1315 (<i>w</i>)	Aromatic Ester C-O (L)
10	1270 – 1210 (<i>s</i>)	Ester C-O stretching (Hy)
11	1054 (<i>s</i>)	C-O-C stretching (aryl-alkyl ether linkage) (H, C, L)
12	1031 (<i>m</i>)	Primary alcohol C-O stretching and deforming (H, C, L)
13	896 – 663 (<i>w</i>)	Aromatic C-H bending (L)

To begin understanding the holistic changes that the biomass undergoes during HTC, the hydrochars were assayed using FTIR to determine the changes in functional groups (Figure 16, Table 2). The broad peak at 3320cm⁻¹ is characteristic of O-H stretching, and is prominent across all reaction conditions. Its diminishment with increased temperature is indicative of the loss of O-H groups as a result of the expulsion of water from the solid product, and the dehydration of the biopolymers. A single strong peak at 1031cm⁻¹ indicates that much of the O-H present exists as primary alcohols, which may be found in abundance in all major components of lignocellulose. This peak remains strong over 200 °C and 230 °C, and also begins to evolve numerous sub-peaks, possibly indicating the evolution of C-O ester bonds. At 260 °C, this large peak diminishes greatly, as do many of the new C-O ester peaks. C=O carbonyl groups (1730-1698cm⁻¹) are also reduced with increasing temperature, likely as a result of decarboxylation reactions of the cellulose, leading to the production of formic acid and CO₂²⁵. These reductions, combined with the shrinkage of the 3400cm⁻¹ peak, indicate a substantial loss of oxygen-containing functional groups, leading to an overall purging of oxygen from the

feedstock¹⁵³. The ability to remove oxygen from a given fuel is an important asset of HTC, and is partly responsible for boosting the higher-heating value of the hydrochar⁶.

A pair of small, yet sharply defined peaks at 2920 and 2850 indicate the presence of aliphatic (cellulose and hemicellulose) and aromatic C-H (lignin) respectively. Neither peak is greatly affected at any of the reaction conditions examined, suggesting that C-H bonds are quite resilient to HTC. Aromatic C-H bending may also be indicated by a collection of medium-strength signals in the 896-663 cm^{-1} region. The influence of lignin can also be discerned by the weak peaks at 1370 cm^{-1} and 1315 cm^{-1} , indicating the bending of phenolic O-H and aromatic C-O bonds respectively.

At 1510 cm^{-1} , a small peak in all reaction conditions indicates the presence of amide bonds in the untreated saltbush, and may also indicate N-O in the hydrochars. Such nitrogenous functional groups can be attributed to the presence of protein within the biomass.

In untreated saltbush, a weak double peak can be observed at 1455 – 1425 cm^{-1} , indicative of O-H bending in alcohol and carboxylic acids. This signal becomes slightly stronger in hydrochars, potentially indicating the formation of products such as oligo- and monosaccharides via the hydrolysis of the glycosidic bonds to form alcoholic and carboxylic acid terminal groups.

The strong peak appearing at 1054 cm^{-1} , present in all conditions except 260 °C, is indicative of C-O-C aryl-alkyl linkages between esters. Such bonds are associated with both glycosidic bonds and the coupling bonds of lignin, implying that lignocellulose is particularly rich in these linkages. The sharp decline in the linkage peak is therefore strong evidence of significant depolymerisation of lignocellulose at 260 °C.

Figure 17 shows the overall changes in the composition of saltbush over the HTC reaction. Untreated saltbush is comprised of up to 73% total lignocellulose, with protein (8%), ash (5%) and other non-lignocellulosic components (14%) making up the remainder. Total

lignocellulose declines progressively as HTC reaction severity increases, reaching a minimum of 23% after 60 minutes at 260 °C.

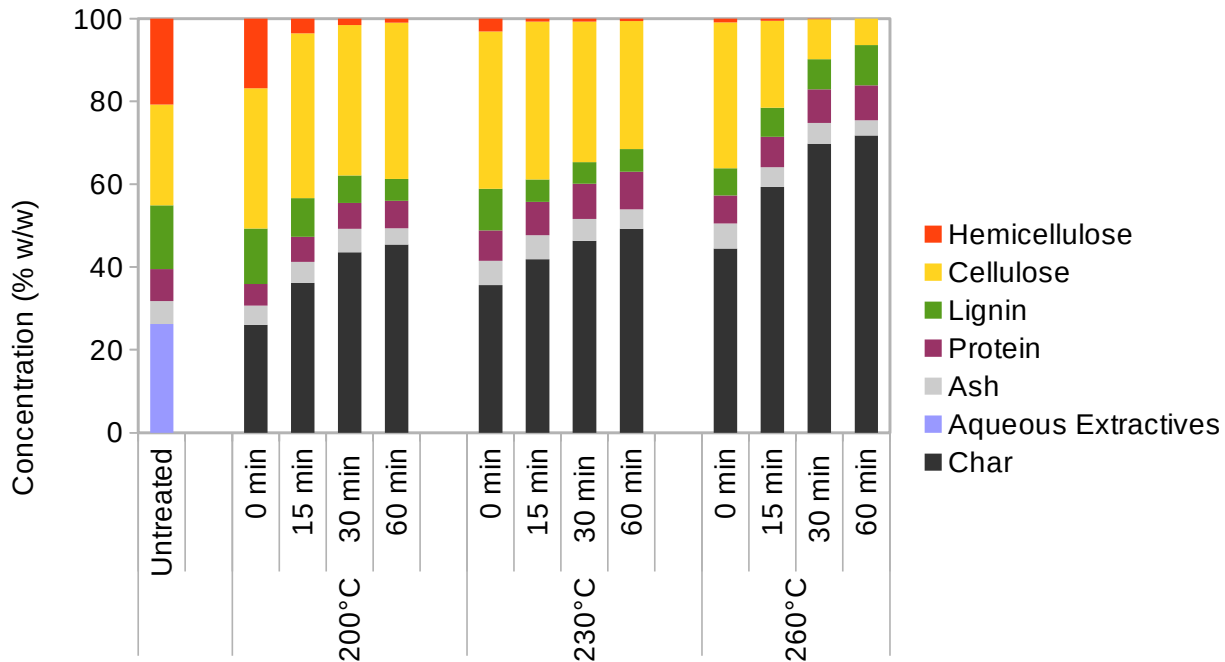


Figure 17: Total biochemical composition of untreated saltbush and hydrochars following HTC at different temperatures (200 °C – 260 °C) and different isothermal holding times (0 min – 60 min). Char and aqueous extractive portions calculated by difference.

Hemicellulose content was determined via the quantification of acid-soluble monosaccharides: mannose, ribose, rhamnose, glucose, galactose, xylose, arabinose, fucose, and the acidic residues glycosidic and galactosidic acid. The total hemicellulose content was calculated from the sum of all acid-soluble monosaccharide. Cellulose was quantified via a modified Updegraff acid-hydrolysis method, wherein all non-crystalline cellulosic material is removed via hot acid-hydrolysis, and the crystalline cellulose content is determined from the remainder on a weight by weight basis. The advantages of quantifying cellulose on a weight/weight basis as opposed to the traditional Updegraff method (where the crystalline cellulose is dissolved in anthrone in sulphuric acid after the hot acid hydrolysis and quantified via UV-absorption) include speed and simplicity.

Untreated saltbush contains 21% hemicellulose, 24% cellulose, and 15% lignin, which each decline to minima of almost 0%, 6% and 10% respectively. Ash content declined slightly from 5% to 3%, while protein content (or the nitrogenous remnants thereof) remains relatively constant between 9% and 6% across all reaction conditions.

Other non-lignocellulosic components of the biomass include such compounds as monomeric and oligomeric sugars, phenolic glycerides, alditols, aliphatic acids¹⁷², as well as nucleotides and lipids, all here collectively termed aqueous extractives. For the purposes of this model, these aqueous extractives are assumed to degrade instantly under HTC conditions.

The protein content in the untreated feedstock, and nitrogenous products in the hydrochars, was approximated by the multiplication of the nitrogen content of the samples by a protein conversion factor of 6.25¹⁷⁰. Due to the water-soluble nature of many proteins, it may be expected that protein content might follow a similar trajectory as that seen in the hemicellulose. However, this is not the case, with levels of reported nitrogen (indicative of protein) remaining relatively constant over time. At even slightly elevated temperatures, proteins readily denature. In this denatured state, they become highly insoluble and sticky, preventing their extrusion from the cell wall, and thus facilitating their incorporation into the mass of the hydrochar.

The char content, the carbonaceous product of the degradation of lignocellulose, was calculated by difference. As hemicellulose and the aqueous extractives degrade very rapidly, cellulose and hydrochar quickly establish themselves as the dominant components within the HTC samples; even by the relatively mild reaction conditions of 30 minutes at 200 °C, the hydrochars are already comprised of $\frac{1}{3}$ cellulose and $\frac{1}{3}$ char.

4.3.2 Biochemical Changes in HTC

The rate of reaction and activation energy of the degradation of each lignocellulosic component were modeled using Arrhenius kinetics. Further analysis into the precise reaction mechanism of each lignocellulosic component is beyond the scope of this project, and instead the behaviours of the individual components were estimated based on a simplified mechanistic

model, drawn from and building upon several points in the literature^{88,108}, and supported by the kinetic models. The models presented here had the best overall fit to the entirety of the dataset, across all temperatures and times for a given biochemical component. The simplicity of these models occasionally lead to low coefficients of determination (r^2) for individual temperatures, even though the overall fit across the bulk of the data was acceptable. As such, these models primarily offer insight into the mechanisms involved during the degradation of each component during HTC by describing the data as it is observed, as opposed to offering predictions about HTC behaviour.

Previous studies in the literature have identified two different principle kinds of solid product (Figure 18); the physically intact yet thermally converted remainder of non-hydrolysed biomass, called primary char. The second product is the result of a two-step reaction pathway wherein lignocellulose is degraded into soluble intermediates, which then undergo subsequent condensation and repolymerisation reactions to form carbonaceous microspheres, called secondary char, or “coke”^{84,85}.

The two components believed to become incorporated into the primary char, cellulose and lignin, were assumed to undergo two separate reaction pathways according to Trajano *et al.* 2013⁸⁸; Mechanism 1, which involves solid-solid conversion to carbonaceous char without the need for depolymerisation and solubilisation. Mechanism 2, by contrast, involved hydrolysis and depolymerisation into soluble intermediates, which then underwent repolymerisation reactions to form secondary char. Under HTC conditions in saltbush, it is assumed that Mechanism 2 is the favoured pathway. Cellulose was assumed to degrade via Mechanism 2 into monomeric glucose, which then underwent aromatisation and polymerisation reactions to become secondary char. Hemicellulose was assumed favour Mechanism 2, prefferentially degrading into its monosaccharide constituents, which in turn were converted to secondary char and gaseous products. So too were the other assorted non-lignocellulosic components of saltbush (lipids, phenolics, free sugars etc), here collectively termed aqueous extractives (AQ). Lignin, as detailed below, is believed to undergo both pathways, with a portion favouring Mechanism 1, and a portion favouring Mechanism 2 (Figure 18). It was experimentally determined that under HTC conditions 22% of the lignin is inert; this

was taken to imply that the temperatures and pressures involved in HTC are insufficient to activate Mechanism 1 in lignin. As a result, approximately 78% of lignin degrades and repolymerises via Mechanism 2, while the remainder remains intact and is incorporated directly into the primary char body.

The mechanistic model can therefore be summarised as Equations (14) – (18):

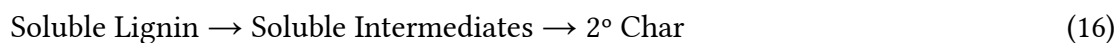
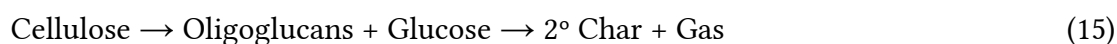


Table 3: Kinetic parameters for the degradation of lignocellulose during HTC. SSE: sum of squares error; k : Temperature-Dependent reaction rate constant; r^2 : Coefficient of determination; E_a : Activation energy; A_0 : Arrhenius constant. Rate constants presented are averages over the holding time at reaction temperature, not including warm-up time. Lignin refers exclusively to that portion of lignin that undergoes HTC degradation.

	Reaction Order (n)	SSE	200 °C		230 °C		260 °C		E_a (kJ mol ⁻¹)	A_0 (s ⁻¹)
			k (s ⁻¹)	r^2	k (s ⁻¹)	r^2	k (s ⁻¹)	r^2		
Hemicellulose	1	33	0.061	0.92	0.136	0.87	0.323	-0.27	61	3.1×10^5
Cellulose	0.5	49	0.009	0.30	0.048	0.81	0.290	0.98	127	8.8×10^{11}
Lignin	1	32	0.053	0.99	0.127	0.66	0.323	0.37	66	9.5×10^5

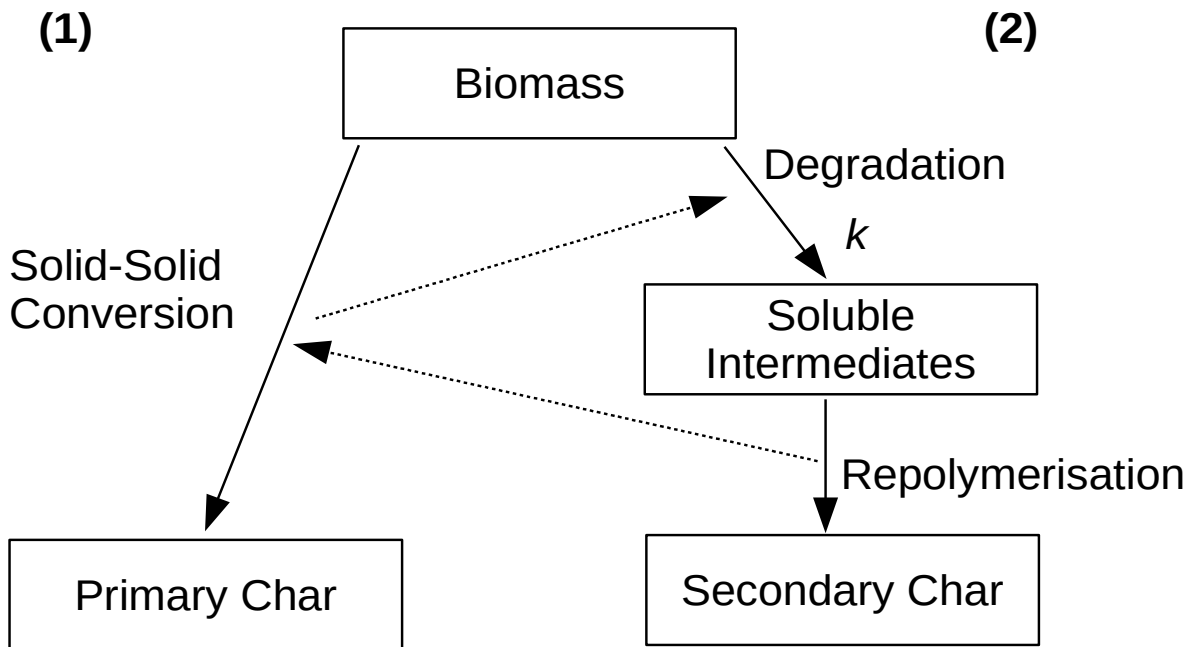


Figure 18: Model of lignocellulose degradation during HTC. Adapted and modified from Dinjus et al. 2011 and Karayıldırım et al. 2008^{85,86}. Dotted lines indicate the interconnectedness of the two mechanisms.

Figure 19A shows how hemicellulose is highly vulnerable to hydrothermal degradation. This is consistent with previous findings in the literature^{93,160,173}. The full determination of monosaccharides allows for a more detailed and accurate depiction of non-cellulosic polysaccharides in biomass than previous literature, which merely estimates the hemicellulose content from the sum of glucose and xylose amounts¹⁶³. The limitations of such estimation are made instantly clear upon the realisation that in saltbush, xylose and glucose account for a mere 41% of total non-cellulosic monosaccharides (Figure 19B). Total hemicellulose declines dramatically after even brief exposure to mild HTC; after only 15 minutes at 200 °C, total hemicellulose content has declined to just 12% of that of untreated saltbush. At higher temperatures, hemicellulose is almost entirely eliminated before the holding temperature has even been reached (Figure 19A). This is in large part because the chemical structure of hemicellulose leaves the β -(1→4) glycosidic linkages between monosaccharide subunits exposed to hydrolysis. Without the crystalline structure of cellulose or the heavily crosslinked, hydrophobic nature of lignin, hemicellulose cannot prevent water from accessing the glycosidic

bonds, which under hydrothermal conditions (starting at 200 °C) are capable of autocatalysing the hydrolytic cleavage of the linkage²⁶. Successive cleavages reduce the superstructure of hemicellulose to soluble fragments, greatly increasing the surface area exposed to attack, and thus accelerating the reaction, leading to the exponential loss of total hemicellulose observed.

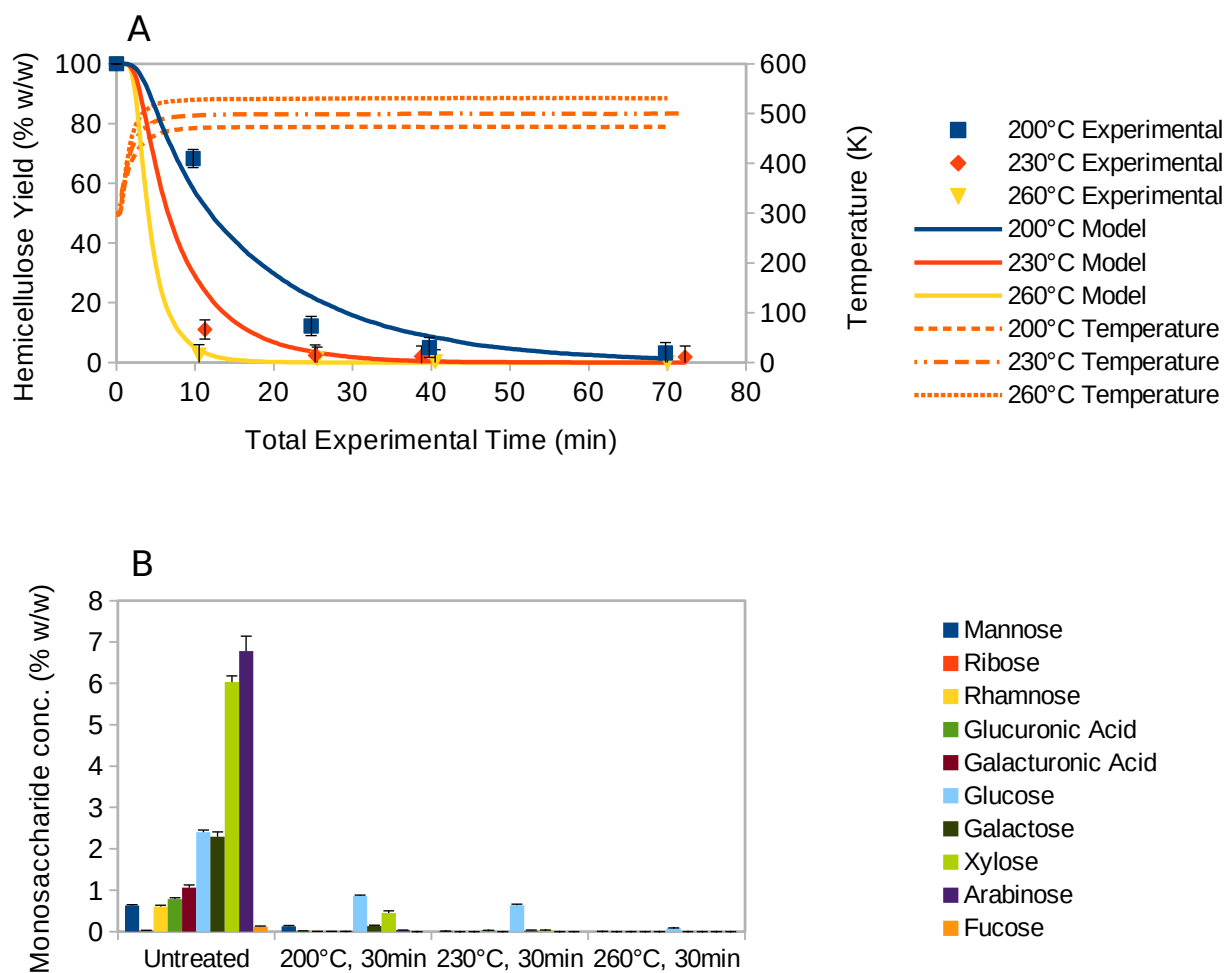


Figure 19: Degradation and first order Arrhenius kinetic modeling of hemicellulose within saltbush following HTC at different temperatures (200 °C – 260 °C) and different isothermal holding times (0 min – 60 min). (A) First order kinetic model. (B) Monosaccharide profile of untreated saltbush and selected hydrochars. Error bars represent a single standard deviation.

Comparing first and second order reaction models, the first order model is on the whole a closer fit than the second order model, with a minimised difference of 32.1 compared to 61.6.

This is further reflected in the coefficient of determination (r^2) values of the 200 °C and 230 °C temperature series, which are maximised for those temperatures under a first order model (Supplementary Table 1). The second order model for 260 °C, by contrast, has the highest r^2 of any reaction order for that temperature. The activation energy and pre-exponential factor of hemicellulose were determined to be respectively 66 kJ mol⁻¹ and 3.1×10^5 s⁻¹ (Table 3).

All monosaccharides decline heavily over HTC, with most sugars assayed fully depleted by 30 minutes at 230 °C. Glucose is the most apparently resistant sugar, persisting in tiny quantities even after 60 minutes at 260 °C, as were trace quantities of mannose and xylose. Glucose is not particularly thermostable in subcritical water, readily degrading into aromatic furfural and 5-hydroxymethyl furfural, as well as simpler molecules such as lactic, formic and acetic acid^{26,102}. One possible explanation of the observed higher “resistance” of glucose to HTC may be that all, or almost all, of the hemicellulosic glucose has in fact degraded completely, and the residual spike of glucose is actually cellulosic glucose that has been partly decrystallised

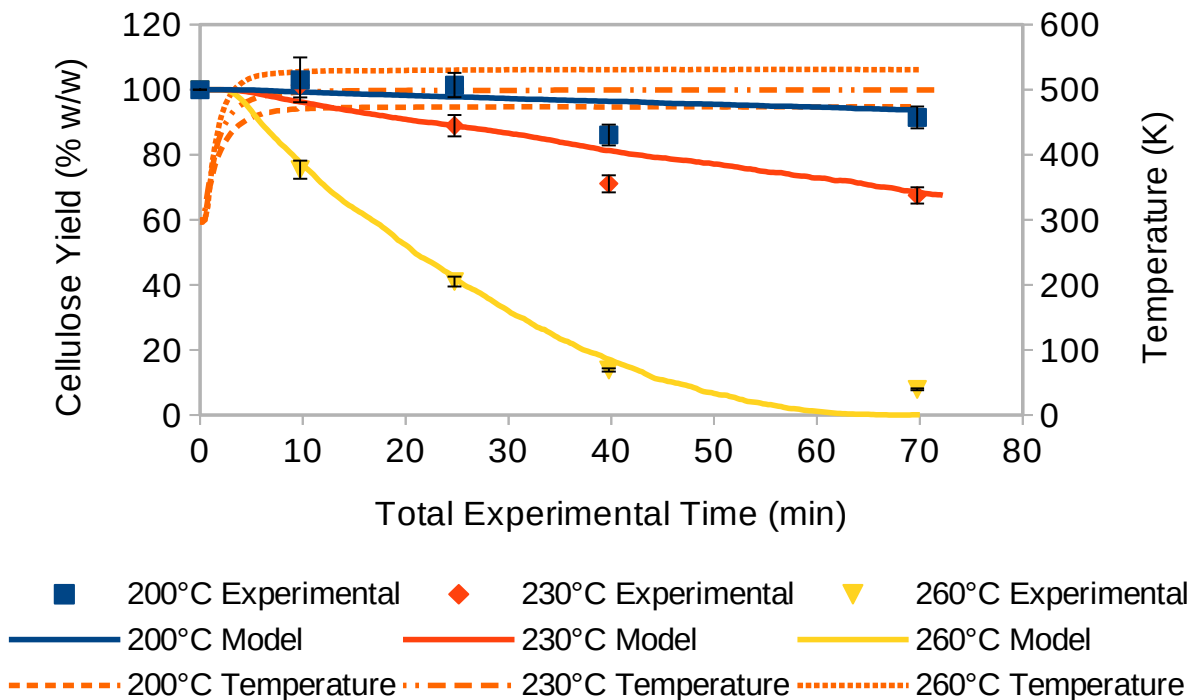


Figure 20: Degradation and 0.5th order Arrhenius kinetic modeling of cellulose within saltbush following HTC at different temperatures (200 °C – 260 °C) and different isothermal holding times (0 min – 60 min). Error bars represent a single standard deviation

and is therefore susceptible to the mild acid-hydrolysis used to release monosaccharides prior to quantification.

Figure 20 shows how cellulose proved to be markedly more resistant to hydrothermal degradation than hemicellulose, especially at 200 °C and 230 °C, again consistent with the literature^{93,161,173}. After 60 minutes at holding temperature, cellulose levels were reduced by a mere 11% and 33% respectively, compared to almost complete elimination under the same conditions for hemicellulose. It is only at 260 °C that pronounced degradation occurs, with only 8% of cellulose remaining after 60 minutes.

The high resistance of cellulose to hydrothermal degradation is due to its crystalline structure, which shields the glycosidic linkages between the glucose monomers from degradation. In contrast to hemicellulose, which typically exhibits α -(1→4) as well as β -(1→4) glycosidic linkages, cellulose exclusively utilises β -(1→4)⁶⁴. This changes the geometry of the polymer chain, conferring upon it two-fold screw axis geometry, which facilitates the formation of hydrogen bonds both within a given cellulose chain, and also particularly between chains. Such intermolecular hydrogen bonds allow multiple chains to neatly overlap one another. Repeated overlapping builds a regular, crystalline matrix that is highly hydrophobic and insoluble, thus excluding water from the superstructure⁶⁴. The consequences of this exclusion of water on hydrothermal degradation are twofold; the first is that because of the profoundly anhydrous environment in the interior of the crystalline microfibrils, hydrolysis cannot occur from within the structure, only from the outer surface. The second is that, because of the screw-axis geometry of the chains and the tight interlacing of the crystalline matrix, the β -(1→4) bonds on the outer surface of the microfibrils are still not very exposed to water, hence dramatically reducing the degree of cellulose degradation. This stability in subcritical water is well supported in the literature, especially with pure cellulose experiments^{26,160–162}. Deguchi *et al.* proposed that prior to hydrolysis, cellulose must undergo decrystallisation in order to expose the β -(1→4) bonds; such a mechanism would require an accompanying enthalpy of decrystallisation. It was thus determined that crystalline cellulose fibres were stable in subcritical water up to 307°C, above which the fibres begin to dissolve. In the current study, however, it is clear that cellulose displays only partial stability at 230 °C, and dissolves rapidly

above this. This apparent reduction in the energy required for degradation lends credence to the suggestion by Reza *et al.* 2013¹⁰⁸ that the chemical environment of hydrothermal carbonisation in biomass is radically different to that in pure component HTC, with the effect of reducing the energy requirements for reacting lignocellulose.

For the 200 °C and 230 °C series, the models attempted to fit a more or less linear relationship between residence time and cellulose degradation, while for the 260 °C series, the fit was exponential. The pseudo-linear model produced for the two cooler temperatures inflected very little across the different reaction orders tested, while the lower portion of the 260 °C model shifted dramatically between the reaction orders of 1, 2, and 0.5 (data not shown), the non-integer reaction order that produced the best fit between data and model. While the 0.5th reaction order produced the highest r^2 for both 230 °C and 260 °C (0.81 and 0.99 respectively), it led to a predicted level of cellulose two orders of magnitude lower than that which was experimentally determined. Across any reaction order tested, the 200 °C model consistently resulted in the poorest fit, with the r^2 ranging between 0.25 and 0.29 for the 0.5th, 1st and 2nd order reaction models (data not shown). While the sheer complexities of the interconnecting reactions that occur during HTC mean that any given kinetic model can only be an approximation at best, the fact that the model that gives the closest overall fit to the data (in terms of r^2 and minimised difference) is the 0.5th order model suggests that there could be multiple coinciding mechanisms involved with the degradation of cellulose. Using the 0.5th order model, the activation energy of cellulose was calculated to be 127 kJ mol⁻¹ respectively.

Compared to the literature, the activation energies of the two principle polysaccharides of lignocellulose were found to be much lower than those reported for pure feedstock experiments, and are much closer to, albeit slightly higher than, the values formulaically estimated for loblolly pine (Table 4). Given that hemicellulose degrades readily under the same conditions, it is unlikely that the observed stability of cellulose is due to an increase in the enthalpy of hydrolysis of the glycosidic linkages. Rather, the most likely explanation is that at 200 °C and 230 °C, there is insufficient energy to overcome the enthalpy of decrystallisation, while at 260 °C there is. This leads to much slower reaction times in the cooler temperatures as degradation can only occur on the surface of the crystalline fibrils, while at 260 °C, when the

fibril has been softened and the crystalline matrix disrupted, water can penetrate into the fibril and thus dramatically accelerate the rate of degradation.

Table 4: Published values for hemicellulose and cellulose in pure refined feedstock and biomass HTC experiments

	Saltbush (kJ mol ⁻¹)	Pure Feedstock (kJ mol ⁻¹)	Loblolly Pine (kJ mol ⁻¹)
Hemicellulose	66	135 ¹¹³	29 ¹⁰⁸
Cellulose	134 (1 st order) 127 (0.5 th order)	215 ²⁶	77 ¹⁰⁸

Figure 21 shows how, unlike hemicellulose and cellulose, instead of approaching zero, the lignin content approached a constant of 22%. Lignin content was measured by incubating the hydrochars in 25% acetyl bromide in glacial acetic acid and the dissolved lignin was quantified via UV absorption. The portion that did react demonstrated very similar behaviour to that of hemicellulose, with a significant amount lost during the heat up phase, especially at the higher temperatures; at 260 °C, lignin content had fully degraded to this constant level before even achieving the holding temperature.

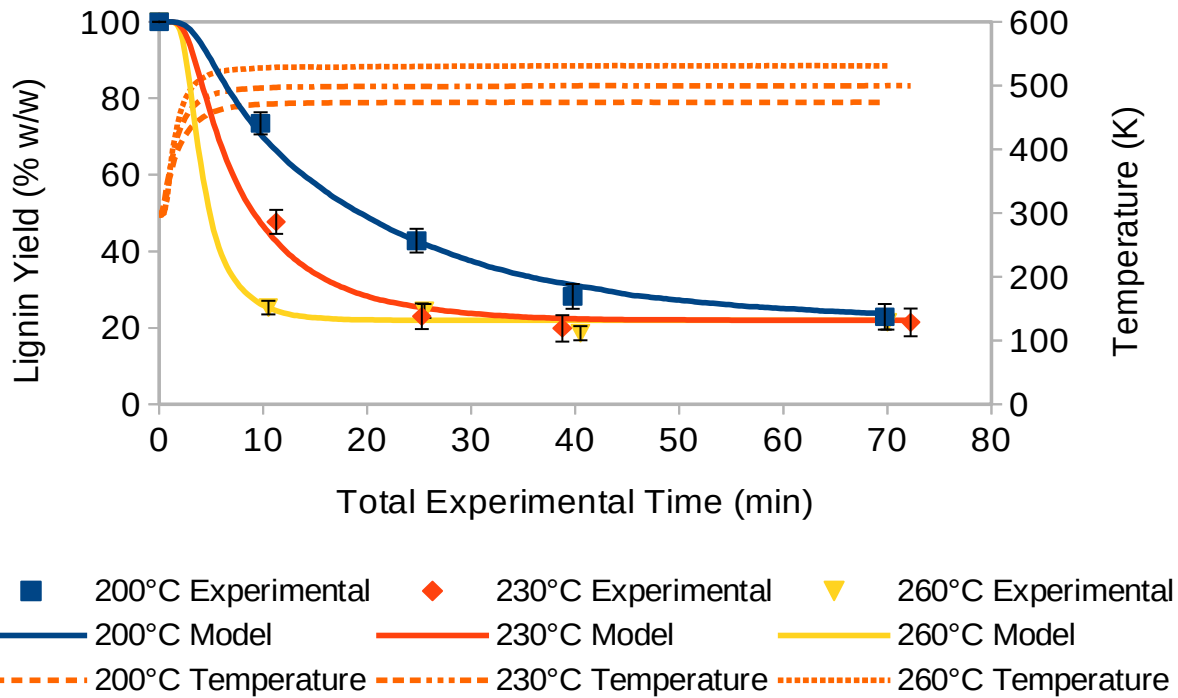


Figure 21: Degradation and first order Arrhenius kinetic modeling of lignin within saltbush following HTC at different temperatures (200 °C – 260 °C) and different isothermal holding times (0 min – 60 min). Error bars represent a single standard deviation.

The first order model for lignin produces a closer overall fit to the experimental data, judged by the minimised difference, of any biochemical component and model investigated here (Table 3). While certain non-integer reaction orders produce a closer fit for certain temperature series, such as 0.8 for 230 °C ($r^2=0.87$ vs 0.50), each of these produced dramatically higher minimised differences, and frequently produced negative r^2 values for the 260 °C series. Thus, it may be concluded that a pseudo-first order reaction model may be the most appropriate for lignin.

Interestingly the kinetic parameters given in the first order model for the reacting portion of lignin very closely match those of hemicellulose (Table 3), implying that they undergo a similar reaction mechanism. Dinjus *et al.* postulates that carbohydrates preferentially react via Mechanism 2, while lignin prefers Mechanism 1, with the assumption

that lignin hardly reacts during normal HTC conditions. This common assertion, that lignin is inert during HTC, is at odds with the data presently obtained.

Much of the current understanding of lignin HTC is derived from experiments utilising pure (kraft) lignin, the results of which are mixed. Some studies indicate that pure lignin is stable in subcritical water up to 260 °C^{114,160}, while others suggest that it does in fact react⁸⁸. However, as has been noted with cellulose, the chemical environment of reacting biomass has a profound effect on the reaction rate of the reacting component, reducing the energy required for degradation to occur. It appears that a similar phenomenon occurs with lignin. In particular, it has been suggested that interactions with the highly heterogeneous carbohydrate makeup of biomass have a pronounced effect on the solubility of lignin in HTC, facilitating its extraction. Lignin has been noted to undergo concurrent hydrolysis-depolymerisation and condensation-repolymerisation reactions during HTC. Lignin is usually a solid-phase reactant, but undergoes numerous phase changes over the course of HTC, passing through “glassy” and “rubbery” transition states, followed by coalescence, migration, and finally extrusion through the cell wall⁸⁸. In a study investigating the fate of the different monolignol subunits after HTC, it was found that guaiacyl subunits were more prevalent in the HTC liquor than other types of monolignols⁸⁸. This is despite the fact that guaiacyl subunits have a higher capacity than other monolignols for cross-linkages both within the greater lignin body, as well as to polysaccharides in hemicellulose. Such a propensity ought to facilitate both resistance to hydrolysis as well as promote condensation reactions, and thus one would therefore expect guaiacyl lignin to be the most stable under HTC, but in fact the opposite is observed. Trajano *et al.* concluded that the greater crosslinking of guaiacyl and syringyl lignin subunits alters and abets the reactivity of lignin as a whole under HTC conditions⁸⁸.

The fact that lignin degrades to a constant, rather than to elimination, suggests that lignin itself may undergo both mechanisms simultaneously. It is possible that a portion of the lignin undergoes Mechanism 2 via hydrolysis of the β -O-4 or β -O-5 ether bonds between monolignol subunits, while other portions crosslinked by β - β or β -5 bonds are resistant to hydrolysis, and thus preferentially follow solid-solid conversion as in Mechanism 1. Under the conditions used here, it is possible that Mechanism 1 occurs slowly, if at all. As a result of this,

the lignin capable of undergoing Mechanism 2 degrades readily, leaving only the portion of HTC-stable lignin as a remainder.

As a means of tracking the changes that take place within biomass over the course of the HTC reaction, the techniques presented here offer a significant advantage over previous methods in the depth and precision they can provide. It is now possible to directly and accurately measure the degradation of each major biochemical constituent of lignocellulosic biomass, independently of all the others. In particular, the ability to determine with accuracy the levels of lignin in biomass and hydrochar is a tremendous benefit, and one which has proved elusive and difficult until now. In finally being able to reliably measure the primary components of biomass during HTC, it is now possible in the future to develop more elaborate mechanistic and kinetic models that include such additional factors as chain fragmentation and population balances, such that a more complete view of the complexities of HTC can be elucidated.

4.4 Conclusions

Hydrochars formed from the hydrothermal carbonisation of Australian saltbush were subjected to rigorous biochemical compositional analysis followed by kinetic modeling to ascertain and quantify the changes in lignocellulose over the course of the hydrothermal reaction. It was determined that hemicellulose was the most susceptible to hydrothermal degradation ($n = 1$, $E_a = 66 \text{ kJ mol}^{-1}$), while cellulose was the most resistant ($n = 0.5$, $E_a = 127 \text{ kJ mol}^{-1}$). Hydrothermally active lignin demonstrated similar reactivity to hemicellulose ($n = 1$, $E_a = 61 \text{ kJ mol}^{-1}$), although a fifth of the lignin proved to be inert under HTC conditions. It is hoped that the techniques developed and presented here can serve as universal standards for compositional and kinetic analysis of lignocellulosic hydrochars. Moving into the future, these techniques will be used to analyse the biochemical changes of different kinds of biomass, lignocellulosic and not, to ascertain how different biomass compositions affect the process and products of the HTC reaction. Such additional knowledge will allow for the construction of more detailed and complex mechanistic and kinetic models that more finely reflect the realities of hydrothermal carbonisation.

4.5 Acknowledgments

This project was funded and supported by the Australian Research Council Centre of Excellence in Plant Cell Walls CE110001007. B. Keiller acknowledges the Australian Federal Government for providing a Research Training Scholarship. The authors would like to acknowledge Jelle Lahnstein and Andrea Matros for their invaluable assistance in designing cellulose and lignin assay methods.

Chapter 5

Paper III

Biochemical Compositional and Kinetic Modelling of Hydrothermal Carbonisation of Hemp

Benjamin G. Keiller[†], Matthew Potter[‡], Rachel A. Burton[†], and Philip J. van Eyk^{ ‡}*

[†] School of Agriculture, Food and Wine, University of Adelaide, Waite Campus, Glen Osmond, SA 5064

[‡] School of Chemical Engineering and Advanced Materials, University of Adelaide, Adelaide, SA 5005


* Corresponding Author

This manuscript was written with contributions from all authors. All authors have given approval to the final version of the manuscript

Statement of Authorship

Title of Paper	Biochemical Compositional Analysis and Kinetic Modelling of Hydrothermal Carbonisation of Hemp
Publication Status	<input type="checkbox"/> Published <input type="checkbox"/> Accepted for Publication <input type="checkbox"/> Submitted for Publication <input checked="" type="checkbox"/> Unpublished and Unsubmitted work written in manuscript style
Publication Details	N/A

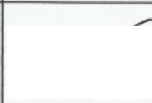
Principal Author


Name of Principal Author (Candidate)	Benjamin Keiller
Contribution to the Paper	Conception, Analysis, Drafting
Overall percentage (%)	70%
Certification:	This paper reports on original research I conducted during the period of my Higher Degree by Research candidature and is not subject to any obligations or contractual agreements with a third party that would constrain its inclusion in this thesis. I am the primary author of this paper.
Signature	 Date 10.12.19

Co-Author Contributions

By signing the Statement of Authorship, each author certifies that:

- i. the candidate's stated contribution to the publication is accurate (as detailed above);
- ii. permission is granted for the candidate to include the publication in the thesis; and
- iii. the sum of all co-author contributions is equal to 100% less the candidate's stated contribution.

Name of Co-Author	Matthew Potter
Contribution to the Paper	Analysis, Drafting
Signature	 Date 07 / 12 / 2019

Name of Co-Author	Rachel A. Burton
Contribution to the Paper	Conception, Drafting
Signature	 Date 11/12/19

Hydrothermal Carbonisation of Novel Biomasses

Name of Co-Author	Philip J van Eyk		
Contribution to the Paper	Conception, Analysis, Drafting		
Signature		Date	13-01-20

5.0 Abstract

Hydrothermal carbonisation (HTC) is a technology used to convert biomass and other feedstocks into a high-energy “hydrochar” with numerous potential applications in solid fuels, activated carbons, and carbon sequestration, among others. The conversion of lignocellulosic biomasses involves a complex, interconnected set of reactions that result in the breakdown of hemicellulose, cellulose and lignin, the precise mechanisms and kinetics of which are at present poorly understood. Hemp stem and seed hulls are subjected to HTC at three temperatures (200 °C, 230 °C, 260 °C), and four residence times (0, 15, 30, 60 minutes), and the hydrochars produced were analysed for hemicellulose, cellulose and lignin content. The degradation for each macromolecule was characterised using Arrhenius kinetics, and it was found that hemicellulose degraded rapidly with a 1.3rd order reaction ($E_a^{\text{Stem}} = 58 \text{ kJ mol}^{-1}$, $E_a^{\text{Hull}} = 67 \text{ kJ mol}^{-1}$), while cellulose degraded more slowly ($E_a^{\text{Stem}} = 113 \text{ kJ mol}^{-1}$, $n = 1.0$, $E_a^{\text{Hull}} = 112 \text{ kJ mol}^{-1}$, $n = 1.5$). A portion of lignin in each hemp tissue was found to be inert under HTC conditions; Hull lignin degraded rapidly to a constant level of 31% in a first order reaction ($E_a = 22 \text{ kJ mol}^{-1}$), while two models were built describing stem lignin, one with an assumed inert portion of 34% ($E_a = 98 \text{ kJ mol}^{-1}$, $n = 1.0$), and another with an assumed inert portion of 21% ($E_a = 81 \text{ kJ mol}^{-1}$, $n = 2.0$).

5.1 Introduction

Hydrothermal carbonisation is a thermochemical process wherein biomass is treated at high temperature with water at between 180 °C to 260 °C and at pressures between 5 MPa to 7 MPa^{25,27,32,93,120}. Exposure to such conditions trigger the breakdown and degradation of the biochemical constituents of the biomass, including hemicellulose, cellulose and lignin, thereby converting the biomass into a black, porous char. Such chars, or “hydrochars”, exhibit heightened fuel properties, such as an increased higher heating value, reduced oxygen content, and lower ash content, often closely approximating or bettering those of fossil coal^{32,153}. HTC therefore has a lot of potential as a means for producing biofuel. However, there is much that remains poorly understood particularly regarding the mechanism and kinetics of the carbonisation process.

Much of the difficulty in investigating the mechanics of the HTC reaction is the sheer complexity of the process. The carbonisation process is the result of many different reactions occurring concurrently, including, but not limited to, hydrolysis, decarboxylation, dehydration, condensation, repolymerisation, and aromatisation²⁵. Each of the three principle components of biomass, hemicellulose, cellulose and lignin, are chemically and structurally distinct, and accordingly behave very differently under HTC conditions. Cellulose is the main component of biomass, typically making up 35% to 55% dry weight of many plant tissues⁶³, and is constructed of long chains of glucose moieties joined to one another via β -(1 \rightarrow 4) glycosidic bonds. These chains then aggregate together into tough, insoluble crystalline fibrils that make up the backbone of the plant cell wall. Enclosed within the crystalline matrix, the glycosidic linkages of cellulose are protected from hydrolysis by the hydrophobic nature of the fibrils and thus cellulose is the slowest reacting component of biomass^{26,162}. Non-cellulosic polysaccharides, frequently referred to under the broad term hemicellulose, are a diverse class of sugar polymers that form an interlocking web around the cellulose fibrils, and are much more structurally variable than the comparatively simple cellulose. Due to lack of a protective crystal structure, the glycosidic linkages of hemicellulose are completely exposed to the sub-critical water molecules, and thus undergo hydrolysis readily. Hemicellulose, accordingly, is widely reported to be the fastest reacting component of lignocellulose, frequently degrading completely within minutes^{26,27,160}. Lignin, in contrast to the other two lignocellulosic components, is not a saccharide, but is instead a highly disordered aromatic polymer produced primarily in the secondary cell wall, where it performs functions related to the structural reinforcement of the cell wall. Lignin synthesis is deeply intricate and flexible¹⁵⁸, and results in a chaotic network of crosslinks within lignin itself, as well as to other parts of the plant cell wall, particularly hemicellulose. The manner in which lignin behaves during HTC is therefore very complex, with some authors stating that lignin undergoes numerous phase changes within the plant cell wall^{86,88}, while others state that it undergoes degrees of hydrolysis to form various aromatic aldehydes¹⁰⁰, while yet others claim that lignin is highly resistant or even inert under HTC conditions^{86,88,114}. However, almost all current knowledge of the mechanisms of HTC of biomass come from studies utilising single, purified model compounds as reaction feedstocks. There is very little information about how these compounds actually behave in whole biomass, or even if the present understanding is a representative model for whole biomass.

Understanding the mechanisms of the HTC reaction is important because it will help to inform the reaction kinetics, which are in turn essential to understand because they impact the design and operation of the production reactors as one scales up from the lab bench to industry. Therefore, in order to truly understand the mechanics and hence kinetics of HTC, compositional analysis must be performed on whole biomass. Such evaluation has been previously performed on Australian saltbush, where it was found that the activation energies for all major biochemical components was notably lower in whole biomass compared to the model compound studies¹⁷⁴. Hemicellulose degraded extremely rapidly, while cellulose was more resistant, as expected. What was surprising, however, was that lignin was found to be only partially susceptible to hydrothermal degradation, with 22% of the lignin being inert up to 60 minutes at 260 °C. The portion of lignin which did degrade did so with almost identical reaction kinetics to hemicellulose. It is apparent that the chemical environment within whole biomass profoundly affects the manner in which lignocellulose degrades during HTC, and it stands to reason that the finer variations in the compositions of different biomasses play a role in influencing the reaction. To further this understanding, HTC of different biomasses must be compared.

Hemp (*Cannabis sativa*) is a perennial plant with a very long history of human usage for its fibre and seed. Hemp products are highly versatile, and have found uses in textiles, paper, building insulation, biocomposites, plastics, paints, food additives, dietary supplements, cosmetics, and many others besides¹⁷⁵⁻¹⁷⁸. It is highly productive, and may be planted at high densities, resulting in potential annual fibre and seed yields of 7000 kg/ha and almost 900kg/ha respectively¹⁷⁹. As a result of its flexible and productive nature, industrial hemp usage (defined as hemp containing low levels of psychoactive THC; lower than 0.5 – 1% depending on the jurisdiction^{180,181}) has been growing very rapidly as ever more countries and local governments decriminalise its application. In 2017, the South Australian Parliament legalised the use of hemp for industrial purposes, ushering in a brand new industry in the state¹⁸⁰. With large amounts of waste products anticipated, especially waste fibre and the hulls of the seeds, it is prudent to begin considering options for sustainably treating and upcycling these waste streams into useful products. One option for doing so is hydrothermal carbonisation.

As such, in order to investigate the fuel capacities of hemp hydrochar as well as gain a broader and deeper understanding of the HTC process, The research reported this paper had the following broad aim: to subject hemp stem and seed hull to hydrothermal carbonisation, to determine the chemical and compositional changes in the feedstock during the HTC process, and from this determine the kinetics and mechanism of the HTC reaction.

5.2 Methods and Materials

5.2.1 Hydrothermal Carbonisation

Hemp stems were supplied by the South Australian Research and Development Institute (SARDI) and seed hulls were supplied by Hemp Foods Australia. These fractions were finely milled in a knife mill, and the 400 – 750 µm size fraction was taken. Prior to experiments, the feedstocks were dried in an oven for 24 hours at 105 °C. The HTC reaction took place in a custom-built batch reactor, according to previously published methods^{10,153,174} with the following modifications: a larger stainless steel reactor was used, with a wall thickness of 3 mm and a total volume of 50 mL; dried hemp fractions were mixed with deionised water to produce a slurry (25 g total weight) with a 10% solids content and added to the reactor. The reactor was sealed, pressurised and heated in line with the published methods¹⁵³. In brief, the interior atmosphere of the reactor was purged of oxygen, and the reactor was heated in a fluidised bed. At the conclusion of reaction time, the reactor was removed from the bed and quenched in water.

HTC reactions were performed at three reaction temperatures (200 °C, 230 °C, 260 °C) and four residence times (0 min, 15 min, 30 min, 60 min), wherein residence time refers to the time when the interior temperature of the reactor reaches 98% of the given reaction temperature. Thus, 0 minutes at 200 °C refers to an instance where the reactor was heated to 198 °C and then immediately quenched in water. All experiments were performed in duplicate.

The solid, liquid and gas yields of the HTC reaction were recorded. To determine the gas yield, the change in mass of the reactor before and after the reactor was vented to exhaust was calculated using Equation 19:

$$\text{Gas Yield (\%)} = \frac{(m_{AR} - m_{PV}) - (m_{N_2} - m_i)}{m} \quad (19)$$

Where m is defined as the dry mass of the untreated hemp feedstock, m_i is the initial mass of the dry, empty reactor, m_{N_2} is the mass of the reactor after pressurising with nitrogen pre-reaction, m_{AR} is the mass of the reactor post-reaction, and m_{PV} is the mass of the reactor after venting to exhaust.

The solid yield is the yield of the dried solid hydrochar product. The solid fraction of the reaction products was separated from the liquid fraction via vacuum filtration using two filter papers. The bulk of the hydrochar was collected on the first filter paper, unwashed. This portion of the hydrochar was used for compositional analysis. The remaining hydrochar portion stuck to the walls of the reactor was rinsed off with water onto the second filter paper. This rinsed portion, due to the possibility of water contamination of the ash yield, was used only to calculate the final total solid yield, and then discarded. Total solid (hydrochar) yield was thus calculated from Equation 20.

$$\text{Solid Yield (\%)} = \frac{(m_{P1} - m_{P1+S}) - (m_{P2} - m_{P2+S})}{m} \quad (20)$$

where m is the dry mass of the untreated feedstock, m_{P1} and m_{P2} are respectively the masses of the first and second filter papers, and m_{P1+S} and m_{P2+S} are the combined masses of the two filter papers and the washed and unwashed hydrochar portions.

The liquid yield was calculated from the percentage difference between the gas and solid yields from the total, as shown in Equation 21.

$$\text{Liquid Yield (\%)} = 1 - \text{Gas Yield (\%)} - \text{Solid Yield (\%)} \quad (21)$$

5.2.2 Compositional Analysis

Hemicellulose, cellulose, lignin, and protein content were determined as described in Chapter 4 (Keiller *et al.*, (2019)¹⁷⁴. The methods here have been given in brief. All experiments were performed in duplicate, and for the calculation of the yields of hemicellulose, cellulose and lignin, the total error was estimated via error propagation with the mass error estimate of the HTC mass yield¹³⁸.

Hemicellulose

Hemicellulose was determined from the non-cellulosic carbohydrate content. Untreated feedstocks and hydrochars were incubated in 1 M sulphuric acid at 100 °C for 3 hours, and the supernatant was diluted 20 times. The acid-soluble monosaccharides within the supernatant were derivatised with 1-phenyl-3-methyl-5-pyrazoline (PMP) in an alkaline environment, and the concentrations of the derivatives were determined via hydrophilic interaction liquid chromatography using a Kintex 2.5 µm C18 100 × 3 mm 100A column.

Alcohol-Insoluble Residue

Prior to cellulose and lignin analysis, feedstocks and hydrochars were washed numerous times to attain the alcohol-insoluble residue (AIR). The samples were washed sequentially in 70%, 100% ethanol, acetone and methanol, with each wash being followed by centrifugation and the disposal of the supernatant.

Cellulose

Cellulose content was determined using a modified Updegraff method. The alcohol-insoluble residue (AIR) was incubated in a mixture of 4:6:1 water : glacial acetic acid : nitric acid at 100 °C for three hours. The cellulose content was determined on a weight-by-weight basis.

Lignin

The lignin content was determined via the acetyl bromide method. The alcohol-insoluble residue was incubated in a mixture of 25% acetyl bromide in 98% glacial acetic acid for 1 hour at 70 °C. The supernatant containing the dissolved lignin was transferred to a new tube, and 2 M NaOH and 0.5 M hydroxylamine hydrochloride were added. The lignin solution was diluted

with glacial acetic acid, and the UV absorbance at 280 nm was recorded. The lignin content was calculated against a standard curve determined using TCI alkaline lignin as a standard, taking into account the high ash content of the standard (49%).

Ultimate analysis (CHN) was determined on a Perkin Elmer 2400 series II CHNS analyser, and the oxygen content determined by difference. The crude protein content of the untreated feedstocks, as well as the quantity of proteinaceous reaction products in the hydrochar were calculated by multiplying the nitrogen content by the conversion factor of 6.25.

Aqueous extractives content of the untreated feedstocks was calculated by difference between the total mass of the starting material, and the sum of hemicellulose, cellulose, lignin, protein and ash. The secondary char content was calculated in the same manner, but using the hydrochar instead of the raw material.

The higher heating value (HHV) was calculated using the Dulong Equation (Equation 22)⁴³:

$$\text{HHV} = (0.3383 \times \% \text{Carbon}) + (1.422 \times \% \text{Hydrogen}) - (\% \text{Oxygen} \div 8) \quad (22)$$

The ash content was determined by incubating the samples at 550 °C for 5 hours in a Labec laboratory muffle furnace¹⁸². The ash content was calculated on a weight-by-weight basis from the difference between the pre-incubation sample mass and the post-heating remainder.

5.2.3 Kinetics Method

The degradation of the biochemical components of hemicellulose, cellulose and lignin over the course of the HTC reaction were modelled using Arrhenius kinetics.

For a given n^{th} order reaction, the concentration of a particular biomass component can be predicted at any time point by Equation 23:

$$-\frac{dc_t}{dt} = k_n c_t^n \quad (23)$$

Where:

c_t is the predicted concentration (%)

k is the temperature dependent reaction rate constant (J min^{-1})

n is the reaction order

t is the total reaction time (mins)

Equation 23 can be integrated with a given initial concentration of c_i to give Equation 24 for a first order reaction, and Equation 25 for a general n^{th} order reaction:

$$c_t = c_i \exp(-kt) \quad (24)$$

$$c_t = \left(\frac{1}{kt \times (n-1)} + \frac{1}{c_i^{n-1}} \right)^{\frac{1}{n-1}} \quad (25)$$

Much of the previous HTC kinetic literature operates under the assumption of constant temperature for the duration of the reaction. However, the batch reactor utilised for this study required a short heat-up period, resulting in a steady increase in the temperature-dependent rate constant k . To account for this, the rate constant was sequentially recalculated at 15 second intervals with the temperature at that time point, using Equation 26:

$$k = A_0 \exp\left(\frac{-E_a}{RT}\right) \quad (26)$$

Where:

A_0 is the pre-exponential factor (s^{-1})

E_a is the activation energy (J),

R is the universal gas constant of ($8.314 \text{ J mol}^{-1} \text{ K}^{-1}$)

T is the temperature (K)

The average reaction rate at the HTC reaction temperature (200 °C, 230 °C, 260 °C) was taken from the average k value between reaction time 0 minutes, and reaction time 60 minutes. The activation energy E_a and pre-exponential factor A_0 were calculated together via a least sum of squares optimisation procedure by minimising the difference between the experimental and predicted values using the DEPS evolutionary algorithm in LibreOffice Solver. Models were produced with reaction orders from $n = 0.1$ to $n = 2$ in increments of 0.1. Goodness of fit was judged via the lowest square sum error (SSE) for a given reaction order, as well as the coefficient of determination (r^2).

5.3. Results and Discussion

Hemp stems and seed hull were subjected to hydrothermal carbonisation at three reaction temperatures (200 °C, 230 °C, and 260 °C) and four reaction times (0, 15, 30, and 60 minutes).

5.3.1 Global changes in biomass composition

Figure 22 shows the total changes across the entire HTC reaction system in the solid, liquid and gas phases, as well as the compositions of the solid phase biomass and hydrochars. Solid yield, represented in Figure 22A and 22B as the sum of the hemicellulose, cellulose, lignin, protein or proteinaceous remnants, ash, ash and secondary char fractions, fell steadily for both biomasses with increasing time and temperature. Higher temperatures lead to a greater reduction of the solid yield, with consistently greater losses observed over the 260 °C series than either of the lower temperature series.

A trend common to both biomasses is that after an initial rapid loss, the solid fraction of a given reaction condition plateaus off after 15 minutes at a given reaction temperature. For example, at 200 °C, both hull and stem hydrochar yields stabilise at around 65%, and at 230 °C they level off at approximately 60%. The only point of divergence is at 260 °C, where the hull hydrochars level off after 30 minutes to 48%, while the stem tissue continuously declines over the entire time of the experiment until it reaches a minimum of 31%; the lowest solid yield of any reaction condition. Liquid yields are consistently lower than solid yields (with the single

exception of stem tissue at 260 °C after 15 minutes), and gas yields are in turn consistently lower than liquid yields. Gas yields tend to increase as time and temperature rise, with higher yields observed at higher temperatures. However, gas yields remain a small percentage of the total reaction system, barely rising above 10% for either tissue at the two cooler temperatures, and even after an hour at 260 °C, the gas yield does not exceed 22% for stem or hull. Liquid yields tend to behave as a mirror reflection of the solid yield. Thus, for many reaction conditions, the liquid yield rises to a maximum, and then plateaus off after 15 minutes, in an opposing manner to the solid yields.

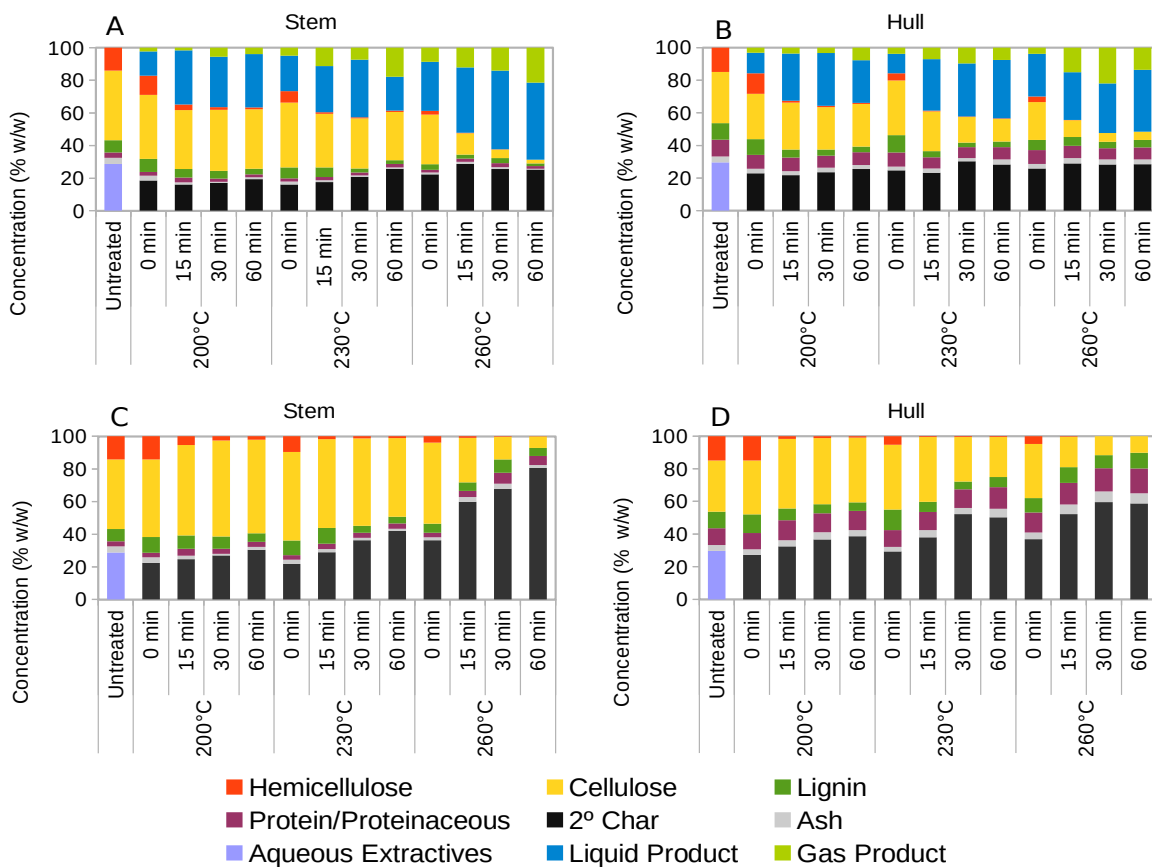


Figure 22: Yields of liquid, gas, and biochemical macromolecule across whole HTC reaction system of hemp stems (A) and seed hulls (B) and hydrochars following HTC at different temperatures (200 °C – 260 °C) and different isothermal holding times (0 min – 60 min). Total biochemical compositional changes of untreated hemp stems (C) and seed hulls (D), and of the HTC hydrochars. Char and aqueous extractive portions calculated by difference.

This plateau lies consistently at around 30% for all temperatures and tissues, with the only major exception being stems at 260 °C, which achieves a 30% liquid yield after just the heat-up period, eventually attaining a nearly 50% liquid yield after 30 minutes. This particular reaction condition has both the highest liquid yields, and among the highest gas yields (22%, shared with hull at 260 °C for 30 minutes) of any sample studied here. This is indicative of considerable hydrolytic and decarboxylic breakdown of the biomass into soluble products, which in turn undergo further degradation into gaseous products^{25,32}.

A fine-grained biochemical and elemental analysis of the untreated feedstocks revealed that the composition of hemp stem and seed hulls are broadly similar, but with a few key differences. Both tissues have cellulose as their largest constituent, making up 31% of seed hulls, and 43% of stems. This higher proportion of cellulose in stems is a result of the presence of the hemp fibres, which are themselves comprised of between 55% and 78% cellulose¹⁸³, which provides hemp fibres with their highly valued strength. Compared to other biomasses, the cellulose content of hemp stems is in the lower range of that observed in various stalk tissues (ranging from 45% for tobacco stalks to 72% for sunflower stalks), while hulls lie more towards the mid range of similar shells and husks (between 25% for olive husks, up to 57% for sunflower shells)⁷⁴. Both hemp stem and seed hulls have more cellulose than saltbush (24%)¹⁷⁴. Over the course of the HTC reaction, the cellulose content is relatively stable across 200 °C and 230 °C in both tissues, with degradation accelerating rapidly at the highest temperature, leading to residual cellulose levels of about 5% in stems and 2% for hulls in the solid product after an hour at 260 °C. Hemicellulose makes up a smaller proportion of either tissue than cellulose, at 14% – 15% for both stems and seed hulls, a slightly smaller proportion than saltbush (21%). In both tissues, this falls to almost 0% after an hour at any temperature. Lignin is present in lower amounts than either polysaccharide in both tissues, comprising 10% of seed hulls and 8% of stems. This is slightly lower than the 15% recorded for saltbush, and much lower than the levels seen in typical woody biomasses, which range from 17% to 32% across various softwoods, hardwoods and herbages¹⁸⁴. The lignin content in both tissues also decreased steadily over the course of the HTC reaction, although far less precipitously than either of the carbohydrates, eventually falling to just 4% for hulls and 1.5% for stems under the highest reaction severities. Lignin is more difficult to remove from the solid phase since there is a substantial portion

which is inert under HTC conditions, as discussed below. Seed hulls have a higher amount of protein than stems, at 10% to 3% respectively. Levels of protein, or the nitrogenous products of denatured proteins, are remarkably stable across the various treatment conditions, with total crude protein falling only slightly to 7% for hulls and 1% for stems after 60 minutes at 260 °C.

Both stems and hulls have an ash content of 4%, which decreases over the course of the reaction, a widely known aspect of HTC^{32,120,130,153}. The reduction in ash differs between the two tissues, with stem losing ash more rapidly, eventually retaining a minimum of 1% after just 30 minutes at 230 °C, while hulls only fall slightly to 3% after 0 minutes at 230 °C. What is interesting is that, as a proportion of the hydrochar (Figures 22C and 22D), after these minima the ash content actually increases steadily with greater reaction severity for both tissues. After a full hour at 260 °C, stems eventually rose back up to 3%, while hulls exceeded the original, untreated ash content by increasing to 6%. Hydrochars reabsorbing inorganics from the hydrothermal medium has been observed before, particularly phosphorus^{130,150,153}, and may be caused by an increase of porosity within the hydrochar, caused by the degradation of hemicellulose^{148,149}, leading to the reabsorption of water-soluble phosphates.

In addition to the principle lignocellulose components, hemp also contains a wide assortment of other biochemicals, including nucleic acids, sterols, phenols, and lipids. These extraneous biochemicals, collectively termed “aqueous extractives” make up just under 30% of each tissue. In keeping with previous methods and literature^{108,185}, aqueous extractives are assumed for the purposes of estimating the carbonaceous char content to degrade instantly upon exposure to hydrothermal water. This char content, although reasonably constant at around 25% for hulls and 20% for stems from a whole system perspective (Figure 22A and 22B), quickly establishes itself as the dominant fraction in the hydrochars (Figure 22C and 22D). After 60 minutes at 200 °C, 230 °C and 260 °C, this char fraction makes up 30%, 42% and 80% of stem hydrochars, and 38%, 50% and 58% of hull hydrochars.

Figure 23A and 23B shows the elemental changes that the hemp biomass underwent during the HTC reaction on a dry, ash-free basis. In both tissues, carbon was enriched in the

solid phase, with this increased carbonisation being driven by the purging of oxygen. The greater the reaction severity, the higher the carbon content, and the lower the oxygen content.

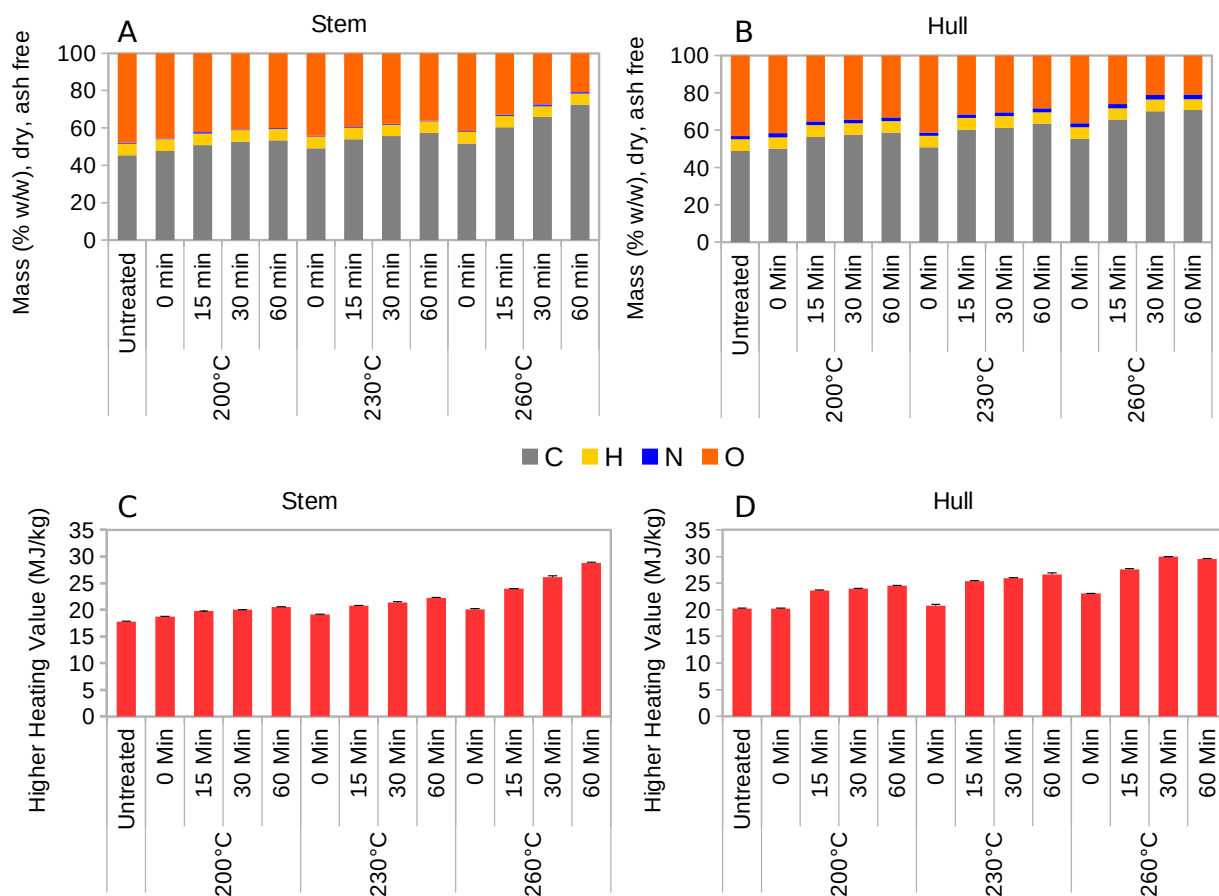


Figure 23: Ultimate analysis of untreated feedstock and HTC hydrochars of hemp stems (A) and seed hulls (B) on a dry, ash-free basis, and calculated higher heating values of untreated feedstock and hydrochars of hemp stem (C) and seed husks (D) produced at different temperatures (200 °C – 260 °C) and different isothermal holding times (0 min – 60 min). Error bars represent a single standard deviation.

Both tissues undergo rather similar degrees of carbonisation, with initial carbon contents for untreated stems and hulls of 45% and 49% respectively rising to 73% and 70% respectively after 60 minutes at 260 °C. In a mirrored fashion, oxygen losses are also very similar between the two biomasses, with initial oxygen contents of 49% for stems and 43% for hulls falling to 23% and 21% respectively under the same conditions. Hydrogen is almost constant, falling very slightly from 6.5% to 5.7% for hulls and from 6.2% to 5.6% for stems under

the most severe conditions. These trends are expected from the hydrothermal carbonisation reaction, and are driven by dewatering and decarboxylation reactions that remove oxygen from the feedstock in the form of water and carbon dioxide^{25,32,93,120,153}. As expected, this reduction in oxygen content lead to an increase in the higher heating values (HHV) for the hemp biomass, as shown in Figures 23C and 23D. The rise in higher heating values is again of a similar magnitude between the two tissues, with stem rising from 18 MJ kg⁻¹ for the untreated feedstock to 30 MJ kg⁻¹ after 60 minutes at 260 °C, and hulls rising from 20 MJ kg⁻¹ to 30 MJ kg⁻¹ under the same conditions. Given how Australian lignites typically exhibit HHVs in the range of 24 – 30 MJ kg⁻¹, this demonstrates that these hydrochars can potentially be used as a renewable solid fuel replacement for coal.

5.3.2 Mechanism of hydrochar production

The solid product of the HTC reaction is on the whole termed “hydrochar”, yet it is made up of two different kinds of char product; the unreacted or partially converted remains of the feedstock, and an aromatic condensate that forms carbonaceous nanospheres^{84,85}. These two kinds of char have been termed “primary char” and “secondary char” respectively, and are produced by two separate, yet interconnected mechanisms: Mechanism 1 involves the solid-solid conversion of biomass into primary char, whilst Mechanism 2 involves the two-step process of the degradation of biomass into soluble intermediates, followed by the polymerisation of these intermediates to secondary char^{85,86,88,174}. This is illustrated in Figure 24.

Using this twin-pathway model as an overall framework of the HTC reaction individual biochemical components are believed to preferentially undergo different mechanisms, although it is apparent that there is a great deal of overlap between them. Hemicellulose and cellulose are assumed to primarily undergo Mechanism 2, while lignin is assumed to undergo both 1 and 2. Lignin, as detailed below, is made up of hydrothemally soluble and insoluble fractions, and as such contributes to the formation of both primary and secondary char. The reaction mechanisms of protein within biomass during HTC are poorly understood, but protein is assumed to denature and become incorporated into the primary char, and may then undergo subsequent Maillard reactions with carbohydrates to form soluble intermediates^{145,147}. Detailed protein analysis is beyond the scope of this study, however. Finally, aqueous extractives are

assumed to instantly degrade to soluble and gaseous products^{108,186}. These pathways are described in Equations 27 – 32:

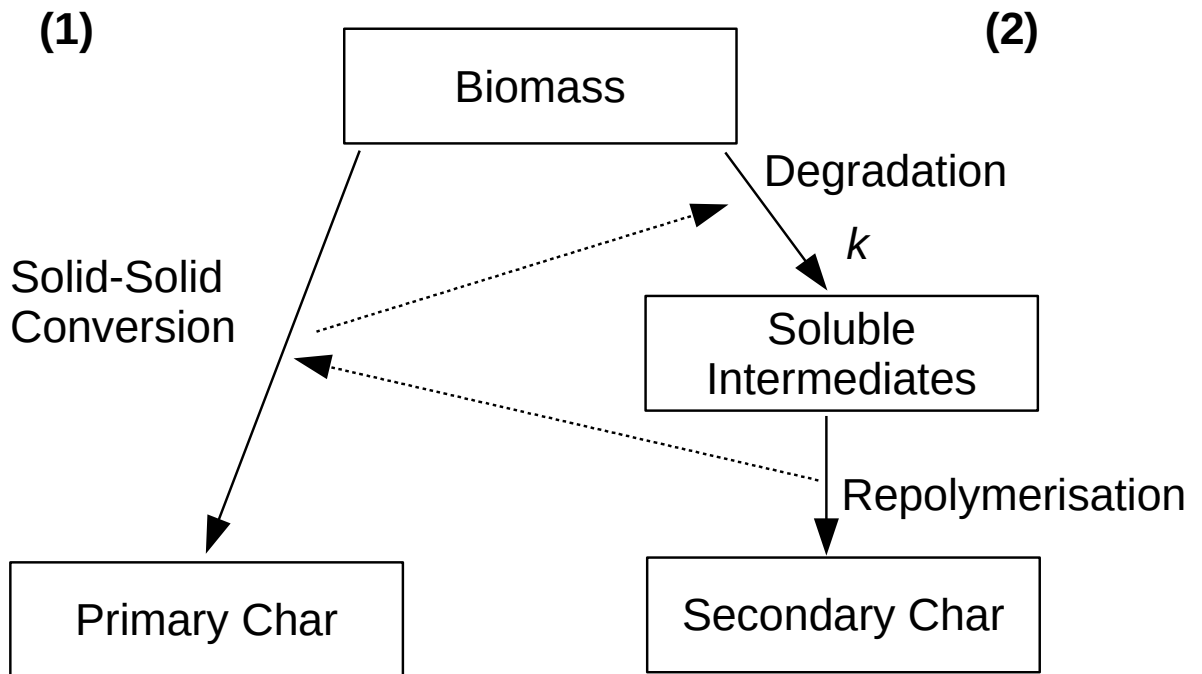


Figure 24: Proposed mechanism for the conversion of biomass into hydrochar during HTC

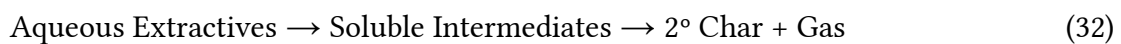
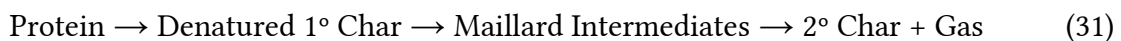
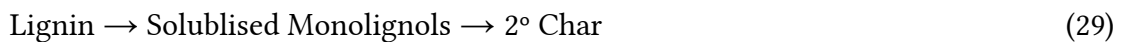
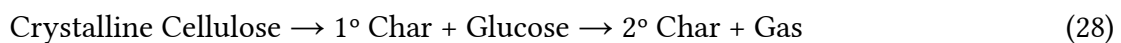
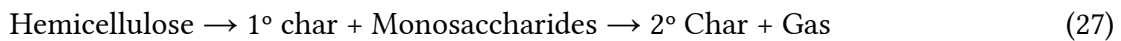


Table 5: Kinetic parameters for the degradation of key biochemical components during HTC of hemp. k : Reaction rate constant at given temperature; E_a : Activation energy; A_0 : Arrhenius constant. Rate constants presented as averages over the holding time at reaction temperature, not including heat-up phase.

		Reaction Order (n)	SSE	200 °C		230 °C		260 °C		E_a (kJ mol ⁻¹)	A_0 (s ⁻¹)
				k (s ⁻¹)	r^2	k (s ⁻¹)	r^2	k (s ⁻¹)	r^2		
Stem	Hemicellulose	1.3	21	0.02	0.99	0.04	0.97	0.10	0.98	58	5.0×10^4
	Cellulose	1.0	70	0.002	-3.97	0.012	-1.15	0.047	0.99	113	6.6×10^9
	Lignin (34% inert)	1.0	86	0.02	0.94	0.09	0.50	0.31	0.33	98	1.5×10^9
	Lignin (21% inert)	2.0	89	0.0003	0.92	0.001	0.66	0.003	0.18	81	2.5×10^5
Hull	Hemicellulose	1.3	45	0.03	0.95	0.09	0.99	0.20	0.16	67	8.7×10^5
	Cellulose	1.5	54	0.0003	-2.05	0.0015	0.90	0.0038	0.98	112	4.2×10^8
	Lignin	1.0	88	0.08	0.95	0.11	0.74	0.14	-0.26	22	1.9×10^1

Figure 25 shows the degradation of hemicellulose over the course of HTC, which is more rapid and more comprehensive than any other major biochemical component. All reaction temperatures for both tissues trend very rapidly towards zero, with almost all hemicellulose lost in both tissues after only 15 minutes. This includes substantial loss during the heat-up period, especially at high temperatures; at 260 °C, where both feedstocks lost almost 80% of their hemicellulose before even reaching the holding temperature. It appears that stem hemicellulose is slightly more resistant to hydrothermal degradation than its seed hull counterpart, particularly at 200 °C. After 15 minutes, hull hemicellulose falls below 10%, and eventually comes to rest at 4% after an hour at 200 °C, while stem hemicellulose just barely falls below 10% after the same time and temperature. At 230 °C, hull hemicellulose falls to 30% after 15 minutes, while stem hemicellulose only reaches 49% under the same conditions. After 15 minutes at 230 °C, and at all time points at 260 °C, the hemicellulose of both tissues undergoes near total hydrolysis. This is due to the autocatalytic hydrolysis of the β -(1→4) and β -(1→3) glycosidic linkages between the monosaccharide moieties, which releases the monosaccharides into the hydrothermal medium as solubilised sugars. The freed sugars then undergo aromatisation to form furfural and 5-(hydroxymethyl)furfural. Under continued exposure the

hydrothermal conditions, 5-HMF undergoes sequential aldol condensation reactions to form the secondary char^{40,94}. As such, the hydrolysis of hemicellulose is an important contribution to the formation of secondary char.

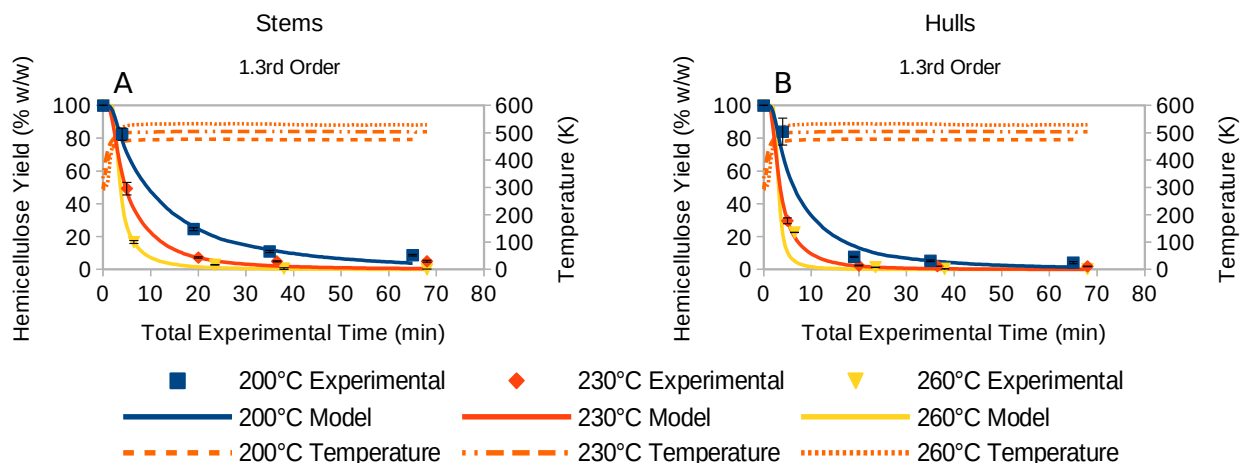


Figure 25: Degradation and Arrhenius kinetic modeling of hemicellulose within hemp following HTC at different temperatures (200 °C – 260 °C) and different isothermal holding times (0 min – 60 min). (A) 1.3rd order kinetic model of stem hemicellulose. (B) 1.3rd kinetic model of seed hull hemicellulose. Error bars represent one standard deviation.

Both hull and stem hemicellulose had a closer fit to a first order kinetic model than a second order model, judged by a lowest square sum error (SSE), although both tissues had their closest fit to a model with a reaction order of 1.3 (Table 5). Regardless of reaction order, stem hemicellulose consistently had much closer fits to the models, with coefficients of variance (r^2) over 0.90 for every reaction order tested. By comparison, seed hull hemicellulose had a relatively less good fit across the board, with a consistently higher SSE at each reaction order as well as wide variation in coefficients of variance. Compared to saltbush hemicellulose, which undergoes a first order hydrolysis reaction during HTC and was found to have an activation energy of 66 kJ mol⁻¹ and rate constants of 0.06 s⁻¹, 0.14 s⁻¹ and 0.35 s⁻¹ for 200 °C, 230 °C, and 260 °C respectively, both stem and hull tissues were found to have similar kinetics. Stems had an activation energy of 58 kJ mol⁻¹, while seed hulls had an activation energy of 67 kJ mol⁻¹, although both tissues consistently had slightly lower reaction rate constants than those observed in saltbush (Table 5, Table 3).

Figure 26 shows that the principle monosaccharide in both hemp tissues is xylose, which by itself makes up a full 12% of seed hull (81% of total hull hemicellulose), and 7% of stem tissue (52% of total stem hemicellulose). The second most prevalent monosaccharide in hemp hemicellulose is glucose, which makes up less than 2% of the total composition of either tissue, and all other monosaccharides are present in concentrations well below that. In comparison, the monosaccharide profiles of both hemp tissues are very similar to saltbush, with high levels of xylose, and other monosaccharides present at levels of around 2% or less. One notable point of difference is that saltbush has high levels of arabinose (8% total concentration), higher even than xylose, while in hemp arabinose is present only at trace levels.

That hull hemicellulose is notably more susceptible to hydrothermal degradation than either hemp stem tissue or saltbush is interesting. A principle element of hemicellulose is arabinoxylan, a polysaccharide with a predominately xylose backbone and numerous arabinose substituents, which often carry further substitutions of other monosaccharides and various acidic and acetyl side groups¹⁸⁷. The composition of arabinoxylan directly influences the overall structure of the polysaccharide, and determines the manner in which it integrates into the plant cell wall. The higher the xylose to arabinose ratio, the more substituted and branched the polysaccharide is likely to be, and the more soluble and labile it is as a result. Conversely, the lower the xylose : arabinose ratio, the more linear, crystalline and insoluble the polymer^{187,188}. Less-substituted xylans, because of their higher crystallinity, tend to form closer associations with cellulose due to the co-crystallisation of the linear polysaccharide with the cellulose microfibril¹⁸⁹⁻¹⁹². In contrast, highly branched arabinoxylans tend to form ferulate crosslinks to lignin, thereby providing strong interconnections within the cell wall as a whole¹⁹³.

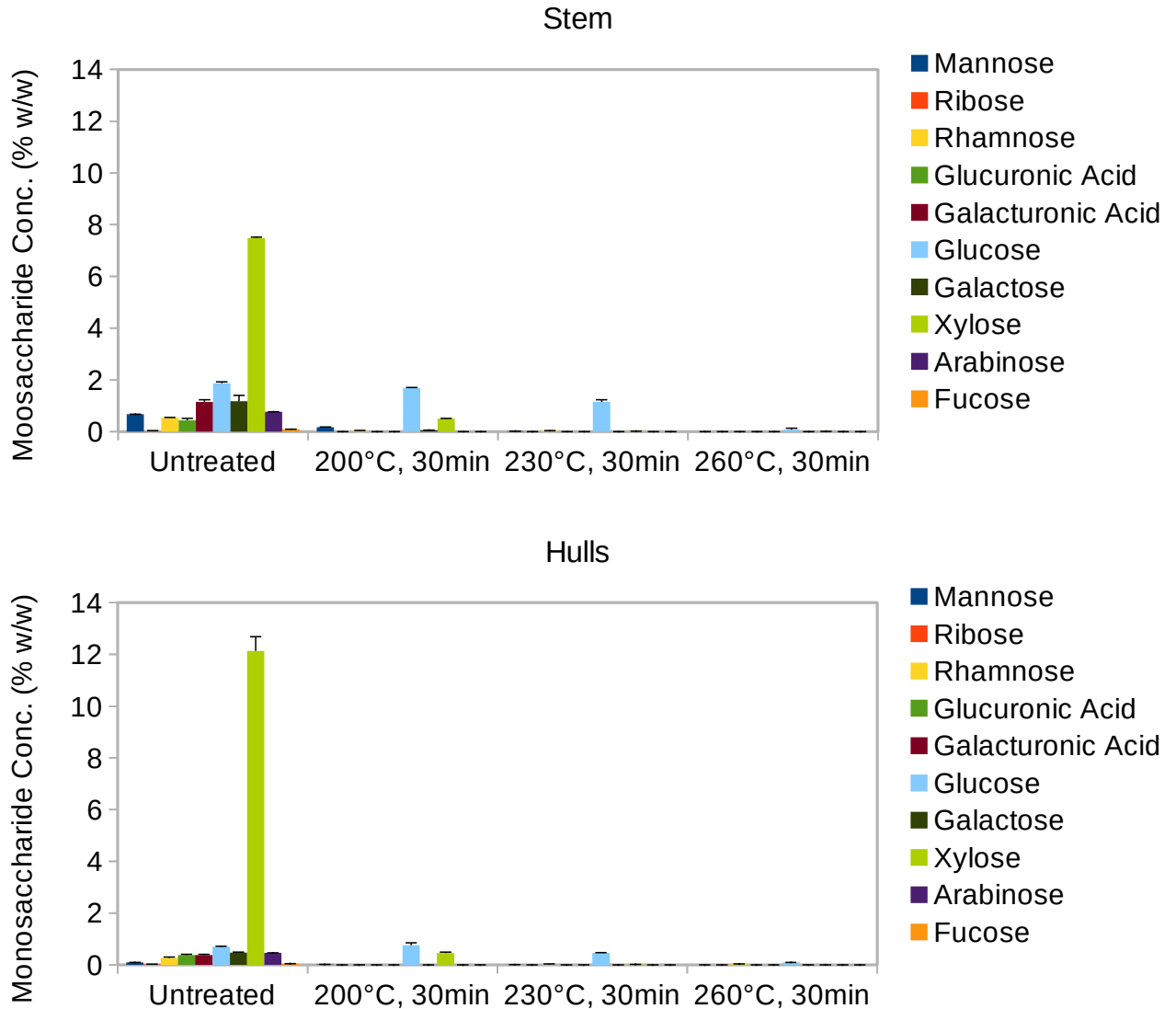


Figure 26: Monosaccharide profiles of untreated hemp stem and seed hull, and select hydrochars following HTC at different temperatures (200 °C – 260 °C) and one isothermal holding time (30 min). Error bars represent a single standard deviation.

The very low xylose : arabinose ratio (0.04) and overall homogeneity of hull hemicellulose imply a roughly linear xylan with very few substitutions, while the slightly higher ratio (0.1) and greater diversity of monosaccharides present in stems suggests a more substituted, but still xylose-dominant polysaccharide. Given the lower activation energy and higher rate constants of the hull hemicellulose, it may be that any co-crystallisation with cellulose is not enough to compensate for the loss of cross-linking with lignin.

Figure 27 shows that cellulose was far more resistant to hydrothermal degradation than hemicellulose for either tissue. There was very little degradation at 200 °C, with both stem and hull losing only 15% – 17% respectively after a full hour at reaction temperature. At 230 °C, cellulose degradation increased slightly but remained relatively slow for stem tissue, losing 31% after an hour at reaction temperature, while hull tissue showed much greater degradation, losing 56% under the same conditions. The greatest losses were observed at 260 °C, with both tissues losing 70% of the initial cellulose content after 15 minutes at reaction temperature. After the full hour at this high temperature, hull tissue eventually lost 84% of cellulose, and stem tissue lost 95%. This greater resistance to the autohydrolytic effect of HT water is due to the crystalline matrix that cellulose exhibits, which protects the β -(1 \rightarrow 4) glycosidic bonds from hydrolysis^{26,194}. Given the rapid acceleration of degradation at 260 °C, however, it seems that at this higher temperature the crystalline structure may be weakened. This stands in contrast to model compound experiments with purified cellulose, which demonstrate that cellulose is stable up to 307 °C in HT water²⁶.

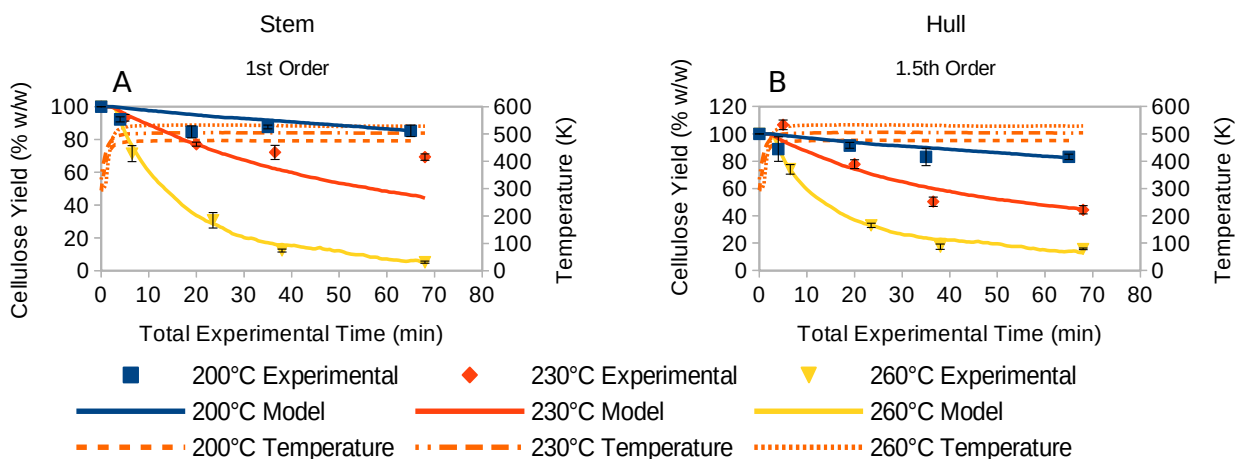


Figure 27: Degradation and Arrhenius kinetic modeling of cellulose within hemp following HTC at different temperatures (200 °C– 260 °C) and different isothermal holding times (0 min – 60 min). (A) First order kinetic model of stem cellulose. (B) 1.5th order kinetic model of seed hull cellulose. Error bars represent one standard deviation.

In both tissues, the first order models produced an overall closer fit than the second order models, although hulls had the closest fit of all cellulose models tested to a 1.5th order

model (SSE: 53). Indeed, hull first and second order models had very similar square sum errors at around 60, only slightly higher than the 1.5th order model which may imply a certain amount of complexity to the underlying mechanism that makes it difficult to tease out the precise reaction order using the simple method presented here. All hull cellulose models have a very close fit to the 260 °C series, with r^2 values of over 0.96 for any reaction order. Fits to the 230 °C series are highly variable, ranging from 0.09 for the first order model, to 0.89 for the second order model, while fits for the 200 °C are very poor, with negative coefficients of variance across the board. The activation energies for hull cellulose ranged from 103 kJ mol⁻¹ (first order) to 117 kJ mol⁻¹ (second order), while the reaction constants showed a very wide spread from first to second order models (Table 5). In contrast to the somewhat opaque hull fits, the much closer fit of stem cellulose to the first order model than the second order model convincingly indicates that stem cellulose undergoes first order degradation. Under this first order model, stem cellulose had an activation energy of 113 kJ mol⁻¹, and reaction constants of 0.002 s⁻¹, 0.012 s⁻¹ and 0.047 s⁻¹ at 200 °C, 230 °C and 260 °C respectively.

Regardless of tissue or model, the activation energies of hemp celluloses were consistently lower than those for saltbush, which was found to be 134 kJ mol⁻¹ for a first order reaction. The rate constants for saltbush were also slightly lower than the ranges shown by any of the hemp cellulose models. An additional difference is that saltbush cellulose was also found to fit a 0.5th order model the most closely; neither of the hemp tissues form a close fit with a reaction order less than one. However, the differences between the three biomasses are far less than the differences between cellulose and hemicellulose for any feedstock. Such differences in the kinetic behaviours of cellulose could be explained by structural variance between the two tissues. Hemp stem tissue contains a large amount of cellulose-reinforced fibres, which are not only very difficult to mill finely, but are also highly insoluble. As a consequence, water may not have had as ready access to stem cellulose than to that in the husk tissue. Another potential factor could be the fact that the solid fraction in the hull experiments was much better at retaining the inorganics than stems. Certain inorganic elements, especially sodium, have been found to have a catalytic effect on hydrothermal reactions¹⁹⁵, and by retaining these in the solid phase, this higher inorganics content could potentially have the effect of slightly increasing the rates of cellulose hydrolysis at the cooler temperatures relative to stems. One final

consideration concerns the interaction between cellulose and xylan. It has been established that it is likely that hull hemicellulose consists of linear, non-substituted xylans that tend to co-crystallise with the cellulose fibrils. It is possible that as the xylans are rapidly degraded, they leave behind a more ragged, frayed, or otherwise weakened cellulose fibril surface, making hull cellulose more susceptible to attack than its stem counterpart. X-ray diffraction experiments investigating the differences in cellulose crystallinity between the two tissues would be necessary to demonstrate this.

Figure 28 shows how the lignin within hemp degraded to a constant value, instead of trending toward zero as for the polysaccharides. This is consistent with previous findings in saltbush, where approximately 22% of the lignin was inert during HTC, and the remainder possessed very similar reaction kinetics to hemicellulose. In seed hull, the inert portion was calculated from the average of all lignin yield data points at 30 and 60 minutes at all temperatures. The inert portion comprised approximately 31% of the total lignin, while the remaining 69% proved to be highly reactive, fully depleting to the inert portion after 30 minutes at 200 °C and 15 minutes at 230 °C. In stems, the inactive portion was more difficult to identify due to slower degradation at 200 °C and 230 °C; two possible values are considered here. An upper value for the inert portion, calculated from the average of lignin values for 15 to 60 minutes at 260 °C and 30 to 60 minutes at 230 °C, was found to be 34%, while a lower value, taken from the lowest lignin value, 260 °C for 60 minutes, was found to be 21%. Degradation is much lower at 200 °C for stem tissue than it is for any other condition in either tissue, remaining above 60% after 30 minutes, and eventually falling to a minimum of 45% after the full hour. At 230 °C, lignin degrades almost as slowly as the 200 °C series for the first fifteen minutes at reaction temperature, falling to 77% after 15 minutes (compare 70% for 15 minutes at 200 °C), and then falls very sharply during the next fifteen minutes to 33%, where it remains for the remaining duration of the reaction. At 260 °C, as with all previous tissues and biochemical components, the loss is most severe, with 55% of the lignin removed during the heat up period, and 79% removed after an hour at reaction temperature.

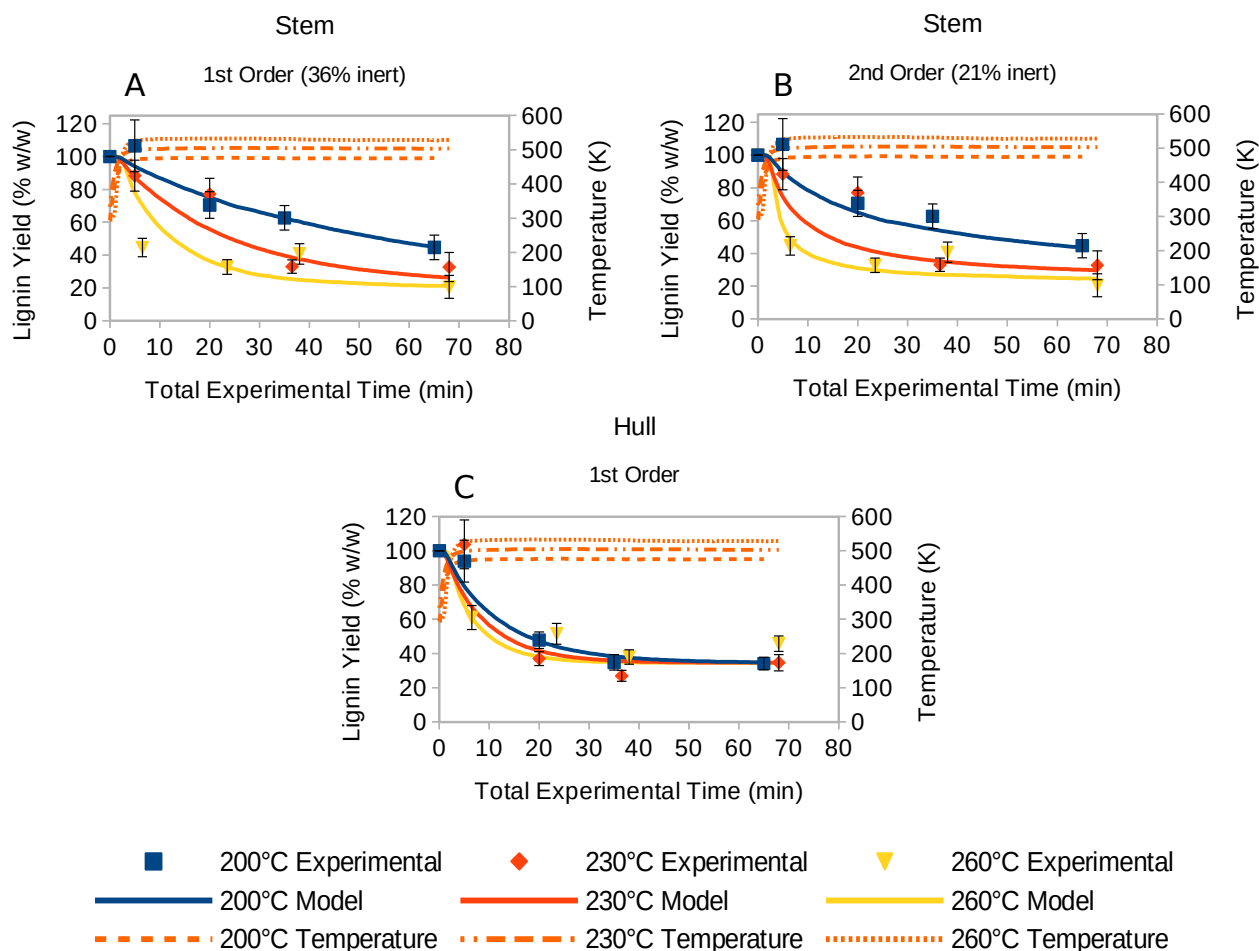


Figure 28: Degradation and Arrhenius kinetic modeling of lignin within hemp following HTC at different temperatures (200 °C– 260 °C) and different isothermal holding times (0 min – 60 min). (A) First order kinetic model of stem lignin cellulose (36% inert portion). (B) Second order kinetic model of stem lignin (21% inert portion). (C) First order kinetic model of seed hull lignin. Error bars represent one standard deviation.

Hydrothermally active hull lignin degrades in a first order reaction, with an activation energy of 22 kJ mol⁻¹, and closely grouped reaction constants of 0.08 s⁻¹, 0.11 s⁻¹ and 0.19 s⁻¹ at 200 °C, 230 °C and 260 °C respectively. Each of the hull lignin curves are very similar, with predicted lignin yields for 260 °C never more than 13% lower than those for 200 °C for any time point. Kinetic modeling for stem lignin differed depending on what the proportion of HTC-stable lignin was assumed to be. For the higher-bound estimate of 34%, HT-active lignin was found to undergo first order degradation, with an activation energy of 98 kJ mol⁻¹, and rate

constants of 0.02 s^{-1} , 0.09 s^{-1} , and 0.31 s^{-1} at $200\text{ }^{\circ}\text{C}$, $230\text{ }^{\circ}\text{C}$ and $260\text{ }^{\circ}\text{C}$. For the lower-bound estimate of 21% however, HT-active stem lignin was found to react via a second order reaction, with a slightly lower activation energy of 81 kJ mol^{-1} , but much lower rate constants of 0.0003 s^{-1} , 0.001 s^{-1} and 0.003 s^{-1} for $200\text{ }^{\circ}\text{C}$, $230\text{ }^{\circ}\text{C}$ and $260\text{ }^{\circ}\text{C}$.

The HT-active lignin of saltbush was found to have almost identical kinetic parameters to saltbush hemicellulose, and thus it was assumed that the reaction mechanism was the same for the two components. This was found to be also true for hemp seed hulls, which had almost the same activation energies and Arrhenius constants, although the rate constants were slightly lower in the lignin model. In stem tissue, by comparison, the picture is more complex. Assuming a 34% inert lignin portion and a first order reaction, the rate constants were similar to those in the corresponding hemicellulose model, although again, slightly lower. However, the activation energy and Arrhenius constant for lignin were much higher, almost double those of the hemicellulose. And in comparing the model for stem 21% inert lignin and stem hemicellulose, there is very little agreement between the first order hemicellulose and second order lignin models, as might be expected.

The difference in the response between the two kinds of hemp lignins to HTC is wider than any other biochemical component assayed here. That the two tissues have not only varying portions of HTC- stable lignin, but also that the stem lignin is notably slower reacting than the hull lignin strongly suggests that the composition of the lignins are different. Lignin is mainly comprised of three phenolic alcohols, or monolignols: *p*-coumaryl alcohol, coniferyl alcohol, and sinapyl alcohol, each differentiated only by the degree of methylation. When incorporated into the plant cell wall, these monolignols form *p*-hydroxyphenyl (H), guaiacyl (G) and sinapyl (S) lignin subunits respectively⁷². The manner in which the monolignols come together is highly complex, and is driven by the radicalisation of the monolignols, which then polymerise by forming covalent crosslinks at numerous points along the monomers. The points at which crosslinks can form is determined by the locations of the resonance-stabilised free radicals within the monolignols, which are in turn determined by the type of monolignol^{72,196}. G-subunits form a rich amount of β -5, 5-5 and β - β crosslinks, leading to more resilient lignin, while lignin rich in S-subunits, which favour β -O-4 ether linkages, is slightly less so¹⁵⁸. H-

lignin, formed from the unmethylated *p*-coumeryl alcohol, does not form cross-links within the lignin superstructure, but instead is only found in nature as “pendant chains” on the outside of the polymer^{197,198}. The ratios of G and S subunits within lignin therefore have a profound impact on the structural integrity of the macromolecule, and thus its propensity for degradation. Because of the binding and reinforcing role that lignin plays in the plant cell wall, any changes in the structural strength of lignin has knock-on effects for the stability of the whole biomass. It was found in *in vitro* studies utilising blends of kraft lignin and cellulose that shifting from pure G-lignin to various mixtures of G, S and H lignins, as well as other related lignic subunits led to a reduction in the amount of sugars released during fungal digestion, while reducing the amount of crosslinking lead to a large increase (in some cases over double) of sugar release¹⁹⁶. In light of this, it is clear that the composition of lignin has a profound impact on the degradation of lignocellulosic biomass during HTC. NMR studies on hemp lignin would allow for the quantification of G and S lignin, and see if the G:S ratio was in some way responsible for the different behaviours observed. Given the current reliance in the field on stock kraft lignin as a lignin analogue, this is an area which is deeply understudied.

Almost all prior HTC literature on the HTC mechanisms of biomass conversion have been conducted with idealised model compounds in order to make generalised statements about the behaviour of whole biomass. And yet, it has been demonstrated that while there are broad similarities between the various biochemical components across different biomasses, at a more refined level there are substantial differences in the biochemical compositions even between various tissues of the same species. The cumulative effect of these differences produces substantial variation in the types and amounts of the reaction products.

5.4 Conclusion

The compositional changes that occur during the HTC of hemp were assessed, and found to be broadly similar to those that occur in other lignocellulosic biomasses. While hemicellulose was found to be the most sensitive to hydrothermal hydrolysis regardless of tissue type, there were subtle differences in the behaviour of cellulose between stem and seed hull tissues. Lignin was the most complex of the biochemical components investigated, and the differences observed between the two discrete tissues of the same plant are indicative of the

great interconnected complexity of biomass and the reactions that occur during HTC of whole biomass. Further studies on other kinds of biomass, as well as more fine-grained analyses of the degradation mechanism within whole biomass are necessary to more fully round out our knowledge of the reaction mechanics. It is hoped that one day, with a more comprehensive understanding of the HTC reaction, it may be possible to predict based on the composition of a given biomass the products and ideal conditions for that feedstock.

5.5 Acknowledgments

This project was funded and supported by the Australian Research Council Centre of Excellence in Plant Cell Walls CE110001007.

The Authors would like to thank the Australian Federal Government for providing a Research Training Scholarship to B. Keiller, and would also like to thank Phoebe Chilman for her invaluable assistance in performing the HTC reactions and Tony Hall of the University of Adelaide, Physical Sciences, for performing the CHN analysis.

Chapter 6

Paper IV

Biochemical Compositional and Kinetic Modelling of Hydrothermal Carbonisation of Macroalgae

Benjamin G. Keiller¹, Phoebe Chilman², Rocky de Nys³, Rachel A. Burton¹, Philip J. van Eyk²

1 School of Agriculture, Food and Wine, University of Adelaide, Adelaide, South Australia, Australia

2 School of Chemical Engineering and Advanced Materials, University of Adelaide, Adelaide, South Australia, Australia


3 MACRO - The Centre for Macroalgal Resources and Biotechnology, College of Science and Engineering, James Cook University, Townsville, Queensland, Australia

This manuscript was written with contributions from all authors. All authors have given approval to the final version of the manuscript

Statement of Authorship

Title of Paper	Biochemical Compositional Analysis and Kinetic Modelling of Hydrothermal Carbonisation of Macroalgae
Publication Status	<input type="checkbox"/> Published <input type="checkbox"/> Accepted for Publication <input type="checkbox"/> Submitted for Publication <input checked="" type="checkbox"/> Unpublished and Unsubmitted work written in manuscript style
Publication Details	N/A


Principal Author


Name of Principal Author (Candidate)	Benjamin Keiller		
Contribution to the Paper	Conception, Analysis, Drafting		
Overall percentage (%)	70%		
Certification:	This paper reports on original research I conducted during the period of my Higher Degree by Research candidature and is not subject to any obligations or contractual agreements with a third party that would constrain its inclusion in this thesis. I am the primary author of this paper.		
Signature		Date	17-12-19

Co-Author Contributions

By signing the Statement of Authorship, each author certifies that:

- i. the candidate's stated contribution to the publication is accurate (as detailed above);
- ii. permission is granted for the candidate to include the publication in the thesis; and
- iii. the sum of all co-author contributions is equal to 100% less the candidate's stated contribution.

Name of Co-Author	Phoebe Chilman		
Contribution to the Paper	Analysis, Drafting		
Signature		Date	05/12/2019

Name of Co-Author	Rocky de Nys		
Contribution to the Paper	Conception, Drafting		
Signature		Date	06/01/20

Chapter 6 (Paper IV) – Biochemical Composition & Kinetic Modelling of HTC of Macroalgae

Name of Co-Author	Rachel A. Burton		
Contribution to the Paper	Conception, Analysis, Drafting		
Signature		Date	17/12/19

Name of Co-Author	Philip J van Eyk		
Contribution to the Paper	Conception, Analysis, Drafting		
Signature		Date	13-01-20

6.0 Abstract

Hydrothermal Carbonisation (HTC) is a thermochemical process by which biomass is converted into an energy-dense “hydrochar”, which can possess very similar properties to fossil lignites. Such hydrochars potentially represent a renewable replacement for coal. Despite growing interest in HTC in recent years, there are many aspects that remain unknown about the process, especially the mechanisms. Two species of macroalgae, the freshwater *Oedogonium intermedium* and the saltwater *Ulva ohnoi*, were subjected to HTC at three reaction temperatures (200 °C, 220 °C, 240 °C) and five retention times (0 min, 5 min, 15 min, 30 min, 60 min). The untreated feedstock and the hydrochars were assayed to determine levels of the major biochemical components; hemicellulose, cellulose, protein, and ash. The degradation of each biochemical component was modelled using Arrhenius reaction kinetics across a range of reaction orders (n), and the activation energy (E_a), Arrhenius pre-exponential factor (A_0) and rate constant (k) were determined for each model. It was found that hydrochar yields for *Oedogonium* were consistently higher than for *Ulva* for any temperature or time. Hemicellulose degraded extremely rapidly, completely disappearing within minutes at any temperature ($n = 1$, $E_a^{Ulva} = 136 \text{ kJ mol}^{-1}$, $E_a^{Oedogonium} = 115 \text{ kJ mol}^{-1}$). Cellulose degraded more slowly, and with different mechanisms between the two species; *Oedogonium* cellulose degraded via a simple first order reaction ($E_a = 130 \text{ kJ mol}^{-1}$), while *Ulva* cellulose appeared to degrade in two parallel first order reactions, one fast and the other slow ($E_a^{Fast} = 148 \text{ kJ mol}^{-1}$, $E_a^{Slow} = 112 \text{ kJ mol}^{-1}$). Protein appeared to undergo a similar parallel mechanism in both species, with *Ulva* ($E_a^{Fast} = 88 \text{ kJ mol}^{-1}$, $E_a^{Slow} = 74 \text{ kJ mol}^{-1}$) proteins degrading faster on the whole than those in *Oedogonium* ($E_a^{Fast} = 148 \text{ kJ mol}^{-1}$, $E_a^{Slow} = 112 \text{ kJ mol}^{-1}$). These complex behaviours of key biochemical compounds are impossible to elucidate in idealised feedstock experiments, and these findings highlight the need for whole biomass HTC compositional studies.

6.1 Introduction

As carbon emissions rise and natural resources deplete, there is a growing urgency to move away from fossil fuels and adopt low-emission, renewable energy sources as soon as possible. Biofuels, combustible fuels derived from biomass, have long been upheld as a potential key weapon in the fight against climate change, due in large part to the high

abundance and low cost of biomass as a feedstock. However, despite increased political and industrial interest in biofuels, there remain numerous challenges and drawbacks with conventional biofuel technology. Bioethanol and bio-diesel produced from crops such as corn, sugar cane and palm oil make up the majority of the current biofuel market, but because these fuels are produced from food crops, they attract controversy by competing directly with land used for food production. The change in land-use from cropping to fuel production, or opening virgin land to plantations can result in biofuels producing up to twice the carbon emissions over their life cycle than fossil fuels²³. If biofuels are to fulfill their promise as a truly sustainable energy source, the chosen feedstock must have a low impact on land use.

Macroalgae are photosynthetic aquatic plants that occur widely across the world in both fresh and salt water environments¹⁹⁹. They are differentiated from microalgae in that they possess a much more sophisticated multicellular structure that allows them to generate complex tissues, and more commonly they are visible with the naked eye. Marine macroalgae, or seaweeds, are already extensively cultivated as a source of food and phycocolloid food additives, with an estimated annual production of 30 million tonnes in 2017²⁰⁰. With a high growth rate, strong capacity to fix atmospheric CO₂, and ability to thrive on excess nitrogen and phosphorus in waste water, macroalgae have attracted considerable interest into other uses, such as bioremediation²⁰¹, and especially as a source of biofuels^{202–206}. Macroalgae are considered a promising feedstock for a variety of biofuels, including conventional fuels such as bioethanol, bio-diesel and biogas, and also more advanced thermochemical processes such as pyrolysis and hydrothermal liquefaction. Much of this optimism is owed to the fact that as aquatic plants, by their very nature they do not compete with food crops for arable land or potable water²⁰⁷. Macroalgae for biomass can be cultivated in the sea, or in enclosures (ponds, tanks) on non-productive land^{203,208}, and could be utilised synergistically to treat waste water from aquaculture, municipal waste water treatments, and agriculture. Algae can also be used to capture the carbon emissions produced from coal and gas-fired power plants^{209,210}. They have a higher photosynthetic efficiency than terrestrial plants (6 – 8%, compared to 1.8 – 2.2%)²¹¹, and therefore have a higher productivity per unit area than many land-based plants²⁰⁸. These capabilities make macroalgae very attractive as a fuel biomass.

One fuel option that has been little considered for macroalgal biofuels is hydrothermal carbonisation (HTC). HTC is a thermochemical process wherein biomass is heated in high-pressure, high-temperature subcritical water at temperatures between 180 °C and 260 °C^{25,32}. Under such conditions, the biomass is converted into a carbonaceous, porous char, or hydrochar, with greatly improved thermal qualities. The changes that occur within biomass during the HTC reaction are poorly understood, and almost all the literature on the subject is concerned with terrestrial lignocellulosic biomass⁹⁸. Typically, studies designed to investigate the changes of lignocellulose have done so by taking a single purified component (such as hemicellulose, cellulose, tannins, or glucose), and using it as an idealised feedstock^{26,41,101,116}. Such an approach, while simple and convenient, is sharply limited in that the reaction environment of a single component does not accurately resemble the extremely complex interactions that occur during HTC of whole biomass. This is a profound weakness when attempting to model the kinetics of the breakdown of lignocellulose during HTC.

An alternative method is to take the biochemical compositional analysis of the whole biomass prior to HTC, and then using the mass yield of the hydrochar product, combined with assumptions about the carbonisation behaviour of each component within the biomass, to model the degradation of each component as a first order Arrhenius reaction. One such study on loblolly pine¹⁰⁸, estimating that hemicellulose degraded to liquid and gas, the cellulose converted to char as well as liquid and gas, and lignin being inert, calculated that the activation energies of cellulose and hemicellulose were a mere fraction of those calculated for pure feedstock experiments. This approach, while more sophisticated than pure feedstock experiences, remains imprecise, as the content and composition of the lignocellulose is estimated based on the composition of the untreated feedstock. Additionally the untreated biomass composition was determined using a crude fibre analysis, which was designed for characterising animal feed, and therefore imprecise. An improved method is to independently measure the content of each individual component as it degrades over the course of the HTC reaction.

Previously, Australian saltbush was treated with HTC, and the untreated feedstock and hydrochars were subjected to rigorous compositional analysis to accurately determine the

content of hemicellulose, cellulose and lignin at each point during the HTC reaction¹⁷⁴. It was found that hemicellulose was eliminated from the biomass within minutes at any reaction temperature, and at higher temperatures was almost fully removed before the holding temperature was even reached. Cellulose, protected by its more crystalline structure⁶⁴, was more resistant to HTC degradation at lower temperatures, but still underwent considerable removal at 260 °C. The accurate measurements of the remaining concentrations of each component were then used directly to create models for the lignocellulosic degradation during HTC, and the kinetic parameters were found again to be dramatically less than those obtained from pure feedstock experiments.

Macroalgae are in some respects well suited for hydrothermal conversion, as they have a very high water content, up to 88% in some species²⁰³. Many thermochemical pretreatments such as torrefaction and pyrolysis require the feedstock to be dried down prior to processing, which can be energy-intensive and costly. By virtue of taking place in water, HTC does not require feedstocks to be pre-dried, and performs well with feedstocks with a solid content of 10 – 30%²⁵. However, macroalgae also contains a large portion of inorganics⁴⁴, which in a combustible fuel manifests as ash. Ash in fuels presents serious problems during combustion, and can lead to slagging and fouling of furnaces⁸¹. Such a high ash content renders other thermochemical technologies problematic, but this issue can be mitigated by using HTC, which has been shown to be able to reduce the inorganics content of a given biomass^{43,130,153}. However, the extent to which the inorganics can be removed from the macroalgae is unknown. Indeed, while both marine and freshwater macroalgae have already been studied using the related procedure of hydrothermal liquefaction^{205,206,212-214}, which produces an oil product similar to crude oil, there are very few studies on HTC of algae of any sort.

One recent study by Smith et al, 2016⁴⁴ performed HTC on three species of marine macroalgae (seaweeds), *Laminaria digitata*, *Laminaria hyperborea* and *Alaria esculenta*, at 200 °C and 250 °C for 60 minutes. The biomass underwent numerous changes, including an increase in higher heating value (up to 26 MJ kg⁻¹), a decrease in the inorganic content, a purging of molecular oxygen, and an altered elemental composition that closely resembled brown coal. Each of these changes is consistent with the literature on HTC²⁵, although it was noted that

compared to lignocellulosic biomass such as *Miscanthus*, the hydrochar yields were lower. This was attributed to the differences in biochemical composition between terrestrial and aquatic biomasses. In contrast to the lignocellulose of terrestrial plants, macroalgae has no lignin, and contains a high proportion of polysaccharides, many of which are unique^{215,216}. Additionally, there is considerable variation in macroalgae composition²¹⁷, not only between species, but also within the same species seasonally and geographically^{44,80}, and this is an important consideration to take into account. There have also been limited studies on HTC of single-cell microalgae, principally as means of processing the lipids within the microalgae as a precursor for bio-diesel production^{147,218}. Although the results of these studies broadly align with our basic understanding of the HTC process, key questions regarding the behaviour of the core biochemical components that make up macroalgae remain outstanding.

Two species of macroalgae have been chosen for this study, the freshwater macroalga *Oedogonium intermedium* and the marine macroalga *Ulva ohnoi* (commonly known as “sea lettuce”). These were chosen for their high growth rates and robustness, making them suitable for use in bioremediation⁸⁰. There is compositional data on both species in the literature^{80,219–222}, however, it is not complete, and often does not distinguish between hemicellulose and cellulose within “total carbohydrate” measurements. This distinction is important when considering the different behaviours of the two polysaccharides under HTC conditions^{25,26,160,223}.

As such, this study aimed to subject both *O. intermedium* and *U. ohnoi* to rigorous compositional analysis to accurately determine hemicellulose, cellulose, and protein content, prior to their use for HTC. The resultant hydrochars will then be subjected to the same analysis, to determine the loss of each component over the course of the HTC reaction, and allow kinetic calculation of the degradation of each component during the HTC reaction.

6.2 Methods and Materials

6.2.1 Hydrothermal Carbonisation

Two species of macroalgae, *Oedogonium intermedium* and *Ulva ohnoi* (hereafter referred to by genus alone) were cultivated at the Marine and Aquaculture Research Facilities Unit

(MARFU) at James Cook University. The biomass as supplied (containing approximately 10% water content) was milled in a Retsch knife mill, and the 150 – 500µm size fraction obtained via sieving. The samples were subsequently fully dried in an oven at 105 °C for 24 hours.

The HTC reaction took place in a custom-built batch reactor, according to prior methods¹⁵³ with minor modifications as outlined here. The reactions were performed using a stainless steel reactor with a wall thickness of 3 mm, and a total volume of 50 mL. Macroalgae was mixed with deionised water to create a 10% slurry by weight (25 g total weight) and added to the reactor. The reactor was then sealed and pressurised according to prior methods and heated in an electronically heated fluidised bed (Techne, model: SBL-2D)¹⁵³.

Three reaction temperatures (200 °C, 220 °C, and 240 °C) and five residence times (0 min, 5 mins, 15 min, 30 min, and 60 min) were used, with residence time beginning when the internal temperature of the reactor reaches 98% of the chosen reaction temperature. These temperatures were chosen based on observations during prior research with HTC of macroalgae, where macroalgae (*Oedogonium*) processed at 260 °C resulted in very low mass yields (>30%)¹⁰. Thus, a lower maximum temperature of 240 °C was selected. All HTC experiments were performed in duplicate.

Solid, liquid and gas yields of the HTC reaction were recorded. The gas yield is determined from the change in mass of the reactor before and after the reactor is vented to exhaust, as in Equation 33:

$$\text{Gas Yield (\%)} = \frac{(m_{AR} - m_{PV}) - (m_{N_2} - m_i)}{m} \quad (33)$$

Where m is the dry mass of the untreated macroalgae feedstock, m_{AR} is the mass of the reactor post-reaction, m_{PV} is the mass of the reactor post-vent, m_{N_2} is the mass of the reactor after pressurising with nitrogen pre-reaction, and m_i is the mass of the dry, empty reactor.

The solid yield is determined from the dry weight of the solid hydrochar product, as in Equation 34. The solid product was separated by filtration through two filter papers. The bulk

of the hydrochar product was collected in the first filter paper unwashed, to be used for compositional analysis. The remainder of the hydrochar that was stuck to the walls of the reactor, was rinsed out onto the second filter paper with water. Because of the potential of the rinsing action to alter the concentration of the water-soluble contents of the hydrochar, the char collected on the second filter paper was used only for calculating the total solid yield, and then discarded.

$$\text{Solid Yield}(\%) = \frac{(m_{P1} - m_{P1+S}) - (m_{P2} - m_{P2+S})}{m} \quad (34)$$

where m is again the dry mass of the untreated feedstock, m_{P1} and m_{P2} are the masses of the first and second filter papers respectively, and m_{P1+S} and m_{P2+S} are the combined mass of the filter papers and the hydrochar product.

The liquid yield was calculated from the difference between the solid and gas yields, as in Equation 35:

$$\text{Liquid Yield}(\%) = 1 - \text{Gas Yield}(\%) - \text{Solid Yield}(\%) \quad (35)$$

6.2.2 Compositional Analysis

Hemicellulose, cellulose, and protein content were determined according to the methods described in Keiller *et al.* (2019)¹⁷⁴, and are recounted here in brief. All experiments were conducted in duplicate, and in calculating the yields of the aforementioned macromolecules, the total yield error was calculated via error propagation using the estimated error of the HTC solid yield¹³⁸.

Hemicellulose content was calculated from the sum concentration of acid-soluble monosaccharides determined via HPLC; after incubation in 0.5M sulfuric acid for 3 hours at 100 °C, the acid-soluble monosaccharides were derivatised with 1-phenyl-3-methyl-5-pyrazoline (PMP), and then quantified with liquid chromatography.

Cellulose content was determined using a modified Updegraff method¹⁶⁸. The alcohol-insoluble residue (AIR) was digested in a 4:6:1 water : glacial acetic acid : nitric acid mixture at 100 °C for three hours. The cellulose content was then determined on a weight-by-weight basis.

Ultimate analysis (CHN) was performed on a Perkin Elmer 2400 series II CHNS analyser, and the oxygen content determined by difference. The crude protein content of the untreated feedstocks as well as the content of the proteinaceous degradation products within the hydrochar were calculated by multiplying the nitrogen content by the conversion factor of 5²²⁴.

The higher heating value (HHV) was calculated using the Dulong Equation⁴³, as in Equation 36:

$$\text{HHV} = (0.3383 \times \% \text{Carbon}) + (1.422 \times \% \text{Hydrogen}) - (\% \text{Oxygen} \div 8) \quad (36)$$

The ash content was determined by incubating the samples at 550 °C for 5 hours in a Labec laboratory muffle furnace¹⁸². The ash content was calculated on a weight-by-weight basis from the difference between the pre-incubation sample mass and the post-heating remainder.

The remainder of the sample (the total dry weight less the sum of hemicellulose, cellulose, protein, and ash) was termed aqueous extractives in the untreated feedstock¹⁰⁸, and secondary char in the hydrochars.

6.2.3 Kinetics Method

The degradation of hemicellulose, cellulose and protein within macroalgae during HTC was modeled using Arrhenius kinetics.

For a given, n^{th} order reaction, the concentration of a given biochemical component can be modelled using Equation 37.

$$\frac{-dc_t}{dt} = k_n c_t^n \quad (37)$$

Hydrothermal Carbonisation of Novel Biomasses

Where:

k is the temperature dependent reaction rate constant (J min^{-1})

n is the reaction order

c_i is the concentration of a particular biomass component (%)

t is time (mins)

Equation 37 can be integrated with a initial concentration of c_i to give Equation 38 for a first order reaction, and Equation 39 for a general n^{th} order reaction:

$$c_t = c_i \exp(-kt) \quad (38)$$

$$c_t = \left(\frac{1}{kt \times (n-1)} + \frac{1}{c_i^{n-1}} \right)^{\frac{1}{n-1}} \quad (39)$$

The batch reactor required a heat-up period prior to achieving the desired holding temperature. To account for the attendant change in temperature-dependent rate k , the rate was sequentially recalculated at 15 second intervals, using the temperature at that time point. The rate constant was calculated using the Arrhenius Equation, as given in Equation 40:

$$k = A_0 \exp\left(\frac{-E_a}{RT}\right) \quad (40)$$

Where:

A_0 is the pre-exponential factor (s^{-1})

E_a is the activation energy (J),

R is the universal gas constant of ($8.314 \text{ J mol}^{-1} \text{ K}^{-1}$)

T is the temperature (K)

The reaction rate presented here is the average k taken across the entire holding time period, from 0 minutes to 60 minutes, and thus does not include the initial heat-up period. The average k for each reaction temperature for each given reaction order n (in intervals of $n = 0.1$) was used to calculate the activation energy E_a and pre-exponential A_0 factor using a least sum of

squares methodology. The square root of the difference between the model and the experimental data was minimised using DEPS evolutionary algorithm in LibreOffice Solver. Goodness of fit was judged via the lowest square sum error (SSE) for a given reaction order. In addition, the coefficient of determination (r^2) was calculated.

6.3 Results and Discussion

Two species of macroalgae (*Oedogonium intermedium* and *Ulva ohnoi*) were subjected to HTC at three reaction temperatures (200 °C, 220 °C, and 240 °C), and five residence times (0 minutes, 5 minutes, 15 minutes, 30 minutes, and 60 minutes).

Figure 29 shows how higher holding temperatures and longer reaction times lead to a lower solid yield in both species. Under HTC conditions, water begins to autocatalyse reactions such as hydrolysis, decarboxylation, dehydration and others, leading to a breakdown of the principle components of biomass. *Ulva* consistently produced lower solid yields than *Oedogonium*, with a significant amount of material lost during the initial heatup phase; even at 200 °C, 39% of starting material is lost before the holding temperature is reached. *Oedogonium* by contrast seems to be more resistant, with only 10% lost under the same conditions. At the highest temperature runs, *Ulva* loses 55% of starting material before reaching 240 °C, while *Oedogonium* initial losses are much less at 28% loss. The highest reaction condition of 60 minutes at 240 °C produced the lowest solid yield for both species, at 15% yield for *Ulva*, and 32% yield for *Oedogonium*. The solid yields for both species of macroalgae are consistently lower than those for lignocellulosic biomasses such as saltbush and hemp at every temperature point. This is likely due to the presence of lignin in terrestrial plants, which reinforces the cell wall, and is partially inert during HTC. Additionally, as detailed below, there may be differences in the degree of crystallinity within macroalgal cellulose that impairs its ability to withstand hydrothermal degradation, leading to lower solid yields.

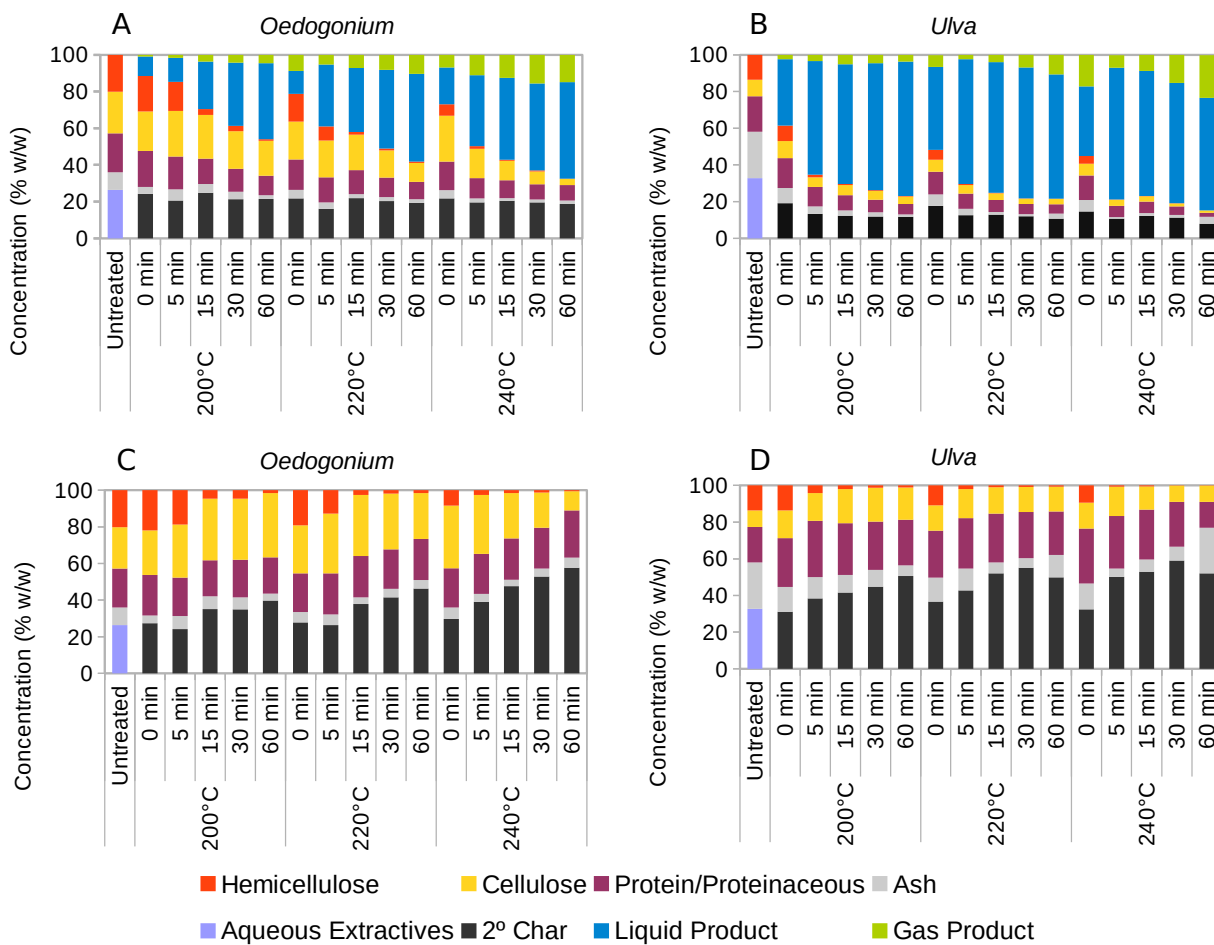


Figure 29: Global changes in macroalgae biomass composition during HTC. Total biochemical composition of untreated *Oedogonium* (A) and *Ulva* (B) and hydrochars produced at different temperatures (200 °C – 240 °C) and different isothermal holding times (0 min – 60 min), as well as total liquid phase and gas phase products (Solid product yield corresponds to the sum of hemicellulose, cellulose, proteinaceous products, ash and 2° char). Total solid phase compositions of *Oedogonium* (C) and *Ulva* (D)

In contrast with the solid yield, greater reaction severity leads to an increase in the liquid and gas yields. In *Ulva*, a considerable amount of the solid material is converted into aqueous products, with the liquid yield consistently exceeding the solid yield after only a few minutes at the reaction temperature. Under each reaction condition, *Ulva* liquid yields are consistently higher than the equivalent sample in *Oedogonium*, sometimes up to 30% greater, as at 240 °C for 5 minutes. *Oedogonium* liquid yields only exceed 50% of the total HTC product at

the most severe reaction condition of 240 °C for 60 minutes; under all other conditions, the liquid yield makes up the minority of the total products. For *Ulva*, by contrast, the aqueous product is the dominant product for all reaction conditions except the 0 minute samples. The gas yields for both species are significantly lower than either solid or liquid yields, with the single exception of *Ulva* at 240 °C for 60 minutes, where the solid yield is 15% and the gas yield is 23%. This is also the highest gas yield observed in this study. The highest gas yield for *Oedogonium* was 16% under the same conditions.

The difference in yields between the two species is a result of the difference in biochemical composition. On the whole, *Ulva* had a lower carbohydrate content than *Oedogonium*, with *Ulva* exhibiting a 14% hemicellulose content and a 9% cellulose content (23% total carbohydrates), while *Oedogonium* possesses a 43% total carbohydrate content, split roughly evenly between 20% hemicellulose and 23% cellulose. Macroalgae are rich in a wide variety of phytochemicals, including carotenoids, phenolics, flavanoids, nucleic acids and lipids²²⁵, here collectively termed “aqueous extractives” and calculated by difference. The aqueous extractive contents of the two algae are similar, at 26% for *Ulva* and 33% for *Oedogonium*, while the protein contents of the two feedstocks were even closer, at 19% for *Ulva* and 21% for *Oedogonium*. The biggest discrepancy between the two feedstocks was in the ash content, which was 2.5 times higher in *Ulva* (25%) than in *Oedogonium* (10%). Consistent with saltbush and hemp, all carbohydrates were subject to removal over the course of the HTC reaction, with higher reaction severity leading to a higher rate of removal. As a fraction of the solid phase, hemicellulose falls to 1% or below for *Oedogonium* after an hour at any temperature, while in *Ulva* hemicellulose is reduced to a similar level at even relatively mild conditions such as 15 minutes at 200 °C, and eventually is almost completely removed at just 0.05% of the hydrochar after 60 minutes at 240 °C. Cellulose levels, as a result of the rapid loss of the hemicellulose and the assumed instantaneous hydrolysis of the aqueous extractives^{108,185}, briefly increase as a proportion of the hydrochar, before eventually falling to a minimum of around 10% for both species under the highest severity. In contrast to the carbohydrates, although there is an overall loss of “protein”, or proteinaceous material content as a proportion of the entire hydrothermal system (Figures 29A and 29B), as a proportion of the solid product the proteinaceous material content is mostly stable, or even increases slightly over the course of

the HTC reaction. For *Oedogonium*, the proportion of proteinaceous material in the solid phase is more or less constant at around 21%. For *Ulva*, the proteinaceous material content of the hydrochars was concentrated at most reaction conditions, rising quickly to a maximum of 31% after 5 minutes at 200 °C, although the median hydrochar protein content is 26% for this feedstock. After a full hour at the highest temperature, the proteinaceous material content of *Ulva* hydrochar declines to 14%.

Ash was also removed from the solid phase by the HTC reaction, one of the most well studied and most important properties of the hydrothermal process with regards to any eventual application in a fuel context^{10,43,120,133,153}. Despite *Ulva* having a higher initial ash content than *Oedogonium*, ash reduction was much faster and more comprehensive in *Ulva*, with 70% to 75% of ash lost during the heat up period. After 60 minutes at 200 °C, 95% of the total ash content had been removed from the hydrochar. Interestingly, although the 220 °C and the 240 °C temperature series showed an even more rapid initial ash reduction, after 30 minutes both higher temperatures began to show an increase in ash content, implying that the ash was being reabsorbed back into the hydrochar from the liquid phase. By 60 minutes at 260 °C, the ash content of the hydrochar had almost reached the same 25% level as the untreated biomass (this particular condition was assayed for ash content for an additional two replicates to confirm [standard deviation = 1.02%]). There is some precedent for this; it has been observed that phosphorus is occasionally reabsorbed back into the hydrochar at high reaction severities in experiments, possibly as a result of the increased porosity of highly processed hydrochars^{130,150,153}. *Oedogonium* does not show such a reabsorption, and indeed features a consistently lower rate of ash removal; only 50% of ash is removed during the heat up period, and all reaction temperatures converge on a maximum ash depletion of around 80% after an hour at reaction temperature.

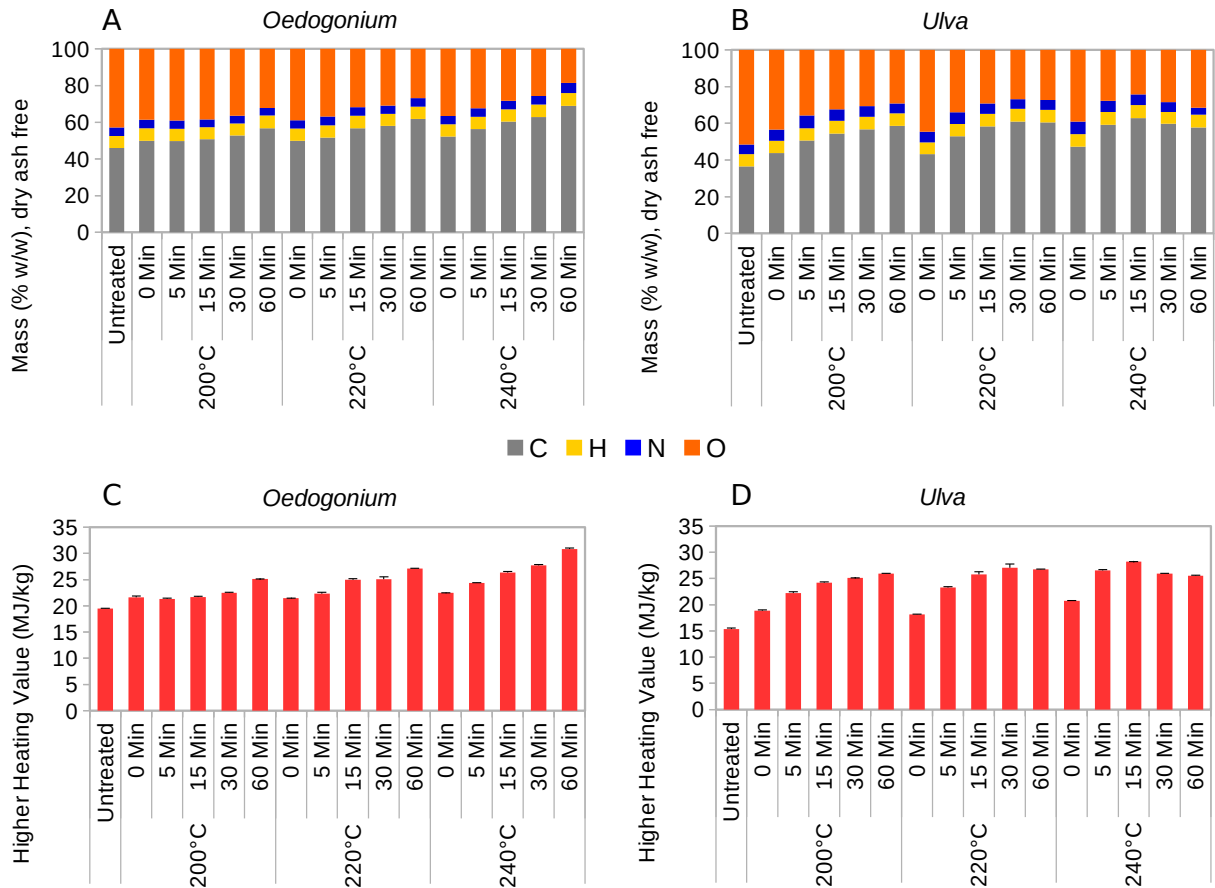


Figure 30: Ultimate Analysis of untreated feedstock and HTC hydrochars of *Oedogonium* (A) and *Ulva* (B) on a dry, ash free basis, and calculated higher heating values of untreated feedstock and HTC hydrochars of *Oedogonium* (C) and *Ulva* (D) produced at different temperatures (200 °C – 240 °C) and different isothermal holding times (0 min – 60 min). Error bars indicate one standard deviation.

Figures 30A and 30B show the changes in the elemental content of the biomass as a result of hydrothermal treatment, on a dry, ash-free basis. Relative to the untreated feedstock, carbon is enriched in the hydrochars in both species, especially in *Oedogonium*, where the carbon content rises steadily from an initial 46% to 69% after 60 minutes at 240 °C. The rise in carbon content in *Oedogonium* is concurrent with the rise in reaction severity, with more severe conditions leading to a higher carbon content. In this manner, *Oedogonium* behaves in a very similar manner to lignocellulosic biomasses such as saltbush and hemp. By contrast, the carbon content of *Ulva*, although it does rise above the initial level of 37%, does not rise consistently with increased reaction severity. Rather, the carbon content appears to peak at around 63%.

After 30 minutes at 220 °C, the carbon content of *Ulva* hydrochars plateaus at 61%, while at 240 °C, the carbon content peaks at 63% after 15 minutes, and then actually decreases thereafter to 58%. The rise in carbon content is driven by the loss of oxygen, caused by the removal of water and carbon dioxide from the feedstock as a result of dehydration and decarboxylation reactions^{25,32,93,120,153}. In *Oedogonium*, the oxygen content falls smoothly with increasing reaction severity from 43% to 19%, while in *Ulva* the oxygen content falls from an initial 52% to a minimum of 24% at the carbon peak of 15 minutes at 240 °C, an approximately 50% reduction for both species. The hydrogen content of both species is small, with untreated *Ulva* containing 5%, while *Oedogonium* had 6%. Consistent with findings in other biomasses, the hydrogen content is little affected by the HTC reaction compared to other elements, rising slightly to 6% in *Ulva* and 7% in *Oedogonium*. Figures 30C and 30D show the dramatic rise of higher heating value (HHV) as the reaction severity increases, in line with the changes in oxygen and carbon content. Untreated macroalgae have a similar HHV to other kinds of biomass, including lignocellulosic material, which typically lies between the ranges of 15 MJ kg⁻¹ to 20 MJ kg⁻¹ ⁶. Untreated *Ulva* has an HHV of 15 MJ kg⁻¹, while *Oedogonium* has a slightly higher value of 20 MJ kg⁻¹, which is more similar to those of hemp stem and hulls. Over the course of the HTC reaction, the HHVs of both species is increased, with *Oedogonium* rising consistently to a maximum value of 31 MJ kg⁻¹ after 60 minutes at 240 °C, while in *Ulva*, the peak is 25 MJ kg⁻¹ at 15 minutes at 240 °C, under the same conditions that yield the lowest oxygen content. As with saltbush and hemp, the highest HHVs are well within the range seen with Australian lignites⁹, meaning that hydrochars produced from macroalgae could well be utilised as a renewable replacement for coal and coke. Additionally, the removal of ash from the macroalgae, especially from *Ulva*, means that macroalgal hydrochars have a very low ash content compared to both brown and black coals (3% – 12%)⁹, the result of which is lower risk of slagging and fouling of furnaces in thermal applications

It has been observed that within hydrochar there are two broad types of solid product: the unreacted or partially reacted remnant of the biomass feedstock, called primary char, and carbonaceous nanospheres called secondary char^{84,85}. This has led to the postulation of a twin-pathway mechanistic model (Figure 31), where Mechanism 1 involves the solid-solid conversion of biomass to primary char, and Mechanism 2 is a two-step process that involves the initial

degradation of the biomass to soluble intermediates, followed by the repolymerisation of those intermediates to secondary char^{85,86,88,174}. These reactions are not mutually exclusive, and there is significant overlap and intermixing between the two mechanisms.

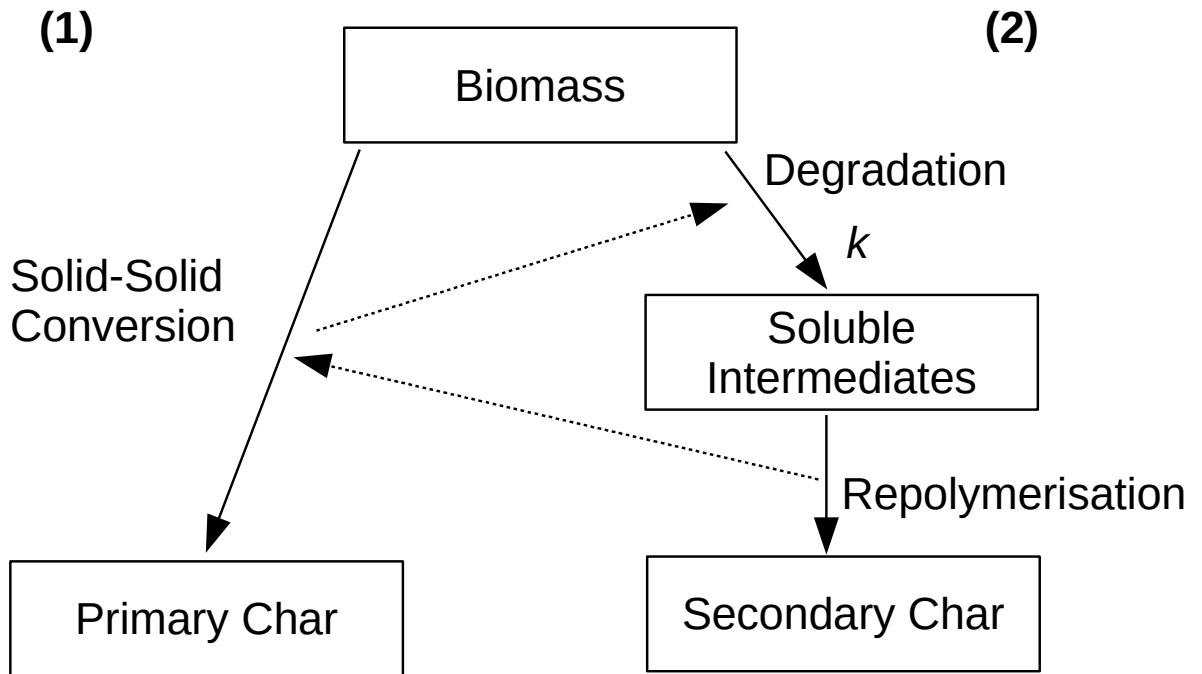
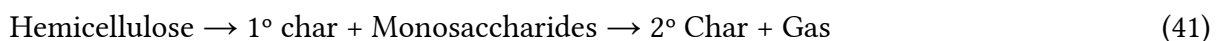


Figure 31: Proposed Mechanism of biomass degradation in HTC. (1) Mechanism 1. (2) Mechanism 2. Dotted lines represent the interconnectedness of the reactions.

Using this twin-pathway model as a conceptual framework, the reaction mechanisms of each of the principle biomass components can be represented as follows. Hemicellulose, and cellulose are assumed to degrade to their respective water-soluble monomers, which then undergo repolymerisation reactions to form the secondary char. Protein, as discussed below, is assumed to initially denature into a sticky mass (possibly becoming part of the primary char), followed by the degradation of the denatured mass to soluble intermediates. Gaseous products are assumed to be formed from the further decomposition of the water-soluble products.

This can be summarised in Equations 41 – 45



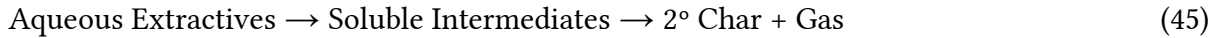
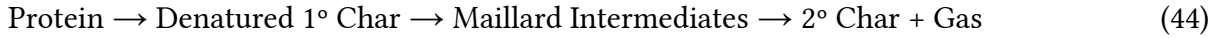
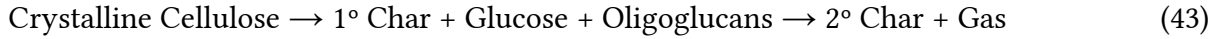
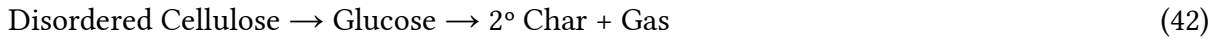


Table 6: Kinetic parameters for the degradation of key biochemical components during HTC of macroalgae. *k*: Reaction rate constant at a given temperature; *E_a*: Activation energy; *A₀*: Arrhenius constant; *n*: Reaction order; *SSE*: Sum of Squares Error. Rate constants presented as averages over the holding time at reaction temperature, not including warm-up time.

		<i>n</i>	<i>SSE</i>	200 °C		220 °C		240 °C		<i>E_a</i> (kJ mol ⁻¹)	<i>A₀</i> (s ⁻¹)
				<i>k</i> (s ⁻¹)	<i>r</i> ²	<i>k</i> (s ⁻¹)	<i>r</i> ²	<i>k</i> (s ⁻¹)	<i>r</i> ²		
<i>Ulva</i>	Hemicellulose	1.2	58	0.06	0.99	0.21	0.21	0.89	0.98	138	4.5 × 10 ¹³
	Cellulose (1-step)	4.8	62	9.0 × 10 ⁹	0.72	8.1 × 10 ⁹	0.99	4.1 × 10 ⁸	0.88	155	1.6 × 10 ⁸
	Cellulose (Fast)	1.0	80	0.05	0.76	0.20	0.90	0.93	0.94	148	7.3 × 10 ¹⁴
	Cellulose (Slow)			0.002		0.005		0.016		113	
	Protein (1-step)	3.8	43	4.0 × 10 ⁷	1.00	9.1 × 10 ⁷	0.98	2.4 × 10 ⁶	0.82	92	4.0 × 10 ³
	Protein (Fast)	1.0	53	0.13	0.98	0.27	0.96	0.68	0.94	88	4.7 × 10 ⁸
	Protein (Slow)			0.003		0.006		0.013		74	
<i>Oedogonium</i>	Hemicellulose	1.0	68	0.04	0.89	0.13	0.88	0.46	0.67	115	1.7 × 10 ¹¹
	Cellulose (1-step)	0.1	67	0.19	0.44	0.57	0.99	2.07	N/A	130	5.3 × 10 ¹¹
	Cellulose (Fast)	1.0	75	8.0 × 10 ⁻⁷³	0.41	1.0 × 10 ⁻⁶⁹	0.78	1.0 × 10 ⁻⁶⁶	0.99	767	4.3 × 10 ¹¹
	Cellulose (Slow)			0.003		0.012		0.039		132	
	Protein (1-step)	5.4	40	5.7 × 10 ¹¹	0.86	1.4 × 10 ¹⁰	0.99	4.3 × 10 ¹⁰	0.87	104	1.3 × 10 ¹
	Protein (Fast)	1.0	46	0.03	0.94	0.08	0.67	0.16	0.94	92	4.2 × 10 ⁸
	Protein (Slow)			0.0005		0.001		0.193		90	

Hemicellulose content was determined via the quantification of acid-soluble monosaccharides. Using standards for typical sugars in lignocellulosic vegetative material, the

following sugars were quantified: mannose, ribose, rhamnose, glucose, galactose, xylose, arabinose, fucose, and the acidic residues glycosidic and galactosidic acid. In addition to these sugars, additional signal peaks were detected, likely manuronic and guluronic acid, components of alginate. These additional signal peaks were quantified using xylose as an estimate for the molecular weight. The hemicellulose content was determined by taking the sum of all quantified monosaccharides.

Figure 32 shows how the monosaccharide profile of the two species is different, with *Oedogonium* hemicellulose being comprised almost entirely of glucose and mannose (36% and 51% of the total *Oedogonium* hemicellulose profile respectively), with galactose and an assortment of trace monosaccharides making up the remainder. *Ulva* exhibits a more varied monosaccharide profile, with high amounts of rhamnose, glucuronic acid, and glucose, moderate amounts of galactose and xylose, and a large collection of alginate monosaccharides. The high levels of rhamnose, glucuronic acid and xylose derive from ulvan²¹⁵. Ulvans differ from terrestrial hemicellulosic polysaccharides by consisting of a backbone of repeating sulphated disaccharide units, referred to as ulvobiuronic acid and ulvanobioses. The principle glycosidic bonds in ulvans are α - and β -(1 \rightarrow 4), as in hemicellulose, although (1 \rightarrow 3) and (1 \rightarrow 2) bonds also occur. The ionic nature of ulvans means that they are highly responsive to changes in pH and solution conductivity, leading to an aggregated, particulate conformation at low pH, and a more open conformation at high pH. This in turn leads to profound changes in the gelling properties of the polysaccharide, with more open conformations leading to higher viscosities. How these properties manifest in the subcritical water of an HTC system is unknown, and likely complex. Given how subcritical conditions simultaneously lower the viscosity and raise the ionic product of water, leading to higher quantities of OH⁻ and H₃O⁺ ions²⁸, predicting how ionic polysaccharides may behave in an HTC system is difficult, and is an understudied area of HTC research. However, judging from the rapid loss of hemicellulose from *Ulva*, in a comparable manner to *Oedogonium* and other feedstocks, it seems that on the whole ionic polysaccharides degrade in much the same manner as other hemicelluloses.

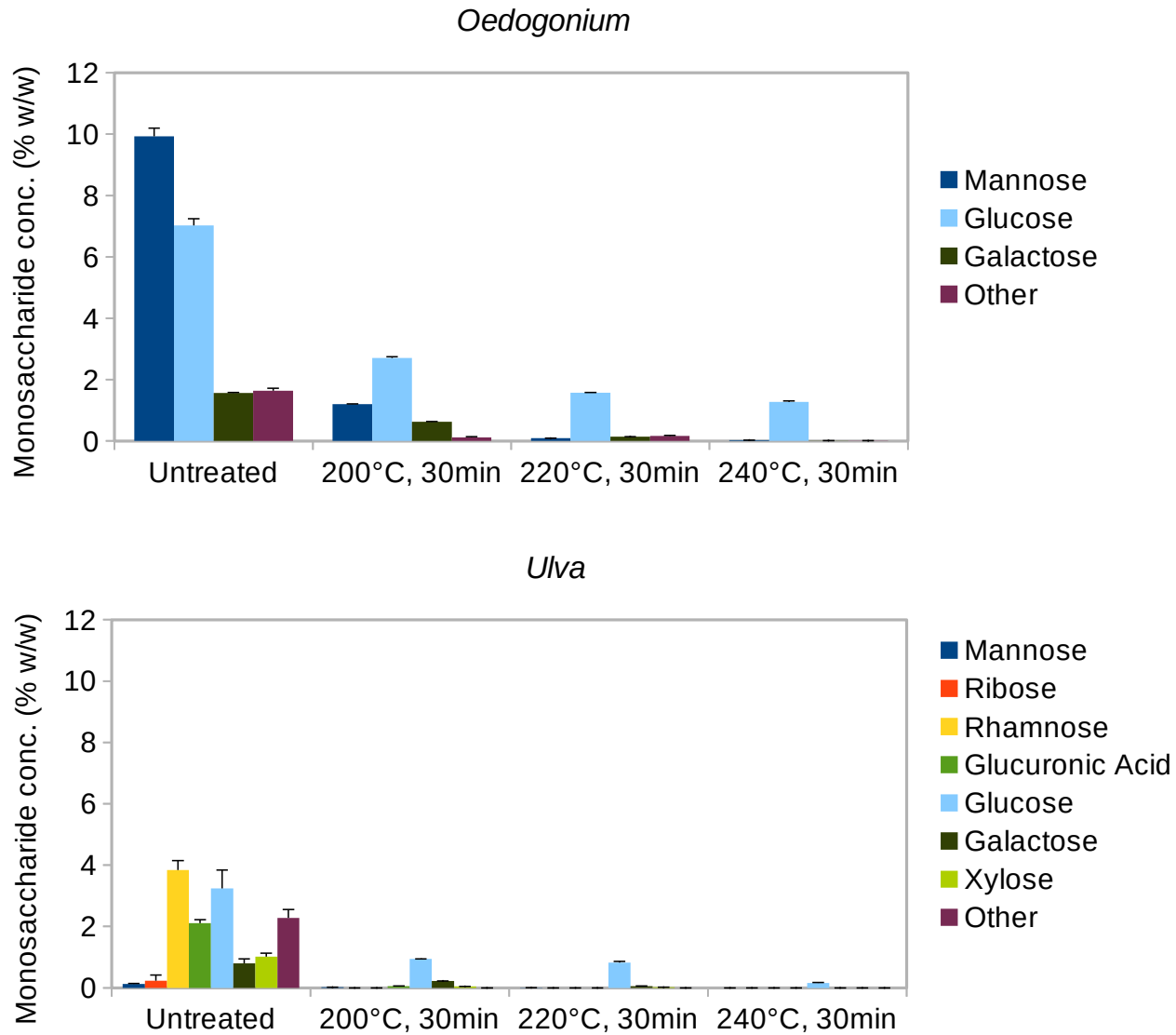


Figure 32: Monosaccharide profiles of untreated *Oedogonium* and *Ulva*, and select HTC hydrochars following HTC at different temperatures (200 °C – 240 °C) and one isothermal holding time (30 min). Error bars represent a single standard deviation.

Figure 33 shows this rapid degradation of hemicellulose during HTC, with hemicellulose content trending towards zero across all reaction conditions and species. *Ulva* hemicellulose in particular seems to be very susceptible to HTC degradation, more so than in *Oedogonium*. At each time and temperature point, *Ulva* hemicellulose retentions are lower than in *Oedogonium*, especially during the 200 °C series; after 5 minutes at 200 °C, *Oedogonium* retains 79% of hemicellulose, while *Ulva* retains only 26%. For both species, degradation is especially rapid at

240 °C, with both macroalgae strains losing 99% of their hemicellulose within 5 minutes at reaction temperature. Of the biochemical components assayed here, hemicellulose was the most obviously and consistently first order, while *Ulva* did have a slightly closer fit to a 1.2nd order model, however this may simply have been a measure of fitting to noise in the data.

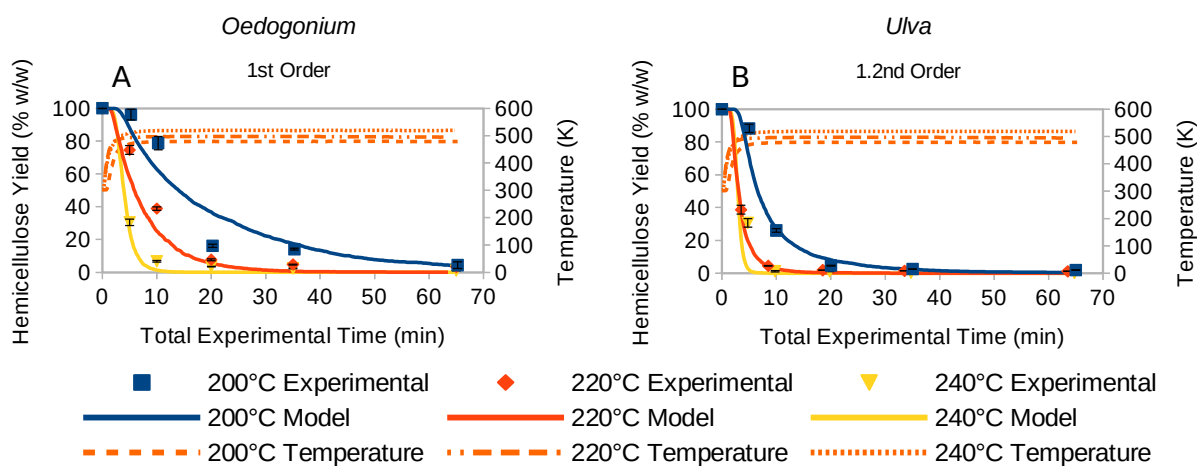


Figure 33: Degradation and Arrhenius kinetic modeling of hemicellulose within macroalgae following HTC at different temperatures (200 °C – 240 °C) and different isothermal holding times (0 min – 60 min). (A) First order kinetic model of *Oedogonium* hemicellulose. (B) 1.2nd order kinetic model of *Ulva* hemicellulose. Error bars correspond to one standard deviation.

Compared to woody biomasses like saltbush, the rate constants of macroalgae hemicellulose were largely comparable, with *Oedogonium* being very similar. At 200 °C, 220 °C, and 240 °C, *Oedogonium* hemicellulose had k rate constants of 0.04 s⁻¹, 0.13 s⁻¹ and 0.46 s⁻¹ respectively (Table 6), very similar to those of saltbush, especially at the lower temperatures¹⁷⁴. *Ulva* hemicellulose had an identical rate constant at 200 °C to both *Oedogonium* and saltbush, but had rather higher reaction rates at higher temperatures, with 0.21 s⁻¹ at 220 °C and 0.89 s⁻¹ at 240 °C. This is possibly a result of the catalytic effect of the high ash content. Despite the similarities in reaction rates to saltbush, both species of macroalgae showed much higher hemicellulose activation energies than terrestrial plants, with *Oedogonium* showing 115 kJ mol⁻¹ and *Ulva* showing 138 kJ mol⁻¹, compared to the 66 kJ mol⁻¹ of saltbush, 58 kJ mol⁻¹ for hemp stem and 67 kJ mol⁻¹ for hemp seed hull.

Figure 34 shows how, compared to hemicellulose, cellulose is more resistant to hydrothermal degradation, with *Ulva* cellulose again proving to be more readily hydrolysed during HTC than its *Oedogonium* counterpart. In *Ulva*, all temperatures led to a rapid loss of crystalline cellulose, with 40% of cellulose hydrolysed with 5 minutes at 200 °C, and up to 60% lost across the same time at 240 °C. In contrast, *Oedogonium* cellulose reacts far more slowly, especially at the cooler temperatures; after a full 60 minutes at 200 °C, *Oedogonium* loses only 17% of cellulose. Despite these differences at cooler temperatures, both species exhibit very rapid cellulose loss at 240 °C, with both falling to just 15% of the initial cellulose content after 60 minutes.

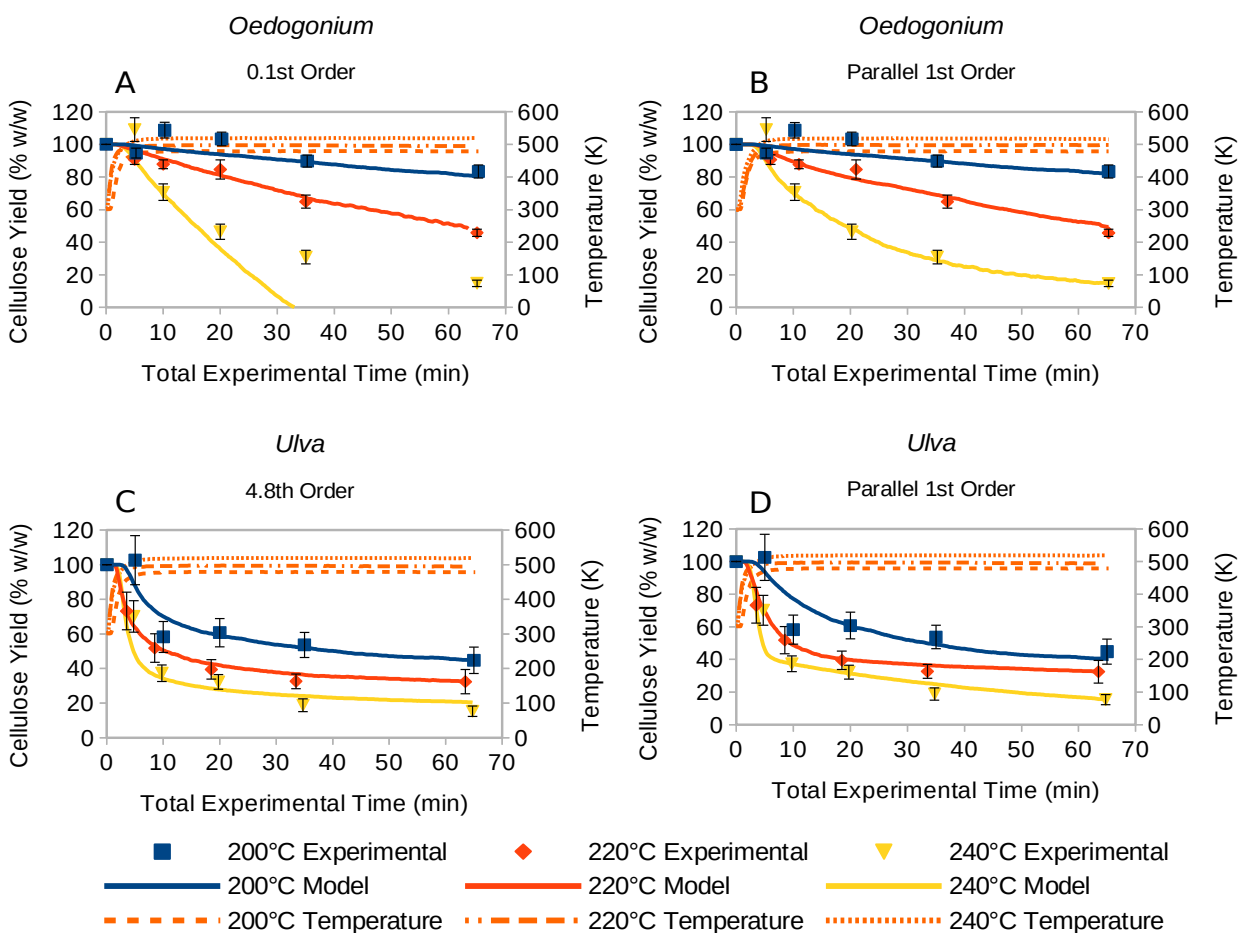


Figure 34: Degradation and Arrhenius kinetic modeling of cellulose within macroalgae following HTC at different temperatures (200 °C – 240 °C) and different isothermal holding times (0 min – 60 min). (A) 0.1st order kinetic model of *Oedogonium* cellulose. (B) Parallel first-order kinetic model of *Oedogonium* cellulose. (C) 4.8th order kinetic model of *Ulva* cellulose. (D) Parallel first order kinetic model of *Ulva* cellulose. Error bars represent one standard deviation.

This high degree of stability under hydrothermal conditions is due to the crystalline nature of cellulose. By aggregating into a rigid, regular matrix, water is excluded from accessing the β -(1 \rightarrow 4) glycosidic linkages between the glucose monomers of cellulose, making hydrolysis reactions more difficult. In addition, the interior of the cellulose fibril is highly hydrophobic. Thus, any hydrolysis must occur from the outside of the fibril towards the interior. By contrast, hemicellulose lacks the crystalline structure of cellulose, and thus the constituent glycosidic linkages are exposed to water molecules on all sides, leaving it highly prone to hydrolysis.

The fact that there is such a significant discrepancy of cellulose degradation between the two species is noteworthy, as it might be expected that crystalline cellulose ought to behave in a similar manner regardless of origin. One possible explanation for this could be that *Ulva* contains a high amount of ash: 25% on a dry basis, compared to just 10% for *Oedogonium*. Being a saltwater species, large portion of this ash in *Ulva* would be sodium, which has been shown to have a catalytic effect on hydrothermal reactions¹⁹⁵. Another possibility is that there are structural differences between the cellulose of either species. Cellulosic microfibrils as they occur within the cell walls are not uniformly crystalline, but instead often contain amorphous regions where the glucose strands are not arranged into a regular matrix⁶³. Without the protection of the crystal matrix, these disordered sections would be more exposed to hydrolytic attack. Additionally, cellulose microfibrils *in situ* are not perfectly straight and smooth, but contain numerous kinks, twists, nanopores and other morphological irregularities, the sum of which lead to a significant increase in the total surface area of the entire cellulose body⁶³. X-ray diffraction analysis of *U. lactuca* cellulose fibrils did not find conclusive evidence for strong crystallinity within the fibrils, suggesting that the fibril crystals may be very small²²⁶. This has been reported in other species of *Ulva* as well²²⁷, and thus it appears likely that this is a property shared with *U. ohnoi* as well.

Kinetically, this variance in crystallinity results in very different reaction rates. In *Oedogonium*, the experimental data of cellulosic degradation fit much closer to a first order model (SSE = 76) than a second order model (SSE = 81) (Figure 34A), although it is worth noting that the SSE continues to drop with reaction orders less than 1.0, eventually reaching a minimum of 67 at an

improbable reaction order of 0.1 (Table 6). Given the unlikelihood of a genuine reaction order of 0.1 (the 240 °C model predicts a cellulose content of 0 after 30 minutes, while the real value is 31%, causing a failure of the r^2 calculation), it is assumed that *Oedogonium* reacts with at least a pseudo-first order reaction. As with hemicellulose, the kinetics of *Oedogonium* cellulose are rather similar to those of saltbush. The rate constants at 200 °C and 220 °C for saltbush are 0.0009 s^{-1} and 0.005 s^{-1} , similar albeit slightly lower than those found for *Oedogonium* in a first order reaction scheme (0.0003 s^{-1} and 0.009 s^{-1} respectively). At 240 °C, however, saltbush has a reaction rate of 0.035 s^{-1} , a near perfect match for the value found for *Oedogonium* at the same temperature. In addition, the activation energies of saltbush ($134.4 \text{ kJ mol}^{-1}$), hemp stem (113 kJ mol^{-1}) and hemp seed hull (112 kJ mol^{-1}) are very close to the *Oedogonium* values ($130.4 \text{ kJ mol}^{-1}$), suggesting a very similar reaction scheme to lignocellulosic biomass.

Ulva, by contrast, is very different. The second order model fits the data more closely (SSE = 95) than the first order model (SSE = 135), but even then the fit is far less good than for *Oedogonium* cellulose, or indeed hemicellulose for either species. Indeed, the reaction order that provides the closest fit is a 4.8th reaction order (SSE = 62) (Figure 34C), which entails reaction rates in the range of $1 \times 10^{-9} \text{ s}^{-1}$ (Table 6). As previously noted, *Ulva* cellulose is possibly much less crystalline than the in *Oedogonium*, raising the possibility that a twin-parallel degradation scheme may be present within *Ulva* cellulose, wherein one reaction involves the rapid hydrolysis of the disordered cellulose and the second reaction involves slower hydrolysis of the more crystalline portion. To this end, a second kinetic model was built to see if this was more representative of the data. In this new model, two parallel first order reactions were assumed, and the sum of the two models was fit to the experimental data in the same manner as above. The kinetics of the slow crystalline degradation were initially set to be identical to those of *Oedogonium*, while the initial settings of the fast reaction were set to those of *Ulva* hemicellulose. The proportion between the two types of cellulose was initially estimated to be 60% : 40% crystalline : disordered, and was then computationally solved simultaneously with the parallel reactions.

It was found that this parallel reaction model fit the data for *Ulva* cellulose more closely than either first or second order single reaction models (SSE = 80) (Figure 34D). As well as the

closest sum of squares difference, the r^2 values for each reaction temperature are significantly greater than those for either first and second order models (Table 6). The proportion of disordered cellulose was found to be slightly higher than crystalline cellulose, at 57% to 43%. The kinetics of the fast and slow reactions did not deviate much from their initial settings after the computational minimising, remaining similar to the values for *Ulva* hemicellulose and *Oedogonium* cellulose respectively (Table 6). This may suggest that the kinetic characters for these reactions do indeed resemble those of hemicellulose for the fast reaction and crystalline cellulose for the slow reaction. However, if the kinetics of the hydrolysis of disordered cellulose were so similar to hemicellulose, the question arises as to why this disordered cellulose remained after the Updegraff hot acid hydrolysis used to quantify the crystalline cellulose content, and did not degrade with the rest of the hemicellulose. It is possible, given the lower temperature of the Updegraff assay compared to the HTC reaction (100 °C compared to 200 °C – 240 °C) that the structure of disordered cellulose, either through a partially crystalline nature, or being protected by the truly crystalline portions of the fibril, was able to resist the milder conditions when the fully amorphous and unprotected hemicellulose was not. When the same parallel reaction model was applied to *Oedogonium*, it was found that the model produces a slightly less good fit than the first order model (SSE = 75) (Figure 34B). In this model, it was calculated that only 6% of the cellulose was disordered and that it reacted near instantaneously, with reaction rate constants in excess of 10^{-60} s^{-1} at all temperatures. Owing to the implausible instantaneous reaction rates and the lower goodness of fit, this parallel reaction model was rejected in the case of *Oedogonium* cellulose.

Protein, as calculated from the dry, ash-free nitrogen content, made up the single largest portion in terms of dry weight percentage for both species, comprising 21% of *Oedogonium*, and 19% of *Ulva* (Figure 29). This is in contrast with terrestrial plants, especially woody plants, which typically possess less than 5% protein on a dry weight basis⁶. The profile of nitrogen (and thereby protein/proteinaceous reaction products) retention in macroalgae is noticeably different from those of woody biomasses, such as saltbush and hemp, as shown in Figure 35. While macroalgae nitrogen yield follows a curve, as with the carbohydrates, in woody biomasses the nitrogen yield falls a small to moderate amount during the heat up phase (10-30%), and then remains constant, regardless of time or temperature (Figures 13, 17 and 22). This

may be a factor of the relative amount of protein in each biomass; in saltbush protein only makes up a mere 8% of the dry weight of the biomass, while both species of macroalgae have approximately one quarter of their dry weight as protein. In keeping with the trend observed with the polysaccharides, *Ulva* is more susceptible to protein degradation than *Oedogonium* is, with protein content falling by around 70% after an hour at 200 °C and 220 °C, and by 89% after 60 minutes at 240 °C. *Oedogonium* protein content fell by 50% after an hour at 200 °C, and by up to 60% after a hour at 240 °C. As with carbohydrates, protein is lost from the biomass via hydrolysis reactions, this time with the hydrolysis of the peptide bond between amino acids. This C-N bond is more stable than the glycosidic bonds present in carbohydrates, resulting in a slower hydrolysis rate of the peptides^{26,228}. However, the manner in which the amino acids breakdown further is complex, and appears to vary across different amino acids and different pH ranges of the medium, with some amino acids, such as leucene, isoleucene, phenylalanine, serine and threonine and histidine being less stable than others at lower pH ranges^{82,229}. This complexity is reflected in the kinetics observed here.

In a similar manner to the *Ulva* cellulose, the reaction orders with the lowest SSE were implausibly high, at 3.8 for *Ulva* (SSE = 43) and 5.4 for *Oedogonium* (SSE = 40) (Table 6). It seems unlikely, then, that the mechanism of protein degradation is a simple hydrolysis scheme. Indeed, during the HTC reaction, it is likely that the proteins within the biomass quickly denature to become a sticky, hydrophobic mass that does not hydrolyse easily¹⁴⁵. It has been suggested that this nitrogenous, semi-solid material may undergo subsequent Maillard reactions with carbohydrates to form heterocyclic compounds and piperazinediones, which may contribute to the dehydrative formation of secondary char^{82,145,147}.

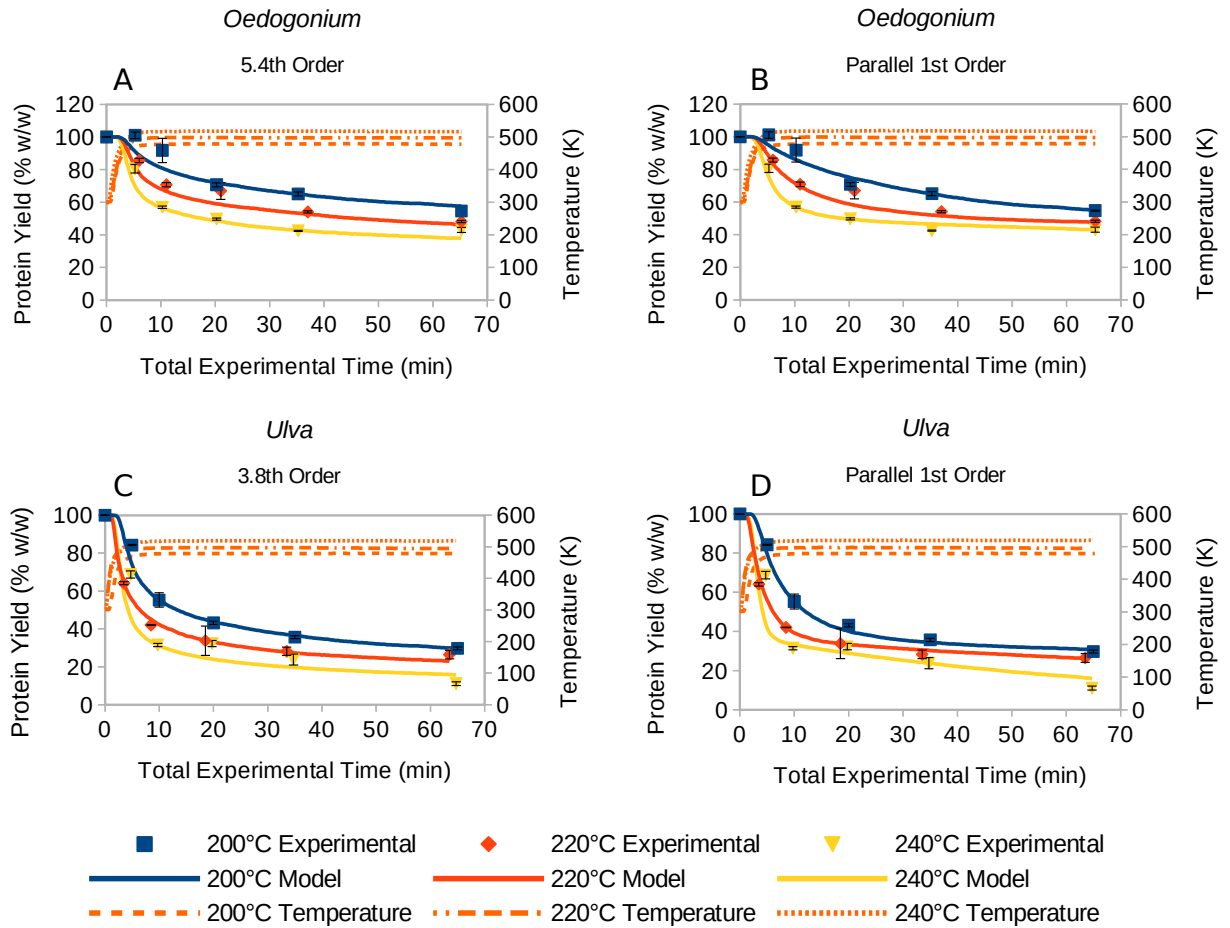


Figure 35: Degradation and Arrhenius kinetic modeling of protein within macroalgae following HTC at different temperatures (200 °C – 240 °C) and different isothermal holding times (0 min – 60 min). (A) 5.4th order kinetic model of *Oedogonium* protein. (B) Parallel first order kinetic model of *Oedogonium* protein. (C) 3.8th order kinetic model of *Ulva* protein. (D) Parallel first order kinetic model of *Ulva* protein. Error bars represent one standard deviation.

A parallel reaction model, wherein the fast reaction corresponds to the hydrolysis of the denatured protein mass, and the slow reaction corresponds to the Maillard and dehydration reactions of the protein mass, was constructed and applied to the protein data for both species. In this case, denaturation was assumed to have occurred instantaneously. For both species, the parallel reaction models had much higher values of goodness of fit than the first and second order models, but slightly less than the higher reaction order models ($SSE_{Ulva} = 53$, $SSE_{Oedogonium} = 46$) (Figure 35B and 35D). In *Oedogonium*, the proportion between fast and slow reacting protein was found to be almost half and half, at 51% to 48%. The activation energies for the two

reactions were very similar, at around 90 kJ mol^{-1} , while the Arrhenius constant for the fast reaction was higher than that for the slow reaction, at 4.17×10^8 compared to 3.32×10^6 (Table 6). The rate constants of the fast reaction begin at $200 \text{ }^\circ\text{C}$ at the same level as those for hemicellulose at 0.03 s^{-1} , but rises much more slowly with increasing temperature, reaching only 0.19 s^{-1} at $240 \text{ }^\circ\text{C}$. The slow reaction is even slower, rising from just 0.0005 s^{-1} at $200 \text{ }^\circ\text{C}$ to 0.003 s^{-1} at $240 \text{ }^\circ\text{C}$. In the *Ulva* parallel model, the proportion of fast to slow reacting protein was much higher, at 63% fast to 37% slow. The activation energies of both reactions were slightly lower in *Ulva* than in *Oedogonium*, at 88 kJ mol^{-1} for the fast reaction and 74 kJ mol^{-1} for the slow reaction. The rate constants for both reactions were faster in *Ulva* than *Oedogonium* at all temperatures, ranging from 0.12 s^{-1} to 0.68 s^{-1} over the temperature series for the fast reaction, and 0.003 s^{-1} to 0.012 s^{-1} for the slow reaction.

The remainder of the total solid mass is assumed to comprise of so-called aqueous extractives, a catch-all term referring to sterols, nucleic acids, phenolics and other biochemical compounds dissolved in the cytoplasm of the cell. In *Ulva*, this was found to comprise 28% of the dry weight of the alga, while in *Oedogonium*, this was found to be 17% (Figure 29). In keeping with previous kinetic modeling in the literature, this portion of the biomass was assumed to react instantaneously during HTC^{108,174}. After this assumption, the remaining portion of the hydrochars was then assumed to be made up of secondary char. As the reaction severity increased, the portion of secondary char also increases, until a full half of the total weight of the hydrochar is made up of secondary char after 60 min at $240 \text{ }^\circ\text{C}$ (50% for *Oedogonium*, and 48% for *Ulva*) (Figure 29). While determining the secondary char content by difference may be a reasonable assumption at higher reaction severities, when the biomass is highly disrupted and converted, at the very lowest severities the implication arises wherein the aqueous extractives are instantly converted directly into secondary char. This makes it difficult to accurately model the formation of secondary char formation as it condenses from the aqueous phase.

Moving into the future, a fuller understanding of the products formed during the HTC reaction, especially regarding the secondary char as distinct from the primary char would be

extremely useful in building a whole-system kinetic model that not only describes the degradation of the biomass, but also the formation of the products.

6.4 Conclusion

Two species of macroalgae, *Oedogonium intermedium* and *Ulva ohnoi*, were subjected to hydrothermal carbonisation, and the biochemical composition of the resultant hydrochars was finely characterised through a detailed analysis. A variety of kinetic models were built to describe the degradation of these biochemical components. It was found that, while some components such as hemicellulose and *Oedogonium* cellulose conform to a simple first order hydrolysis reaction, other components such as protein and *Ulva* cellulose undergo more complex reaction schemes, involving multiple simultaneous reactions. This consideration of how the same macromolecule within different biomasses behaves during HTC has not been well studied, and illustrates the importance of performing whole-biomass kinetic studies.

6.5 Acknowledgments

This project was funded and supported by the Australian Research Council Centre of Excellence in Plant Cell Walls CE110001007. The Authors would like to thank Matthew Potter for his invaluable assistance with the HTC reactions, Tony Hall of the University of Adelaide, Physical Sciences, for performing the CHN analysis, and the Australian Federal Government for providing a Research Training Scholarship to support the work of the researchers.

Chapter 7

Thesis Conclusions and Future Directions

7.1 Thesis Conclusions and Key Findings

This thesis explores the hydrothermal carbonisation of various novel biomasses, in particular the mechanisms and kinetics by which the biomass is thermally converted into hydrochar. Overall, it has been demonstrated that hydrothermal carbonisation is a highly versatile process that is capable of generating energy-enriched hydrochars from a wide variety of biomasses, both terrestrial and aquatic. Such novel biomasses as saltbush, hemp, and macroalgae, exhibit numerous characteristics that make them favourable as a potential biofuel feedstock. All of them have high growth rates, and can be readily grown on sub-optimal land, either in semi-arid, salt-blighted locations as in saltbush, or in vats on non-productive land as in macroalgae. In doing so, these biomasses avoid competing with food crops for resources and land, and as such side-step the controversies associated with first-generation biofuels. Additionally, these biomasses each have numerous different human applications, some of which command a high market value. Saltbush cultivation as a means of soil remediation and as a source of drought-resistant forage for sheep is growing, catering to a rising demand for sustainable agriculture and upmarket saltbush lamb. Industrial and dietary hemp products such as textiles, flour, food additives, building materials, insulation, plastics, and many others besides, are rapidly gaining in popularity across the globe. And macroalgal products, especially ulvans, are widely hailed for their remarkable bioactivity, while the macroalgae themselves can be used to treat contaminated water, and also as a food source. Together, these novel biomasses represent an important facet in an emerging bioeconomy, wherein biological material is utilised holistically and sustainably in order to deliver new value and products in an environmentally-friendly manner.

Hydrothermal carbonisation has the potential to be a keystone technology in this new bioeconomy, in converting waste or excess biomass into hydrochar and liquid products which may be utilised as a liquid fertiliser, soil enhancement, or as a renewable solid fuel source. The present research has demonstrated that each of the biomasses studied here are suitable for the production of hydrochar for thermal applications (Papers I, III and IV), with longer residence times at higher temperatures leading to hydrochars with greater higher heating values and lower ash content than typical lignites. To understand the manner in which the biomass was converted into hydrochar, a variety of biochemical analysis techniques were developed to

Hydrothermal Carbonisation of Novel Biomasses

accurately quantify the key biochemical components of the feedstocks, thus allowing the changes within the feedstock to be tracked with accuracy (Papers II, III and IV). Using this information, a twin pathway mechanistic schematic was produced to describe the carbonisation process, with Mechanism 1 involving solid-solid conversion of the biomass into primary char, and Mechanism 2 involving a two-step process where the biomass degrades into soluble intermediates which then condense and repolymerise into secondary char. Finally, the degradation of the principle biochemical components in whole biomass, corresponding to the initial degradation step of Mechanism 2, was described using a simple Arrhenius kinetic model.

7.1.1 Fuel Properties of HTC of novel biomasses

HTC of all three feedstocks lead to significant thermal upgrading of the biomass. The more severe the reaction conditions, the higher the HHV of the hydrochars, with the most severe conditions elevating the energy content of the hydrochar to levels observed in lignites, at between 27 and 31 MJ kg⁻¹. This was chemically driven by the removal of oxygen from the solid phase, as a result of dehydration and dewatering reactions. In the process, this lead to an increase in the overall carbon content of the hydrochar. In addition to the boost in HHV, HTC consistently lead to a reduction in the ash content of the solid phase, even in biomasses with very high inorganic contents, such as marine seaweed. In general, as with HHV and oxygen content, higher reaction severity lead to greater effect, with ash reduction at the higher severities resulting in hydrochars with highly favourable ash levels compared to fossil coals. However, it was noted in some cases, inorganics were absorbed back into the solid phase under high reaction severities. In saltbush, phosphorous was reabsorbed at 260 °C, while in *Ulva ohnoi*, enough inorganics were reabsorbed after 60 minutes at 220 °C and 240 °C that the total ash content of the hydrochars was almost identical to that of the untreated feedstock, making up a quarter of the entire solid fraction by mass. Obtaining the highest quality solid fuels from these novel biomasses is therefore not as simple as merely processing the feedstocks at the highest conditions possible. Another consideration for wider scale adoption of HTC of these biomasses is that there is an inverse relationship between high heating value and hydrochar yield; for most of the biomasses studied here, the mass yields after half an hour at 260 °C or 240 °C are less than 40%, and for *Ulva*, the mass yields at the highest reaction conditions are less than 20%. With the necessarily low price of solid fuels, it remains an open question as to

whether these low yields of high-quality fuel are more economically valuable than larger quantities of lower-quality fuel. Such considerations are outside the scope of this thesis, however.

7.1.2 Compositional Analysis of Hydrochars

The biomasses examined here, while each distinct from a taxonomic perspective, shared numerous compositional properties (Table 7). Each had a hemicellulose content of between 14% and 20%, had crystalline cellulose as their largest compositional fraction at between 40% and 25% (with the single exception of *Ulva*), and had an aqueous extractive content of around 30%. The lignocellulosic biomasses had similarly small amounts of lignin, at around 8-15%, while also having similar protein contents of around 10% (hemp stem had a very small protein content of 3%). The macroalgae both had protein levels of 20%. These broad similarities across the different biomasses resulted in consistencies across the various hydrochars, as noted above regarding their fuel properties. Where there was significant divergence in the composition, such as in the low level of crystalline cellulose and high content of *Ulva*, there were greater differences observed in the hydrochar yield, as well as the HHV of those hydrochars produced.

The physical structure of a biochemical component determines its behaviour during hydrothermal carbonisation. The reaction rates of polysaccharides are principally determined by their crystallinity, with non-crystalline polysaccharides hydrolysing extremely rapidly, while crystalline polysaccharides, notably cellulose, are more resistant, especially at lower temperatures. The crystallinity of cellulose, and the advantages it offers in resisting HTC degradation are well known, but it appears that the degradation of hemicelluloses as well can be slowed by increased crystallinity afforded by the structure of the arabinoxylan backbone. The degradation of proteins is poorly understood, especially in a whole biomass system, but appears to be more complex than a simple hydrolytic pathway, possibly involving Maillard reactions with carbohydrates. Lignin is comprised of two fractions: HTC-soluble lignin, and HTC-insoluble lignin, with soluble lignin being the dominant fraction in the feedstocks investigated in this thesis. HTC-soluble lignin reacts very rapidly, frequently with similar kinetic parameters to hemicellulose, implying that the mechanisms may be similar.

Table 7: Summary of concentrations of each biochemical macromolecule (% w/w) in each feedstock (untreated, and select hydrochars) studied in this thesis.

		Hemicellulose	Cellulose	Lignin	Protein	Ash	Aqueous Extractives	Char
Saltbush	Untreated	20.7	24.4	15.4	7.7	5.6	26.2	0.0
	200°C 60 min	1.0	37.3	5.3	6.6	4.0	0.0	45.9
	230°C 60 min	0.6	30.5	5.5	9.1	4.7	0.0	49.6
	260°C 60 min	0.0	5.9	9.7	8.4	3.7	0.0	72.2
Hemp Stem	Untreated	14.2	42.6	7.5	3.1	3.8	28.8	0.0
	200°C 60 min	1.9	57.4	5.3	3.1	1.8	0.0	30.5
	230°C 60 min	1.1	48.1	4.0	3.3	1.3	0.0	42.0
	260°C 60 min	0.0	7.0	5.0	5.5	1.9	0.0	80.7
Hemp Hull	Untreated	15.0	31.3	10.2	10.3	3.6	29.6	0.0
	200°C 60 min	0.9	39.6	5.3	11.7	3.8	0.0	38.6
	230°C 60 min	0.5	24.6	6.2	13.2	5.4	0.0	50.2
	260°C 60 min	0.0	10.2	9.6	15.1	6.1	0.0	58.9
Ulva	Untreated	13.6	9.0	0.0	19.3	25.3	27.7	0.0
	200°C 60 min	1.1	17.6	0.0	25.0	5.7	0.0	46.3
	220°C 60 min	0.7	13.6	0.0	23.7	12.2	0.0	45.6
	240°C 60 min	0.1	9.1	0.0	14.0	24.9	0.0	47.8
Oedogonium	Untreated	20.2	22.7	0.0	21.2	9.6	17.3	0.0
	200°C 60 min	1.6	35.1	0.0	19.6	3.9	0.0	32.0
	220°C 60 min	1.6	25.0	0.0	22.4	4.7	0.0	38.6
	240°C 60 min	0.6	10.4	0.0	25.9	5.5	0.0	50.0

An interesting finding of this study is that the same biochemical macromolecule can behave differently within different biomasses. It is typically believed that cellulose for example reacts in more or less the same way across all biomasses. However, it was found that *Ulva* cellulose was far more susceptible to hydrothermal degradation than its *Oedogonium* and lignocellulosic counterparts, likely playing a large role in *Ulva* subsequently having the lowest hydrochar yields of any biomass studied here. Such a finding would be impossible to achieve by relying entirely upon purified crystalline cellulose as an idealised feedstock, which is usually sourced from wood pulp. Other important influences on the hydrochar yield are likely to be the amount of HTC-inert lignin, the degree of cross-linking between the various cell wall components, and the level of catalytic inorganics present in the feedstock.

7.1.3 Kinetics of the Principle Biochemical Components of biomass

The degradation of the principle biochemical components was described using simplified Arrhenius kinetic models, summarised in Table 8. In this manner, it was possible to estimate the energy requirements of the HTC reaction, thus contributing to the design of more efficient reactors and chemical processes. While the models presented here were calculated to find the optimum reaction order, due to the tremendous complexity of the HTC reaction, it is important to note that such orders are only pseudo-orders at best. Nevertheless, it is possible to make some informed statements about the kinetics of the components. Hemicellulose, across any biomass studied here, reacts with a pseudo-first order reaction, as does HTC-soluble lignin. The only exception to this was hemp stems with an assumed 21% HT-insoluble content, which formed the closest fit with a second order model, the only component to do so. Cellulose was the most inconsistent of the compounds to model, with optimal reaction orders ranging from 0.1 to 1.5. This probably reflects the complex interaction of factors such as differing degrees of crystallinity, the amount of catalytic inorganics, the morphology of the cellulose fibrils themselves, any softening of the fibrils during the reaction, and the amount of cross-linking between the cellulose fibrils and other cell wall components. For some components, such as macroalgal protein and *Ulva* cellulose, a parallel reaction scheme involving two simultaneous first order reactions produced a better fit to the data than a single order scheme, which produced implausibly high reaction orders. In each model presented here though, the activation energies of the components as measured in whole biomass were consistently lower than those obtained from purified model compounds. In light of this, it is recommended that future kinetic studies on HTC of biomass omit the use of model compounds, as they are not representative of what occurs within whole biomass.

Hydrothermal Carbonisation of Novel Biomasses

Table 8: Summary of Kinetic Parameters of the biochemical macromolecules and feedstocks and models examined within this thesis. k : Reaction rate constant at a given temperature; E_a : Activation energy; A_0 : Arrhenius constant; n : Reaction order; SSE: Sum of Squares Error. Rate constants presented as averages over the holding time at reaction temperature, not including warm-up time.

	Feedstock and Model	n	SSE	200 °C		220 °C		240 °C		E_a (kJ mol ⁻¹)	A_0 (s ⁻¹)
				k (s ⁻¹)	r^2	k (s ⁻¹)	r^2	k (s ⁻¹)	r^2		
Hemicellulose	Saltbush	1	33	0.061	0.92	0.136	0.87	0.323	-0.27	61	3.1×10^5
	Hemp Stem	1.3	21	0.02	0.99	0.04	0.97	0.1	0.98	58	5.0×10^4
	Hemp Hull	1.3	45	0.03	0.95	0.09	0.99	0.2	0.16	67	8.7×10^5
	<i>Ulva</i>	1.2	58	0.06	0.99	0.21	0.21	0.89	0.98	138	4.5×10^{13}
	<i>Oedogonium</i>	1	68	0.04	0.89	0.13	0.88	0.46	0.67	115	1.7×10^{11}
Cellulose	Saltbush	0.5	49	0.009	0.3	0.048	0.81	0.29	0.98	127	8.8×10^{11}
	Hemp Stem	1	70	0.002	-3.97	0.012	-1.15	0.047	0.99	113	6.6×10^9
	Hemp Hull	1.5	54	0.0003	-2.05	0.0015	0.9	0.0038	0.98	112	4.2×10^8
	<i>Ulva</i> (1-step)	4.8	62	9.0×10^9	0.72	8.1×10^9	0.99	4.1×10^8	0.88	155	1.6×10^8
	<i>Ulva</i> (Fast Reaction)	1	80	0.05	0.76	0.2	0.9	0.93	0.94	148	7.3×10^{14}
	<i>Ulva</i> (Slow Reaction)			0.002		0.005		0.016		113	
	<i>Oedogonium</i> (1-step)	0.1	67	0.19	0.44	0.57	0.99	2.07	N/A	130	5.3×10^{11}
	<i>Oedogonium</i> (Fast Reaction)	1	75	8.0×10^{-73}	0.41	1.0×10^{-69}	0.78	1.0×10^{-66}	0.99	767	4.3×10^{11}
	<i>Oedogonium</i> (Slow Reaction)			0.003		0.012		0.039		132	
Lignin	Saltbush	1	32	0.053	0.99	0.127	0.66	0.323	0.37	66	9.5×10^5
	Hemp Stem (34% Inert)	1	86	0.02	0.94	0.09	0.5	0.31	0.33	98	1.5×10^9
	Hemp Stem (21% Inert)	2	89	0.0003	0.92	0.001	0.66	0.003	0.18	81	2.5×10^5
	Hemp Hull	1	88	0.08	0.95	0.11	0.74	0.14	-0.26	22	1.9×10^1
Protein	<i>Ulva</i> (1-step)	3.8	43	4.0×10^7	1	9.1×10^7	0.98	2.4×10^6	0.82	92	4.0×10^3
	<i>Ulva</i> (Fast Reaction)	1	53	0.13	0.98	0.27	0.96	0.68	0.94	88	4.7×10^8
	<i>Ulva</i> (Slow Reaction)			0.003		0.006		0.013		74	
	<i>Oedogonium</i> (1-step)	5.4	40	5.7×10^{11}	0.86	1.4×10^{10}	0.99	4.3×10^{10}	0.87	104	1.3×10^1
	<i>Oedogonium</i> (Fast Reaction)	1	46	0.03	0.94	0.08	0.67	0.16	0.94	92	4.2×10^8
	<i>Oedogonium</i> (Slow Reaction)			0.0005		0.001		0.193		90	

7.2 Future Directions

7.2.1 Develop a database on the compositions of different biomasses and hydrochars

The mass yield of the HTC reaction, as well as the properties of the hydrochars, is highly reliant upon the composition of the feedstock. With the methods presented here, it is possible to gain a more complete knowledge of the feedstocks as well as the hydrochars than has been previously utilised in HTC research. By applying these methods to an ever wider variety of biomasses, it will be possible to build a database containing information about not only the compositions of different feedstocks, but also the products and the properties of those products. From there, it should be possible to develop a model that could predict the ideal conditions for generating a given product from a given biomass for which the composition was known. Such a database would be an indispensable tool in scaling up hydrothermal technologies in the coming years.

7.2.2 Develop better methods of differentiating primary and secondary char

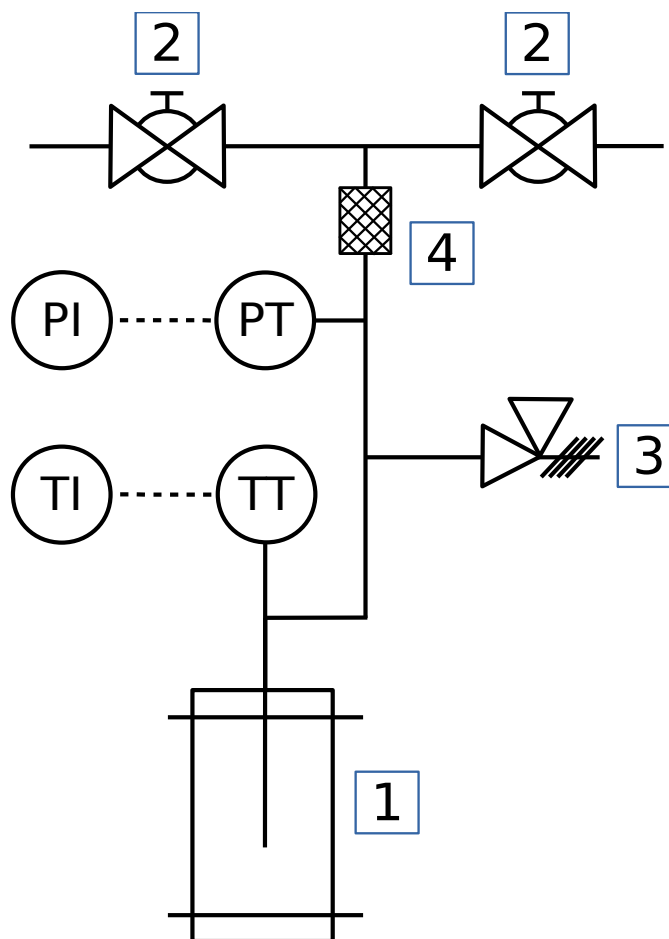
At present, secondary char is calculated by difference from the sum of all other components for which quantities are known. This is the same method used to calculate the aqueous extractives, which are assumed to react instantaneously under HTC conditions. However, this is merely an estimate, and the result of this is that for the lower reaction severities, the “secondary char” content is almost identical to the aqueous extractive content. While this does not present an issue with studying the degradation step of Mechanism 2, without an accurate measure of the amount of secondary char being produced, it is impossible to accurately describe the repolymerisation step. Additionally, by developing better means of quantifying the secondary char, it may be possible to draw a finer distinction within the primary char as well: truly unreacted biomass components, and thermally converted products. With more accurate measures of the products, combined with the knowledge of the degradation reactions, it should be possible to develop holistic kinetic and mechanistic models that describe the entire HTC process.

7.2.3 Investigate the mechanisms by which hydrochar reabsorbs inorganic elements

High levels of inorganic elements in the hydrochar are detrimental to not only fuels, but also to other applications for hydrochars, such as soil amendment or activated carbons. While under most conditions the inorganics of the feedstock are dissolved into the aqueous medium, for certain biomasses, especially *Ulva*, significant amounts of inorganics were reabsorbed back into the solid phase under very high reaction severities. Even for feedstocks that had an overall decrease in total ash content, such as saltbush, certain elements like phosphorus are reabsorbed under high temperatures even as other elements are purged. The mechanisms of this are little understood, and may be related to increased porosity of hydrochars processed under high temperatures. Understanding the manner in which the inorganics are reabsorbed is essential to designing processes that produce hydrochars with the smallest ash content possible.

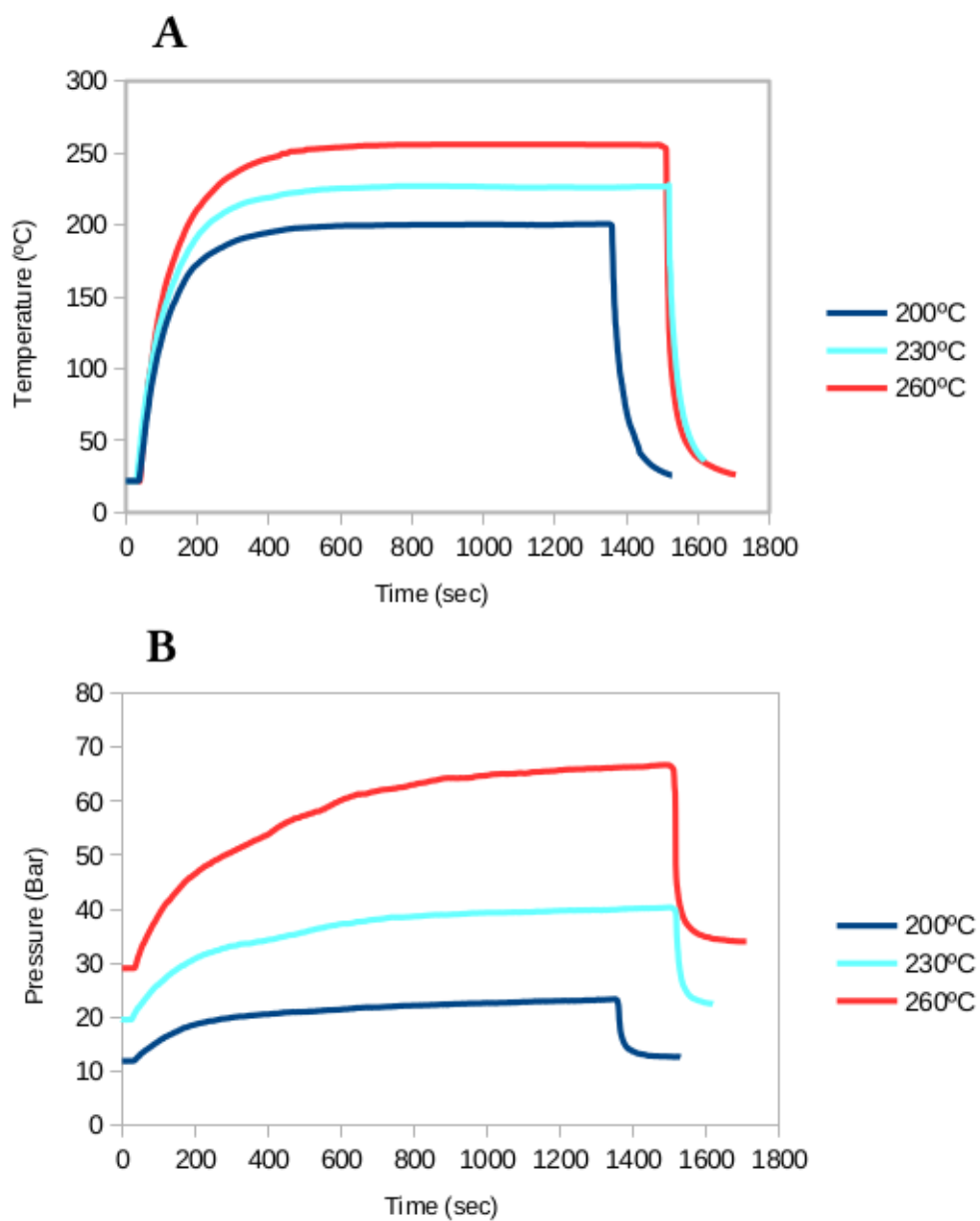
Appendix

Figure of Hydrothermal Carbonisation Reactor



Supplementary Figure 1: Schematic diagram of the custom HTC reactor. PT: Pressure Transducer. PI: Pressure Indicator. TT: Thermocouple. TI: Temperature Indicator. 1: Reactor Tube. 2: Hand-Operated Ball Valves. 3. Safety Pressure Relief Valve. 4: Sintered Stainless Steel Filter

Temperature and pressure profiles of HTC of saltbush, 15 minute runs



Supplementary Figure 2: Temperature and pressure profiles of saltbush HTC after 15 minute runs.

(A) Temperature profile (B) Pressure profile

Supplementary Table 1. Table of statistically significant groupings of various fuel properties and chemical compositions of hydrochars produced from saltbush, determined via Student's *t*-test ($p=0.05$).

		200 °C				230 °C				260 °C			
Time (mins)	Untreated	0	15	30	60	0	15	30	60	0	15	30	60
HHV	a	b	c	d	e	c	e	e	f	e	g	g	h
Volatile Matter	a	a	b	bc	b	c	c	c	d	cd	e	f	g
Fixed Carbon	a	b	c	c	cd	cd	cd	d	e	cd	f	g	h
Ash	a	bd	bc	ce	bf	c	c	cd	bd	c	bde	bde	f
Carbon	a	b	c	d	e	d	ef	ef	g	f	h	i	k
Hydrogen	ad	a	b	bc	b	ac	bcd	b	b	b	bde	be	be
Nitrogen	a	b	a	c	d	e	f	g	h	c	e	f	fg
Sulphur	a	a	a	a	a	a	a	a	a	a	a	a	a
Oxygen	a	b	c	d	d	d	e	e	f	e	g	h	i
Sodium	a	b	bc	be	d	b	c	b	d	b	e	d	f
Chloride	a	bc	b	c	d	bc	e	bc	f	b	g	f	h
Calcium	a	b	c	cd	de	d	de	de	ef	de	cd	fg	g
Potassium	a	bd	bf	bd	cdg	bd	b	bd	deg	bef	df	deg	g
Phosphorus	a	b	b	b	c	bd	e	bd	f	b	g	h	i

Bibliography

1. UN Development Programme. NDC Global Outlook Report 2019. (2019).
2. IPCC. Climate Report 2018. (2018).
3. UN Environment Program. Emissions Gap Report 2019. (2019).
4. BP. BP Energy Outlook 2019. (2019).
5. Naik, S. N., Goud, V. V., Rout, P. K. & Dalai, A. K. Production of first and second generation biofuels: A comprehensive review. *Renew. Sustain. Energy Rev.* **14**, 578–597 (2010).
6. Jenkins, B. M., Baxter, L. L., Miles, T. R. & Miles, T. R. Combustion properties of biomass. *Fuel Process. Technol.* **54**, 17–46 (1998).
7. Hellwig, M. Basics of the combustion of wood and straw. *Energy Biomass 3rd EC Conf. Held Venice 25-29 March 1985* 793–798 (1985).
8. Bridgwater, A. V. Review of fast pyrolysis of biomass and product upgrading. *Biomass Bioenergy* **38**, 68–94 (2012).
9. Durie, R. A. *The Science of Victorian Brown Coal: Structure, Properties of Consequences for Utilisation*. (Butterworth Heinemann, 1991).
10. Lane, D. J. *et al.* Effect of Hydrothermal Carbonization on the Combustion and Gasification Behavior of Agricultural Residues and Macroalgae: Devolatilization Characteristics and Char Reactivity. *Energy Fuels* **32**, 4149–4159 (2018).
11. Biofuels Mandates Around the World: 2016: Biofuels Digest. <http://www.biofuelsdigest.com/bdigest/2016/01/03/biofuels-mandates-around-the-world-2016/>.
12. Annual Ethanol Production. *Renewable Fuels Association* <https://ethanolrfa.org/statistics/annual-ethanol-production/>.
13. International Energy Agency - Transport biofuels. *International Energy Agency* <https://www.iea.org/tcep/transport/biofuels/> (2019).
14. Raman, S. *et al.* Integrating social and value dimensions into sustainability assessment of lignocellulosic biofuels. *Biomass Bioenergy* **82**, 49–62 (2015).
15. Ribeiro, B. E. Beyond commonplace biofuels: Social aspects of ethanol. *Energy Policy* **57**, 355–362 (2013).
16. Avery, D. Biofuels, Food or Wildlife? The massive land costs of U.S. Ethanol. *Issue Anal.* (2006).
17. Mitchell, D. A Note on Rising Food Prices. (2008).
18. Gilbert, C. L. How to Understand High Food Prices. *J. Agric. Econ.* **61**, 398–425 (2010).
19. Baffes, J. & Haniotis, T. Placing the 2006/08 Commodity Price Boom into Perspective. (2010).
20. Keyzer, M. A., Merbis, M. D. & Voortman, R. L. The Biofuel Controversy. *Econ.* **156**, 507–527 (2008).
21. Arneeth, A. *et al.* Historical carbon dioxide emissions caused by land-use changes are possibly larger than assumed. *Nat. Geosci.* **10**, 79–84 (2017).
22. Henders, S., Persson, U. M. & Kastner, T. Trading forests: land-use change and carbon emissions embodied in production and exports of forest-risk commodities. *Environ. Res. Lett.* **10**, 125012 (2015).
23. Searchinger, T. *et al.* Use of U.S. Croplands for Biofuels Increases Greenhouse Gases Through Emissions from Land-Use Change. *Science* **319**, 1238–1240 (2008).
24. Hansen, A. C., Zhang, Q. & Lyne, P. W. L. Ethanol–diesel fuel blends -- a review. *Bioresour. Technol.* **96**, 277–285 (2005).
25. Funke, A. & Ziegler, F. Hydrothermal carbonization of biomass: A summary and discussion of chemical mechanisms for process engineering. *Biofuels Bioprod. Biorefining* **4**, 160–177 (2010).
26. Peterson, A. *et al.* Thermochemical biofuel production in hydrothermal media: A review of sub- and supercritical water technologies. *Energy Environ. Sci.* **1**, 32–65 (2008).
27. Tekin, K., Karagöz, S. & Bektaş, S. A review of hydrothermal biomass processing. *Renew. Sustain. Energy Rev.* **40**, 673–687 (2014).
28. Möller, M., Nilges, P., Harnisch, F. & Schröder, U. Subcritical Water as Reaction Environment: Fundamentals of Hydrothermal Biomass Transformation. *ChemSusChem* **4**, 566–579 (2011).

29. Bedeaux, D. & Kapral, R. The effective reaction rate and diffusion coefficients for a two-phase medium. *J. Chem. Phys.* **79**, 1783–1788 (1983).
30. Toor, S. S., Rosendahl, L. & Rudolf, A. Hydrothermal liquefaction of biomass: A review of subcritical water technologies. *Energy* **36**, 2328–2342 (2011).
31. Fang, J., Zhan, L., Ok, Y. S. & Gao, B. Minireview of potential applications of hydrochar derived from hydrothermal carbonization of biomass. *J. Ind. Eng. Chem.* **57**, 15–21 (2018).
32. Libra, J. A. *et al.* Hydrothermal carbonization of biomass residuals: a comparative review of the chemistry, processes and applications of wet and dry pyrolysis. *Biofuels* **2**, 71–106 (2011).
33. Bergius, F. *Die Anwendung hoher drucke bei chemischen Vorgängen und eine nechbildung des Entstehungsprozesses der Steinkohlen.* (W. Knapp, 1913).
34. Dieguez Alonso, A. *et al.* Towards Biochar and Hydrochar Engineering—Influence of Process Conditions on Surface Physical and Chemical Properties, Thermal Stability, Nutrient Availability, Toxicity and Wettability. *Energies* **11**, 496 (2018).
35. Assarsson, A. Some reactions during chip storage and how to control them. *Pulp Pap Mag Can* (1969).
36. Lehtikangas, P. Storage effects on pelletised sawdust, logging residues and bark. *Biomass Bioenergy* **19**, 287–293 (2000).
37. Liu, Z., Quek, A. & Balasubramanian, R. Preparation and characterization of fuel pellets from woody biomass, agro-residues and their corresponding hydrochars. *Appl. Energy* **113**, 1315–1322 (2014).
38. Escala, M., Zumbühl, T., Koller, Ch., Junge, R. & Krebs, R. Hydrothermal Carbonization as an Energy-Efficient Alternative to Established Drying Technologies for Sewage Sludge: A Feasibility Study on a Laboratory Scale. *Energy Fuels* **27**, 454–460 (2013).
39. Ma, P.-Y. *et al.* Determination of Combustion Kinetic Parameters and Fuel Properties of Hydrochar Prepared from Hydrothermal Carbonization of Bamboo. *BioResources* **12**, 3463–3477 (2017).
40. Borrero-López, A. M. *et al.* High added-value products from the hydrothermal carbonisation of olive stones. *Environ. Sci. Pollut. Res.* **24**, 9859–9869 (2017).
41. Danso-Boateng, E., Shama, G., Wheatley, A. D., Martin, S. J. & Holdich, R. G. Hydrothermal carbonisation of sewage sludge: Effect of process conditions on product characteristics and methane production. *Bioresour. Technol.* **177**, 318–327 (2015).
42. Ghanim, B. M., Pandey, D. S., Kwapinski, W. & Leahy, J. J. Hydrothermal carbonisation of poultry litter: Effects of treatment temperature and residence time on yields and chemical properties of hydrochars. *Bioresour. Technol.* **216**, 373–380 (2016).
43. Smith, A. M., Singh, S. & Ross, A. B. Fate of inorganic material during hydrothermal carbonisation of biomass: Influence of feedstock on combustion behaviour of hydrochar. *Fuel* **169**, 135–145 (2016).
44. Smith, A. M. & Ross, A. B. Production of bio-coal, bio-methane and fertilizer from seaweed via hydrothermal carbonisation. *Algal Res.-Biomass Biofuels Bioprod.* **16**, 1–11 (2016).
45. Naisse, C. *et al.* Effect of physical weathering on the carbon sequestration potential of biochars and hydrochars in soil. *GCB Bioenergy* **7**, 488–496 (2015).
46. Sevilla, M., Antonio Maciá-Agulló, J. & B. Fuertes, A. Hydrothermal carbonization of biomass as a route for the sequestration of CO₂: Chemical and structural properties of the carbonized products. *Biomass Bioenergy* **35**, 3152–3159 (2011).
47. Malghani, S. *et al.* Carbon sequestration potential of hydrothermal carbonization char (hydrochar) in two contrasting soils; results of a 1-year field study. *Biol. Fertil. Soils* **51**, 123–134 (2015).
48. Abel, S. *et al.* Impact of biochar and hydrochar addition on water retention and water repellency of sandy soil. *Geoderma* **202–203**, 183–191 (2013).
49. Röhrdanz, M. *et al.* Hydrothermal carbonization of biomass from landscape management – Influence of process parameters on soil properties of hydrochars. *J. Environ. Manage.* **173**, 72–78 (2016).
50. Breulmann, M., van Afferden, M., Müller, R. A., Schulz, E. & Fühner, C. Process conditions of pyrolysis and hydrothermal carbonization affect the potential of sewage sludge for soil carbon sequestration and amelioration. *J. Anal. Appl. Pyrolysis* **124**, 256–265 (2017).

51. Islam, Md. A., Tan, I. A. W., Benhouria, A., Asif, M. & Hameed, B. H. Mesoporous and adsorptive properties of palm date seed activated carbon prepared via sequential hydrothermal carbonization and sodium hydroxide activation. *Chem. Eng. J.* **270**, 187–195 (2015).
52. Jain, A., Balasubramanian, R. & Srinivasan, M. P. Hydrothermal conversion of biomass waste to activated carbon with high porosity: A review. *Chem. Eng. J.* **283**, 789–805 (2016).
53. Erkelens, M., Ball, A. S. & Lewis, D. M. The application of activated carbon for the treatment and reuse of the aqueous phase derived from the hydrothermal liquefaction of a halophytic *Tetraselmis* sp. *Bioresour. Technol.* **182**, 378–382 (2015).
54. Sevilla, M. & B. Fuertes, A. Sustainable porous carbons with a superior performance for CO₂ capture. *Energy Environ. Sci.* **4**, 1765–1771 (2011).
55. Islam, Md. A., Ahmed, M. J., Khanday, W. A., Asif, M. & Hameed, B. H. Mesoporous activated coconut shell-derived hydrochar prepared via hydrothermal carbonization-NaOH activation for methylene blue adsorption. *J. Environ. Manage.* **203**, 237–244 (2017).
56. Enterría, M. *et al.* Effect of nanostructure on the supercapacitor performance of activated carbon xerogels obtained from hydrothermally carbonized glucose-graphene oxide hybrids. *Carbon* **105**, 474–483 (2016).
57. Salinas-Torres, D. *et al.* Electrochemical behaviour of activated carbons obtained via hydrothermal carbonization. *J. Mater. Chem. A* **3**, 15558–15567 (2015).
58. Kambo, H. S., Minaret, J. & Dutta, A. Process Water from the Hydrothermal Carbonization of Biomass: A Waste or a Valuable Product? *Waste Biomass Valorization* **9**, 1181–1189 (2018).
59. Stemann, J., Putschew, A. & Ziegler, F. Hydrothermal carbonization: Process water characterization and effects of water recirculation. *Bioresour. Technol.* **143**, 139–146 (2013).
60. Linstrom, P. J. & Mallard, W. G. Water. in *NIST Chemistry WebBook* vol. NIST Standard Reference Database Number 69 (National Institute of Standards and Technology).
61. Cooper, A. R. & Jeffreys, G. V. *Chemical Kinetics and Reactor Design*. (Oliver & Boyd, 1971).
62. Jones, L., Ennos, A. R. & Turner, S. R. Cloning and characterization of irregular xylem4 (irx4): a severely lignin-deficient mutant of *Arabidopsis*. *Plant J. Cell Mol. Biol.* **26**, 205–216 (2001).
63. Lynd, L. R., Weimer, P. J., Zyl, W. H. van & Pretorius, I. S. Microbial Cellulose Utilization: Fundamentals and Biotechnology. *Microbiol. Mol. Biol. Rev.* **66**, 506–577 (2002).
64. Brown, R. M. Cellulose structure and biosynthesis: What is in store for the 21st century? *J. Polym. Sci. Part Polym. Chem.* **42**, 487–495 (2004).
65. Agbor, V. B., Cicek, N., Sparling, R., Berlin, A. & Levin, D. B. Biomass pretreatment: Fundamentals toward application. *Biotechnol. Adv.* **29**, 675–685 (2011).
66. Saha, B. C. Hemicellulose bioconversion. *J. Ind. Microbiol. Biotechnol.* **30**, 279–291 (2003).
67. Hendriks, A. T. W. M. & Zeeman, G. Pretreatments to enhance the digestibility of lignocellulosic biomass. *Bioresour. Technol.* **100**, 10–18 (2009).
68. Girio, F. M. *et al.* Hemicelluloses for fuel ethanol: A review. *Bioresour. Technol.* **101**, 4775–4800 (2010).
69. Jung, K. A., Lim, S.-R., Kim, Y. & Park, J. M. Potentials of macroalgae as feedstocks for biorefinery. *Bioresour. Technol.* **135**, 182–190 (2013).
70. Scheller, H. V. & Ulvskov, P. Hemicelluloses. *Annu. Rev. Plant Biol.* **61**, 263–289 (2010).
71. Rinaldi, R. *et al.* Paving the Way for Lignin Valorisation: Recent Advances in Bioengineering, Biorefining and Catalysis. *Angew. Chem. Int. Ed.* n/a-n/a (2016) doi:10.1002/anie.201510351.
72. Achyuthan, K. E. *et al.* Supramolecular Self-Assembled Chaos: Polyphenolic Lignin's Barrier to Cost-Effective Lignocellulosic Biofuels. *Molecules* **15**, 8641–8688 (2010).
73. Campbell, M. M. & Sederoff, R. R. Variation in Lignin Content and Composition (Mechanisms of Control and Implications for the Genetic Improvement of Plants). *Plant Physiol.* **110**, 3–13 (1996).
74. Vassilev, S. V., Baxter, D., Andersen, L. K., Vassileva, C. G. & Morgan, T. J. An overview of the organic and inorganic phase composition of biomass. *Fuel* **94**, 1–33 (2012).
75. Huber, G. W., Iborra, S. & Corma, A. Synthesis of Transportation Fuels from Biomass: Chemistry, Catalysts, and Engineering. *Chem. Rev.* **106**, 4044–4098 (2006).

76. Demirbas, A. Use of algae as biofuel sources. *Energy Convers. Manag.* **51**, 2738–2749 (2010).
77. Chen, S. L., Heap, M. P., Pershing, D. W. & Martin, G. B. Fate of coal nitrogen during combustion. *Fuel* **61**, 1218–1224 (1982).
78. Qian, F. P., Chyang, C. S., Huang, K. S. & Tso, J. Combustion and NO emission of high nitrogen content biomass in a pilot-scale vortexing fluidized bed combustor. *Bioresour. Technol.* **102**, 1892–1898 (2011).
79. Vassilev, S. V., Baxter, D., Andersen, L. K. & Vassileva, C. G. An overview of the chemical composition of biomass. *Fuel* **89**, 913–933 (2010).
80. Neveux, N., Magnusson, M., Maschmeyer, T., Nys, R. de & Paul, N. A. Comparing the potential production and value of high-energy liquid fuels and protein from marine and freshwater macroalgae. *GCB Bioenergy* **7**, 673–689 (2015).
81. Ma, Z. *et al.* A comprehensive slagging and fouling prediction tool for coal-fired boilers and its validation/application. *Fuel Process. Technol.* **88**, 1035–1043 (2007).
82. Wang, T., Zhai, Y., Zhu, Y., Li, C. & Zeng, G. A review of the hydrothermal carbonization of biomass waste for hydrochar formation: Process conditions, fundamentals, and physicochemical properties. *Renew. Sustain. Energy Rev.* **90**, 223–247 (2018).
83. Jatzwauck, M. & Schumpe, A. Kinetics of hydrothermal carbonization (HTC) of soft rush. *Biomass Bioenergy* **75**, 94–100 (2015).
84. Knežević, D., van Swaaij, W. & Kersten, S. Hydrothermal Conversion Of Biomass. II. Conversion Of Wood, Pyrolysis Oil, And Glucose In Hot Compressed Water. *Ind. Eng. Chem. Res.* **49**, 104–112 (2010).
85. Karayıldırım, T., Sinağ, A. & Kruse, A. Char and Coke Formation as Unwanted Side Reaction of the Hydrothermal Biomass Gasification. *Chem. Eng. Technol.* **31**, 1561–1568 (2008).
86. Dinjus E., Kruse A. & Tröger N. Hydrothermal Carbonization – 1. Influence of Lignin in Lignocelluloses. *Chem. Eng. Technol.* **34**, 2037–2043 (2011).
87. Donohoe, B. S., Decker, S. R., Tucker, M. P., Himmel, M. E. & Vinzant, T. B. Visualizing lignin coalescence and migration through maize cell walls following thermochemical pretreatment. *Biotechnol. Bioeng.* **101**, 913–925 (2008).
88. Trajano, H. L. *et al.* The fate of lignin during hydrothermal pretreatment. *Biotechnol. Biofuels* **6**, 110 (2013).
89. Sevilla, M. & Fuertes, A. B. The production of carbon materials by hydrothermal carbonization of cellulose. *Carbon* **47**, 2281–2289 (2009).
90. Bruice, 1941-, Paula Yurkanis. *Organic chemistry / Paula Yurkanis Bruice.* (2014).
91. Iryani, D. A., Kumagai, S., Nonaka, M., Sasaki, K. & Hirajima, T. Hydrothermal Carbonisation Kinetics of Sugarcane Bagasse treated by Hot Compressed Water under variabel temperature conditions. *ARNP J. Eng. Appl. Sci.* **11**, 4833–4839 (2016).
92. Antal, M. J., Mok, W. S. L. & Richards, G. N. Mechanism of formation of 5-(hydroxymethyl)-2-furaldehyde from d-fructose and sucrose. *Carbohydr. Res.* **199**, 91–109 (1990).
93. Reza, M. T. *et al.* Hydrothermal Carbonization of Biomass for Energy and Crop Production. *Appl. Bioenergy* **1**, (2014).
94. Jung, D., Zimmermann, M. & Kruse, A. Hydrothermal Carbonization of Fructose: Growth Mechanism and Kinetic Model. *ACS Sustain. Chem. Eng.* **6**, 13877–13887 (2018).
95. Krawielitzki, S. & Kläusli, T. M. Modified Hydrothermal Carbonization Process for Producing Biobased 5-HMF Platform Chemical. *Ind. Biotechnol.* **11**, 6–8 (2015).
96. Yin, S., Pan, Y. & Tan, Z. Hydrothermal Conversion of Cellulose to 5-Hydroxymethyl Furfural. *Int. J. Green Energy* **8**, 234–247 (2011).
97. Falco, C. *et al.* Hydrothermal Carbon from Biomass: Structural Differences between Hydrothermal and Pyrolyzed Carbons via ¹³C Solid State NMR. *Langmuir* **27**, 14460–14471 (2011).
98. Román, S. *et al.* Hydrothermal Carbonization: Modeling, Final Properties Design and Applications: A Review. *Energies* **11**, 216 (2018).
99. Jung, D. & Kruse, A. Evaluation of Arrhenius-type overall kinetic equations for hydrothermal carbonization. *J. Anal. Appl. Pyrolysis* **127**, 286–291 (2017).

Hydrothermal Carbonisation of Novel Biomasses

100. Kang, S., Li, X., Fan, J. & Chang, J. Hydrothermal conversion of lignin: A review. *Renew. Sustain. Energy Rev.* **27**, 546–558 (2013).
101. Knežević, D., van Swaaij, W. P. M. & Kersten, S. R. A. Hydrothermal Conversion of Biomass: I, Glucose Conversion in Hot Compressed Water. *Ind. Eng. Chem. Res.* **48**, 4731–4743 (2009).
102. Kabyemela, B. M., Adschiri, T., Malaluan, R. M. & Arai, K. Kinetics of Glucose Epimerization and Decomposition in Subcritical and Supercritical Water. *Ind. Eng. Chem. Res.* **36**, 1552–1558 (1997).
103. Matsumura, Y., Yanachi, S. & Yoshida, T. Glucose Decomposition Kinetics in Water at 25 MPa in the Temperature Range of 448–673 K. *Ind. Eng. Chem. Res.* **45**, 1875–1879 (2006).
104. Bobleter, O. & Pape, G. Der hydrothermale abbau von glucose. *Monatshefte Für Chem. Chem. Mon.* **99**, 1560 (1968).
105. Amin, S. R. Reforming and decomposition of glucose in an aqueous phase. in (1975).
106. Yong, T. L.-K. & Matsumura, Y. Reaction Kinetics of the Lignin Conversion in Supercritical Water. *Ind. Eng. Chem. Res.* **51**, 11975–11988 (2012).
107. Yong, T. L.-K. & Matsumura, Y. Kinetic Analysis of Lignin Hydrothermal Conversion in Sub- and Supercritical Water. *Ind. Eng. Chem. Res.* **52**, 5626–5639 (2013).
108. Reza, M. T. *et al.* Reaction kinetics of hydrothermal carbonization of loblolly pine. *Bioresour. Technol.* **139**, 161–169 (2013).
109. Reza, M. T. Hydrothermal Carbonization of Lignocellulosic Biomass. (University of Nevada, Reno, 2011).
110. Goering, H. K. & Soest, P. J. V. *Forage Fiber Analyses (apparatus, Reagents, Procedures, and Some Applications)*. (U.S. Agricultural Research Service, 1970).
111. Mittal, A., Chatterjee, S. G., Scott, G. M. & Amidon, T. E. Modeling xylan solubilization during autohydrolysis of sugar maple and aspen wood chips: Reaction kinetics and mass transfer. *Chem. Eng. Sci.* **64**, 3031–3041 (2009).
112. Mittal, A., Chatterjee, S. G., Scott, G. M. & Amidon, T. E. Modeling xylan solubilization during autohydrolysis of sugar maple wood meal: Reaction kinetics. *Holzforschung* **63**, 307–314 (2009).
113. Grénman, H. *et al.* Kinetics of Aqueous Extraction of Hemicelluloses from Spruce in an Intensified Reactor System. *Ind. Eng. Chem. Res.* **50**, 3818–3828 (2011).
114. Zhang, B., Huang, H.-J. & Ramaswamy, S. Reaction Kinetics of the Hydrothermal Treatment of Lignin. *Appl. Biochem. Biotechnol.* **147**, 119–131 (2008).
115. Danso-Boateng, E. *et al.* Kinetics of faecal biomass hydrothermal carbonisation for hydrochar production. *Appl. Energy* **111**, 351–357 (2013).
116. Braghiroli, F. L. *et al.* Kinetics of the hydrothermal treatment of tannin for producing carbonaceous microspheres. *Bioresour. Technol.* **151**, 271–277 (2014).
117. M, B., D, B., F, P., D, C. & L, F. Kinetic and Thermal Modeling of Hydrothermal Carbonization Applied to Grape Marc. *Chem. Eng. Trans.* **43**, 505–510 (2015).
118. BP Energy Outlook, 2018 edition. (2018).
119. Hoekman, S. K., Broch, A. & Robbins, C. Hydrothermal Carbonization (HTC) of Lignocellulosic Biomass. *Energy Fuels* **25**, 1802–1810 (2011).
120. Coronella, C. J., Lynam, J. G., Reza, M. T. & Uddin, M. H. Hydrothermal Carbonization of Lignocellulosic Biomass. in *Application of Hydrothermal Reactions to Biomass Conversion* 275–311 (Springer, Berlin, Heidelberg, 2014). doi:10.1007/978-3-642-54458-3_12.
121. Bach, Q.-V. & Skreiberg, Ø. Upgrading biomass fuels via wet torrefaction: A review and comparison with dry torrefaction. *Renew. Sustain. Energy Rev.* **54**, 665–677 (2016).
122. Patel, B., Guo, M., Izadpanah, A., Shah, N. & Hellgardt, K. A review on hydrothermal pre-treatment technologies and environmental profiles of algal biomass processing. *Bioresour. Technol.* **199**, 288–299 (2016).
123. Geoscience Australia. Deserts. <http://www.ga.gov.au/scientific-topics/national-location-information/landforms/deserts> (2009).
124. Redondo-Gómez, S. *et al.* Growth and Photosynthetic Responses to Salinity of the Salt-marsh Shrub *Atriplex portulacoides*. *Ann. Bot.* **100**, 555–563 (2007).

125. Ben Salem, H. *et al.* Potential use of oldman saltbush (*Atriplex nummularia* Lindl.) in sheep and goat feeding. *Small Rumin. Res.* **91**, 13–28 (2010).
126. Shabala, S., Bose, J. & Hedrich, R. Salt bladders: do they matter? *Trends Plant Sci.* **19**, 687–691 (2014).
127. Dai, B.-Q., Wu, X., De Girolamo, A. & Zhang, L. Inhibition of lignite ash slagging and fouling upon the use of a silica-based additive in an industrial pulverised coal-fired boiler. Part 1. Changes on the properties of ash deposits along the furnace. *Fuel* **139**, 720–732 (2015).
128. Tortosa Masiá, A. A., Buhre, B. J. P., Gupta, R. P. & Wall, T. F. Characterising ash of biomass and waste. *Fuel Process. Technol.* **88**, 1071–1081 (2007).
129. Koppejan, J. & Loo, S. van. *The Handbook of Biomass Combustion and Co-firing*. (Routledge, 2012).
130. Reza, M. T., Lynam, J. G., Uddin, M. H. & Coronella, C. J. Hydrothermal carbonization: Fate of inorganics. *Biomass Bioenergy* **49**, 86–94 (2013).
131. Novianti, S., Nurdiawati, A., Zaini, I. N., Sumida, H. & Yoshikawa, K. Hydrothermal treatment of palm oil empty fruit bunches: an investigation of the solid fuel and liquid organic fertilizer applications. *Biofuels* **7**, 627–636 (2016).
132. Baskoro Lokahita, Muhammad Aziz, Yoshikawa, K. & Takahashi, F. Energy and resource recovery from Tetra Pak waste using hydrothermal treatment. *Appl. Energy* **207**, 107–113 (2017).
133. Benavente, V., Calabuig, E. & Fullana, A. Upgrading of moist agro-industrial wastes by hydrothermal carbonization. *J. Anal. Appl. Pyrolysis* **113**, 89–98 (2015).
134. Gallifuoco, A., Taglieri, L., Scimia, F., Papa, A. A. & Di Giacomo, G. Hydrothermal carbonization of Biomass: New experimental procedures for improving the industrial Processes. *Bioresour. Technol.* **244**, 160–165 (2017).
135. Mäkelä, M., Fullana, A. & Yoshikawa, K. Ash behavior during hydrothermal treatment for solid fuel applications. Part 1: Overview of different feedstock. *Energy Convers. Manag.* **121**, 402–408 (2016).
136. EPA, USA. Microwave assisted acid digestion of siliceous and organically based matrices. *OHW Method* **3052**.
137. Kalra, Y. *Handbook of Reference Methods for Plant Analysis*. (CRC Press, 1997).
138. Bevington, P. R. & Robinson, D. K. *Data reduction and error analysis for the physical sciences*. (2003).
139. Montgomery, D. C. *Design and Analysis of Experiments*. (John Wiley & Sons, 2008).
140. Mayoral, M. C., Izquierdo, M. T., Andrés, J. M. & Rubio, B. Different approaches to proximate analysis by thermogravimetry analysis. *Thermochim. Acta* **370**, 91–97 (2001).
141. Werther, J., Saenger, M., Hartge, E.-U., Ogada, T. & Siagi, Z. Combustion of agricultural residues. *Prog. Energy Combust. Sci.* **26**, 1–27 (2000).
142. Saldarriaga, J. F. *et al.* Fast characterization of biomass fuels by thermogravimetric analysis (TGA). *Fuel* **140**, 744–751 (2015).
143. Department of the Environment and Energy. *Department of the Environment and Energy* <http://www.environment.gov.au/>.
144. Lane, D. J. *et al.* Release of Cl, S, P, K, and Na during Thermal Conversion of Algal Biomass. *Energy Fuels* **29**, 2542–2554 (2015).
145. Heilmann, S. M. *et al.* Hydrothermal carbonization of distiller's grains. *Biomass Bioenergy* **35**, 2526–2533 (2011).
146. Mukherjee, T. & Chatterjee, A. Production of low phosphorus steels from high phosphorus Indian hot metal: Experience at Tata Steel. *Bull. Mater. Sci.* **19**, 893–903 (1996).
147. Heilmann, S. M. *et al.* Hydrothermal carbonization of microalgae II. Fatty acid, char, and algal nutrient products. *Appl. Energy* **88**, 3286–3290 (2011).
148. White, R. J. *Porous Carbon Materials from Sustainable Precursors*. (Royal Society of Chemistry, 2015).
149. Yu, L. *et al.* Carbohydrate-Derived Hydrothermal Carbons: A Thorough Characterization Study. *Langmuir* **28**, 12373–12383 (2012).

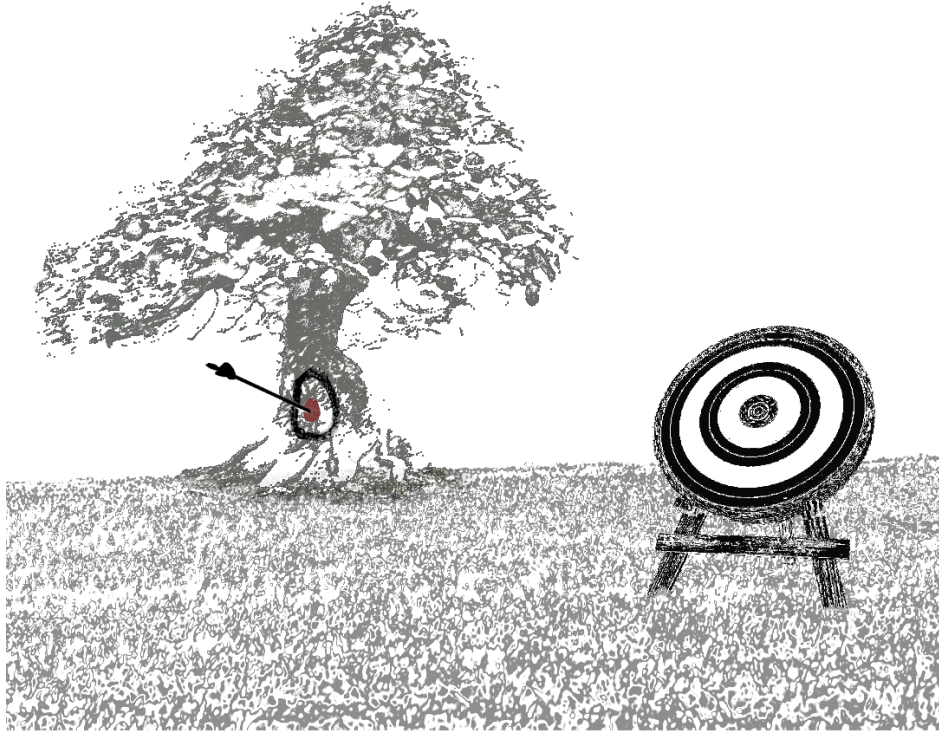
150. Dai, L. *et al.* Engineered hydrochar composites for phosphorus removal/recovery: Lanthanum doped hydrochar prepared by hydrothermal carbonization of lanthanum pretreated rice straw. *Bioresour. Technol.* **161**, 327–332 (2014).
151. World Energy Council. World Energy Resources, Bioenergy 2016. (2016).
152. Klemm, D., Heublein, B., Fink, H.-P. & Bohn, A. Cellulose: Fascinating Biopolymer and Sustainable Raw Material. *Angew. Chem. Int. Ed.* **44**, 3358–3393 (2005).
153. Keiller, B. G., van Eyk, P. J., Lane, D. J., Muhlack, R. & Burton, R. A. Hydrothermal Carbonization of Australian Saltbush. *Energy Fuels* (2018) doi:10.1021/acs.energyfuels.8b03416.
154. Arevalo-Gallegos, A., Ahmad, Z., Asgher, M., Parra-Saldivar, R. & Iqbal, H. M. N. Lignocellulose: A sustainable material to produce value-added products with a zero waste approach—A review. *Int. J. Biol. Macromol.* **99**, 308–318 (2017).
155. Van Dyk, J. S. & Pletschke, B. I. A review of lignocellulose bioconversion using enzymatic hydrolysis and synergistic cooperation between enzymes—Factors affecting enzymes, conversion and synergy. *Biotechnol. Adv.* **30**, 1458–1480 (2012).
156. Burton, R. A., Gidley, M. J. & Fincher, G. B. Heterogeneity in the chemistry, structure and function of plant cell walls. *Nat. Chem. Biol.* **6**, 724–732 (2010).
157. Rowell, R. M., Pettersen, R., Han, J. S., Rowell, J. S. & Tshabalala, M. A. Cell wall chemistry. *Handb. Wood Chem. Wood Compos. Boca Raton Fla CRC Press 2005 Pages 35-74* (2005).
158. Mottiar, Y., Vanholme, R., Boerjan, W., Ralph, J. & Mansfield, S. D. Designer lignins: harnessing the plasticity of lignification. *Curr. Opin. Biotechnol.* **37**, 190–200 (2016).
159. Tillman, D. A., Rossi, A. J. & Kitto, W. D. Properties of Wood Fuels. in *Wood Combustion: Principles, Processes, Economic* 17–46 (Academic Press, 1981).
160. Kang, S., Li, X., Fan, J. & Chang, J. Characterization of Hydrochars Produced by Hydrothermal Carbonization of Lignin, Cellulose, d-Xylose, and Wood Meal. *Ind. Eng. Chem. Res.* **51**, 9023–9031 (2012).
161. Kim, D., Lee, K. & Park, K. Y. Upgrading the characteristics of biochar from cellulose, lignin, and xylan for solid biofuel production from biomass by hydrothermal carbonization. *J. Ind. Eng. Chem.* **42**, 95–100 (2016).
162. Deguchi, S., Tsujii, K. & Horikoshi, K. Crystalline-to-amorphous transformation of cellulose in hot and compressed water and its implications for hydrothermal conversion. *Green Chem.* **10**, 191–196 (2008).
163. Iryani, D. A. *et al.* The Hot Compressed Water Treatment of Solid Waste Material from the Sugar Industry for Valuable Chemical Production. *Int. J. Green Energy* **11**, 577–588 (2014).
164. Fuertes, A. B. *et al.* Chemical and structural properties of carbonaceous products obtained by pyrolysis and hydrothermal carbonisation of corn stover. *Soil Res.* **48**, 618–626 (2010).
165. Comino, P., Shelat, K., Collins, H., Lahnstein, J. & Gidley, M. J. Separation and Purification of Soluble Polymers and Cell Wall Fractions from Wheat, Rye and Hull less Barley Endosperm Flours for Structure-Nutrition Studies. *J. Agric. Food Chem.* **61**, 12111–12122 (2013).
166. Fu, D. T. & O'Neill, R. A. Monosaccharide Composition Analysis of Oligosaccharides and Glycoproteins by High-Performance Liquid Chromatography. *Anal. Biochem.* **227**, 377–384 (1995).
167. Yamamoto, F. M. & Rokushika, S. Study of pH dependence using molecular modeling in reversed-phase liquid chromatography of 1-phenyl-3-methyl-5-pyrazolone derivatives of aldose. *Anal. Chim. Acta* **501**, 143–149 (2004).
168. Burton, R. A. *et al.* Virus-Induced Silencing of a Plant Cellulose Synthase Gene. *Plant Cell* **12**, 691–705 (2000).
169. Barnes, W. & Anderson, C. Acetyl Bromide Soluble Lignin (ABSL) Assay for Total Lignin Quantification from Plant Biomass. *BIO-Protoc.* **7**, (2017).
170. Hames, B., Scarlata, C. & Sluiter, A. Determination of Protein Content in Biomass. Laboratory Analytical Procedure (LAP) NREL/TP-510-42625. (2008).
171. Yang, H., Yan, R., Chen, H., Lee, D. H. & Zheng, C. Characteristics of hemicellulose, cellulose and lignin pyrolysis. *Fuel* **86**, 1781–1788 (2007).

172. Minowa, T., Zhen, F. & Ogi, T. Cellulose decomposition in hot-compressed water with alkali or nickel catalyst. *J. Supercrit. Fluids* **13**, 253–259 (1998).
173. Lynam, J. G., Reza, M. T., Yan, W., Vásquez, V. R. & Coronella, C. J. Hydrothermal carbonization of various lignocellulosic biomass. *Biomass Convers. Biorefinery* **5**, 173–181 (2015).
174. Keiller, B. G., Muhlack, R., Burton, R. A. & van Eyk, P. J. Biochemical Compositional Analysis and Kinetic Modeling of Hydrothermal Carbonisation of Australian Saltbush. *Energy Fuels* (2019) doi:10.1021/acs.energyfuels.9b02931.
175. Ranalli, P. & Venturi, G. Hemp as a raw material for industrial applications. *Euphytica* **140**, 1–6 (2004).
176. Amziane, S. & Arnaud, L. *Bio-aggregate-based Building Materials: Applications to Hemp Concretes*. (John Wiley & Sons, 2013).
177. Ingrao, C. *et al.* Energy and environmental assessment of industrial hemp for building applications: A review. *Renew. Sustain. Energy Rev.* **51**, 29–42 (2015).
178. Leson, G. Hemp Foods in North America. *J. Ind. Hemp* (2008).
179. Department of Agriculture, Province of Manitoba. Industrial Hemp Production and Management. *Province of Manitoba* <http://www.gov.mb.ca/agriculture/> (2018).
180. Office of Parliamentary Counsel. South Australian Legislation. (2017).
181. Keller, N. M. The Legalization of Industrial Hemp and What It Could Mean for Indiana’s Biofuel Industry Note. *Indiana Int. Comp. Law Rev.* **23**, 555–590 (2013).
182. Sluiter, A. *et al.* Determination of Ash in Biomass. Laboratory Analytical Procedure (LAP). NREL/TP-510-42622. (2005).
183. Shahzad, A. Hemp fiber and its composites – a review. *J. Compos. Mater.* **46**, 973–986 (2012).
184. Zhu, J. Y. & Pan, X. J. Woody biomass pretreatment for cellulosic ethanol production: Technology and energy consumption evaluation. *Bioresour. Technol.* **101**, 4992–5002 (2010).
185. Reza, M. T., Uddin, M. H., Lynam, J. G., Hoekman, S. K. & Coronella, C. J. Hydrothermal carbonization of loblolly pine: reaction chemistry and water balance. *Biomass Convers. Biorefinery* **4**, 311–321 (2014).
186. Reza, M. T. *et al.* Hydrothermal carbonization (HTC) of cow manure: Carbon and nitrogen distributions in HTC products. *Environ. Prog. Sustain. Energy* **35**, 1002–1011 (2016).
187. Izydorczyk, M. S. & Dexter, J. E. Barley β -glucans and arabinoxylans: Molecular structure, physicochemical properties, and uses in food products—a Review. *Food Res. Int.* **41**, 850–868 (2008).
188. Zhang, Y. *et al.* Wheat bran arabinoxylans: Chemical structure and film properties of three isolated fractions. *Carbohydr. Polym.* **86**, 852–859 (2011).
189. Kabel, M. A., van den Borne, H., Vincken, J.-P., Voragen, A. G. J. & Schols, H. A. Structural differences of xylans affect their interaction with cellulose. *Carbohydr. Polym.* **69**, 94–105 (2007).
190. Linder, Å., Bergman, R., Bodin, A. & Gatenholm, P. Mechanism of Assembly of Xylan onto Cellulose Surfaces. *Langmuir* **19**, 5072–5077 (2003).
191. Dammström, S., Salmen, L. & Gatenholm, P. On the interactions between cellulose and xylan, a biomimetic simulation of the hardwood cell wall. *BioResources* **4**, 3–14 (2009).
192. Busse-Wicher, M. *et al.* The pattern of xylan acetylation suggests xylan may interact with cellulose microfibrils as a twofold helical screw in the secondary plant cell wall of *Arabidopsis thaliana*. *Plant J.* **79**, 492–506 (2014).
193. Ralph, J. Hydroxycinnamates in lignification. *Phytochem. Rev.* **9**, 65–83 (2010).
194. Kruse, A. & Dinjus, E. Hot compressed water as reaction medium and reactant: Properties and synthesis reactions. *J. Supercrit. Fluids* **39**, 362–380 (2007).
195. Ming, J. *et al.* Sodium salt effect on hydrothermal carbonization of biomass: a catalyst for carbon-based nanostructured materials for lithium-ion battery applications. *Green Chem.* **15**, 2722–2726 (2013).
196. Grabber, J. H. How Do Lignin Composition, Structure, and Cross-Linking Affect Degradability? A Review of Cell Wall Model Studies. *Crop Sci.* **45**, 820–831 (2005).
197. Boerjan, W., Ralph, J. & Baucher, M. Lignin Biosynthesis. *Annu. Rev. Plant Biol.* **54**, 519–546 (2003).

Hydrothermal Carbonisation of Novel Biomasses

198. Li, M.-F., Fan, Y.-M., Xu, F. & Sun, R.-C. Characterization of extracted lignin of bamboo (*Neosinocalamus affinis*) pretreated with sodium hydroxide/urea solution at low temperature. *BioResources* **5**, 1762–1778 (2010).
199. Diaz-Piuldo, G. & McCook, L. *Macroalgae (Seaweeds)*. (Great Barrier Reef Marine Park Authority, 2008).
200. Buschmann, A. H. *et al.* Seaweed production: overview of the global state of exploitation, farming and emerging research activity. *Eur. J. Phycol.* **52**, 391–406 (2017).
201. Paul, N. A. & de Nys, R. Promise and pitfalls of locally abundant seaweeds as biofilters for integrated aquaculture. *Aquaculture* **281**, 49–55 (2008).
202. Chen, H., Zhou, D., Luo, G., Zhang, S. & Chen, J. Macroalgae for biofuels production: Progress and perspectives. *Renew. Sustain. Energy Rev.* **47**, 427–437 (2015).
203. Ghadiryanfar, M., Rosentrater, K. A., Keyhani, A. & Omid, M. A review of macroalgae production, with potential applications in biofuels and bioenergy. *Renew. Sustain. Energy Rev.* **54**, 473–481 (2016).
204. Jones, C. S. & Mayfield, S. P. Algae biofuels: versatility for the future of bioenergy. *Curr. Opin. Biotechnol.* **23**, 346–351 (2012).
205. Suganya, T., Varman, M., Masjuki, H. H. & Renganathan, S. Macroalgae and microalgae as a potential source for commercial applications along with biofuels production: A biorefinery approach. *Renew. Sustain. Energy Rev.* **55**, 909–941 (2016).
206. Adeniyi, O. M., Azimov, U. & Burluka, A. Algae biofuel: Current status and future applications. *Renew. Sustain. Energy Rev.* **90**, 316–335 (2018).
207. Singh, A., Nigam, P. S. & Murphy, J. D. Renewable fuels from algae: An answer to debatable land based fuels. *Bioresour. Technol.* **102**, 10–16 (2011).
208. Kraan, S. Mass-cultivation of carbohydrate rich macroalgae, a possible solution for sustainable biofuel production. *Mitig. Adapt. Strateg. Glob. Change* **18**, 27–46 (2013).
209. Wang, B., Li, Y., Wu, N. & Lan, C. Q. CO₂ bio-mitigation using microalgae. *Appl. Microbiol. Biotechnol.* **79**, 707–718 (2008).
210. Um, B.-H. & Kim, Y.-S. Review: A chance for Korea to advance algal-biodiesel technology. *J. Ind. Eng. Chem.* **15**, 1–7 (2009).
211. Aresta, M., Dibenedetto, A. & Barberio, G. Utilization of macro-algae for enhanced CO₂ fixation and biofuels production: Development of a computing software for an LCA study. *Fuel Process. Technol.* **86**, 1679–1693 (2005).
212. Eboibi, B. E.-O., Lewis, D. M., Ashman, P. J. & Chinnasamy, S. Hydrothermal liquefaction of microalgae for biocrude production: Improving the biocrude properties with vacuum distillation. *Bioresour. Technol.* **174**, 212–221 (2014).
213. Elliott, D. C., Biller, P., Ross, A. B., Schmidt, A. J. & Jones, S. B. Hydrothermal liquefaction of biomass: Developments from batch to continuous process. *Bioresour. Technol.* **178**, 147–156 (2015).
214. Gollakota, A. R. K., Kishore, N. & Gu, S. A review on hydrothermal liquefaction of biomass. *Renew. Sustain. Energy Rev.* (2017) doi:10.1016/j.rser.2017.05.178.
215. Kidgell, J. T., Magnusson, M., de Nys, R. & Glasson, C. R. K. Ulvan: A systematic review of extraction, composition and function. *Algal Res.* **39**, 101422 (2019).
216. Iwamoto, K. & Shiraiwa, Y. Salt-Regulated Mannitol Metabolism in Algae. *Mar. Biotechnol.* **7**, 407–415 (2005).
217. Suutari, M. *et al.* Macroalgae in biofuel production. *Phycol. Res.* **63**, 1–18 (2015).
218. Levine, R. B., Pinnarat, T. & Savage, P. E. Biodiesel Production from Wet Algal Biomass through in Situ Lipid Hydrolysis and Supercritical Transesterification. *Energy Fuels* **24**, 5235–5243 (2010).
219. Ortiz, J. *et al.* Dietary fiber, amino acid, fatty acid and tocopherol contents of the edible seaweeds *Ulva lactuca* and *Durvillaea antarctica*. *Food Chem.* **99**, 98–104 (2006).
220. Yaich, H. *et al.* Chemical composition and functional properties of *Ulva lactuca* seaweed collected in Tunisia. *Food Chem.* **128**, 895–901 (2011).

221. Tabarsa, M., Rezaei, M., Ramezanzpour, Z. & Waaland, J. R. Chemical compositions of the marine algae *Gracilaria salicornia* (Rhodophyta) and *Ulva lactuca* (Chlorophyta) as a potential food source. *J. Sci. Food Agric.* **92**, 2500–2506 (2012).
222. Tonetto, A., Oliveira, K. S. & M Domingues, T. Analysis of Biochemical Composition of Three Stream Macroalgae Species. **4**, 111–115 (2014).
223. Álvarez-Murillo, A., Sabio, E., Ledesma, B., Román, S. & González-García, C. M. Generation of biofuel from hydrothermal carbonization of cellulose. Kinetics modelling. *Energy* **94**, 600–608 (2016).
224. Angell, A. R., Mata, L., de Nys, R. & Paul, N. A. The protein content of seaweeds: a universal nitrogen-to-protein conversion factor of five. *J. Appl. Phycol.* **28**, 511–524 (2016).
225. WANG, N. Biological Activities of Tropical Green Algae from Australia. (2016).
226. Lahaye, M., Jegou, D. & Buleon, A. Chemical characteristics of insoluble glucans from the cell wall of the marine green alga *Ulva lactuca* (L.) Thuret. *Carbohydr. Res.* **262**, 115–125 (1994).
227. Ray, B. & Lahaye, M. Cell-wall polysaccharides from the marine green alga *Ulva* “rigida” (ulvales, chlorophyta). Extraction and chemical composition. *Carbohydr. Res.* **274**, 251–261 (1995).
228. Rogalinski, T., Liu, K., Albrecht, T. & Brunner, G. Hydrolysis kinetics of biopolymers in subcritical water. *J. Supercrit. Fluids* **46**, 335–341 (2008).
229. Abdelmoez, W., Nakahasi, T. & Yoshida, H. Amino Acid Transformation and Decomposition in Saturated Subcritical Water Conditions. *Ind. Eng. Chem. Res.* **46**, 5286–5294 (2007).
230. Trif-Tordai, G. & Ionel, I. Waste Biomass as Alternative Bio-Fuel - Co-Firing versus Direct Combustion. (2011) doi:10.5772/25030.



این نیز بگذرد

īn nīz bogzarad

Hoc quoque transibit

Καὶ αὐτὸ περήσει

Ĉi tio ankaŭ pasos

Buydd hyn hefyd yn pasio

Sillumë yando vānuva

În hrossene yedho hen

This too shall pass...